# A Process for Separation by Semi-Continuous Counter-Current Crystallization

By

## Nathan M. Aumock

B.S. Chemical Engineering - University of Wisconsin, 2004
M.S. Chemical Engineering Practice - Massachusetts Institute of Technology, 2006

*Submitted to the Department of Chemical Engineering in partial fulfillment of the requirements for the degree of*

Doctor of Philosophy
at the
Massachusetts Institute of Technology

February 2011

Signature of Author  ……………………………………………………………………………………………………….
Department of Chemical Engineering
December 23, 2010

Certified by  ……………………………………………………………………………………………………….
T. Alan Hatton
Ralph Landau Professor of Chemical Engineering Practice
Thesis Supervisor

Certified by  ……………………………………………………………………………………………………….
Kenneth A. Smith
Gilliland Professor of Chemical Engineering
Thesis Supervisor

Accepted by  ……………………………………………………………………………………………………….
William M. Deen
Professor of Chemical Engineering
Chairman, Committee for Graduate Students

# A Process for Separation by Semi-Continuous Counter-Current Crystallization

By

Nathan M. Aumock

## Abstract

A process is proposed to perform separations via crystallization by using multiple tanks and constraining crystal growth to solid surfaces. Multiple tanks allow multiple recrystallizations to improve product purity and to ensure high recovery of the component of interest. Crystal growth on solid surfaces avoids multi-phase flow handling which can cause operational difficulties. A model is developed for this process for solid solution forming systems which is also applied to batch crystallization for comparison.

The solid product from the process is found to provide enhanced purity (1-2% increase) at yields approaching the batch yield when a large number of tanks are used; the ratio of incorporation rate constants ($\gamma$) is significantly less than one; and the surface equilibrium constant ($K$) is less than order one. The liquid effluent from the process is also a viable product when $\gamma>1$ and $K$ is close to or greater than one. The use of a sweep stream entering at a tank upstream of the feed tank was determined to be undesirable due to diminished yield.

Batch experiments performed to validate the proposed model with asparagine as the component of interest and aspartic acid as the impurity in water were found to be inconclusive. Fitting of parameter values to the liquid phase was not successful due to crystal growth on surfaces other than the designated seed. The parameters $\gamma$ and $K$ fitted to solid phase data were found to be 0.1-3 and 0.4-0.6 respectively which are favorable parameters for use of the semi-continuous process with the solid taken as the product. The presence of crystals on multiple surfaces in the liquid phase indicates that constraint of crystallization to a specific surface was not achieved.

The impurity distribution in the solid layer did not match the model prediction throughout the crystal. Non-uniform initial growth behavior or uneven dissolution of the crystal during analysis could cause the observed behavior. Further experiments should be conducted that increase the ratio of product to accumulation in the liquid phase and employ solid sampling methods that give more consistent results.

Thesis Supervisor: T. Alan Hatton
Title: Ralph Landau Professor of Chemical Engineering Practice

Thesis Supervisor: Kenneth A. Smith
Title: Gilliland Professor of Chemical Engineering

# Acknowledgements

Graduate school is a trying endeavor and no one can complete alone. I'd first like to thank my advisors for their support and encouragement during my time at MIT. Working with both of you has been a valuable experience and I am thankful for your guidance throughout the last 6 years. I'd also like to thank my committee members Professors Trout and Cooney for their input and the Singapore-MIT alliance and the Novartis-MIT Center for Continuous Manufacturing for funding at various stages of my PhD.

Next I'd like to thank Bertold Schenkel, Felix Kollmer and Dragoslav Jetvic from Novartis AG in Basel, Switzerland. Bertold and Felix were heavily involved in the early stages of this project and discussions with them have influenced this work significantly. They also made possible a visit to a Novartis research lab in Basel where Dragoslav was very generous with his time helping me to make the most of the short time I spent there. Thank you all for your help.

I also must thank Diana Bower and the Prather lab for allowing me to use their HPLC over the last few months of my experimental work. With their help I avoided a significant headache that I otherwise would have developed. Thank you again.

The Hatton group is an incredibly fun and friendly place to work. Everyone is willing to lend a helping hand with a derivation or to discuss the best monkey with bird picture on the internet. I'd like to especially thank Saurabh, Sanjoy, Brad, Lino, Fritz, Andrea, Ying D. and Smeet for their help both with work and beyond.

My friends have been invaluable in maintaining my sanity during my time at MIT. The Chemical Engineering Department is a fantastic place to work in particular I'd like to thank Dave, Kevin, the Captain, Matt, Sohan, Melanie, John, Dave, Charles, Ben and Sty for making my time here as enjoyable as it was.

My family back in Minnesota have been very understanding through the years as I explain that no, I am not done yet and no, I do not know when I will be. Thank you all for your support and I'm happy to report that I'm finally done with school.

Finally and most importantly I would like to thank my fiancée, Gina, for her love and support. She has been my strongest supporter in the past few years and I am lucky to have her in my life. I hope that I can as valuable to her in the future.

# Table of Contents

# Table of Figures

11

13

# Table of Tables

# 1.    Introduction

Crystallization is one of the most important chemical separation processes. It is a process in which a species undergoes a transition from a liquid to a solid phase or from a state of dissolution to a solid. It has been used for years to separate and purify chemical compounds. Crystallization can be done in batch or continuous fashion and many processes have been developed to perform batch and continuous crystallizations.

Crystallization is separation process and the methods by which impurities enter a crystal should be considered when designing a unit operation. One common mechanism that occurs for molecules that have very similar structures is solid solution formation. The impurity molecule enters the crystalline lattice in place of a molecule of the desired compound. The replacement can occur over a limited or the full concentration range. This type of impurity inclusions is expected to be important for separations resulting from chemical reactions where by-products with similar structures are generated.

It is expected that impurity incorporation into a growing crystal via solid solution formation will result in a concentration gradient in the crystal. This is expected because once a layer of crystal has been deposited; it will not interact with the subsequent layer of deposition on the time scale of crystal growth from solution. This effect will be especially prominent in a system where growth is occurring on a fixed surface. Growth in solution by seeding with many small particles can minimize the magnitude of this gradient if each individual particle remains small but growth on large particles or large surfaces should allow gradients to develop.

A new semi-continuous process employing multiple crystallization vessels and targeted growth on fixed surfaces is proposed. This process seeks to increase purity with respect to batch crystallizations while also eliminating the need for handling of multi-phase flows. A model of this process is developed with the assumption that impurity inclusion occurs through solid solution formation. The proposed model is analyzed to determine practical implications and the model is validated using batch crystallization experiments.

Before detailing the proposed process which uses crystallization to effect a separation, an overview of crystallization will be given. This will be followed by a description of current industrial crystallization processes. Both batch and continuous operations will be discussed.

17

## 1.1 <u>Crystallization</u>

Crystallization is a process where a compound present in a liquid phase undergoes a phase transformation into the solid phase. The process of crystallization can occur in two ways; solution crystallization for a component in a solution; or melt crystallization for a single compound going from its liquid phase to a solid phase (as in water to ice). Solution crystallization is commonly used for small molecules that may be sensitive to temperature or for compounds produced in limited quantities. This is the case for a large number of pharmaceutical compounds. Melt crystallization is more common for polymer systems and other compounds with low melting points and in large amounts.

Crystallization occurs when the chemical potential of a species in the liquid phase becomes larger than the chemical potential for that species in the solid phase. The amount by which the chemical potential in the liquid exceeds the saturation value is referred to as the driving force for crystallization.

$$\Delta\mu = \mu_{i,L} - \mu_{i,S} \qquad (1.1)$$

where $\mu_{i,L}$ is the chemical potential of species $i$ in the liquid phase and $\mu_{i,S}$ is the chemical potential of species $i$ in the solid phase.

Because it is difficult to measure chemical potentials, the driving force for crystallization is generally expressed in terms of concentrations. The concentration driving force is given in equation (1.2).

$$\Delta C = C_i - C_i^* \qquad (1.2)$$

where $C_i$ is the liquid phase concentration of species $i$ and $C_i^*$ is the saturation concentration of species $i$ in the liquid phase

Two useful quantities related to the concentration driving force are given in the following equations.

$$S_i = \frac{C_i}{C_i^*} \tag{1.3}$$

$$\sigma_i = \frac{C_i - C_i^*}{C_i^*} \tag{1.4}$$

where $S_i$ is the supersaturation ratio of species $i$ and $\sigma_i$ is the relative supersaturation of species $i$. Supersaturation and the driving force for crystallization are directly related quantities. If a driving force for crystallization exists in a system, then the relative supersaturation must be positive and the supersaturation ratio must be greater than one.

Supersaturation can be generated in multiple ways. For solution crystallization the temperature of the solution can be changed, the concentration of the solution can be changed or an additional compound may be added to the solution that changes the solubility of the component of interest. Temperature control and addition of another component are also applicable to melt crystallization but concentration change by solvent evaporation is not possible.

The solubility of a compound is often dependent on the temperature of the solution. Generally the solubility increases as the temperature increases but the converse situation does exist for some molecules, such as calcium sulfate in water.[1] An initially saturated or undersaturated solution may be cooled in order to decrease the saturation concentration so that the solution becomes supersaturated.

Instead of changing the saturation concentration, the concentration of the crystallizing component can be changed by decreasing the amount of solvent. Decreasing the amount of solvent will increase the concentration of the component of interest and this can also generate supersaturation.

A third method for generating supersaturation requires that an added component affect the solubility of the component of interest such that the saturation concentration is lowered enough that supersaturation is generated. This is also known as "salting out" due to the frequent use of electrolytes as the added component.

Other types of crystallization including reactive[2] and extractive[3] crystallization are possible. Reactive crystallization, also known as precipitation occurs when a chemical reaction between multiple compounds results in a crystalline solid product. Extractive crystallization requires the addition of an additional component in the form of a solvent to alter the phase relationship between the species in question. This can be considered a special case of the salting out crystallization.

No matter how supersaturation is generated, both solution and melt crystallization can be divided into two major parts; nucleation and growth. Nucleation refers to the processes leading to formation of the initial solid particle from the liquid phase and growth is addition of more molecules from the liquid phase to that initial solid particle. These two processes will be looked at in the next two sections.

It is possible for the supersaturation to be increased to a point such that solid formation happens immediately. This corresponds to spinodal decomposition[4]. Conversely, although supersaturation occurs for any solution with a concentration higher than the saturation concentration, not all supersaturated solutions will crystallize in a finite period of time. A supersaturated solution may exist in the meta-stable zone where no crystals will be formed unless some external input is applied. Solutions in the meta-stable zone can exist without crystallizing for long periods of time. This consideration applies to solutions that have not undergone nucleation because if a crystal is introduced into a solution in the meta-stable zone, growth and nucleation will occur. Other inputs such as mechanical agitation or the presence of a solid surface can also lead to nucleation as will be described further in the following section.

### 1.1.1 Nucleation

The creation of new solid particles in a liquid phase is referred to as nucleation. Primary nucleation refers to the creation of the initial particle of solid phase in a liquid phase while secondary nucleation refers to any particles that are created when other particles are present.

Primary nucleation is the process by which a critical number of molecules associate in the liquid phase and undergo a phase transformation into the solid phase. This critical number of molecules depends on the chemical in question and is difficult to measure. Nucleation is a

statistical process because it relies on collisions or near collisions of multiple molecules and cannot be characterized by simple parameters.

The average time before a crystal nucleus is observed is known as the induction time which is often used to characterize primary nucleation. The definition of induction time is important because the initial nucleus formed is generally very small and difficult to detect. The reported induction time will often be the time necessary for a crystal nucleus to become visible, either to the naked eye or with optical microscopy.

System parameters including geometry, stirring speed, type of stirring, supersaturation, and impurity concentration can all affect primary nucleation. Geometry and speed and type of stirring can affect how easy it is for the critical cluster of molecules to form in the liquid phase. Supersaturation is very important because the larger the number of molecules in excess of the saturation concentration, the larger the chance that a critical number of them will interact to form a nucleus. The impact of impurities is less obvious but very significant because an impurity can change the energetics of nucleus formation. An impurity can serve to lower the energy needed to form a solid particle thereby reducing the induction time and facilitating nucleation. The opposite effect were the impurity raises the energy of solid phase formation is also possible.

The effect of impurities requires that primary nucleation behavior be described as either homogeneous or heterogeneous. Homogeneous nucleation refers to a nucleus that forms through interactions of species present in the liquid phase including the component of interest and the solvent. Dissolved impurity molecules may also participate in homogeneous nucleation although they would be unlikely to do so unless they were structurally similar to the component of interest. Heterogeneous nucleation occurs when any solid species is involved in the formation of the initial solid particle. Heterogeneous nucleation can be caused by the surface of the vessel in which the crystallization is performed or by dust or other small particles present in solution.[5-11] Porous materials can also impact nucleation.[12]

It is very difficult to have exclusively homogeneous nucleation because so many different materials can lead to heterogeneous nucleation and making perfectly clean solutions is difficult in practice. In general heterogeneous nucleation will dominate except at extremely high

supersaturations where the number of molecules of the component of interest is much larger than the number of solid impurities present so that it is more likely for molecules to interact without being affected by a solid impurity.[8] One method for studying homogeneous nucleation at moderate supersaturations involves suspension of extremely pure supersaturated droplets in an immiscible solvent.[13, 14]

If nucleation occurs on a material that has a matching crystal structure to the component being crystallized this process is called epitaxy. When the crystal structure of the material matches or very nearly matches the crystal structure of the crystallizing component then the energy barrier to nucleation is reduced[15]. Various examples of epitaxy have been reported in the literature including the use of thin films[16-22] and other crystals[23-26] as the surface for nucleation. A special case of epitaxy occurs when crystals of the component being crystallized are added to the solution in order to facilitate nucleation. This process is referred to as seeding and in this case nucleation is not necessary as growth will generally begin immediately upon addition of the seeds.

Secondary nucleation is the formation of new solid particles in the presence of other solid particles of that same species. Common modes of secondary nucleation are particle breakage and contact nucleation. When a crystal particle breaks into two or more pieces the total number of particles in solution will increase. Contact nucleation is a process by which a crystal will move across a solid surface, such as an impeller blade or a vessel wall, and will generate a new solid particle. This new particle is not created by breakage of the first particle but instead results from the interactions of the surface of a formed crystal and a second surface. It is thought that this may result in very high local supersaturations which result in the nucleation of a particle but this phenomenon is not well understood. [27, 28]

The meta-stable zone is the range of supersaturations defined by a lack of primary nucleation for a given system. The system will maintain that supersaturation without generating any crystal nuclei until an external input such as an impurity addition, seed crystal addition, mechanical agitation, temperature change or solvent evaporation results in a nucleus and subsequent crystal growth. Once nucleation is induced in these solutions growth and secondary nucleation will result in the liquid phase concentration approaching the equilibrium value over

time.  Foreign surfaces can also induce nucleation in a system initially in the meta-stable zone. This occurs because the width of the meta-stable zone actually depends on all system parameters, including foreign surfaces and particles.[29, 30]  These solids serve to change the meta-stable zone width just as they change the energetic requirements for nucleation.

The thermodynamic nucleation rate has been modeled by several different approaches. The nucleation rate (with units of number of nuclei/time/volume) is often assumed to have an Arrhenius dependence on temperature as shown in equation (1.5).

$$J = Ae^{\frac{-\Delta G_C}{kT}}$$
(1.5)

where $A$ (number of nuclei/time/volume) and $\Delta G_C$ (energy/molecule) are the pre-factor and the energy barrier to nucleation respectively.  The role of a specific nucleation model is to evaluate these expressions.  The induction time is often assumed to be proportional to the inverse nucleation rate because induction time data are easy to collect[31].  This approximation has been used to estimate the factor $A$ using experimental data[32-34].

In classical nucleation theory as developed primarily by Gibbs, Volmer and Becker and Döring.[31, 35, 36] the energy barrier is related to that necessary to form a critically sized cluster. The cluster is assumed to be spherically shaped and described by the radius, $r$.  The energy of a cluster of arbitrary size ($\Delta G$) is found by balancing the surface excess free energy ($\Delta G_S$) with the volume excess free energy ($\Delta G_V$) of the cluster.  The sum of these two energies as a function of cluster size will exhibit a maximum and this corresponds to the energy necessary ($\Delta G_C$) to form a critical sized cluster ($r_C$).  The qualitative behavior of these energies as a function of cluster size is shown in Figure 1.

Figure 1 shows that a cluster larger than the critical size decreases its energy by growing larger while a cluster smaller than the critical size will decrease its energy by decreasing in size. This explains why a cluster of a critical size is necessary for a solid phase to persist.  The energy of this critical cluster is given by the following equation.

$$\Delta G_C = \frac{4\pi \gamma r_C^2}{3} \tag{1.6}$$

where $\gamma$ is the surface energy of the interaction between the cluster and the bulk solution. This quantity can be related to the supersaturation by using the Gibbs-Thomson equation relating solubility to particle size. For a non-electrolyte, this equation can be written as the following.

$$\ln S = \frac{2\gamma v}{kTr} \tag{1.7}$$

where $v$ is the molecular volume and $k$ is the Boltzmann constant. Using equation (1.7) to re-place $r_C$ in equation (1.6) gives the critical energy as a function of temperature, surface energy and supersaturation.

$$\Delta G_C = \frac{16\pi \gamma^3 v^2}{3k^2 T^2 (\ln S)^2} \tag{1.8}$$

The rate of nucleation is then found by using the energy of this critical cluster size in an Arrhenius type expression as shown in equation (1.9).

$$J = A\exp\left(\frac{16\pi \gamma^3 v^2}{3k^2 T^2 (\ln S)^2}\right) \tag{1.9}$$
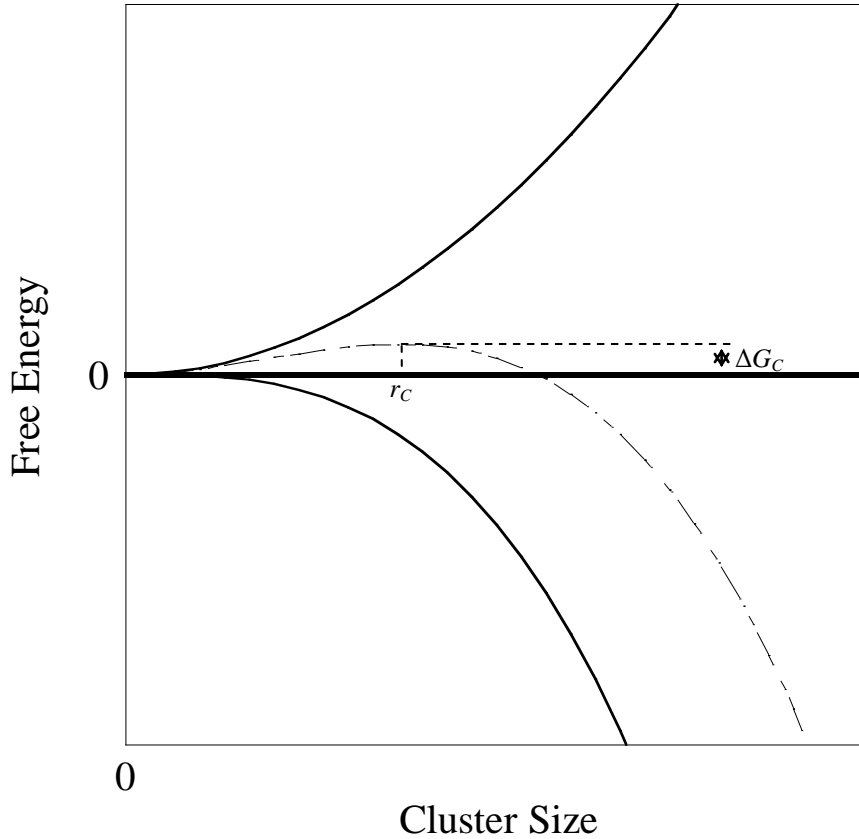
**Figure 1. Free energy diagram for classical nucleation theory showing the surface and volume excess free energies.**

Classical nucleation theory predicts that the nucleation rate will depend on the absolute temperature, the supersaturation and the surface energy between the forming solid particle and the bulk liquid. This surface energy in this model is equal to the bulk surface energy between solid and liquid but it is unlikely that a continuum model is the best choice for a process occurring on a molecular level. Newer nucleation rate expressions seek to account for the molecular nature of this process and improve upon the simple result from classical nucleation theory.

Various methods to improve nucleation modeling have been attempted. A kinetic model for nucleation has been developed by the combined work of Kolmogorv, Avrami and Johnson and Mehl[37-39]. This kinetic model along with the classical thermodynamic model have been extended and improved by various authors.[32, 40-48] A simplified model for engineering purposes has also been proposed[49].

Models for nucleation have also been developed that focus on the molecular nature of nucleation. Density functional theory has been used to remove the need for bulk surface tension values[50, 51] while variational transition state theory was used to calculate directly the forward and reverse reaction constants for molecular clusters of various sizes. [52]

Molecular simulations have also been used to model nucleation.[53-56] The difficulty with this approach is that a large simulation area or a long simulation time is necessary to observe a nucleation event.[57, 58] Molecular simulations are in concept better than the classical nucleation theory but they depend on the intermolecular potentials used and in some cases require significant computer power. These methods will surely improve as advances are made in these two fields.

### 1.1.2  Growth

After a solid particle is present in solution, that particle will incorporate more molecules from solution and increase in size through crystal growth. Growth is a simpler process to model than nucleation because there is no induction time before it begins. Once a crystal is present growth will continue until the concentration in the solution has reached its saturation value (supersaturation becomes 0).

Various models for crystal growth have been proposed. They include birth and spread, surface energy, adsorption layer and diffusion-reaction. The birth and spread and adsorption models are similar and both require 2-dimensional nucleation on the surface of a crystal to propagate growth. The birth and spread models assume that a new surface layer is nucleated at a corner or some defect in the crystal and growth then spreads across the surface of the crystal from this nucleus. Other surface nucleation events can occur on the same surface as the first or on top of the growing surface. Many of these models have been developed for crystal growth from a vapor phase but are generally appropriate for solution crystallization as well. Some of the assumptions made in their development need to be adjusted for crystallization from solution.

The adsorption models assume that molecules from the bulk liquid first adsorb to the surface of the crystal without being immediately incorporated into the crystal lattice.[59, 60] The

first adsorption model is credited to Volmer in 1939[31] with heavy influence from the work of Gibbs.[35]  The adsorbed molecules are then free to move over the surface of the crystal until they encounter an edge or a kink where the interaction energy becomes strong enough to in-corporate that molecule into the crystal.  This method then requires active edges, defects or kinks in the crystal surface for growth to occur.  It has been postulated that these edges can be generated by 2-dimensional nucleation.

An alternative to this is the Burton-Cabrera-Frank (BCF) theory that gives a model for spiral growth of a crystal.[61]  With a spiraling growth surface, there is always an edge present so that surface nucleation events are not necessary.  BCF theory predicts the following crystal growth rate for growth from the vapor phase:

$$R = A\sigma^2 \tanh\left(\frac{B}{\sigma}\right) \tag{1.10}$$

where $R$ is the crystal growth rate (length/time), $\sigma$ is the relative supersaturation ($C_i/C_i^*$-1) and $A$ and $B$ are complicated temperature-dependent constants.  The most important point to take from this expression is that crystal growth will be proportional to $\sigma^2$ at low supersaturations and $\sigma$ at higher supersaturations[*].  The meaning of high and low supersaturations depends on physical properties of the system.  The BCF theory has been adapted more explicitly to solution crystallization.[62, 63]

Surface energy theories predict that the shape and growth rate of crystals will be de-termined by overall minimization of surface energy.  This was initially proposed by Gibbs as an analogy to a droplet immersed in a fluid that minimizes its energy by minimizing its surface area.[35]  Different faces of a crystal will have different molecular interactions with the solvent and so will have different surface energies.  Growth will occur in order to minimize this energy over the sum of all faces of the crystal.   This approach has not been shown to match experi-

---

[*] $\lim\limits_{x \to 0} \tanh\left(\dfrac{1}{x}\right) = 1$ and $\tanh\left(\dfrac{1}{x}\right) = \dfrac{1}{x} + O\left(\dfrac{1}{x^3}\right)$

mental data regarding the dependence of crystal growth on supersaturation and so is not widely accepted.

The diffusion-reaction approach combines transport of a molecule to the surface of the crystal and then incorporation of that molecule into the crystal. This approach was developed as a modification of a purely diffusive mechanism by Berthoud[64] and Valeton[65]. The kinetics of these steps are considered separately with either one potentially being the rate limiting step. The rate expressions for these two steps are given in equations (1.11) and (1.12).

$$\frac{dm}{dt} = k_d A \left( C - C_j \right) \tag{1.11}$$

$$\frac{dm}{dt} = k_r A \left( C_j - C^* \right)^r \tag{1.12}$$

where $\frac{dm}{dt}$ is change of crystal mass with time, $k_d$ and $k_r$ are the diffusion and reaction rate constants, $r$ is the order of the surface integration reaction, $A$ is the surface area for crystal growth, $C$ is the bulk concentration, $C^*$ is the saturation concentration and $C_j$ is an intermediate concentration between $C$ and $C^*$ that is determined by the balance of mass transfer and reaction rates.

These equations show that the two steps of the growth process operate under different driving forces and can have different dependences on their respective driving forces. Measurement of the intermediate concentration $C_j$ is difficult so often the two expressions are combined into equation (1.13)[66].

$$\frac{dm}{dt} = k A \left( C - C^* \right)^g \tag{1.13}$$

where $k$ is now the overall rate constant and $g$ is the order of the overall crystallization process. The exponent $g$ must be determined experimentally and it does not have a fundamental significance in the way in which an exponent in chemical reaction kinetics would.

Crystals that have high surface roughness have been shown to have a kinetic growth expression with first order dependence on the supersaturation.[67] Rough surfaces provide many sites at which molecules may be added to the crystal so that generation of an active site is not a limiting process. A surface entropy factor[†] has been defined by Jackson[68] that can provide guidance as to when a surface will have first order dependence on the supersaturation.

$$\chi = \frac{4\varepsilon}{kT} \tag{1.14}$$

where $k$ is Boltzmann's constant, $T$ is the temperature and $\varepsilon$ is the potential energy change per solid-fluid bond. Smaller values of x correspond to a rougher surface and when $\chi$ is less than approximately three, growth will occur with a first order dependence on the supersaturation. For higher values of $\chi$ (smoother surfaces) other growth mechanisms will apply. Evaluation of $\chi$ and comparison to experimental data has been studied by other authors.[69, 70]

The surface entropy factor refers to the microscopic surface of the crystal where new molecules are added. The macroscopic roughness of a surface is not addressed by this consideration although it can have an effect on the crystal growth rate and does have an effect on the nucleation kinetics as discussed in section 1.1.1.

If the surface integration reaction is order 1 ($r = 1$), then $g$ will also be one and the overall rate constant $k$ can be easily related to the diffusion and reaction rate constants:

$$k = \frac{k_d k_r}{k_d + k_r} \tag{1.15}$$

The diffusion-reaction approach to modeling crystallization is very attractive from an engineering perspective and has been used in the literature.[71-73] The only physical information about the crystallizing species required is the solubility as a function of temperature. The rate constant $k$ and empirical order $g$ can be determined experimentally. This allows a framework

---

[†] The symbol for this value in the original articles is $\alpha$, but $\chi$ is used here to avoid confusion with the separation factor to be defined in section 1.2.2.

developed with this formulation to be applicable to a large number of compounds with only a few experiments.

### 1.1.3  Crystal Size Distribution

The combined details of the nucleation and growth processes along with system operating parameters dictate the final distribution of the number and size of crystals in solution crystallization.  Control of the crystal size distribution is often one of the key goals when performing an industrial crystallization.  The first experimental study of the size distribution from a continuous crystallizer was done by Montillon and Badger in 1927[74] and the basis for a large portion of subsequent theoretical work was done by McCabe in 1929[75, 76].  Generally it is desired to have the majority of crystals in a small size range in order to simplify other unit operations downstream of the crystallization.  It may in some cases also be important to have crystals that are bigger than some critical size.

The crystal size distribution is modeled using a population balance[77] which keeps track of the number of crystals present in the system as a function of the crystal size.

$$n = f\left(L\right) \tag{1.16}$$

where $n$ is the crystal population density in number of crystals per unit size per unit volume and $L$ is a characteristic dimension of the crystal.  The population balance takes into account both nucleation and growth kinetics along with the operating parameters of the crystallizer.  Other factors that may be important depending on the system include size dependent crystal growth rate and the rate of secondary nucleation

The moments of the crystal size distribution give valuable information about the crystal product.  The zeroth moment gives the number of crystals $N$, the second moment gives the surface area $A$ and the third moment gives the mass $M$ up to a certain size $L$.  These moments are given in equations  (1.17) to (1.19).

$$N = \int_0^L n \, dL \tag{1.17}$$

$$A = \int_0^L nL^2 \, dL \tag{1.18}$$

$$M = \int_0^L nL^3 \, dL \tag{1.19}$$

Key parameters used to control the crystal size distribution are the supersaturation, stirring properties and method for generating initial crystals. The supersaturation can be controlled either by temperature changes, solvent evaporation or salting-out so that a prescribed level of supersaturation is always present. This could be done so that supersaturation is high at the beginning when nucleation is desired and then becomes much smaller so that growth occurs but nucleation is minimized later during the crystallization process.

Control of the stirring is important because it has a significant effect on secondary nucleation.[78] Vigorous stirring can lead to particle breakage or contact nucleation that can significantly affect the particle distribution by creating a large number of very small particles.

Because nucleation is a difficult process to predict and control, many industrial crystallizations seek to minimize nucleation all together. Seed particles are added to the solution instead of waiting for primary nucleation to occur. These seed particles then can immediately undergo growth so that the kinetics of the overall process becomes more easily defined. If these seed crystals have a very narrow size distribution then the process can be designed to minimize secondary nucleation so that the final size distribution will also be narrow. This is done by choosing a very low supersaturation in order to minimize primary nucleation and choosing operating parameters such that secondary nucleation is also minimized.

### 1.1.4 Polymorphism

An individual compound may be capable of existing in more than one crystalline state. The property of having more than one chemically identical but different crystalline structure is called polymorphism. The physical properties of different crystal polymorphs will generally be

different. This has important consequences in pharmaceutical applications where dissolution and other physical properties are very important for consumable products.[66]

The achieved polymorphs can be influenced by the rate of crystallization, the temperature, the solvent and the presence of impurities. The rate of crystallization is generally controlled by the supersaturation and larger supersaturations can lead to different polymorphs. The temperature at which the crystallization is carried out can also dictate the polymorph of the crystal. Different solvents will interact differently with the crystallizing component and this can also impact the structure of the crystal formed from that solution. Impurities can also play a role in the structure of the crystalline product by disrupting the structure of the crystal and making another form more energetically favorable.

The initial polymorph that is formed during crystallization may not be the most stable polymorph of that crystal. The initial polymorph may be influenced by kinetic factors or by impurities but given enough time the crystal will transition into the most thermodynamically stable polymorph.[66] The amount of time necessary for this transition to occur can be extremely long and so newly grown crystals must be observed over the time frame in which they would be used to see if any polymorphic transitions occur.

Discovery of different polymorphs for a specific compound is largely done by trial and error. Various temperatures, supersaturations and impurity concentrations are employed and the resulting polymorph is noted.[79] Impurities in the form of solid surfaces can also sometimes be very useful in generating different polymorphs. It is difficult to say definitively that all polymorphs have been determined because there is no way currently to know all of the possible polymorphs.

Simulation methods have become more popular and are another way to study possible polymorphs available to a given substance.[80-82] Advances in computational capability can lead to predicted polymorphs that cannot be obtained experimentally. Knowing the structure of a particular polymorph does not provide sufficient information on what to do to obtain that polymorph in practice.

## 1.2 <u>Impurity Incorporation During Crystallization</u>

Crystallization is a purification unit operation and so the methods by which impurities are included in the crystal must be considered. Different mechanisms for impurity incorporation include adsorption, inclusions, co-crystal formation, and solid solution formation. The first two mechanisms can occur in any system depending on operating conditions while the last two mechanisms relate to thermodynamic states that are only applicable to certain chemical systems.

Understanding the mechanism of impurity incorporation is important when designing crystallization processes in order to maximize purity of the product. While any species can adsorb to the surface of a growing crystal, only certain species will be able to form a solid solution or a co-crystal solid with a given component of interest. The particular equipment, temperature profiles and operating times of a given separation can be chosen in order to minimize the effect of the most important impurity incorporation mechanism for a given crystallization.

### 1.2.1 *Non-thermodynamic Impurity Incorporation*

Adsorption of impurities to the surface of a growing crystal can have a dramatic effect on the crystal growth process. The adsorbing molecule could be either the solvent or any species present in solution that is not the component of interest. Molecules adsorbed to the surface of a growing crystal can reduce the growth rate of that crystal even at low concentrations. This occurs because the adsorbed impurity occupies a site on the surface where the component of interest could incorporate into the crystal.[83, 84] Because adsorption may occur preferentially on a certain face of the crystal, impurities can also affect the morphology of the growing crystal. If the dominant growth face in the absence of impurities is impeded due to impurity adsorption then other faces will continue to grow which can result in a different final morphology.[85, 86] The supersaturation can also effect the adsorption of impurities. Models of the effects of impurity adsorption using the Langmuir adsorption isotherm[87-89] and other approaches have been developed.

Inclusions occur when the growing crystal traps an impurity inside the crystal structure. This is more commonly found in fast growing crystal systems with larger crystal sizes.[90, 91] The

solution in which crystallization takes place is a common inclusion.  These solvent inclusions will decrease the purity of the final product because they contain a high level of impurity in relation to the growing crystal.  Inclusions can also be generated if the crystal is generated by heterogeneous nucleation on an impurity particle or a designed nucleation surface.  Inclusions can be formed when the edges of a crystal face grow faster than the center allowing a depression to form in which an impurity can be trapped.[92-94]  They can also be formed by the collision of dendrites under conditions resulting in dendritic crystal growth.[95]

### 1.2.2   Thermodynamic Impurity Incorporation

Impurity incorporation in a growing crystal can also occur due to formation of a thermodynamically stable phase.  Types of binary phases that may be encountered include co-crystals and solid solutions.  Both of these thermodynamic states will be represented on the phase diagram of the system of interest.  Preparing phase diagrams for real systems that include a solvent, the component of interest and multiple impurities is very difficult because of the large number of parameters.  Real phase diagrams are extremely useful in designing a crystallization operation but are unfortunately not widely available.

A co-crystal is composed of two or more distinct compounds organized in a regular way in the crystal lattice.  A co-crystal can be represented by a unit cell with a formula such as $A_nB_m$. The component of interest and the impurity are arranged in a regular pattern throughout the crystal.  The solvent in solution crystallization can also be the impurity in the crystal.  The resulting co-crystals are called solvates for general solvents and hydrates[96] when the solvent is water. If the solvate is undesirable, the isolated solvate crystals can be dried in order to remove the solvent.

A solid solution occurs when a crystal is able to incorporate an impurity into the crystalline lattice in an irregular way.  Solid solutions are a very common method of impurity incorporation and have also been referred to as mixed crystals.  The impurity may replace a molecule of the component of interest or it may be able to fit in the interstitial space in the crystal lattice. The amount of impurity present in the crystal will depend on the solution concentrations and the temperature and pressure of the system.  The concentration of the impurity can also

change if conditions in the bulk are changed which is not possible for a co-crystal. Purification of a system that forms solid solutions will require multiple recrystallizations in order to attain high purity product.

Compounds that have very similar structures are more likely to form a solid solution because they form by substitution of an impurity for the component of interest in the crystal lattice.[97-101] Introducing an impurity into the crystal lattice causes strain on the crystal and if the strain is too great then the crystal cannot grow any further.[102] Compounds with similar structures are more likely to substitute into the crystal lattice without preventing further growth. Various models have been developed to predict impurity concentrations in solid solutions using kinetic[103, 104] and thermodynamic[105-108] approaches. An important parameter in models addressing the impurity distribution in solid solutions is the distribution coefficient,

$$D_i = \frac{C_{i,S}}{C_{i,L}}$$

(1.20)

where $C_{i,s}$ is the concentration of component $i$ in the solid phase and $C_{i,L}$ is the concentration of component $i$ in the liquid phase. This quantity relates the concentrations of a species in the liquid and solid phases for a system at equilibrium. Another useful quantity is the separation factor.

$$\alpha_{ij} = \frac{D_j}{D_i} = \frac{C_{j,S}/C_{j,L}}{C_{i,S}/C_{i,L}} = \frac{C_{j,S}C_{i,L}}{C_{i,S}C_{j,L}}$$

(1.21)

The separation factor is an equilibrium measure of the separation of species $i$ and $j$ after crystallization. A separation factor of one indicates there has been no change in the relative amounts of $i$ and $j$ from the liquid to the solid phase. A separation factor greater than one indicates that there is relatively more species $j$ compared to species $i$ in the solid phase than the

liquid phase, or the solid phase has been enriched in species $j$. Conversely, for separation factors less than one $i$ is enriched in the solid phase compared to the liquid phase.

Values for $D_i$ and $\alpha_{ij}$ can be determined from an appropriate phase diagram. Given a temperature, the equilibrium concentrations in the solid and liquid phase can be read from the diagram and used to calculate a distribution coefficient or a separation factor. Unfortunately phase diagrams are not available for a large number of systems, especially for ternary systems necessary for solution crystallization, which often requires that these parameters be measured at the appropriate operating conditions.

Rosenberger and Riveros developed an equation to estimate the separation factor for crystallization from melt and from solution.[109] The simplified equation for crystallization from solution depends on the ratio of solubilities of the component of interest and the impurity in the liquid phase and the heat of solution of adding the impurity to the solid phase. These parameters can be measured allowing determination of the separation factor.

The non-equilibrium nature of many crystallization operations has also been addressed. An effective separation factor is found by taking into account the diffusion boundary layer thickness and the growth rate of the crystal.[110] The diffusion boundary layer thickness must be estimated to use this approach but it is generally true that decreasing the boundary layer thickness will result in an effective separation factor that is closer to the equilibrium value. The boundary layer thickness depends strongly on the agitation and can be decreased with more vigorous agitation of the solution.[111]

Even with the use of effective separation factors previous solution crystallization results focus on the average impurity concentration of the solid product.[112] No model has been found for crystallization from solution that addresses impurity gradients in solid solutions. This issue has been studied extensively for melt crystallization as summarized by Sloan and McGhie[113].

## 1.3    Types of Industrial Crystallization Unit Operations

There are a wide variety of industrial crystallization operations. These operations can be run batch wise, continuously or somewhere in between. Different processes make use of all three methods for generating supersaturation; temperature control, solvent evaporation and

addition of a component affecting solubility of the component of interest. The most common methods for generating supersaturation are temperature and solvent evaporation so those will be the focus here. A few of these processes will be detailed in order to frame the discussion of the new process that is proposed in the next chapter.

### 1.3.1  Industrial Solution Crystallization Operations

The first industrial crystallization to be discussed which is also the simplest is tank crystallization.[114, 115] This operation may be carried out with or without agitation. The feed solution is charged to the tank where either cooling or evaporation is carried out in order to induce crystallization. Cooling may be via convection from the tank to the environment over a long period of time or it can be accomplished using a jacketed vessel and a heat transfer medium such as water. Internal coils may also be used for cooling but these are prone to encrustation of crystals which reduces the efficiency of cooling. The temperature of the tank is often varied with time during batch crystallization in order to control the supersaturation and product size distribution. Optimal cooling profiles for seeded batch crystallizations have been calculated and implemented in practice.[116-118]

Evaporation can be done by long term exposure to the environment (open tank), solar evaporation, or steam heating. Solar evaporation is used in large open-air ponds to recover salt from salt water[119, 120] but is in principle a large unstirred tank. Steam can be introduced through a coil inside the tank in order to provide energy for solvent evaporation. This type of crystallizer is a batch operation and is simple to operate and cheap to build but can be labor intensive and offers lower productivity than other methods.

Another type of unit operation is the trough crystallizer. This is a continuous crystallization operation where a feed solution is fed to a long unit that can be agitated or otherwise propelled in order to move the solution along the length of the trough with crystals exiting at the far end. The length of the device or speed of conveyance is adjusted in order to establish the desired operating time in the crystallizing unit. In its simplest implementation, crystallization occurs due to cooling associated with natural convective exchange with the surroundings.

Units have also been designed that incorporate direct cooling by using internal coils, jacketing the trough or by spraying of a coolant such as water on the exterior of the trough.[66]

The Oslo-Krystal crystallizer[121] is a more complicated unit operation that can deliver crystals continuously with a narrow size distribution. This unit operation is an example of a circulating liquor crystallizer in which the solution is circulated while the crystalline particles are not. This is accomplished by very careful determination of flow rates in the device so that the crystals remain fluidized in one section of the crystallizer. The solution without crystals is circulated through an external loop, where supersaturation is generated either by cooling or by evaporation, before being recirculated to the region of the crystallizer where the crystals are present. A schematic of this crystallizer using evaporation to generate supersaturation is shown in Figure 2.

The amount of supersaturation generated must be small so that nucleation does not occur during the solution circulation. The supersaturated solution when reintroduced to the crystals results in crystal growth. As the crystals grow they sink lower in the vessel until they reach a desired size and position in the tank at which point they are discharged as a slurry. Careful control is necessary to ensure that nucleation does not occur in the solution circulation loop and that the crystals remain fluidized in the desired location in the crystallizer.
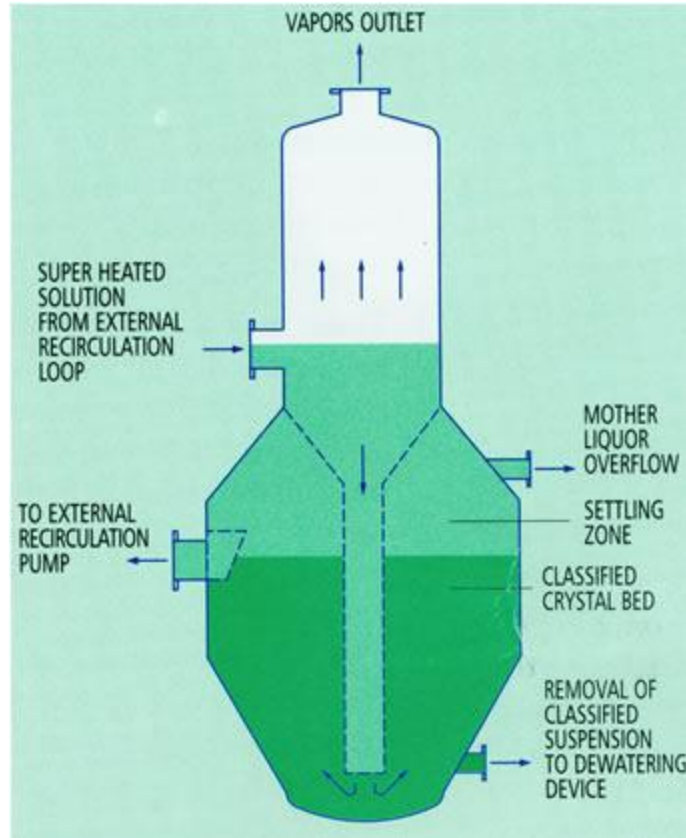
**Figure 2. Picture of an Oslo-Krystal type continuous crystallizer. Feed is added in the external recirculation loop before heating.**[122]

Another common type of crystallizer is the draft-tube with agitation crystallizer. The most common example of this is the draft-tube baffled crystallizer[123], shown schematically in Figure 3. A draft tube with an agitator is placed in a larger tank such that the top of the draft tube is below the liquid level in the tank. The feed is introduced at the base of the draft tube. The hot solution moves up the draft tube and solvent boils at the liquid surface giving supersaturation. The supersaturated solution then falls along the side of the draft tube and passes through a fluidized bed of particles in the same way as in an Oslo-Krystal crystallizer. There is an internal liquor recycle loop again similar to an Oslo-Krystal unit which serves to fluidize the crystals outside of the draft tube. The baffle in the wall serves to minimize crystals in the solution recycle loop. The product crystals are removed from the bottom of the vessel once they have achieved the desired size.
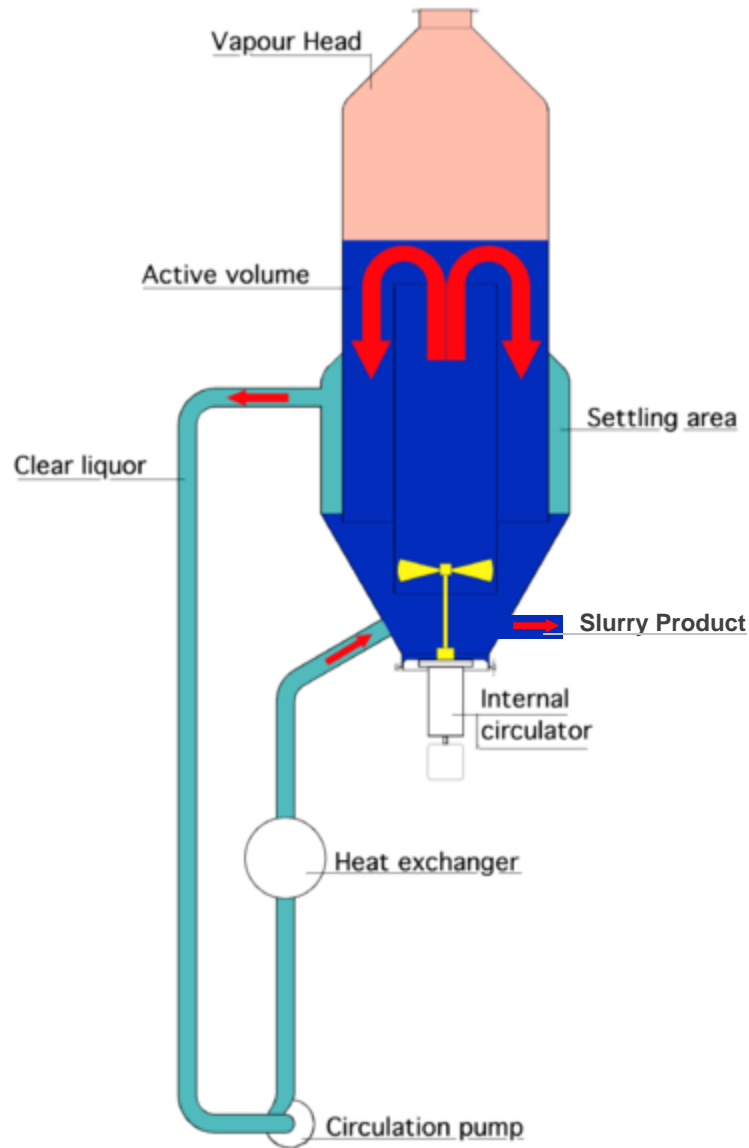
**Figure 3.** Picture of a draft-tube and baffle crystallizer.[124] The feed enters at the bottom of the draft tube. Supersaturation is generated by evaporation of solvent from the liquid surface just above the outlet of the draft tube.

The continuous crystallizations described above all deliver a slurry of crystalline particles entrained in solution as the product. The difference between the stirred tank and trough versus the Oslo-Krystal or the DTB crystallizer is that the stirred tank and trough deliver a wide size distribution of crystal particles while the latter two methods are designed to give tighter size distributions. But the cost of the tighter size distribution is the need for careful control of operating parameters to maintain fluidization of crystal particles in the crystallizer.

All of these crystallization operations can also be operated as cascades of individual crystallization operations to allow better control of the required heat transfer. Multiple stages allow the temperature gradient needed to achieve the desired yield to distributed over the tanks, such that smaller temperature differences can be used in each tank to minimize encrustation of the cooling elements and give overall better energy efficiency. The use of a multiple stage cascade to impact the crystal size distribution has also been explored but no significant benefit has been found.[125-127]

### 1.3.2   *Industrial Melt Crystallization Operations*

In melt crystallization, supersaturation is generated via temperature control. This temperature control, generally in the form of cooling, is introduced through cooled surfaces. Fouling of the cooling surfaces by crystal growth is a significant concern. This is more important than in solution crystallization because the amount of the feed that is crystallized is generally much higher in melt crystallization than in solution crystallization.[66] Also, the feed density can be much higher in melt crystallization which makes uniform stirring very difficult. The stirred tank operations used in solution crystallization are not useful for melt crystallization.

A sweat tank crystallizer is one of the simplest units for melt crystallization. A melt is charged to a tank and cooled through a jacket or internal elements. Initial crystal formation will occur on the cooling surfaces. Once the feed has totally solidified, steam will be introduced into the unit in order to re-melt the crystals. The steam will also serve to sweat out impurities trapped in the melt so that the final product will have higher purity than the initially formed solid. If the composition of the melt is continuously monitored, the product can be collected once the desired purity threshold has been reached.

Scraped surface crystallizers deal with cooling element encrustation by physical removal of the solid layer. The melt is passed through a tube with the cooling medium exposed to the outer wall of the tube, often in the annular region of a second pipe encasing the first. The crystallization occurs on the interior wall of the pipe but a scraping mechanism serves to remove crystals from the surface and allow new crystals to form. This scraping operation can lead to

very small crystals due to breakage but this type of operation has been used effectively for crystallization of fats and waxes.[128-130]

Various column crystallizers have also been used for melt crystallization.[131-133] The general principle as first developed by Arnold and then extended by Schildknecht[134] is to introduce a liquid feed to the middle of column. The liquid will then be pushed towards the top of the column while crystals that are formed will fall towards the bottom of the column. The movement of these crystals may be aided by a conveyor. At the bottom of the column is a heater that melts some of the crystals to provide a liquid flow that moves counter-currently to the solid particles in order to provide purification. There is also a chiller at the top of the column in order to promote crystallization. The overall operation of this type of system is very similar to a distillation column with a condenser, with the understanding that the product is removed from the bottom in the crystallization compared to the top for distillation.

The column crystallizer has been extended further by Brodie and the Tsukishima Kikai Company. Brodie[135] introduced a column crystallizer with a temperature gradient throughout the column. The column is broken into several segments with individual heat exchangers in order to impose a gradient. The presence of heat exchangers requires the use of a scraping operation to keep the heat transfer surfaces functioning. This scraping operation also serves to convey the crystals towards the outlet of the column. The Tsukishima Kikai process uses a series of cooling crystallizers instead of the column to impose a temperature gradient. Multiple stirred tanks can approximate the performance of a column while allowing for easier imposition of a temperature gradient.

The Sulzer MWB crystallizer[136] is a falling film crystallizer that can be staged sequentially in order to improve purifications. The ability to stage this operation allows for the separation of mixtures that form solid solutions. The melt to be separated is passed over a solid surface. Crystallization is induced by cooling of the surface. A falling film is used instead of a filled tube to improve the mixing properties of the melt in order to approach ideal impurity distribution coefficients. Periodically the melt added to the top of the crystallizer is heated before being passed over the surface of the growing crystal. This heated melt will dissolve a small amount of the crystal and sweat out some of the impurities present. After the desired amount of crystal is

grown, it is removed from the process by heating the surface on which crystallization occurred. This melts the crystal on the wall and allows the entire crystal mass to be removed from the crystallizer. This crystal mass can then be melted completely before being removed as the product or being fed to a subsequent step in order to increase purity.

An alternative to temperature control using cooled surfaces is to directly inject the cooling medium into the melt.[137-139] Either air or some liquid may be injected directly into the melt in order to induce crystallization without causing the walls to become covered in crystal. This approach is not widely used but does provide an interesting alternative to cooled surfaces. Complications can arise if the cooling medium is incorporated into the crystal either as an inclusion or directly in the crystal structure.[140] Any subsequent separations necessary to remove the cooling medium from the crystal would have to be considered before implementing this type of operation.

## 1.4 Summary of Crystallization and Industrial Unit Operations

The basic processes of crystallization are nucleation and growth and models for these two processes from the literature have been discussed. It is evident that nucleation is a more difficult phenomenon to predict and control and often times it is avoided in practical crystallizations by the addition of seed crystals. The various methods for impurity incorporation during crystallization were also discussed. The formation of solid solutions is a common method for impurity incorporation and the separation of solid solutions requires multiple crystallization operations. Solid solutions may have inhomogeneous distributions of impurity but no previous study of this phenomenon for solution crystallization was found. Impurity distribution in solid solution formation from the melt has been studied previously.

The major types of industrial crystallization operations have also been presented for both solution and melt crystallization. The counter-current column crystallization used in melt crystallization is attractive for separation of a solid-solution because multiple recrystallizations are carried out in a single operation.

Industrial crystallizations from solution generally have multiphase mixtures during the crystallization and as the product. Crystal particles are distributed throughout the solvent in a

43

slurry.  This approach has the advantage of allowing control of the crystal size distribution and of easier control of heat transfer during crystallization.  But the slurry nature of these processes can lead to processing difficulties.

A process that did not involve multiphase flow would be advantageous from an operational perspective.  One way to avoid multiphase flows would be to constrain growth to occur on fixed surfaces so that the amount of solid particles in the bulk is minimized.  This type of process would also not have to worry about encrustation of heat transfer elements because this behavior would be built into the design of the system.  The crystal size distribution would also be unimportant because a polycrystalline mass would be developed and this mass could be dissolved in order to deliver the product as a liquid stream.

A greater focus on the impurity distribution during crystallization would be necessary than in suspension crystallizations.  The large number of crystals formed and the vigorous stirring allow use of average concentrations in suspension operations but growth on solid surfaces would require the impurity concentration over the course of the crystallization to be accounted for.  This is in much the same way as the impurity profiles are studied for melt crystallizations.

The solid surfaces could also be used to avoid the need for nucleation.  An initial layer of crystals could be generated on the solid surface so that the complicated kinetics of nucleation could be neglected when designing the process.

A process based on these basic principles will be discussed in the next chapter.  A model will also be introduced that can predict impurity concentration profiles in the solid phase.

# 2.  Counter-Current Crystallization Process

Crystallization unit operations are very important in industrial purifications.  Traditional crystallizations have been performed in a batch manner and although continuous crystallization operations have been developed, the required multi-phase flow handling can lead to complications.  High purity products from crystallization can require multiple recrystallization operations.  A crystallization operation that worked in a continuous or semi-continuous manner while providing multiple recrystallizations to enhance product purity would be advantageous for industrial separations.

A new process is proposed here that utilizes crystallization in a counter current, semi-continuous manner.  Staging crystallizations in a counter current manner is done in order to facilitate multiple crystallizations which are expected to lead to a higher purity product.  The proposed process will also attempt to avoid solids handling operations such as filtering and drying by confining crystal growth to defined growth surfaces and dissolving the crystalline product in order to remove it as a liquid.  Solids handling is often the source of complications and malfunctions[141-143] during operation and eliminating solid phase handling operations should increase process reliability.  The proposed process is semi-continuous but could be operated as part of a continuous process if two were operated in parallel.

Processes similar to the one proposed here have been studied in the past.  A semi-continuous counter-current crystallization operation has been performed using a series of connected tanks.  A diagram of this taken from an article in *Simulation* is shown in Figure 4.  This process works by first charging a discrete amount of liquid to the left side of the cascade and allowing that liquid to overflow and fill the rest of the tanks with the overflow from the last tank taken as the product.  All valves are then closed and the tanks are cooled so that batch crystallization occurs in all tanks.  After crystallization is completed, a wash liquid is introduced at the right end of the cascade which overflows in the opposite direction and the amount that overflows from tank one is removed as the waste.  This process removes the mother liquor preferentially to the crystals which have settled to the bottoms of the tanks.  After the waste is removed, the tanks are heated in order to dissolve the crystals before adding more of the feed.[144, 145]
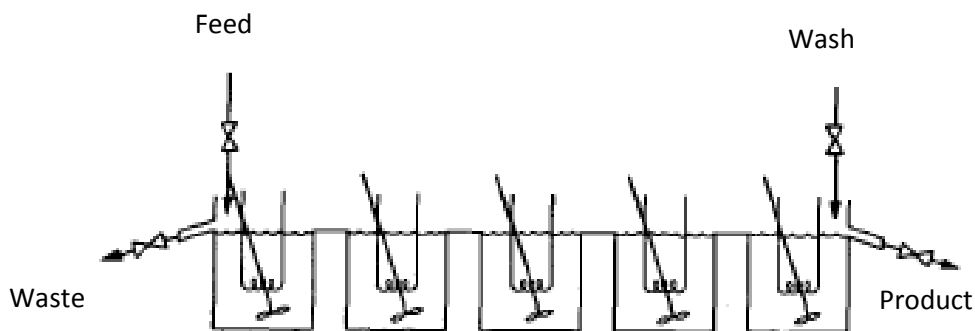
**Figure 4.  Diagram of continuous crystallization process developed by Godfrey.**[145]

Another previous process developed by the Upjohn Corporation achieves counter current operation by performing a batch crystallization, removing the resulting crystals and introducing them to the previous tank and moving the solution to the next tank in the series.  The crystals moved to the previous tank in the cascade act as the seed crystals for that crystallization.  This process employs a cascade of tanks divided into an enriching and a stripping section.  A diagram of this process from an article in *Industrial and Engineering Chemistry* is shown in Figure 5.  This process provides counter current action and the ability to perform multiple recrystallizations in order to improve purity but requires handling of multiphase flows and significant material handling.[146, 147]

The proposed process will differ from previous solution crystallization processes by constraining crystallization to a solid surface and by accounting for the kinetics of impurity incorporation.  Previous processes were studied in terms of equilibrium crystallization only and so any possible advantages available from kinetic considerations were ignored.  The physical equipment necessary for this process will be simple although the operation will require more sophisticated planning and execution than single-pass continuous crystallizations.
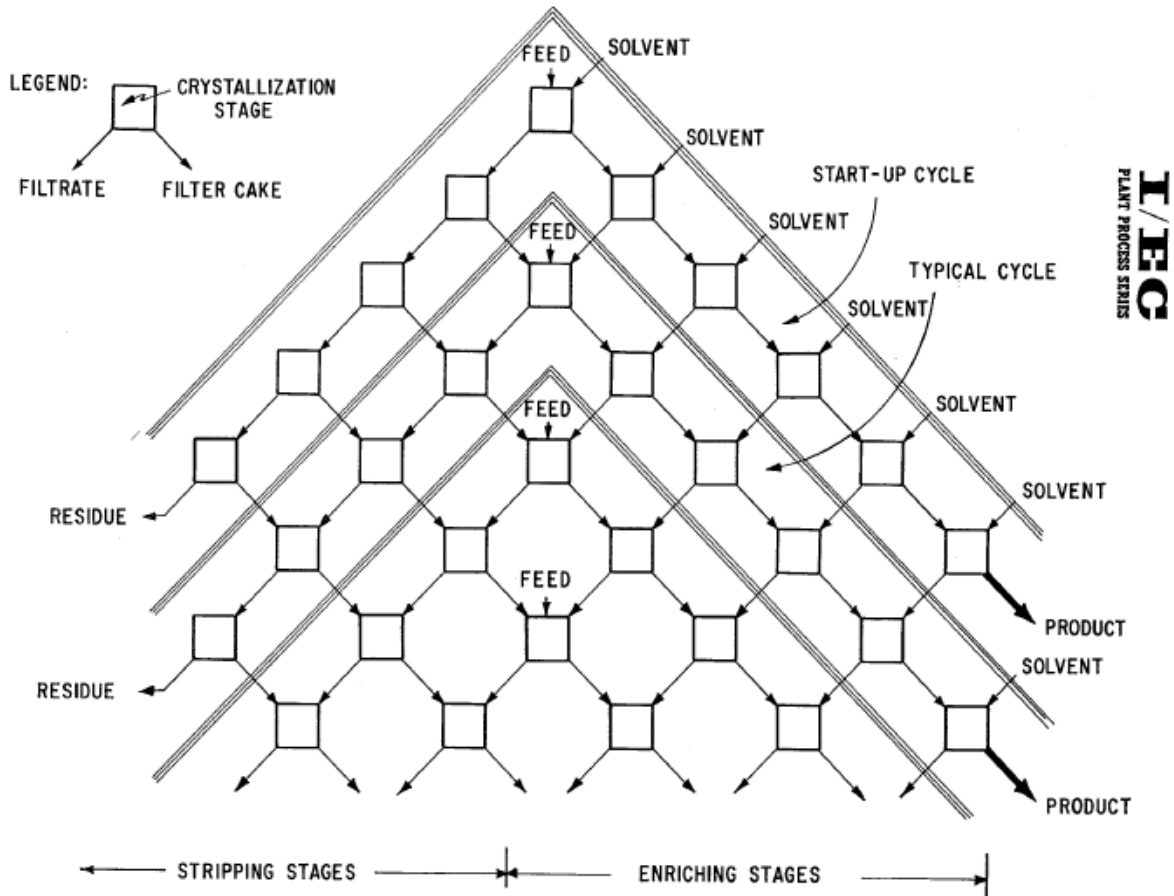
**Figure 5.** Schematic of the Upjohn process for counter-current crystallization.[147]

First the process will be described and explained. Then a model for batch crystallization will be outlined before being adapted to the process. Analysis of these models and results from model simulations will conclude this chapter.

## 2.1 Process Overview

The proposed counter-current crystallization (CCC) process consists of a series of vessels in which crystallization occurs on defined surfaces semi-continuously. A schematic of the process is shown in Figure 6 for a cascade with an arbitrary number of vessels N and a feed stream entering at tank F which is between tanks 1 and N.
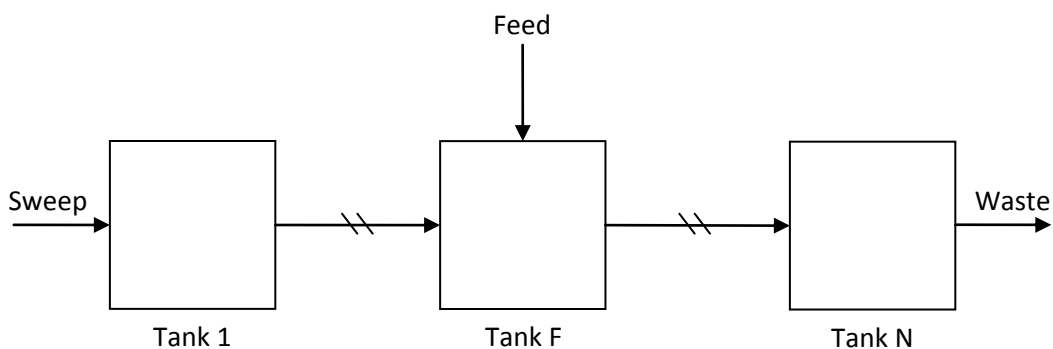
**Figure 6. Schematic of a multi-stage counter-current crystallization process with feed entering at an intermediate tank and waste being removed from tank N. The sweep stream entering at tank one may be omitted.**

Figure 6 shows the feed entering at stage F which is between the first and last stages, a sweep stream at the first stage and a waste stream leaving from the last stage (stage N). The feed stream could be added at any tank including the first or last tank and the sweep stream can be omitted entirely. If a sweep stream is not used the feed will be introduced at stage 1. As will be seen below, the product is removed from the first tank. The intent of the sweep stream is to sweep impurity out of tank one and increase the overall product purity and it could be either a pure solvent stream or some type of recycle stream.

Crystal growth will be designed to occur on fixed surfaces in each tank. These surfaces will act as seeds for crystallization so that nucleation is not necessary. To this end, the surfaces can be functionalized or otherwise treated in order to strongly promote crystal growth; they can be physically coated with seed crystal through rapid sudden cooling of a highly supersaturated solution; or they can be coated by evaporation after dipping the surface in a supersaturated solution. A designed surface is the preferred method but a method for developing such a surface for an arbitrary compound is not currently available. Seeding via evaporative coating has been demonstrated and is currently accessible for use with this process.

Supersaturation will be generated in this process by cooling. Other methods to generate supersaturation such as anti-solvent addition and solvent evaporation could potentially be used but this description will assume that cooling is used. The cooling can occur in two ways. The first is to operate each tank isothermally. The feed will enter at a higher temperature than the tank so that upon cooling to the tank temperature the solution will be supersaturated. Me-

thods for implementing this temperature control are jacketing of the vessels or insertion of a cooling coil into the vessel.

In this type of operation the heat transfer equipment should be designed to maintain the bulk liquid in each tank at nearly the same temperature as the crystallization surface. This will require strong mixing and sufficient heat removal or generation from the temperature control device to maintain the liquid volume of each tank at the desired temperature. The bulk temperature must be controlled tightly so that the supersaturation generated throughout each tank is small and homogeneous nucleation is minimized. The relationship between bulk temperature and supersaturation is given by the solubility as a function of temperature data for the component of interest.

If a uniform temperature throughout the tank is not achieved in practice the slight temperature gradient that is developed will depend on the relationship between the ambient temperature and the desired temperature of the tank. If the desired temperature is greater than the ambient temperature the temperature gradient will result in a lower temperature of the liquid compared to the temperature at the surface of the jacket or cooling coil. And if the ambient temperature is greater than the desired temperature, the temperature of the liquid will be greater than the temperature at the surface of the jacket or cooling coil. The magnitude of this temperature gradient is determined by the stirring rate, system geometry, system materials of construction and the ambient and desired temperature values.

If the bulk temperature in a tank is controlled at a value less than the ambient temperature then the temperature gradient will likely result in temperature control surfaces coated with crystal. This will hamper further temperature control and should be avoided. Alternatively, the bulk temperature can be held somewhat above the ambient temperature. This situation requires the feed to be much hotter than the ambient temperature so that upon cooling to the vessel temperature the supersaturation of the solution is increased. The high temperature required to avoid encrustation of the cooling surfaces by this approach would result in lower yields since the saturation concentration of most species decreases with temperature.

The second method of generating supersaturation is to cool the desired surfaces for crystallization relative to the bulk liquid. This method is a natural extension of using cooling

coils in the tank volume because it combines the necessary cooling element with the designated surface for crystallization. In this situation, the bulk temperature in each tank will be higher than the temperature at the crystallization surface. The benefits of this approach are that crystallization in the bulk will be decreased due to decreased homogeneous nucleation and any secondary crystals formed could dissolve in solution. This method eliminates the problem of fouling of the cooling surfaces because growth on the cooling surfaces is now the desired outcome. The cooling surface can now be held at the lowest possible temperatures in order to maximize the amount of crystallization without any operational complications.

The temperature in each stage is controlled separately such that different tanks may have different temperatures. In the case where the growth surfaces are cooled, each tank could have two controllable temperatures, one corresponding to the bulk liquid (controlled by an external jacket) and the other at the surface of the crystal growth surface (controlled by internal coolant flow).

### 2.1.1 Process Description

In the following description of the operation of this process, A refers to the component of interest, B refers to an impurity and the cascade will consist of three stages with feed at stage two and a sweep stream at stage one. This description can be generalized to any number of stages with or without a sweep stream. Even though three tanks are used during the growth phase, a fourth tank will be used to facilitate liquid handling and product removal. In general, for an N stage growth cascade, the process will require N+1 total tanks.

The operation consists of two phases: a growth phase and a product removal phase. During the growth operation crystal will grow on the designated surface in each tank while the feed and sweep streams are added continuously to the cascade. In the product removal phase, a liquid transfer operation will occur that mixes the crystals in one tank with the liquid from the tank immediately upstream of that tank. The crystals in every tank are then dissolved by heating and the contents of the first tank are removed as the product. The redissolution occurs so that the so the product can be removed in the liquid phase and the component of interest can be recrystallized in order to improve the purity of the product.
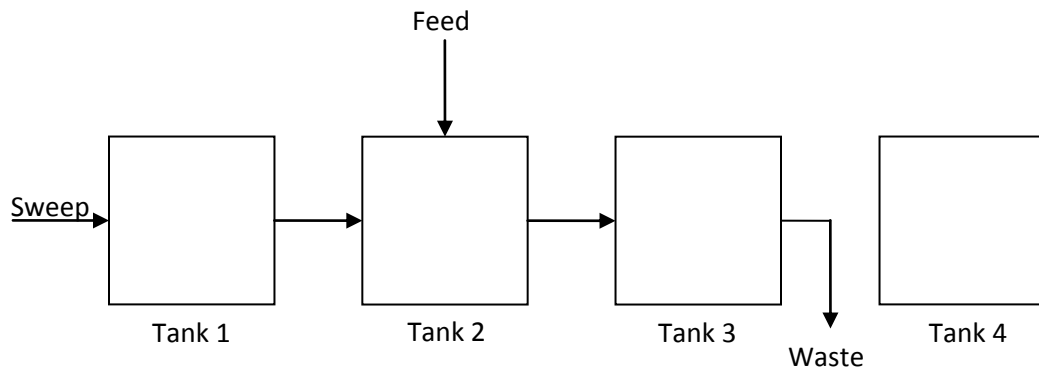
**Figure 7. Schematic of the equipment to be used in a counter-current crystallization process with three active tanks and four total tanks.**

A schematic of the tanks during the growth phase is shown in Figure 8. The relative sizes of the letters A and B give a qualitative idea of the amount of that species present. The crystal is represented by the grey rectangle at the bottom of each tank and the size qualitatively represents the amount of crystal.
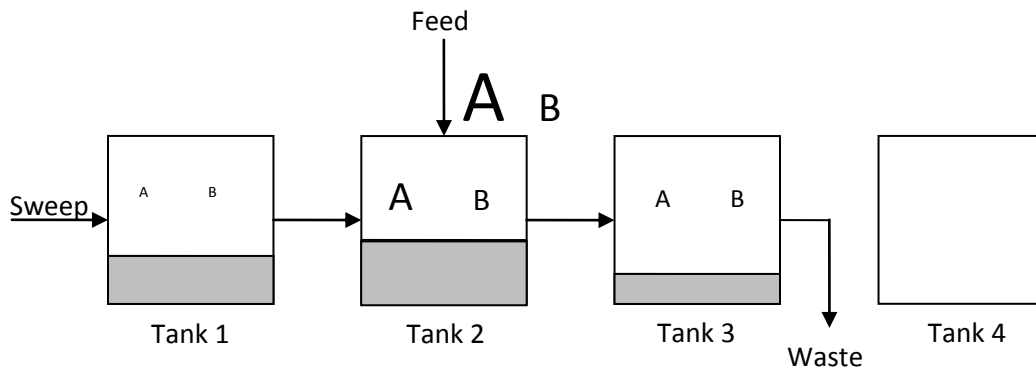


**Figure 8. Schematic of processing vessels during growth operation showing relative amounts of impurity and component of interest.**

The growth operation is run until a predetermined end point is reached. This endpoint could be based on time or it could be based on an amount of crystal grown in a particular tank. If this process is run for too long with fast growing crystals and a very concentrated solution there is the potential to fill the tank with crystal which would cause the process to fail by pre-

venting further fluid flow. The end point for the growth phase could also be constrained by other processing operations up or downstream from this unit operation.

After this stop condition has been met, the flow to the cascade is stopped. The liquid tank contents are then transferred in the following manner while the crystal remains in its original tank. The liquid contents of the third tank are moved into a fourth tank that was unused during the growth phase. The liquid contents of the second tank are then transferred into the third tank. Then the contents of the first tank are emptied into the second tank.

Note that there can be a complication with this transfer operation. The liquid from tanks 1, 2 and 3 is being added to tanks 2, 3 and 4 respectively with tanks 2 and 3 still containing crystals. If the liquid volume of tank 1 or 2 plus the crystal volume of tank 2 or 3 respectively is greater than the total volume of the vessel then there would be overflow. This can be avoided as follows. Liquid is transferred from tank 1, 2 or 3 to tank 2, 3, or 4 until all the liquid is transferred or until tank 2, 3 or 4 is full. If there is still liquid in tank 1 after this process is applied to the entire cascade, that liquid is transferred to tank 4 along with the liquid from tank 3. All four tanks will be full or less than full following this procedure.

At this point tank 1 contains only crystal while tanks 2 and 3 contain crystal and solution. Pure solvent is added to tank one and the contents of all tanks are heated in order to dissolve the crystal. The amount of solvent needed in tank 1 is determined by the solubility of the product and the concentration requirements for subsequent processing operations. Once fully dissolved, the contents of tank one are removed as the product. The result of this operation is that tanks 2, 3 and 4 are full of liquid at varying concentrations of species A and B while tank 1 is empty. Tank 1 becomes the unused tank during the next growth operation.
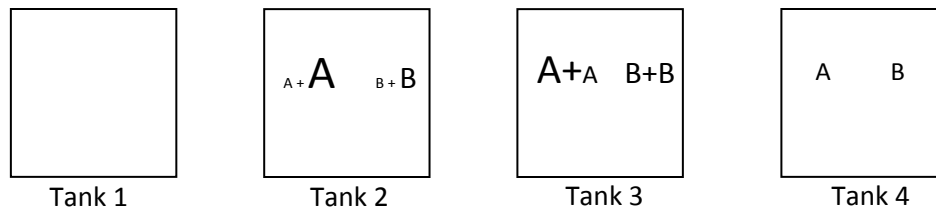
**Figure 9. Schematic showing the contents of the tanks in the cascade after removal of product and dissolution of crystal. The two sets of letters in tanks 3 and 4 indicate the contribution from the dissolved crystal and the liquid phase.**

The next step is to nucleate the system so that growth can be resumed. This nucleation is achieved by one of the methods listed earlier.
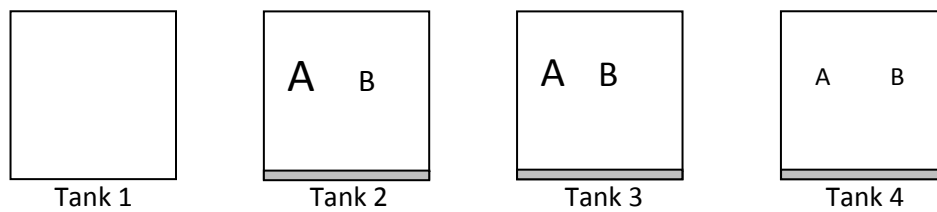


**Figure 10. Contents of tanks in CCC process after nucleation has occurred.**

Once this nucleation has occurred, the location of the feed stream, sweep stream and waste stream are moved one tank down the cascade and the process is repeated.
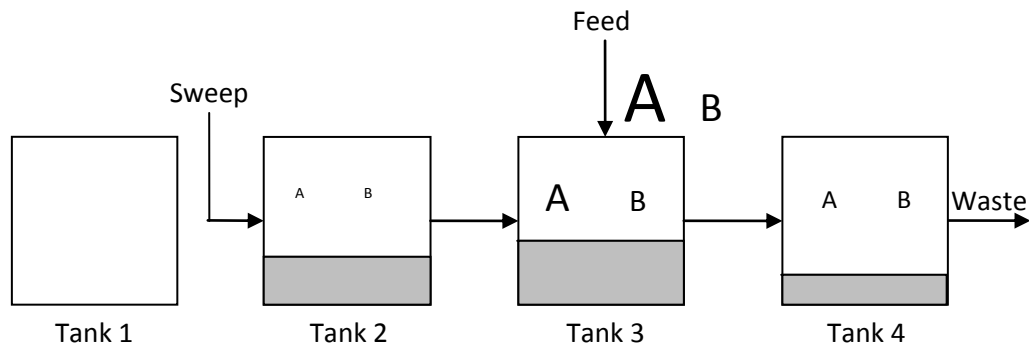


**Figure 11. Schematic of cascade during the growth operation after the input and output streams have been shifted.**

It was earlier mentioned that there is the possibility for overflow when transferring the liquid contents after the growth operation. There is also the possibility that tanks will be under-filled after this transfer operation. If a tank is not full at the beginning of the next growth operation, the outflow from that tank remains zero until the tank is full, at which point outflow is resumed.

### 2.1.2 Alternative Processing Method

The process described above utilized an extra tank for the liquid transfer operation. An alternative method of operation is to discard the entire liquid contents of the last tank as waste. The liquid transfer operation as described could then be completed without the need for an extra tank. The tank from which the product was removed in one cycle becomes the tank from which the effluent leaves in the next cycle. An overview schematic of this mode of operation is given in Figure 12.

This implementation of the process without the use of an extra tank is simpler because it requires less equipment and less liquid transfers. The performance for implementation of this process with and without an extra tank will be discussed in section 2.4.6.
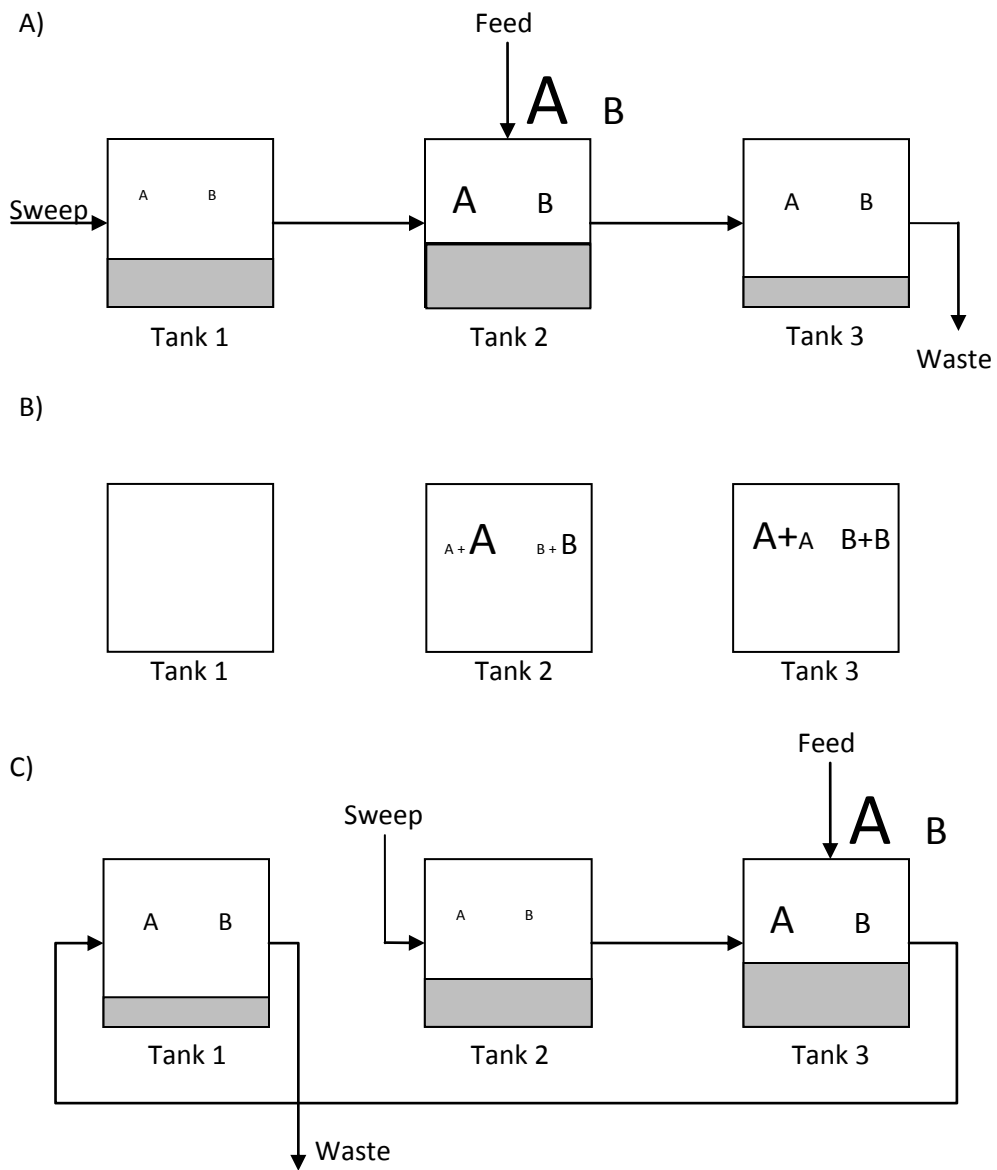
**Figure 12. Schematic of process operation when liquid contents of last tank in cascade are discarded. A) Contents of each tank at the end of one growth cycle. B) Contents of each tank after the liquid transfer operation. Product has been removed and liquid initially in tank 3 has been discarded. C) Conditions at end of next growth cycle after inlet and outlet points have been moved.**

### 2.1.3 *Operational Similarity to Simulated Moving Bed Chromatography*

Although this process seems quite complicated to operate it shares many operational similarities to simulated moving bed chromatography[148]. A simulated moving bed is a practical approximation to a true moving bed process where a separation occurs between a liquid and a solid phase and both phases move counter-currently to each other. Moving a solid phase is not a desirable operation and so the simulated moving bed can be used. The proposed crystallization operation is not an approximation to an ideal separation process design as a simulated moving bed is but it is desirable because it provides multiple recrystallizations which give increased purity.

In a simulated moving bed, feed is added continuously to a multi-stage cascade. The stages are filled with a solid, stationary phase that interacts with the component of interest or the impurity. The species that interacts with the stationary phase will move more slowly through the cascade than the other species, leading to separation. To simulate counter-current operation, the feed and product removal points are periodically shifted in the direction of liquid flow.

This movement of the flow entry and exit points results in the "movement" of the solid phase in the opposite direction of the fluid flow. An equivalent process would be to leave the fluid entry and exit points in place but to move the solid phase one tank in the direction opposite of the fluid flow. This is more difficult than moving the fluid entry and exit points in practice but it may be simpler to envision the counter-current nature of the process with this description. A schematic of a simulated moving bed chromatography unit is shown in Figure 13.
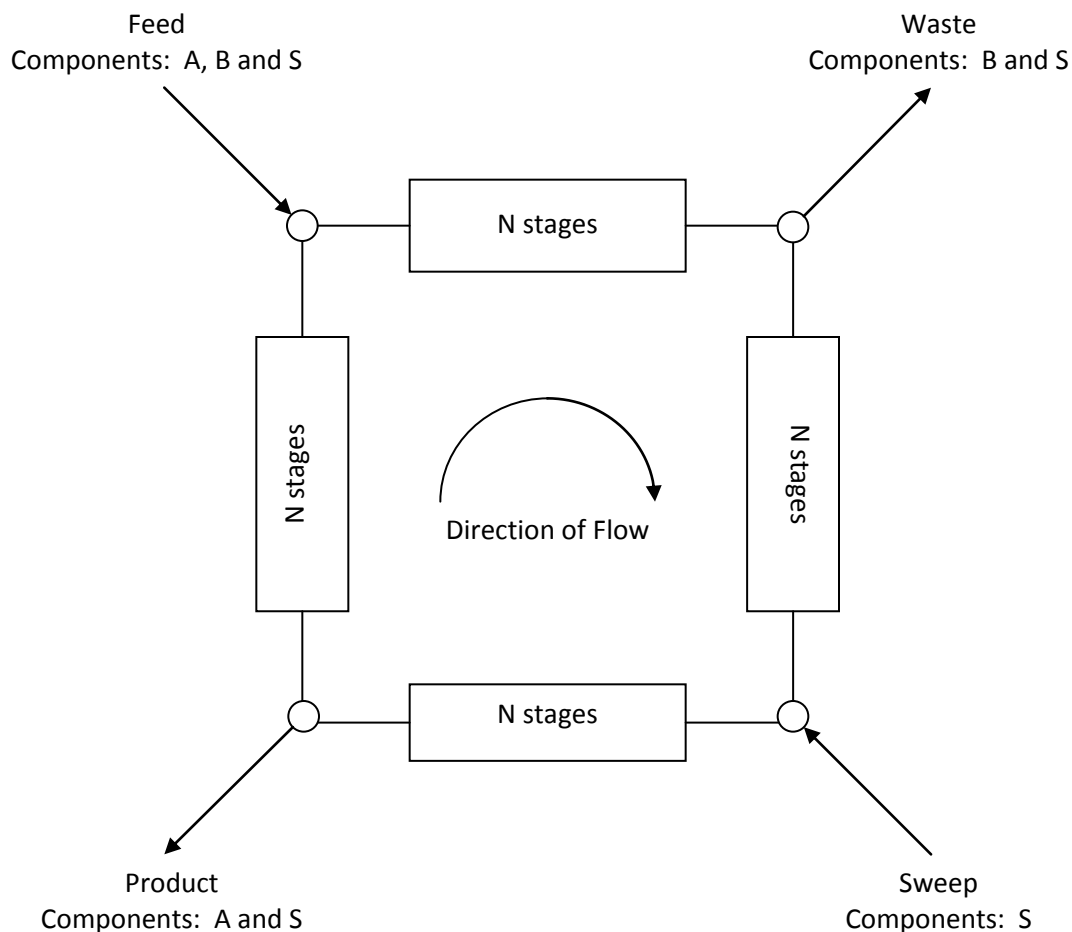
**Figure 13. Schematic of a simulated moving bed chromatography device. A represents the component of interest, B is the impurity and S is the solvent. The block between each inlet/outlet point represents N stages for a 4N stage cascade in total.**

The proposed crystallization process is fundamentally different than simulated moving bed chromatography due to crystallization as the mechanism for separation and the redissolution of the crystal which allows for multiple recrystallizations but it does share similar operating principles. The proposed crystallization process can be viewed as the liquid phase moving in one direction while the crystal moves in the other direction which is similar to the overall result of the SMB process. The feed and withdrawal points also shift along the length of the cascade during the course of a cyclical operation and the equipment must be designed to allow for this to occur. Both the simulated moving bed and the proposed crystallization process will require significant equipment and control infrastructure in order to carry out the complicated process.

The proposed crystallization process will require some additional equipment that has no analog in the SMB process.  The ability to pump liquid between stages is required in order to enact the liquid transfer operation which is used to facilitate the recrystallization operations that increase product purity.  Heat transfer equipment to control the temperature of the bulk liquid in each tank and possibly the temperature at the crystallization surface must also be present.  These are standard, readily available unit operations but the added costs of their construction and operation will need to be considered.

While the simulated moving bed differs significantly from the proposed crystallization operation because of a different underlying mechanism of separation and the use of batch-like recrystallization operations, both have similar operational requirements.  The complicated nature of the proposed crystallization operation should not immediately disqualify it from consideration although it must be considered when designing separations for a specific application.

### 2.1.4   Process Discussion

The proposed process has similarities to both a batch crystallization operation and continuous flow crystallization.  The multiple recrystallizations that occur due to the dissolution and liquid transfer operations are similar to batch recrystallizations while each individual growth cycle operates as a continuous crystallizer.  The benefits of this process are multiple crystallizations of the component of interest, semi-continuous operation and avoidance of multi-phase flows.  Multiple crystallizations serve to increase the purity of the product while semi-continuous operation is important for implementation in an overall continuous process and eliminating multi-phase flows can enhance reliability of the process.  The use of a semi-continuous flow process is important because this process could be implemented in a completely continuous process if two of these counter-current crystallization operations are run in parallel.  Continuous operation should then be possible with the feed continuously flowing to one of the two setups.

Multiple recrystallizations are possible due to the use of multiple stages and redissolution of the crystals after every growth operation.  This also allows for smaller supersaturations to be used in each tank.  Supersaturation results from temperature gradients between the bulk

liquid and the crystal surface and smaller supersaturations also mean smaller temperature differences. This arrangement allows for more economical heat management in addition to the main benefit of multiple recrystallizations. If crystallization occurs such that higher purity solutions give higher purity crystals then limiting the supersaturation in the first tank will also result in higher purity product which is the desired outcome. The multiple tanks allow for the yield to be maintained while getting high crystal purity from a smaller amount of crystallization in the first tank.

The yield can approach the maximum value through careful selection of the number of stages and other operating parameters. The yield is limited by how much of species A leaves the system in the waste stream which is determined by the concentration of A in the final stage and the flow rate of the waste stream. The concentration in the final stage is limited by the solubility of species A in this stage. This solubility usually decreases with temperature so that the practical limitation is the lowest feasible operating temperature.

The performance of the proposed process is compared to batch crystallization run to completion. Batch crystallization is a good comparison because it represents a very common method of purification and a batch operation run until completion will result in a liquid phase concentration equal to the equilibrium concentration of species A at the employed temperature which will give the maximum yield. If this complicated process cannot approach the maximum yield while providing higher purity than the batch operation then it will not be worthwhile. A model is first developed for batch crystallization before it is extended to the semi-continuous process because the batch model is simpler but is readily transferrable to the continuous process.

In order to maximize yield from the semi-continuous process the concentration in the final stage and flow rate out of the final stage could be minimized. While the solubility of species A may be changed only by changing the temperature, the flow rate of the waste stream could be lowered in two ways. If some solvent is evaporated between stages after the feed stage, this will concentrate the stream entering the following stage and decrease the amount of effluent from that stage. The concentrated stream will have a larger supersaturation driving force and will deposit more crystal than the original stream.

The other option is to recycle some of the waste stream. But in order to recycle, some of the solvent must first be evaporated. The waste stream is at the lowest possible concentration of species A (as dictated by the solubility of A) and so adding it directly into the feed stream will only dilute the feed and lead to worse performance. By evaporating some of the solvent, the waste stream is concentrated and can be mixed with the feed stream for a possible improvement in performance. But the recycling of the waste stream will result in a less pure feed material that could diminish the overall purity. A good starting point for the amount of solvent to be evaporated is to match the concentration of species A in the feed and recycle streams. Either method of decreasing the flow rate requires solvent evaporation which would require a significant input of energy.

Although the process has been described with the solid crystal being removed as the product it is possible that a specific chemical system will tend to crystallize the impurity preferentially to the component of interest. In this situation, the "waste" stream may be enriched in the component of interest and could be removed as the product. This would be a desirable situation because the product would already be in liquid form and ready for the next processing operation but this situation is not expected to be common.


## 2.2    Batch Modeling

The initial system to be modeled is a batch reactor with three components: the component of interest (A), the impurity (B) and the solvent (S). A schematic of the system showing the important variables is included in Figure 14.

The variables in Figure 14 are defined as follows: $m_A$, $m_B$ and $m_S$ are the masses (kg) of species A, B and solvent in the liquid phase respectively; $m_{Ac}$ and $m_{Bc}$ are the masses (kg) of each component in the crystal phase; $V_l$, and $V_c$ are the liquid and crystal phase volumes respectively (m$^3$); $C_A^*$ and $C_B^*$ are the equilibrium liquid phase concentrations; and $C_{Ac}^S$ and $C_{Bc}^S$ are the surface concentrations of A and B in the solid phases. The total volume of the reactor is $V_R$. Note that we can define concentrations in the liquid and crystal phases as $m_j/V_j$.
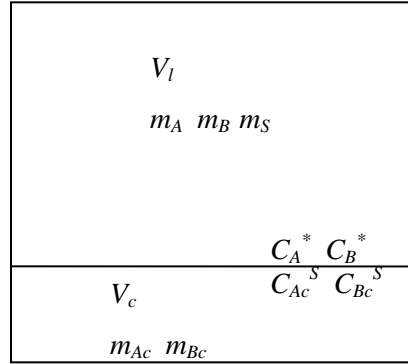
**Figure 14. Drawing of a batch crystallization tank along with all possible variables for use in deriving equation system for batch crystallization model.**

This system has 11 unknowns ($m_A$, $m_B$, $m_s$, $m_{Ac}$, $m_{bc}$, $V_l$, $V_c$, $C_A^*$, $C_B^*$, $C_{Ac}^s$ and $C_{Bc}^s$) Equations (2.1) through (2.5) are mass balances for the batch system.

$$\frac{d(m_A)}{dt} = -ka\left(C_A - C_A^*\right)^n$$

(2.1)

$$\frac{d(m_b)}{dt} = -k_b a\left(C_b - C_b^*\right)^n$$

(2.2)

$$\frac{d(m_s)}{dt} = 0$$

(2.3)

$$\frac{d(m_{Ac})}{dt} = -\frac{d(m_A)}{dt}$$

(2.4)

$$\frac{d(m_{bc})}{dt} = -\frac{d(m_b)}{dt}$$

(2.5)

The new variables in the above equations are $a$, $k_i$ and $n$ which are the surface area for crystal growth, the kinetic incorporation rate constant of species $i$ into the crystal and the exponential dependence of crystal growth on the supersaturation. These quantities are introduced through the crystal growth mechanism and only $a$ is potentially a controllable parameter. Values for the parameters $k_i$ and $n$ must be measured experimentally because they are chemi-

cal system specific. Nucleation is assumed to be present before operation begins and any further nucleation is assumed to be negligible so that it is not included in the model.

For the general case, the surface area for growth will change as crystallization occurs. This can be accounted for in the model by introducing an expression that relates the area for growth to the total amount of crystal in a given tank. This is straightforward for simple geometric shapes such as cylinders and plates and the model can then be solved numerically. If growth occurs on flat plates in one dimension the area for growth is constant. Assuming that the area for growth is constant would also be for growth on cylinders or spheres where the thickness of the crystal layer is much less than the radius of the cylinder of sphere.

The crystal growth expressions combine the two parts of crystal growth; diffusion to the surface and surface integration. Either part of the process could be the rate limiting step. If diffusion to the surface is the limiting step then the parameter $n$ would be equal to one. If surface integration is the limiting factor, or if both processes are important, then $n$ is generally found to have a value between one and two.[37] The specific value is dependent on the chemical system in use. The parameters $k_A$ and $k_B$ will be referred to as incorporation rate constants and will represent a combination of the two steps and no assumption will be made at this point about which process is rate limiting.

The value of $C_A{}^*$ will be given by the saturation concentration of A which is only a function of temperature.

$$C_A^* = f(T)$$

(2.6)

The saturation concentration as a function of temperature is assumed to be known and is input into the model. The temperature in use will also be known so that the value of $C_A{}^*$ is known. The presence of the impurity species will in reality have an effect on the value of $C_A{}^*$ but the ratio of $C_A/C_B$ will be greater than one and this effect will be assumed small.

The equilibrium at the surface between the liquid and solid phases is assumed to obey the equilibrium expression

$$K = \frac{C_A^*}{C_B^*} \frac{C_{Bc}^s}{C_{Ac}^s} \qquad\qquad (2.7)$$

This relationship is similar in form to the separation factor used to measure impurity distribution in separation of solid solutions by crystallization[‡] but instead of relating bulk phase concentrations, Equation (2.7) compares equilibrium liquid concentrations to surface solid concentrations.

The parameter $K$ relates changes in equilibrium liquid phase concentrations to changes in surface solid concentrations which is important for modeling impurity incorporation into the solid. This parameter will be assumed to only depend on temperature. Because $C_A^*$ is known as a function of temperature, $K$ can be used to find the value of the previously unknown parameter $C_B^*$. Requiring that $K$ be constant is a key assumption of this model.

If a batch experiment were allowed to run for a long time so that complete equilibration of the solid and liquid occurred, then the value of $K$ could be measured from the bulk properties of the liquid and solid. Even in this situation, the surface concentration of the solid should be used for calculating the value of $K$ instead of the average solid concentration. If the crystal particle size was kept very small during growth and enough time was allowed for solid diffusion to smooth out any impurity distribution in the solid then the average concentration of the crystals could be used for calculation of $K$. The average concentration is easier to measure but experimentally obtaining crystals that are in equilibrium is expected to be difficult and so the surface concentration is a better choice for determination of $K$.

The ratio of differential crystal growth of species A to species B will be equal to the ratio of the crystal surface concentration at that time, i.e.

$$\frac{d\left(m_{Ac}\right)\big/dt}{d\left(m_{Bc}\right)\big/dt} = \frac{C_{Ac}^s}{C_{Bc}^s} \qquad\qquad (2.8)$$

---

[‡] See section 1.2.2 and equation (1.21).

63

This equation relates the unknown surface concentrations of the solid to the known growth rates of the crystal.

The last three equations describe the volumes in the liquid and solid phases.

$$m_A \overline{V_A} + m_B \overline{V_B} + m_s \overline{V_s} = V_l \qquad (2.9)$$

$$\frac{m_{Ac} + m_{Bc}}{V_c} = \rho_c \qquad (2.10)$$

$$C^s_{Ac} + C^s_{Bc} = \rho_c \qquad (2.11)$$

where $\overline{V_i}$ is the partial mass volume of species $i$ and $\rho_c$ is the density of the crystal.

Equation (2.9) may be simplified for certain systems that form ideal solutions or are dilute. If equation cannot be simplified then the partial mass volumes must be known as functions of the composition of the system and temperature. An appropriate activity coefficient model can be used to find the expressions for partial mass volume.

Equations (2.10) and (2.11) are derived by assuming constant density of the crystal phase. The constant density of the solid is a good assumption because when dealing with systems forming solid solutions the A and B species will be very similar chemically. Equation (2.11) is a special case of equation (2.10) indicating that the surface layer will have the same density as the bulk of the crystal. This is important because of the use of surface concentration in the definition of the surface equilibrium constant $K$.

Assumptions made in developing this model include that the solvent is absent from the crystal (no inclusions or solid solutions with the component of interest or the impurity) and the surface equilibrium constant is only a function of temperature. At the beginning of operation the reactor is full of liquid and a small coating of crystal on a solid surface that will act as a seed for crystal growth.

### 2.2.1 Non-Dimensionalization

This system is put into dimensionless form with the following variables.

$$m_i = \frac{m_i}{C_i^0 V_R} \tag{2.12}$$

$$\tau_2 = \frac{t k_A a \left(C_A^0\right)^{n-1}}{V_R} \tag{2.13}$$

$$\upsilon = \frac{V_l}{V_R} \tag{2.14}$$

$$\lambda_i = C_i^0 \overline{V_i} \tag{2.15}$$

$$\gamma = \frac{k_B}{k_A} \left(\frac{C_B^0}{C_A^0}\right)^{n-1} \tag{2.16}$$

$$\theta_i = \frac{C_i}{C_i^0} = \frac{m_i}{C_i^0 V_l} = \frac{m_i}{\upsilon} \tag{2.17}$$

$$\theta_i^* = \frac{C_i^*}{C_i^0} \tag{2.18}$$

$$\eta = \frac{C_b^0}{C_A^0} \tag{2.19}$$

where $C_i^0$ is the initial concentration in the liquid phase of species $i$. Note that $\theta_A^*$ is equal to the inverse of the supersaturation ratio as defined in the background section[§] and that the incorporation rate constant of species A provides the scale for time. The dimensionless total length of the batch operation will be denoted by $\tau_{2f}$, using the same definition as in equation (2.13) with $t$ set equal to $t_f$ which is the total time for batch crystallization.

Substituting these variables into equations (2.1)-(2.11) gives the dimensionless equation system.

---

[§] $S = C_A^0 / C_A^*$

$$\frac{d\left(m_A\right)}{d\tau_2} = -\left(\theta_A - \theta_A^*\right)^n \tag{2.20}$$

$$\frac{d\left(m_B\right)}{d\tau_2} = -\gamma\left(\theta_B - \theta_B^*\right)^n \tag{2.21}$$

$$\frac{d\left(m_s\right)}{d\tau_2} = 0 \tag{2.22}$$

$$\frac{d\left(m_{Ac}\right)}{d\tau_2} = -\frac{d\left(m_A\right)}{d\tau_2} \tag{2.23}$$

$$\frac{d\left(m_{Bc}\right)}{d\tau_2} = -\frac{d\left(m_B\right)}{d\tau_2} \tag{2.24}$$

$$\theta_A^* = f\left(T\right) \tag{2.25}$$

$$K = \frac{\theta_A^* \; \theta_{Bc}^s}{\theta_B^* \; \theta_{Ac}^s} \tag{2.26}$$

$$\frac{d\left(m_{Ac}\right)\Big/ d\tau_2}{d\left(m_{Bc}\right)\Big/ d\tau_2} = \frac{\theta_{Ac}^s}{\theta_{Bc}^s} \tag{2.27}$$

$$m_A\lambda_A + m_B\lambda_B + m_s\lambda_s = \upsilon \tag{2.28}$$

$$m_{Ac} + m_{Bc}\eta = \rho_c \upsilon_c \tag{2.29}$$

$$\theta_{Ac}^s + \theta_{Bc}^s \eta = \rho_c \tag{2.30}$$

### 2.2.2  Batch Model Analysis

It will also be assumed for the following analysis that the liquid volume is constant (dilute system), the temperature is constant and the parameter $n$ is equal to one.  Note that the initial condition $V_l^0 = V_R$ and the assumption that liquid volume is constant implies that $V_l = V_R$. Under this assumption $\tilde{m}_i = \theta_i$.  Constant temperature means that $K$ and $\theta_A^*$ are constant because both $K$ and $\theta_A^*$ have been assumed to depend only on temperature.  These assumptions

66

limit this model to systems with low saturation concentrations and low supersaturations but allow the development of closed form analytical solutions.

Under these assumptions equation (2.20) becomes:

$$\frac{d(\theta_A)}{d\tau_2} = -(\theta_A - \theta_A^*)$$

(2.31)

This can be solved directly for $\theta_A$ recalling that the initial concentration in dimensionless form is 1 by definition.

$$\theta_A(\tau_2) = \theta_A^* + (1 - \theta_A^*)e^{-\tau_2}$$

(2.32)

In order to solve for $\theta_B$, an expression for $\theta_B^*$ is required. First combine equations (2.23), (2.24) and (2.27) to give equation (2.33).

$$\frac{\theta_{Ac}^s}{\theta_{Bc}^s} = \frac{d(m_{Ac})/d\tau_2}{d(m_{Bc})/d\tau_2} = \frac{-d(m_A)/d\tau_2}{-d(m_B)/d\tau_2} = \frac{-d(\theta_A)/d\tau_2}{-d(\theta_B)/d\tau_2} = \frac{(\theta_A - \theta_A^*)}{\gamma(\theta_B - \theta_B^*)}$$

(2.33)

Then combine equations (2.33) and (2.26) and solve for $\theta_B^*$ to give equation (2.34).

$$\theta_B^* = \frac{\gamma\theta_A^*\theta_B}{K(\theta_A - \theta_A^*) + \gamma\theta_A^*}$$

(2.34)

A solvable differential equation for $\theta_B$ is then given by combining equations (2.21), (2.32) and (2.34). This is presented in equation (2.35).

$$\frac{d\left(\theta_b\right)}{d\tau_2} = -\gamma\left(\theta_B - \frac{\theta_B}{\frac{K}{\gamma}\left(\frac{1}{\theta_A^*}-1\right)e^{-\tau_2}+1}\right) \tag{2.35}$$

The initial condition by definition is $\theta_B{}^0=1$ and the solution to equation (2.35) is given in equation (2.36).

$$\theta_B = \left(\frac{1+e^{-\tau_2}\frac{K}{\gamma}\left(\frac{1}{\theta_A^*}-1\right)}{1+\frac{K}{\gamma}\left(\frac{1}{\theta_A^*}-1\right)}\right)^{\gamma} \tag{2.36}$$

These expressions for the liquid phase concentrations will be useful during the analysis of the model for the semi-continuous process.

### 2.2.3  Discussion of Impurity Concentration when $\gamma \gg 1$

When $\gamma$ is very large, equation (2.34) indicates that the critical concentration of the impurity in the liquid becomes equal to the concentration of the impurity in the liquid.

$$\lim_{\gamma\to\infty}\theta_B^* = \lim_{\gamma\to\infty}\frac{\gamma\theta_A^*\theta_B}{K\left(\theta_A-\theta_A^*\right)+\gamma\theta_A^*} = \theta_B \tag{2.37}$$

This expression also requires that $\gamma \ll K$.

This result indicates that when $\gamma$ is very large there is no resistance to incorporation of the impurity into the solid.  $\gamma$ is the ratio of incorporation rate constants and it will be much greater than one when the incorporation rate constant of the impurity is much greater than the incorporation rate constant of the component of interest.

In this situation the only limitation to impurity addition to the solid phase will be the amount of solid phase present which is controlled by the growth of species A. Impurity will be added to the crystal as soon as the crystal is grown. This means that concentration change in B will have the same time constant as the concentration profile for A. The amount of change in the concentration of B can be different than the change in A but the time scales over which the concentration changes occur will be the same.

## 2.3    CCC Modeling

A model of the semi-continuous process described in section 2.1 was developed in order to estimate the possible benefits of this process and to provide guidance for experimentation. The equations needed to model the semi-continuous process are very similar to the equations that describe batch crystallization.

The following set of equations will be derived for a single tank. These equations can be applied to any number of tanks to give the full equation system for a multi-tank process. The system is shown in Figure 15.
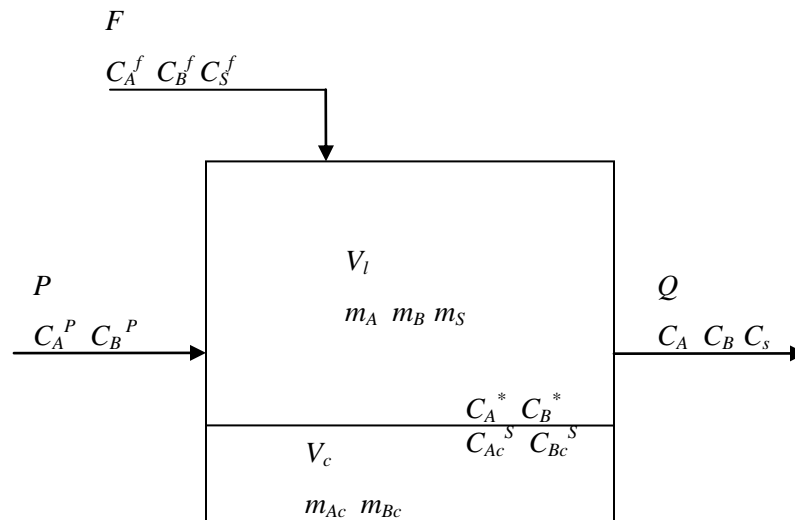


**Figure 15.  Drawing of one tank along with all possible variables for use in deriving equation system for counter-current crystallization model.**

69

The new variables in Figure 15 are defined as follows. $F$ and $P$ are the input volumetric flow rates (m$^3$/s) of the feed and sweep stream respectively; $Q$ is the outlet volumetric flow rate; $C_A^f$, $C_B^f$ and $C_S^f$ are the feed stream mass concentrations (kg/m$^3$) of species A, B and solvent respectively; and $C_A^P$, $C_B^P$ and $C_S^P$ are the sweep stream mass concentrations. Extension of these equations to a multiple tank system can be done by adding a subscript $i$ to each variable in order to denote the tank number. The inlet and sweep conditions could vary with time but are assumed to be known. The temperature and pressure in the tank will be held constant

This system has 12 unknowns ($m_A$, $m_B$, $m_s$, $m_{Ac}$, $m_{bc}$, $V_l$, $V_c$, $C_A^*$, $C_B^*$, $C_{Ac}^s$, $C_{Bc}^s$ and $Q$). The presence of flow alters the mass balance equations from the batch model. The new mass balance equations are given in equations (2.38)-(2.42).

$$\frac{d\left(m_A\right)}{dt} = PC_A^P + FC_A^f - QC_A - k_A a\left(C_A - C_A^*\right)^n \tag{2.38}$$

$$\frac{d\left(m_b\right)}{dt} = PC_b^P + FC_b^f - QC_b - k_b a\left(C_b - C_b^*\right)^n \tag{2.39}$$

$$\frac{d\left(m_s\right)}{dt} = PC_s^P + FC_s^f - QC_s \tag{2.40}$$

$$\frac{d\left(m_{Ac}\right)}{dt} = k_A a\left(C_A - C_A^*\right)^n \tag{2.41}$$

$$\frac{d\left(m_{bc}\right)}{dt} = k_b a\left(C_b - C_b^*\right)^n \tag{2.42}$$

The next six equations are the same as for the batch model.

$$C_A^* = f\left(T\right) \tag{2.43}$$

$$K = \frac{C_A^* \, C_{Bc}^s}{C_B^* \, C_{Ac}^s} \tag{2.44}$$

$$\frac{d\left(m_{Ac}\right)/dt}{d\left(m_{Bc}\right)/dt} = \frac{C_{Ac}^{s}}{C_{Bc}^{s}} \tag{2.45}$$

$$m_{A}\overline{V_{A}} + m_{B}\overline{V_{B}} + m_{s}\overline{V_{s}} = V_{l} \tag{2.46}$$

$$\frac{m_{Ac} + m_{Bc}}{V_{c}} = \rho_{c} \tag{2.47}$$

$$C_{Ac}^{s} + C_{Bc}^{s} = \rho_{c} \tag{2.48}$$

A new equation is needed because of flow through the cascade and it relates to the operation of the system. The chosen constraint will be that the total volume in the reactor ($V_{l} + V_{c}$) is constant. Alternatively, an assumption about the solid phase volume, liquid phase volume or outlet flow rate could be made.

$$V_{R} = V_{l} + V_{c} \tag{2.49}$$

This volume is the volume for a single tank. A cascade of $N$ reactors would have a total volume equal to $NV_{R}$.

### 2.3.1  Non-Dimensionalization

The model equations were non-dimensionalized using the following dimensionless variables.

$$m_{i} = \frac{m_{i}}{C_{i}^{0}V_{R}} \tag{2.50}$$

$$\tau = \frac{tF}{V_{R}} \tag{2.51}$$

$$\upsilon = \frac{V_{l}}{V_{R}} \tag{2.52}$$

$$\lambda_i = C_i^0 \overline{V_i} \qquad (2.53)$$

$$\beta_i = \frac{k_i a \left(C_i^0\right)^{n-1}}{F} \qquad (2.54)$$

$$\gamma = \frac{\beta_B}{\beta_A} = \frac{k_B}{k_A}\left(\frac{C_B^0}{C_A^0}\right)^{n-1} \qquad (2.55)$$

$$\theta_i = \frac{C_i}{C_i^0} = \frac{m_i}{C_i^0 V_l} = \frac{m_i}{\upsilon} \qquad (2.56)$$

$$\theta_i^* = \frac{C_i^*}{C_i^0} \qquad (2.57)$$

$$\psi = \frac{P}{F} \qquad (2.58)$$

$$\phi = \frac{Q}{F} \qquad (2.59)$$

$$\rho_c = \frac{\rho_c}{C_A^0} \qquad (2.60)$$

$$\eta = \frac{C_b^0}{C_A^0} \qquad (2.61)$$

The difference from the batch equations is that the time is now non-dimensionalized using the feed flow rate instead of the incorporation rate constant of A. The dimensionless time in the flow system is denoted as $\tau$ as opposed to $\tau_2$ in the batch system. The dimensionless total length of the growth operation will be denoted by $\tau_f$, using the same definition as in equation (2.51) with $t$ set equal to $t_f$ which is the total time for growth.

These variables when inserted into equations (2.38)-(2.49) give the following dimension-less system of equations.

$$\frac{d\left(m_A\right)}{d\tau} = \psi\theta_A^P + \theta_A^f - \phi\theta_A - \beta_A\left(\theta_A - \theta_A^*\right)^n \qquad (2.62)$$

$$\frac{d\left(m_B\right)}{d\tau} = \psi\theta_B^P + \theta_B^f - \phi\theta_B - \beta_B\left(\theta_B - \theta_B^*\right)^n \tag{2.63}$$

$$\frac{d\left(m_s\right)}{d\tau} = \psi\theta_s^P + \theta_s^f - \phi\theta_s \tag{2.64}$$

$$\frac{d\left(m_{Ac}\right)}{d\tau} = \beta_A\left(\theta_A - \theta_A^*\right)^n \tag{2.65}$$

$$\frac{d\left(m_{Bc}\right)}{d\tau} = \beta_B\left(\theta_B - \theta_B^*\right)^n \tag{2.66}$$

$$\theta_A^* = f\left(T\right) \tag{2.67}$$

$$K = \frac{\theta_A^* \, \theta_{Bc}^s}{\theta_B^* \, \theta_{Ac}^s} \tag{2.68}$$

$$\frac{d\left(m_{Ac}\right)\big/d\tau}{d\left(m_{Bc}\right)\big/d\tau} = \frac{\theta_{Ac}^s}{\theta_{Bc}^s} \tag{2.69}$$

$$m_A\lambda_A + m_B\lambda_B + m_s\lambda_s = \upsilon \tag{2.70}$$

$$m_{Ac} + m_{Bc}\eta = \rho_c\upsilon_c \tag{2.71}$$

$$\theta_{Ac}^s + \theta_{Bc}^s\eta = \rho_c \tag{2.72}$$

$$1 = \upsilon + \upsilon_c \tag{2.73}$$

This system of equations was solved using MATLAB. Starting from an arbitrary initial state the simulation is repeated for many cycles of operation until the concentrations in each tank at the beginning of one growth operation are the same as at the beginning of the next growth operation. This condition is referred to as cyclical steady state.

The mole fraction of the impurity in the solid at the surface is given by equation (2.74).

$$x_{Bc}^s = \frac{C_{Bc}^s}{C_{Bc}^s + C_{Ac}^s} = \frac{1}{1 + \dfrac{C_{Ac}^s}{C_A^0} \dfrac{C_A^0}{C_B^0} \dfrac{C_B^0}{C_{Bc}^s}} = \frac{1}{1 + \dfrac{\theta_{Ac}^s}{\eta \theta_{Bc}^s}}$$

(2.74)

where $\eta$ is the ratio of the initial concentrations of species B to species A as defined in equation (2.61). Once a layer of crystal is deposited, its concentration is assumed constant on the time scale of this process so the value of $x_{Bc}{}^s$ as a function of time will give the concentration profile of the crystal as a function of time. The value of this mole fraction can be calculated from the solution to the above set of equations.

### 2.3.2  Analytical Solution for Yield in Three Stage Cascade

An analytical expression for the yield at cyclic steady state from this process was developed for a three stage cascade with feed at stage two and a sweep stream at stage 1. This is the smallest number of stages able to capture all of the possible advantages of the proposed counter-current crystallization. It was also assumed for this analysis that the temperature in every stage was the same, the parameter $n$ is equal to one, crystal growth only occurs in one planar dimension so that the area for crystal growth is constant and that the system is dilute in A and B so that the liquid volume remains constant. The expression for yield was generated via a stage by stage calculation. It is straightforward to extend this analysis to a system with more stages but the algebra required is significant.

The expression for the yield of a three stage cascade with feed at stage two and a sweep stream is given in equation (2.75). A full derivation of this quantity is included in section 6.2.

$$y = \left[ \beta_A \left( \frac{\psi\theta_0 + \beta_A\theta^*}{\psi + \beta_A} - \theta^* \right) \right]_{\text{tank 1}} +$$

$$\left[ \frac{\beta_A \left( \dfrac{1 + \psi \left( \dfrac{\psi\theta_0 + \beta_A\theta^*}{\psi + \beta_A} \right) + \beta_A\theta^*}{1 + \psi + \beta_A} - \theta^* \right)}{\dfrac{\psi + \beta_A}{\beta_A} - \dfrac{\psi(1 + \psi + \beta_A)}{(1 + \psi + \beta_A)^2 - \beta_A(1 + \psi)}} \right]_{\text{tank 2}} +$$

$$\left[ \frac{\beta_A \left( \dfrac{(1 + \psi) \left( \dfrac{1 + \psi \left( \dfrac{\psi\theta_0 + \beta_A\theta^*}{\psi + \beta_A} \right) + \beta_A\theta^*}{1 + \psi + \beta_A} \right) + \beta_A\theta^*}{1 + \psi + \beta_A} - \theta^* \right)}{\left( \dfrac{1 + \psi + \beta_A}{\beta_A} - \dfrac{1 + \psi}{1 + \psi + \beta_A} \right)\left( \dfrac{\psi + \beta_A}{\beta_A} - \dfrac{\psi(1 + \psi + \beta_A)}{(1 + \psi + \beta_A)^2 - \beta_A(1 + \psi)} \right)} \right]_{\text{tank 3}} \qquad (2.75)$$

Equation (2.75) can be simplified to give the expression for yield from a two stage cascade with feed at stage 1 by setting the sweep stream flow rate to zero. This follows from the sequential nature of the process. A downstream tank is only affected by its nearest neighbor tank in the upstream direction. Setting the sweep flow rate equal to zero results in no outflow from tank one and therefore no input into tank two. It will not be necessary to study this special case because a more general analysis will cover the interesting details of this solution.

Analysis of this solution will be facilitated by looking at the individual yield in each of the three tanks if a single growth operation were run until steady state is achieved in each stage. The expressions for the yield from the three tanks in this situation are given in equations (2.76)-(2.78)

$$y_{\text{ss,tank 1}} = \beta_A \left( \frac{\psi\theta_0 + \beta_A\theta^*}{\psi + \beta_A} - \theta^* \right) \qquad (2.76)$$

$$y_{ss,tank\ 2} = \beta_A \left( \frac{1 + \psi \left( \frac{\psi \theta_0 + \beta_A \theta^*}{\psi + \beta_A} \right) + \beta_A \theta^*}{1 + \psi + \beta_A} - \theta^* \right) \tag{2.77}$$

$$y_{ss,tank\ 3} = \beta_A \left( \frac{(1 + \psi) \left( \frac{1 + \psi \left( \frac{\psi \theta_0 + \beta_A \theta^*}{\psi + \beta_A} \right) + \beta_A \theta^*}{1 + \psi + \beta_A} \right) + \beta_A \theta^*}{1 + \psi + \beta_A} - \theta^* \right) \tag{2.78}$$

Equations (2.75)-(2.78) show that the yield of the counter-current crystallization process at cyclical steady given in equation (2.75) is a weighted sum of the yield from each tank during a single growth phase run until steady state is achieved. The weight on tank 1 is 1 while the weights on the other tanks in the cascade are functions of the dimensionless sweep flow rate $\psi$ and the dimensionless reaction rate $\beta_A$. If the sweep flow rate is set to zero the weighting factor on tank two yield will become one. The weighting factor on the first tank in any cascade will be one because that is the tank from which the product is removed.

The weighting factor for each tank is composed of the weighting factor from the adjacent upstream tank multiplied by an additional unique factor. The weighting factor for the second/feed tank is more complicated that the unique portion of the weighting factor from the third tank. The presence of input streams is seen to result in more complicated weighting factors.

The values of the weighting factors in any tank except tank 1 are strictly less than or equal to one. This indicates that the proposed cyclical process can at best match the yield for a single growth operation run until steady state is achieved if the crystal is collected from all tanks but will likely have worse yield than a single pass operation with recovery from every tank.

Another important point to be gleaned is that the operating time for the growth phase of the counter-current crystallization operation does not affect the cyclical steady state yield under these conditions. Equation (2.75) was generated using the full transient equation system and all terms involving time cancelled out when solving for the yield. As long as the process is

run until cyclical steady state is achieved the duration of each individual growth cycle does not matter. The effect of varying total growth times on the process will be to change the number of cycles necessary to achieve cyclical steady state with shorter growth times requiring more cycles until steady state.

This conclusion is dependent on the assumption used in the derivation of the yield that the liquid volume remains constant. This assumption means that only a small amount of growth can occur because the simulation constrains the sum of liquid and solid volume to be constant. Even in dilute systems a large amount of crystal can be grown if the cascade is operated for long times. This expression for the yield is limited to short operating times and the effect of longer operating times for appreciable crystal growth is discussed below along with the results from the full simulation.

The sweep tank (tank 1) will always decrease overall yield unless the sweep stream concentration is greater than or equal to the saturation concentration. The intended purpose of the sweep stream is to increase the purity of the final product and this expression indicates that any increase in purity will come at a cost of yield unless the sweep stream is highly concentrated in species A. The effect of the sweep stream flow rate and concentration on product purity is analyzed using MATLAB simulations because an analytical solution for the purity was not obtained.

Excessively high sweep stream flow rates can result in zero net crystal growth in tank 1. The product is the crystal formed in tank 1 of the cascade so the sweep stream must be low enough to allow net crystal growth to occur in tank 1. Conditions for which there is no crystal growth in tank 1 were not studied. The sweep stream flow rate can be so high as to eliminate growth in tank 1 while still allowing growth in tanks 2 and 3 but this situation is not important because no product can be removed if there is no growth in tank 1.

Examination of equations (2.76)-(2.78) also shows that the yield from each tank after the feed is less than that from the immediately preceding tank. Adding more tanks in order to increase yield then is subject to diminishing returns. Multiple tanks do increase the overall yield but small increases in yield must be balanced against the increase in equipment and operating costs to perform the cyclical counter current crystallization process in a large cascade.

This analysis was performed under the assumption that the temperature in each stage was constant. Constant temperature also implies that $\beta_A$ is the same in each stage. Moving to a system with different temperature in each stage would complicate the algebra but the same types of relationship would be expected. The main difference would be that instead of only $\beta_A$ appearing in the equations, there would be a $\beta_{A,i}$ for every stage. This modification is not expected to change the preceding analysis.

### 2.3.3 Analytical Purity for Certain Values of the System Specific Parameters

The concentration profile of the impurity cannot be solved for analytically in general using the equation system outlined in section 2.3. But for limited values of the system specific parameters $\gamma$ and $K$ analytical solutions can be determined. The concentration profile of the impurity can be determined when $\gamma \ll 1$ or when $\gamma \gg 1$ and $K \ll 1$ with an arbitrary number of stages with or without a sweep stream.

While solutions are possible for large cascades, a one stage system was used because the results become quite complicated with multiple stages and are difficult to analyze. The derivation of the concentration profiles for this system is discussed in appendix 6.3. A one stage system can provide insight that can inform further study using numerical simulations. The use of a sweep stream with the one stage system is done only to provide insight on the effect of a sweep stream when longer cascades are used. A sweep stream would not be employed in practice with a one stage system.

The availability of an analytical impurity concentration profile allows an analytical expression for the purity to be determined. The purity and yield for the one stage system with a sweep stream at cyclical steady state is given in the following equations for both situations. When $\gamma \ll 1$ the purity is given by

$$p = \cfrac{1}{1 + \eta_B \gamma \left( \cfrac{1}{\cfrac{\left(1 + \psi + \beta_B\right)}{\left(1 + \psi + \beta_A\right)}\left(1 - \left(1 + \psi\right)\theta_A^*\right) + \cfrac{\gamma \theta_A^*}{K}\left(1 + \psi\right)} \right)} \tag{2.79}$$

When $\gamma \gg 1$ and $K \ll 1$ the purity is given by

$$p = \cfrac{1}{1 + \cfrac{\eta_B K}{\theta_A^*}\left(\cfrac{1}{1 + \psi + \cfrac{K\beta_A}{\theta_A^*}\left(\cfrac{1-(1+\psi)\theta_A^*}{1+\psi+\beta_A}\right)}\right)} \qquad (2.80)$$

The yield is independent of the impurity profile so in both cases it is given by

$$y = \frac{\beta_A}{1 + \psi + \beta_A}\left(1 - \theta_A^*\right) \qquad (2.81)$$

Examination of equation (2.81) indicates that the yield will always decrease as $\psi$ is increased.

Studying equation (2.79) it is evident that in order for the purity to be very high the value of the second term in the denominator should be as small as possible. This can be studied by looking at the expressions $\eta_B \gamma$ (term 1) and $\dfrac{1}{\dfrac{(1+\psi+\beta_B)}{(1+\psi+\beta_A)}\left(1-(1+\psi)\theta_A^*\right) + \dfrac{\gamma\theta_A^*}{K}(1+\psi)}$ (term 2). For a real system the value of $\beta_A$ will be order one[**] and $\psi$ will be less than one. When this is true the magnitude of term 2 will also be order one and the purity will largely be determined by the value of the term 1 with slight modification from term 2. When $\gamma \ll 1$ the departure of the purity from one is then seen to be approximately equal to the product of $\eta_B$ and $\gamma$ as shown in equation (2.82).

$$1 - p \approx \eta_B \gamma \qquad (2.82)$$

Although term 1 has the most important effect on the purity, term 2 is of interest because it contains the sweep stream flow rate. Analysis of this term can indicate what effect the sweep stream flow rate has on the purity. Unfortunately term 2 does not behave monotonical-

---

[**] Large values of $\beta_A$ require large reactor volumes or very small flow rates which would be impractical.

ly for all parameter values. No simple analysis is possible but once the relevant system specific parameters are known equation (2.79) could be used to understand how the operating parameters impact the purity from this process.

A more instructive analysis can be performed on equation (2.80) for the situation when $\gamma \gg 1$ and $K \ll 1$. Purity will be higher when the second term in the denominator is as small as possible. The expression determining the purity now consists of two terms: $\dfrac{\eta_B K}{\theta_A^*}$ (term 3) and

$$\dfrac{1}{1+\psi+\dfrac{K\beta_A}{\theta_A^*}\left(\dfrac{1-(1+\psi)\theta_A^*}{1+\psi+\beta_A}\right)}$$ (term 4). The value of term 3 is controlled by the product of $\eta_B$

and $K$ while term 4 will be order one for the parameter values expected for a practical system. This indicates that the departure of the purity from one when $\gamma \gg 1$ and $K \ll 1$ is roughly determined by the product of $\eta_B$ and $K$ as shown in equation (2.83).

$$1-p \approx \eta_B K \tag{2.83}$$

To understand the effect of the sweep stream flow rate on the purity in this situation, term 4 is compared to its value at $\psi=0$. The equality will again be assumed so that increasing $\psi$ gives a decreasing value for this term.

$$\dfrac{1}{1+\dfrac{K\beta_A}{\theta_A^*}\left(\dfrac{1-\theta_A^*}{1+\beta_A}\right)} > \dfrac{1}{1+\psi+\dfrac{K\beta_A}{\theta_A^*}\left(\dfrac{1-(1+\psi)\theta_A^*}{1+\psi+\beta_A}\right)} \tag{2.84}$$

This can be rearranged to give

$$\psi > \dfrac{K\beta_A}{\theta_A^*}\left(1+\dfrac{1-\theta_A^*}{1+\beta_A}\right)-(1+\beta_A) \tag{2.85}$$

If this equality is satisfied then the purity will increase with increasing sweep stream flow rate. If the right hand side of the equality in equation (2.85) is less than zero then any value of the sweep stream flow rate greater than zero will give increased purity. Assuming this is the case and performing some rearrangement gives

$$\frac{K\beta_A}{\theta_A^*}\left(1+\frac{1-\theta_A^*}{1+\beta_A}\right)-(1+\beta_A)<0 \tag{2.86}$$

$$K<\frac{\theta_A^*(1+\beta_A)^2}{\beta_A(1+\beta_A+1-\theta_A^*)} \tag{2.87}$$

$$\frac{1}{K}>\frac{\beta_A}{\theta_A^*(1+\beta_A)}+\frac{\beta_A(1-\theta_A^*)}{\theta_A^*(1+\beta_A)^2} \tag{2.88}$$

Recall that $\theta_A^*$ is order one and note that ratio of $\beta_A/(1+\beta_A)$ or $\beta_A/(1+\beta_A)^2$ will always be between zero and 1 for $\beta_A>0$. This means the right hand side of equation (2.88) will always be order 1. $K$ was constrained at the beginning of the derivation to be much less than one so that $1/K$ will be much greater than one and therefore equality (2.88) is true. This means that equality (2.86) is also true and increasing $\psi$ will result in increased purity when $K<<1$ and $\gamma>>1$.

The analysis in this section has shown that in situations where $\gamma<<1$ or when $K<<1$ and $\gamma>>1$ the departure of the purity from unity is approximately given by the product of $\eta_B$ and $\gamma$ or the product of $\eta_B$ and $K$ respectively for a one stage system. Higher purities will result from lower system specific parameter values ($\gamma$ and $K$) and lower values of the initial concentration ratio of the impurity to the component of interest ($\eta_B$). These parameters will often be fixed by the specific chemical system and a given feed stream concentration but systems with lower values of these parameters will result in higher purity products.

The intended purpose of the sweep stream was to increase product purity and this is seen to be the case under certain conditions although the magnitude of this effect is expected to be small in practical systems ($\beta_A$ order one and $\psi$ order one or less). Also recall that the yield always decreases with increasing sweep stream flow rate. A more general analysis of the effect

81

of different parameters on the purity will be done using the numerical solution to the full model in section 2.4.

### 2.3.4    General Model Comments

The major assumptions made in this model are the temperature dependent equilibrium relationship at the surface and the expressions for crystal growth.  These expressions govern the incorporation of the impurity into the crystal and if they are not reasonable then the results will not be useful.  Experimentation is required in order to determine how valid these assumptions are and to provide guidance for better functional forms if these are not appropriate.

Another assumption is that temperature in each tank and at the crystallization surface can be held constant.  Depending on the amount of crystallization occurring and the size of each tank heat transfer limitations could be important.  This is an important consideration when designing the process equipment which may dictate a particular cooling method.

This model does not assume dilute solutions.  It accounts for variable liquid phase volumes for systems with high concentrations in the liquid phase.  Issues with the liquid transfer operation such as under and overfilling are only expected to apply in concentrated systems so that operation of dilute systems will be less complicated in terms of operational programming.

## 2.4    CCC Model Results

The physical parameter values and variable ranges used in the model simulation are shown in Table 1 and are based on published physical properties of asparagines.[149, 150]  The reason for the use of asparagine properties will be discussed in section 4.2.3 when the model experimental system is discussed but for now it is only necessary to note that the density is in a common range for small molecule solids[150] and the solubility varies strongly with temperature in the vicinity of room temperature.  The mass specific volumes for A and B are at infinite dilution because the solubility of asparagine in water is low.   A and B will have very similar structures in solid-solution-forming systems so the mass specific volume of the impurity will be assumed to be the same as for species A.

| Parameter | Value(s) | | Operational Variable | Range of Values |
|---|---|---|---|---|
| $C_A^*$ | $7.4 \times 10^{-5} e^{.04*T}$ g/kg solvent (T in Kelvin) | | $\psi$ | 0-1 |
| $\rho_C$ | 1543 kg/m$^3$ | | $\beta_A$ | 0.1-100 |
| $V_A^0 = V_B^0$ | $6 \times 10^{-4}$ m$^3$/kg | | $K$ | 0.1-10 |
| $V_s^0$ | 0.001 m$^3$/kg | | $\gamma$ | 0.1-10 |
| $\tau$ | 3 | | | |
| $T$ | 273.15 K | | | |
| $n$ | 1 | | | |
| $C_A^0$ | 25 kg/m$^3$ | | | |
| $C_B^0$ | 2 kg/m$^3$ | | | |

**Table 1.  Parameters values and variable ranges used for MATLAB simulation of semi-continuous counter current crystallization process.**

The value of the parameter $n$ is assumed to be one and growth is assumed to occur in only one dimension.  Planar one-dimensional growth allows the area $a$ to be constant so that $\beta_A$ is only dependent on the feed stream flow rate.  Assuming that $n$ is one will be valid in systems operated at high supersaturations and for systems with microscopically rough surface as discussed in section 1.1.2.  The roughness of the surface of a growing crystal is a property of the specific chemical undergoing growth and must be determined for each unique system.

The use of a dilute system allows equation (2.46) to be simplified.  Instead of using partial mass volumes for A, B and the solvent the mass specific volume at infinite dilution can be used for A and B and the pure component specific volume can be used for the solvent.  This simplification removes the need to find a relationship for the partial mass volumes as a function of the concentration of all species.

The concentration profiles for species A and B in each stage of a three stage cascade with feed at stage two are shown in Figure 16, Figure 17 and Figure 18.  The system and operational parameters in these figures are $K$=0.5, $\gamma$=0.5, $\psi$=0.1, $\beta_A$=2, $\tau_f$=2 and $T$=273.15 K.  Note that the concentration of each species is normalized to the feed concentration of that species so

that the dimensionless concentration of B can be greater than the dimensionless concentration of A even though the actual concentration of A is always higher than B.

These figures show a process occurring with a time constant for $\theta_A$ of roughly 0.5. The time constant for flow-dependent phenomena in tanks 2 and 3 should be approximately one because of the definition of $\tau$ and in tank 1 it should be 10 because the sweep stream flow rate is set to 0.1. However, if this was a batch operation the time constant for $\theta_A$ would instead be given by $1/\beta_A$. This represents the time constant for crystallization which in this case is 0.5. The growth cycle is therefore seen to be dominated by crystallization and behave very much like batch crystallization over the initial period of time. For the impurity, the time constant in the first tank is approximately 1. This is the expected result with $\gamma$ equal to 0.5 and $\beta_A$ equal to 2. This means that the crystallization and flow time constant for the impurity in tanks 2 and 3 are nearly equal. The observed time constant in tanks 2 and 3 are slightly shorter than in tank 1 because the flow rate is much higher allowing some depletion to occur by flow out of the stage in addition to depletion by crystallization.

If the growth cycle is operated for a long period of time, the steady state profile will be achieved and further deposition will be at constant rate and composition. Operating for very long times will result in the average composition of the crystal being controlled by the steady state deposition with the initial transient representing a very small fraction of the total crystal.

These figures demonstrate that the continuous process is controlled by the fastest time constant of the system. The competing time constants are proportional to $1/\beta_A$ and $1/(1+\psi)$. When $\beta_A$ is greater than $1+\psi$ the reaction time constant will be much smaller than the flow time constant and the concentration decrease is controlled by crystallization.
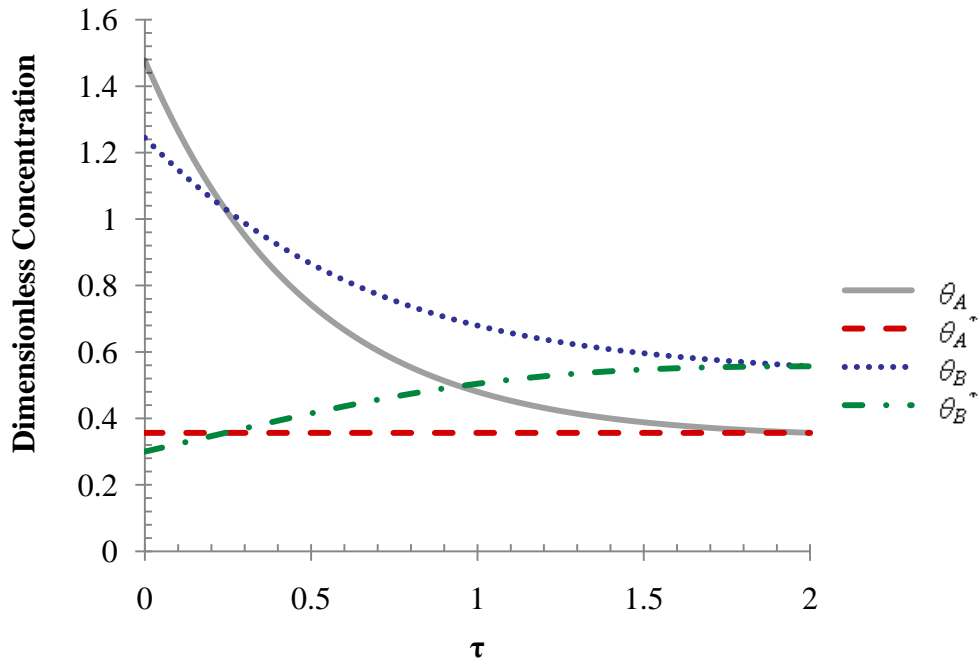
**Figure 16. Dimensionless concentration plots for stage 1 vs. time over one growth cycle after cyclic steady state has been achieved in the semi-continuous process. Simulated process is 3 stages with feed at stage 2 with $K$=0.5, $\gamma$=0.5, $\psi$=0.1, $\beta_A$=2, $\tau_f$=2 and $T$=273.15 K**
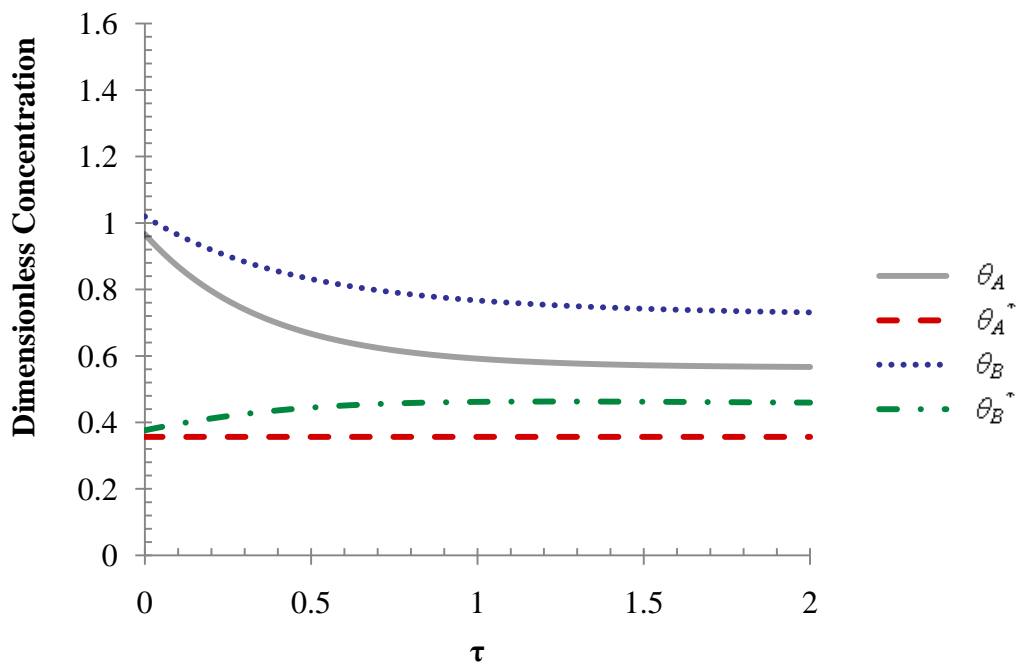


**Figure 17. Dimensionless concentration plots for stage 2 vs. time over one growth cycle after cyclic steady state has been achieved in the semi-continuous process. Simulated process is 3 stages with feed at stage 2 with $K$=0.5, $\gamma$=0.5, $\psi$=0.1, $\beta_A$=2, $\tau_f$=2 and $T$=273.15 K**
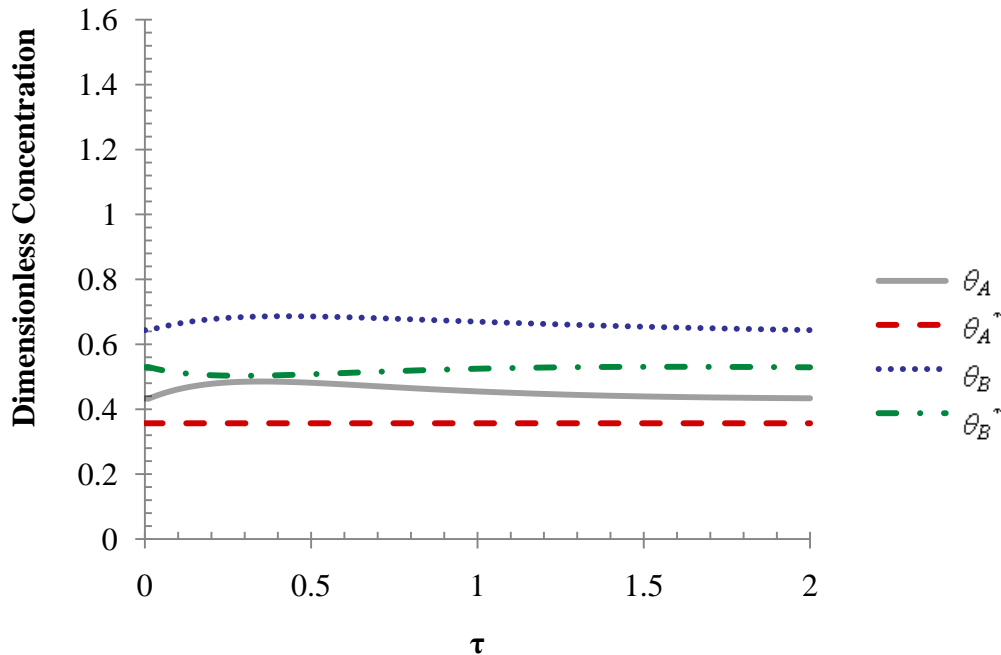
**Figure 18. Dimensionless concentration plots for stage 3 vs. time over one growth cycle after cyclic steady state has been achieved in the semi-continuous process. Simulated process is 3 stages with feed at stage 2 with $K$=0.5, $\gamma$=0.5, $\psi$=0.1, $\beta_A$=2, $\tau_f$=2 and $T$=273.15 K**

The goal of this process is to obtain as much A and as little B as possible. In order to do this, the amount of A leaving the system via flow should be minimized while the amount of B leaving the system via flow should be maximized. Minimizing the loss of species A via flow requires that the crystallization of A be maximized and this will occur when the time constant for crystallization of A is much smaller than the flow time constant. This means that $\beta_A$ should be much greater than 1+$\psi$. In order to maximize the amount of B leaving due to flow the amount of crystallization of B should be minimized which will occur when $\beta_B$ is much less than 1+$\psi$. The values of $\beta_A$ and $\beta_B$ can be manipulated by changing the flow rate of the feed but the ratio of the two is the chemical system specific parameter $\gamma$ which is constant. Combining these two conditions indicates that $\beta_A$ should be much greater than $\beta_B$ ($\gamma$<<1) in order to achieve the best results. This result is to be expected because as $\gamma$ approaches zero the amount of impurity in the crystal becomes zero and the crystal would be perfectly pure.

The mole fraction of impurity at the surface of the growing crystal as a function of time is shown in Figure 19 for the same system.
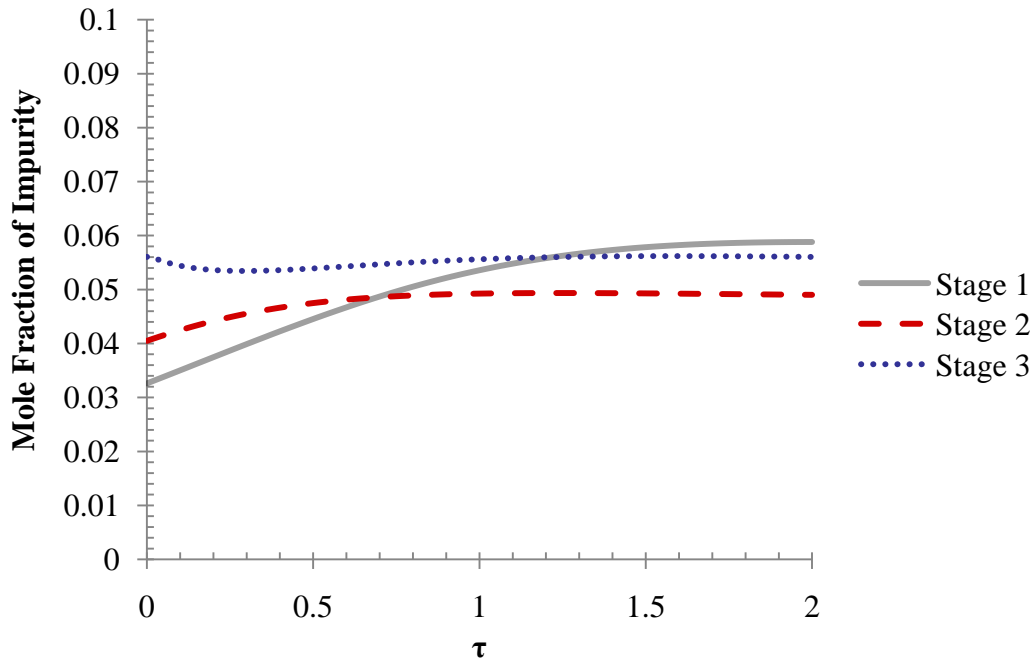
**Figure 19. Mole fraction impurity at the crystal surface vs. time over one growth cycle after cyclic steady state has been achieved in the semi-continuous process. Simulated process is 3 stages with feed at stage 2 with $K$=0.5, $\gamma$=0.5, $\psi$=0.1, $\beta_A$=2, $\tau_f$=2 and $T$=273.15 K**

This plot demonstrates the previously stated conclusion that after the initial transient, crystal will be formed at a constant concentration of impurity. This is seen clearly for tanks 2 and 3. This surface mole fraction of impurity in tank 1 takes longer to approach this constant value because the flow rate is very low and the depletion of species in tank 1 is due to crystallization with very little flow contribution. Figure 19 also indicates that purity at the final surface of the crystal in tank 1 is worse than at the surface of the crystal in tank 2 or tank 3. While the final layer of crystal may have a higher concentration of impurity in tank 1, the overall purity of tank 1 is higher than in tank 2 which is higher than in tank 3. The deposited crystal is dissolved before being removed as product so the average purity of the crystal in each tank is the most important value to consider.

While understanding of the behavior in each tank during the operation of this process is useful, the output from the simulation that is of most interest is the yield and purity of the product when cyclical steady state has been reached. The simulation results in the following sections are presented in plots of purity vs. yield. Each figure will explore the variation of two parameters. A series of curves will be shown for different values of one parameter while each

individual line will consist of multiple simulations done while varying a second parameter. Each point on an individual line will correspond to one simulation calculation with a unique set of values for the parameters. Note that the purity of the feed solution on a solvent free basis used in all simulations is 0.9259.

One of the goals of this process is to provide better performance than a batch operation, assessed by comparison of the yield and purity from a batch crystallization run to completion to those of the cyclical steady state of the counter current process. A batch crystallization run until completion will give the best possible yield for a given set of operating conditions and the proposed counter current process cannot exceed this yield. Better performance will be indicated by close approach to the batch yield but with purity higher than for batch crystallization.

Comparisons of the batch model to the semi-continuous process model will be made only when the chemical system specific parameters ($K$, $\gamma$ and $n$) are constant. Changing these values changes the batch performance and so a clear comparison is not possible. Study of the variation of the chemical system specific parameters is done to understand the different operational regimes and not to determine optimal values. $K$, $\gamma$ and $n$ are dictated by the specific chemical system in use and cannot be varied at will. Batch comparisons will be made when varying controllable operating parameters such as flow rates and times.

### 2.4.1 Effect of the chemical system parameters $K$ and $\gamma$

#### 2.4.1.1 Effects of varying $\gamma$
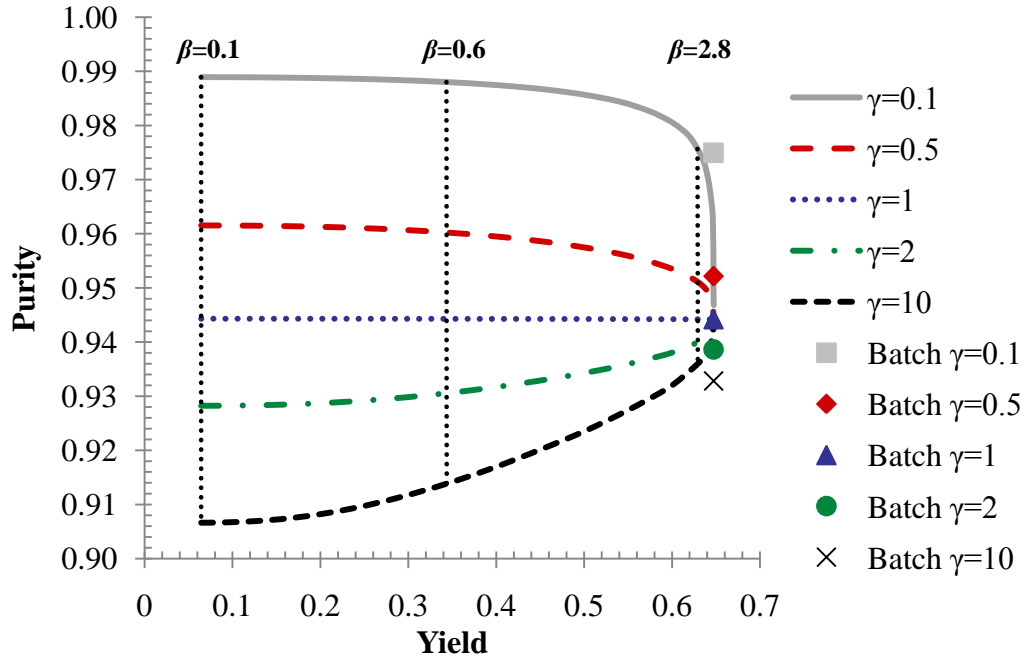


**Figure 20. Plot of purity vs. yield when $\beta_A$ is varied at various values of the constant ratio $\gamma$. $\tau_f$=2, $\psi$=0, 3 stages, feed at stage 1, $K$=0.5, and T=273.15 K. $\beta_A$ varies from 0.1 to 30 moving left to right in each individual line. Vertical dotted lines represent constant values of $\beta_A$ and individual points correspond to the batch comparison points for different values of $\gamma$. The purity of the feed solution is 0.9259.**

Figure 20 shows that the value of $\gamma$ has a significant impact on the performance of the counter-current crystallization process. In all cases the yield increases as the value of $\beta_A$, the incorporation rate constant of species A, increases. Higher incorporation rate constants result in higher yields. For $\gamma$ less than unity, the purity decreases as $\beta_A$ increases while for $\gamma$ greater than one the purity increases as the yield increases. When $\gamma$ is equal than unity, there is no change in purity as the incorporation rate constant of A increases.

When the incorporation rate constant of B is faster than A ($\gamma$>1), the purity of the product is decreased as $\beta_A$ increases. Conversely, when B is added to the crystal at a slower rate than A ($\gamma$<1) the product will become more pure as $\beta_A$ increases. At a given value of $\beta_A$ the purity increases as $\gamma$ approaches zero. This is in line with the definition of $\gamma$ which indicates that

when $\gamma$=0 the incorporation rate of B into the crystal is zero and therefore the product would be perfectly pure.

As $\beta_A$ becomes very high the product from the counter-current crystallization approaches the same final yield and purity for all values of $\gamma$. $\beta_A$ decreases with flow rate but increases with the intrinsic incorporation rate constants and surface area for growth. As $\beta_A$ becomes larger the conditions in each tank are less and less affected by kinetic considerations and the yield and purity approach a value independent of $\gamma$. The final purity is then determined by thermodynamic factors which in this model are represented by $K$ and $\theta_A{}^*$.

### 2.4.1.2  Analysis of Behavior at $\gamma$=1

Figure 20 indicates that the purity does not change when $\beta_A$ changes if $\gamma$=1. The ratio of driving forces is given by

$$\frac{\theta_A - \theta_A^*}{\theta_B - \theta_B^*} \qquad\qquad (2.89)$$

A plot of the ratio of driving forces for crystallization in tank 1 is presented in Figure 21 for $\gamma$ equal to 0.5, 1 and 2.

The ratio of the driving forces is constant and independent of $\beta_A$ only when $\gamma$ =1. The driving force for the impurity, $\theta_B$-$\theta_B{}^*$, is determined by the parameters, $\gamma$, $K$, $\tau_f$ and $Ca^*$ but Figure 21 indicates that it is directly proportional to $\theta_A$-$\theta_A{}^*$ when $\gamma$ =1. By combining equations (2.33) and (2.26) the ratio of driving forces can also be represented as

$$\frac{\theta_A - \theta_A^*}{\theta_B - \theta_B^*} = \frac{K\theta_B^*}{\gamma\theta_A^*} \qquad\qquad (2.90)$$

Recall that $K$, $\gamma$ and $\theta_A{}^*$ are all constant at constant temperature indicating that a constant ratio of driving forces is equivalent to a constant value of $\theta_B{}^*$ in this model.
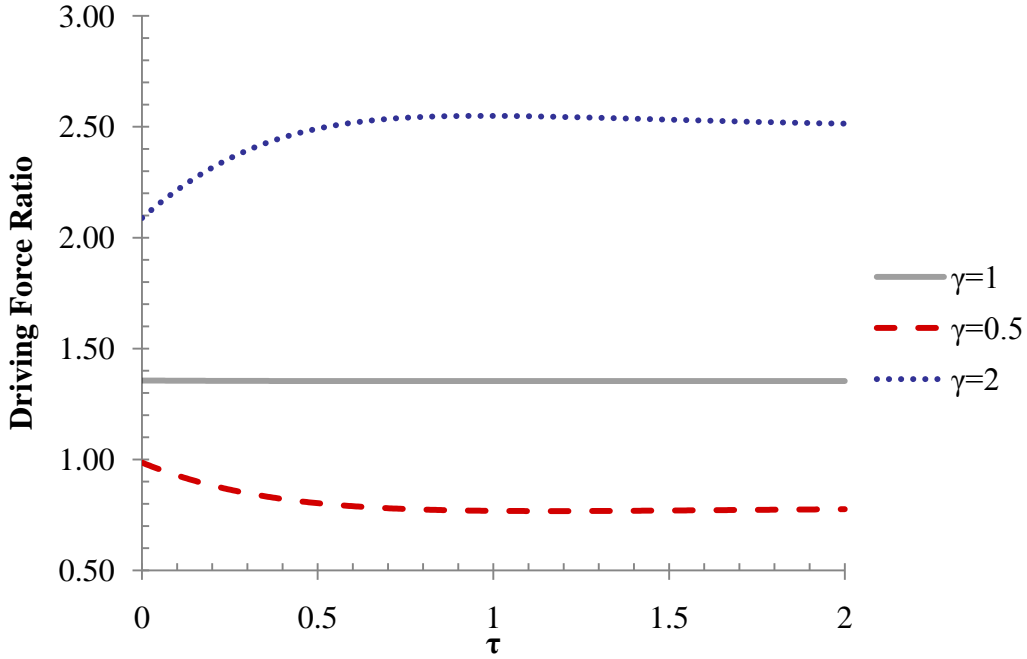
**Figure 21.** Plots of the ratio of crystallization driving forces for A and B in stage 1 vs. $\tau$ for $\beta_A$=2. $\tau_f$=2, $\psi$=0, 3 stages, feed at stage 1, $K$=0.5, and T=273.15 K. $\gamma$ is 2 for the top line, 1 for the middle line and 0.5 for the lower line.

This can be understood in the batch case making use of the analytical expressions for liquid phase concentration developed in section 2.2.2.

$$\theta_B^* = \frac{\theta_B}{\frac{K}{\gamma \theta_A^*}\left(\theta_A - \theta_A^*\right)+1} = \frac{\left(\frac{1+e^{-\tau_2}\frac{K}{\gamma}\left(\frac{1}{\theta_A^*}-1\right)}{1+\frac{K}{\gamma}\left(\frac{1}{\theta_A^*}-1\right)}\right)^{\gamma}}{1+\frac{K}{\gamma}\left(\frac{1}{\theta_A^*}-1\right)e^{-\tau_2}} \tag{2.91}$$

When $\gamma$=1 the following result is obtained.

$$\theta_B^* = \frac{1}{1+K\left(\frac{1}{\theta_A^*}-1\right)} \tag{2.92}$$

This expression is constant when temperature is constant which results in constant purity.

A similar analysis can be done for the semi-continuous process. It was not possible to solve for the concentration of B in the liquid phase analytically in the general case but for a system that has constant liquid phase volume (dilute with short growth times), feed at stage one with no sweep stream and $\gamma=1$ an expression can be generated for the concentration of B during a single cycle which is then used to find an expression for $\theta_B^*$. A full derivation is given in section 6.3. The numerical subscripts on $\theta$ indicate the tank number.

$$\theta_{B1}^*(\tau) = \frac{1}{1 + \dfrac{K}{\theta_A^*}\left(1 - \theta_A^*\right)} + \left(\frac{\theta_{B1}^0}{1 + \dfrac{K}{\theta_A^*}\left(\theta_{A1}^0 - \theta_A^*\right)} - \frac{1}{1 + \dfrac{K}{\theta_A^*}\left(1 - \theta_A^*\right)}\right) *$$

$$\left(\frac{1 + \dfrac{K}{\theta_A^*}\left(\theta_{A1}^0 - \theta_A^*\right)}{\dfrac{K}{\theta_A^*}\left(\theta_{A1}^0 - \dfrac{1 + \beta_A \theta_A^*}{1 + \beta_A}\right) + \left(\dfrac{K}{\gamma\theta_A^*}\left(\dfrac{1 - \theta_A^*}{1 + \beta_A}\right) + 1\right)e^{(1+\beta_A)\tau}}\right)^{\dfrac{1 + \frac{K}{\theta_A^*}\left(1 - \theta_A^*\right)}{\beta_A + 1 + \frac{K}{\theta_A^*}\left(1 - \theta_A^*\right)}}$$

(2.93)

Equation (2.93) is not useful for calculating the numerical value of the product purity from the cascade because it contains the initial concentration of species A and B in tank 1. The initial concentration of A in each tank was eliminated in section 2.3.2 when determining the yield by invoking the conditions of cyclic steady state but that is not possible analytically for species B. This expression is also only applicable to $\gamma=1$ because the integration could not be completed when $\beta_A$ and $\beta_B$ are different.

Consider equation (2.93) at $\tau=0$ and $\tau=\infty$.

$$\theta_{B1}^*(\tau = 0) = \frac{\theta_{B1}^0}{1 + \dfrac{K}{\theta_A^*}\left(\theta_{A1}^0 - \theta_A^*\right)}$$

(2.94)

$$\theta_{B1}^*(\tau = \infty) = \frac{1}{1 + \dfrac{K}{\theta_A^*}\left(1 - \theta_A^*\right)}$$

(2.95)

This result matches the batch result given in equation (2.92) at long times and also at all times if $\theta_{A1}{}^0$ and $\theta_{B1}{}^0$ are equal to 1. The values of $\theta_{A1}{}^0$ and $\theta_{B1}{}^0$ will always be order one because they are normalized but even small differences from unity will be important for very small values of K. Very large values of $K$ will result in $\theta_{B1}{}^*$ approaching zero so that very little absolute change will be observed and this amount of change will be negligible in relation to the initial driving force.

The difference between the value of $\theta_{B1}{}^*$ at $\tau=0$ and $\tau=\infty$ gives the maximum amount of change in $\theta_{B1}{}^*$ for a given set of parameters. This is true because the term on the second line of equation (2.93) is 1 when $\tau=0$ and monotonically decreases to zero as $\tau$ increases. If this difference is small relative to the initial driving force for species B then it can be assumed that $\theta_{B1}{}^*$ is constant. This is the case for all sets of parameters used in the simulation when $\gamma=1$. A constant value of $\theta_{B1}{}^*$ results in a constant incorporation rate ratio of A to B and therefore a constant product purity as seen in the simulation results presented in Figure 20.

Purification is still possible when $\gamma=1$ (unless the value of $K$ is also 1 in which case the product purity will be equal to the feed purity) but there are no benefits to staging in this situation for a system operated at constant temperature. The driving force in every stage along the cascade is essentially the same which results in crystalline product in each stage having the same purity. Multiple recrystallizations will not result in higher purity because the purity in every stage is the same. Discussion of when the proposed staged process is advantageous in relation to the different regimes of $\gamma$ will be addressed in section 2.4.3 after the effects of varying the total number of stages are presented.

### 2.4.1.3   Effect of varying $K$

The effect of $K$ on the yield and purity is shown in Figure 22. The yield does not change as $K$ is varied just as Figure 20 showed that $\gamma$ had no effect on the yield. This is the case because the crystallization of A has been assumed to be independent of B. $K$ and $\gamma$ only affect the amount of B that is incorporated into the crystal and so the yield is unchanged as they are varied.

Figure 22 indicates that at a fixed set of parameters, higher values of $K$ lead to lower purity products. This follows from the definition of $K$ (equation (2.44)) which indicates that if $K$=0, no impurity will incorporate into the crystal and the resulting purity of the crystal will be one. Larger values of $K$ indicate a larger amount of species B in the crystal which will result in lower purity.

Figure 21 also shows that for values of $K$ greater than or equal to one, the maximum purity achieved in batch crystallization is less than the purity of the feed solution. When $\gamma$<1 and $K$>1 the semi-continuous process can still provide higher purity than the feed but only with lower yields. As $K$ becomes much larger than one, achieving purity higher than the feed purity is only possible at lower and lower yields making this process undesirable. This indicates that for systems with values of $K$ much greater than one, crystallization in the manner described should not be used to effect a separation. When $K$ is order one and $\gamma$<1 the proposed process may be able to give the desired performance depending on the actual values of the system specific and operating parameters.

Figure 20 and Figure 22 indicate that higher purity and yield are achieved for smaller values of $K$ and $\gamma$. Systems with $K$>1 should not be used with the proposed semi-continuous process because any increase in purity compared to the starting material will occur at very low yields. As $\beta_A$ is increased, the differences in purity caused by different values of $\gamma$ disappear. The value of $\gamma$ does have important ramifications on the operation of this process and results will be presented below for $\gamma$ =0.5 and 2 in order to represent the two regimes $\gamma$>1 and $\gamma$<1.
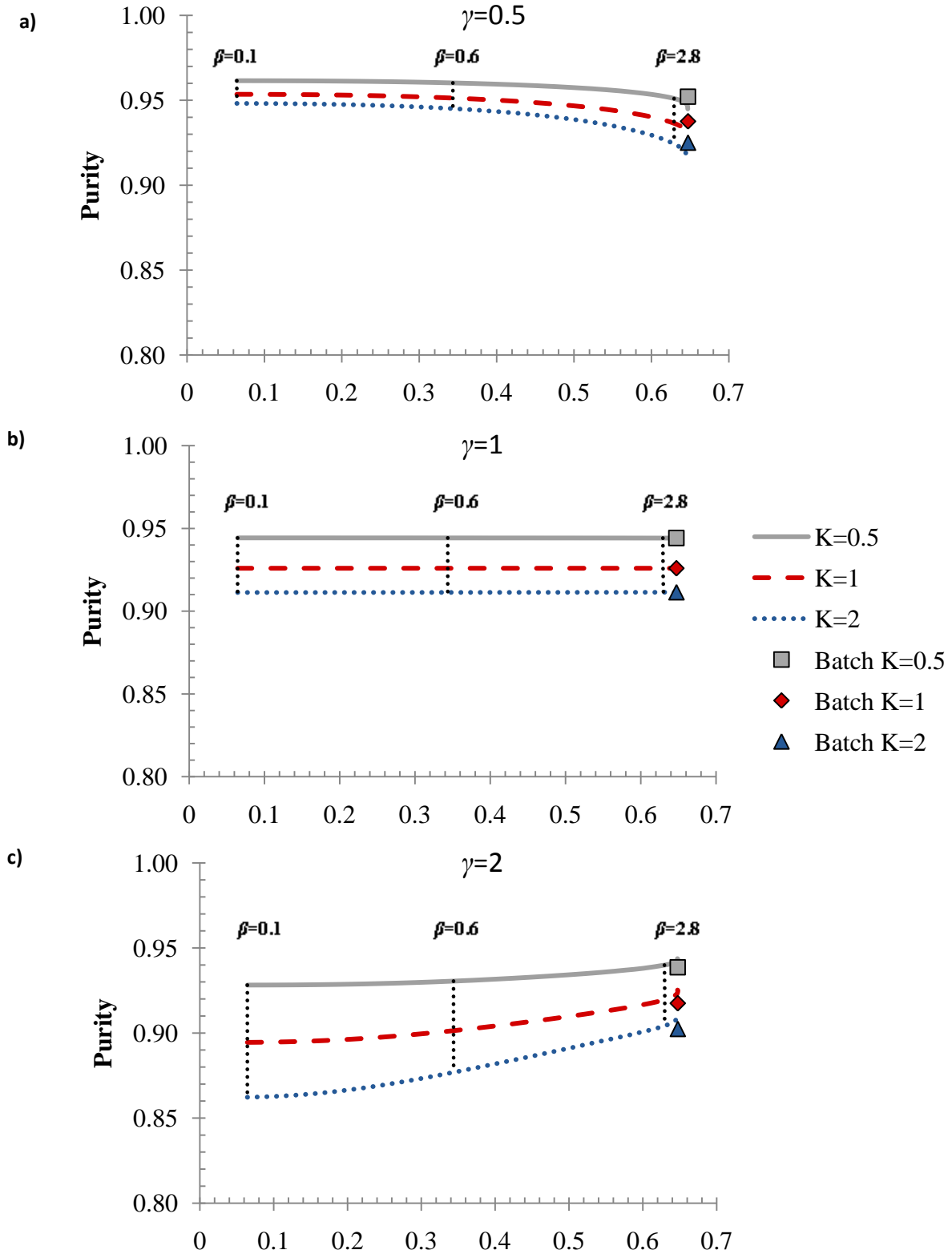
**Figure 22.** Plots of purity vs. yield when $\beta_A$ is varied at various values of the surface equilibrium constant K. $\tau_f$=3, $\psi$=0, 3 stages, feed at stage 1 and T=260 K. $\beta_A$ varies from 0.1 to 30 moving left to right in each individual line. Vertical dotted lines indicate constant $\beta_A$ and the points represent the batch comparison point at a particular value of $K$. The initial purity of the feed is 0.9259. a) $\gamma$=0.5 b) $\gamma$=1 c) $\gamma$=2

### 2.4.2  Effect of varying $\tau_f$

The effect of the duration of the growth stage ($\tau_f$) on yield and purity is shown in Figure 23 for $\gamma=0.5$ and $\gamma=2$ respectively.  The other parameters in the figure are: $T=273.15$ K, $\beta_A=2$, $K=0.5$, $\psi=0$, purity of feed solution is 0.9259 in a 3 stage cascade with feed at stage 1.
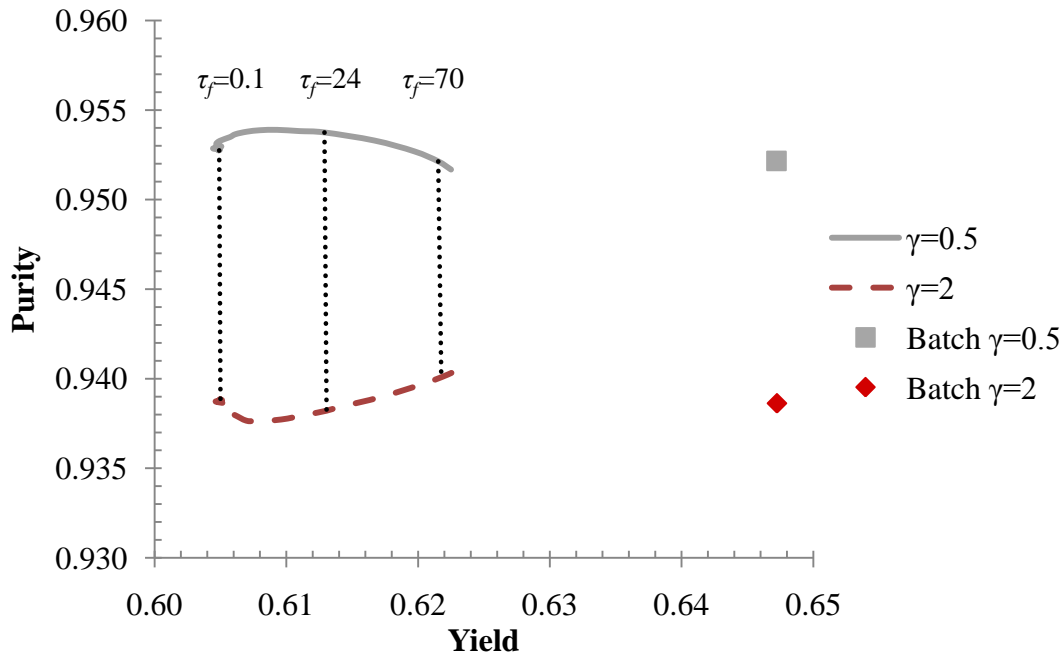


**Figure 23.  Plot of purity vs. yield when $\tau_f$ is varied for $\gamma$ values greater and less than one.  Results are for a 3 stage cascade with feed at stage 1, $\beta_A=2$, $\psi=0$, $K=0.5$ and T=273.15 K.  $\tau_f$ varies from 0.1 to 80 moving from left to right. Vertical dotted lines indicate constant values of $\tau_f$.  $\gamma=0.5$ in the top curve and $\gamma=2$ in the lower curve.  Maximum variation in yield and purity between two points on either line are 3.0  and 0.3% of the smaller value respectively. Purity of the feed solution is 0.9259.**

It was shown in section 2.3.2 that the dimensionless total time of the growth operation does not affect the yield at cyclic steady state for small operating times and dilute systems. This is not true for the full simulation results at long times because Figure 23 indicates that the yield increases with increasing $\tau_f$.

The full simulation results do not follow the analytical solution because the volume of the crystal phase becomes appreciable at long times even for dilute liquid phases.  An appreciable solid phase volume invalidates a key assumption in the derivation of the analytical yield expression and the results should no longer be expected to correspond to the analytical solu-

tion.  Note that at small times the yield is constant which does correspond to the behavior predicted by the analytical solution.

The purity also varies slightly as $\tau_f$ is increased but the value of gamma determines whether the purity increases or decreases.  When $\gamma<1$ the purity goes through a maximum as $\tau_f$ is increased.  Although this change in purity is small it is important and the dependence of the maximum purity on different parameters was studied for $\gamma<1$. For $\gamma>1$ the highest purity is achieved at very short or very long times and goes through a minimum at intermediate times.  This minimum purity is not of interest and was not studied.

Figure 24 and Figure 25 are plots of the value of $\tau_f$ at which the max purity is reached and the purity reached at that time vs. a varied operational parameter.  The studied parameters are $\beta_A$ and $\psi$.

For both $\beta_A$ and $\psi$ the time at which the maximum purity is achieved decreases as the parameter increases.  The behavior of the maximum purity is not the same though as the maximum purity decreases as $\beta_A$ increases but increases while $\psi$ increases.  No conclusions should be drawn about the benefits of using high $\beta_A$ or $\psi$ because the effect on yield has not been addressed.  This will be studied in the next section.  Figure 24 and Figure 25 do show that the variation in maximum purity with both $\beta_A$ and $\psi$ is much greater than the variation shown in Figure 23 when $\tau_f$ is varied.

The change in the purity and yield with varying $\tau_f$ is appreciable but is small compared to the change caused by varying $\beta_A$ or $\psi$.  Subsequent simulation results will be shown for a fixed operating time during the growth stage in order to simplify analysis given the large number of parameters.  The simulation results indicate that an optimal growth time exists with respect to purity for any set of parameters with $\gamma<1$ and that when $\gamma>1$ the shortest possible operating time will give the highest purity.  The yield in either case increases as $\tau_f$ increases.  Other factors such as equipment scheduling, crystal growth blockage of the flow channel, time necessary for crystal dissolution or downstream processing operations should also be accounted for when determining the growth time and these may be more important than the slight increases in purity and yield available at certain values of $\tau_f$.
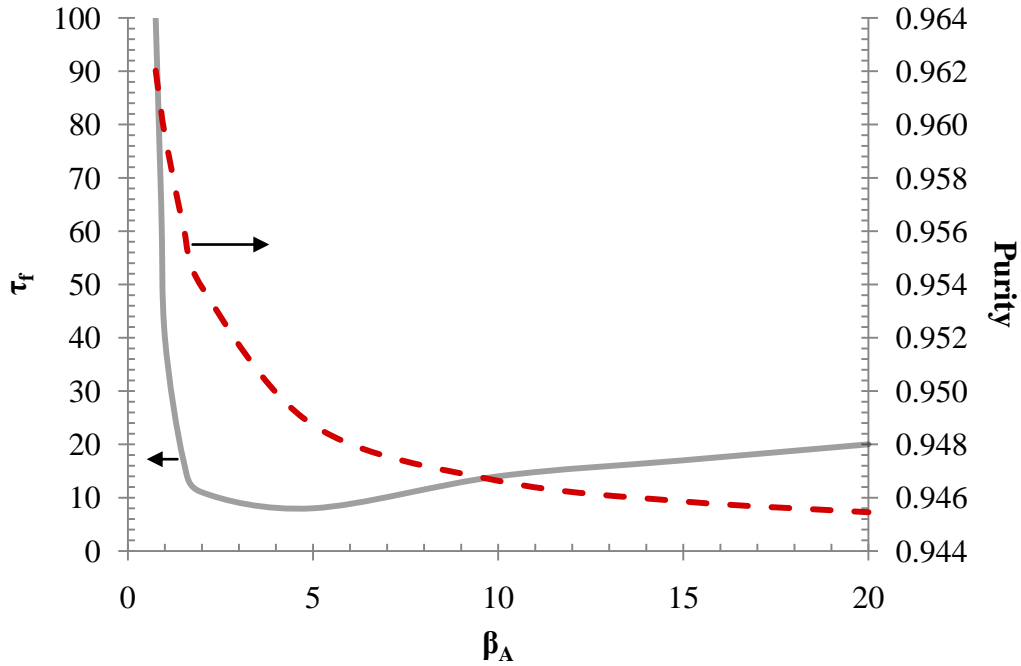
**Figure 24. Growth time at which the maximum purity is achieved and the purity at that time vs. $\beta_A$. Other simulation parameters are $\psi$=0, $\gamma$=0.5, $K$=0.5 and $T$=273.15 K for a 3 stage cascade with feed at stage 1. Purity of the feed solution is 0.9259. The solid, gray line is the growth time at which the maximum purity is achieved and corresponds to the left axis. The red dashed line is the maximum purity and corresponds to the right axis.**
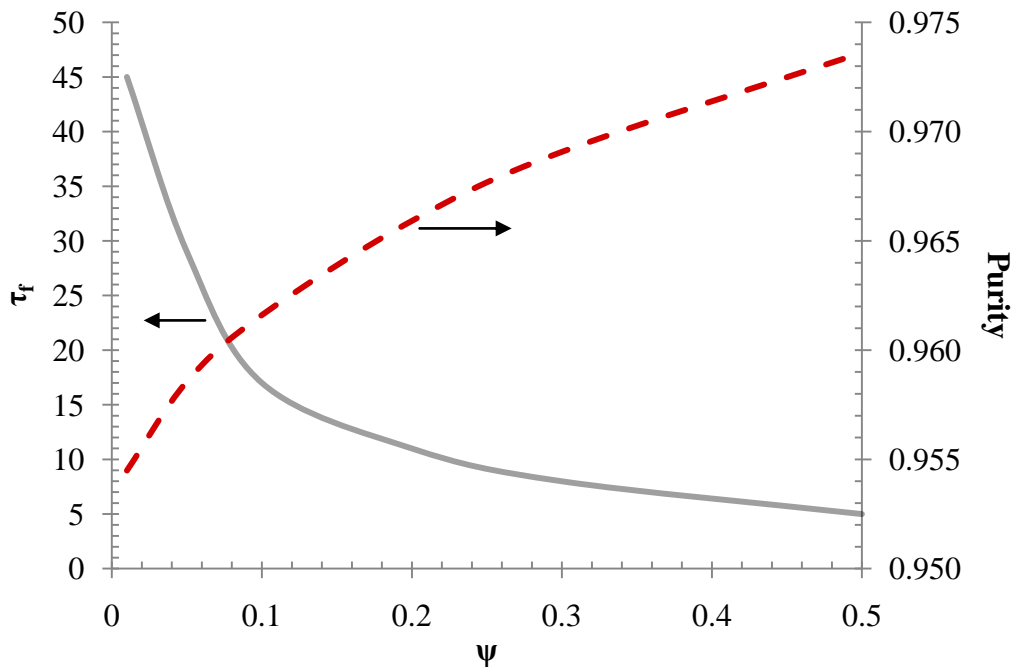


**Figure 25. Growth time at which the maximum purity is achieved and the purity at that time vs. $\psi$. Other simulation parameters are $\beta_A$=2, $\gamma$=0.5, $K$=0.5 and $T$=273.15 K for a 3 stage cascade with feed at stage 1. Purity of the feed solution is 0.9259. The solid, gray line is the growth time at which the maximum purity is achieved and corresponds to the left axis. The red dashed line is the maximum purity and corresponds to the right axis.**

### 2.4.3  Effect of the sweep stream flow rate, feed stage and number of stages

Simulation results showing how the variation of $\beta_A$ and $\psi$ affect the yield and purity of the semi-continuous counter current crystallization operation are presented in Figure 26. These results correspond to a 5 stage cascade with the feed at stage 2, a dimensionless residence time of 3 and a temperature in each stage at the crystallization surface of 273.15 K. The chemical parameters $\gamma$ and $K$ are both 0.5 and the purity of the feed solution is 0.9259.
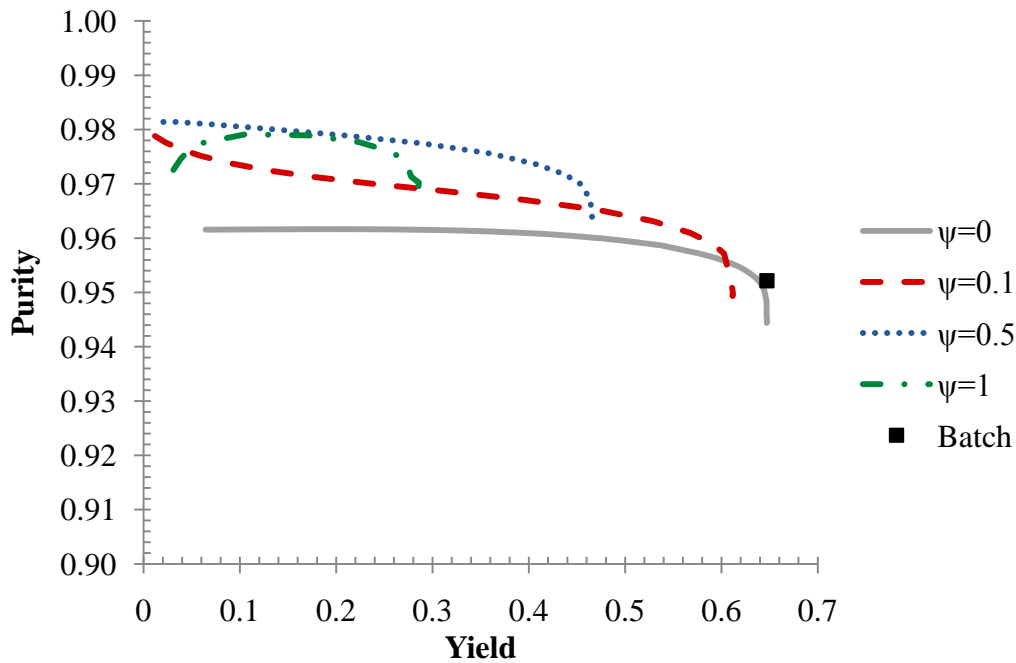


**Figure 26.  Plot of purity vs. yield when $\beta_A$ is varied for various values of $\psi$. Results are for a 5 stage cascade with feed at stage 2, $\tau_f$=3, $\gamma$=0.5, $K$=0.5 and T=273.15 K. Purity of the feed solution is 0.9259. $\beta_A$ varies from a minimum equal to the value of $\psi$ for that line to 100 moving left to right in each individual line.**

From Figure 26, with increasing $\beta_A$ the yield increases while the purity decreases. Recall that $\beta_A$ represents the ratio of volumetric incorporation rate constants into the crystal to feed flow rate. As this value increases, there is more crystal growth compared to flow in the system so the system behaves more like a batch operation. Higher yields result from larger depletion of A in the liquid phase. For these values of $\gamma$ and $K$, larger depletion of A results in greater incorporation of B into the crystal which results in a decrease in purity. The amount of impurity in the crystal increases as the impurity concentration in the liquid phase increases.

The trend with the dimensionless sweep rate ($\psi$) is in the opposite direction. As the sweep rate increases, the yield goes down and the purity goes up at a given value of $\beta_A$. As the sweep stream increases, there is less crystal in the first tank because more material is swept further down the cascade. Less crystal means a lower yield but with less depletion of A relative to B in the liquid phase, the purity of the crystal increases.

The first two curves in Figure 26 for $\psi$=0 and $\psi$=0.1 indicate that while the yield decreases the purity increases markedly when $\psi$=0.1. The best possible result in a system with these values for the chemical-system-specific parameters is higher purity and reduced yield compared to a batch crystallization. The exact optimal operating condition in terms of $\psi$ and $\beta_A$ for this system would depend on the relative value of purity to yield but any increase in purity arising from the use of sweep stream would come at a significant cost in yield. The value of this trade-off must be evaluated on a case-by-case basis but in general the use of a sweep stream is not desirable unless higher purity is much more important than maximum yield.

The individual curves for different values of $\psi$ are not the same length. This occurs because these curves do not represent the same range or values for the parameter $\beta_A$ because some sets of parameters values do not result in crystalline product being grown. Parameter sets that lead to zero product were not studied. The smallest value of $\beta_A$ in each line in Figure 26 is equal to the value of $\psi$ for that line.

A very different situation occurs when $\gamma$ is 2 instead of 0.5. Figure 27 shows the result if all of the parameters are the same as in Figure 26 except for $\gamma$. In this case the purity and yield of the product both increase as the dimensionless incorporation rate constant of species A increases. It is also apparent that the sweep stream has very little effect on the product purity. A slight increase in the maximum attainable purity is apparent when a sweep stream is used but at a significant cost in yield. It is still not possible to achieve a higher yield than a batch crystallization but in this case the purity of the product can exceed the purity of a batch crystallization at nearly the maximum yield if the dimensionless incorporation rate constant is high enough.
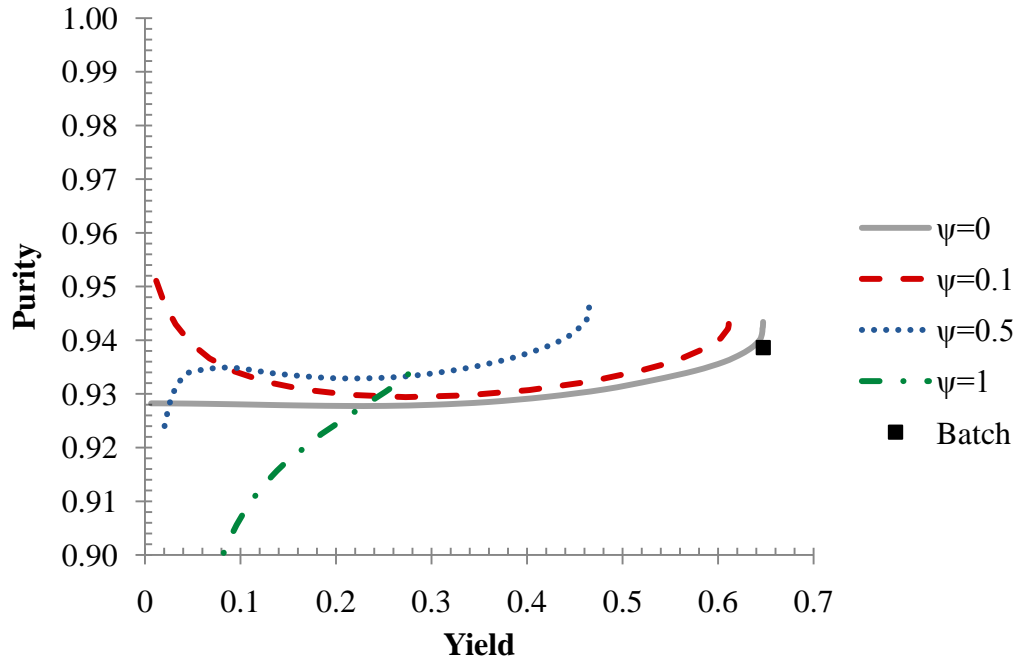
**Figure 27.** Plot of purity vs. yield when $\beta_A$ is varied for various values of $\psi$. Results are for a 5 stage cascade with feed at stage 2, $\tau_f=3$, $\gamma=2$, $K=0.5$ and T=273.15 K. Feed solution purity is 0.9259. $\beta_A$ varies from 0.1 to 100 moving left to right in each individual line.

The same behavior at low values of $\beta_A$ is shown in both Figure 26 and Figure 27. High values of $\psi$ result in purity increasing with increasing $\beta_A$ while small values of $\psi$ result in decreasing purity with increasing $\beta_A$ at small values of $\beta_A$. The behavior at high values of $\beta_A$ is dictated by the system properties $K$ and $\gamma$, while at low values of $\beta_A$ the flow nature of the process is dominant. In the flow dominated regime of Figure 27, there is a transition between the two types of behavior at a value of $\psi$ between 0.1 and 0.5. Further simulations show that the transition occurs at approximately $\psi=0.35$. If this effect is related to the flow nature of the system then a plot similar to Figure 27 but with much lower growth time should show different behavior. This plot is shown in Figure 28 for the same parameters as in Figure 27 except $\tau_f=0.5$.
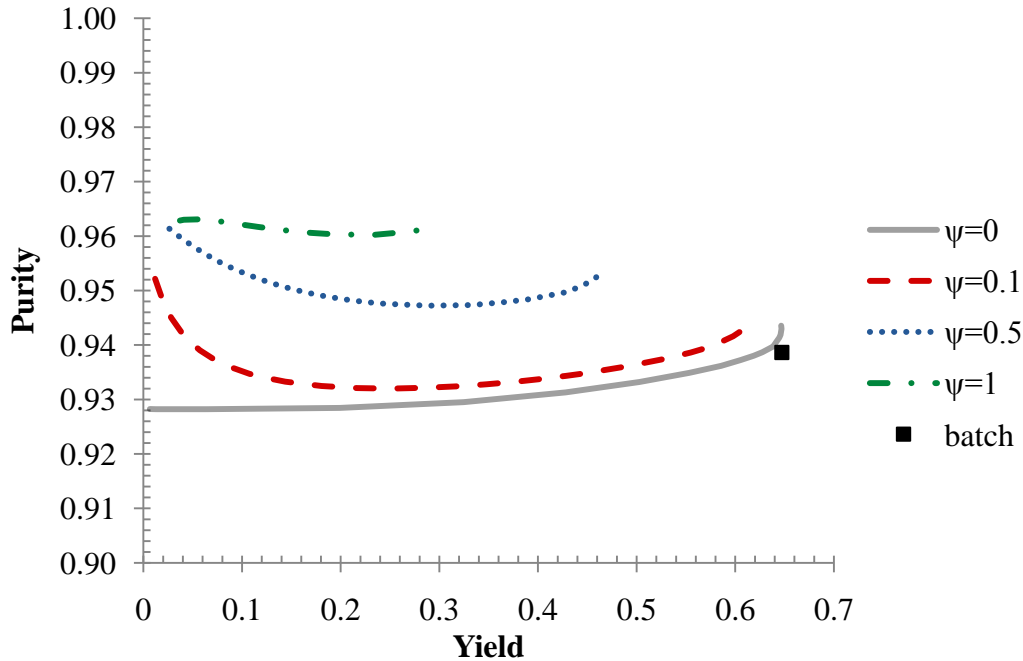
**Figure 28. Plot of purity vs. yield when $\beta_A$ is varied for various values of $\psi$. Results are for a 5 stage cascade with feed at stage 2, $\tau_f$=0.5, $\gamma$=2, $K$=0.5 and T=273.15 K. Feed solution purity is 0.9259. $\beta_A$ varies from 0.1 to 100 moving left to right in each individual line.**

When the growth time is 0.5 the behavior at low values of $\beta_A$ shows decreasing purity with increasing yield for larger values of $\psi$ compared to when $\tau_f$=3. The transition between decreasing and increasing purity at low $\beta_A$ when $\tau_f$=0.5 occurs at approximately $\psi$=0.85. The behavior at low values of $\beta_A$ is controlled by the growth time and the sweep stream flow rate. Operation at low values of $\beta_A$ results in very small yield that are not of interest for practical purposes so these conditions do not need to be studied further.

Figure 29 shows the effect of varying $\beta_A$ and the feed stage position. These results correspond to a 5 stage cascade, dimensionless sweep stream flow rate of 0.1, dimensionless residence time of 3 and temperature at the crystallization surface in every stage of 273.15 K. The chemical parameters $\gamma$ and $K$ are both 0.5 and the purity of the feed solution is 0.9259. Different curves represent operation with the feed entering at a different stage. Each individual curve represents different values of $\beta_A$ for a given feed stage with $\beta_A$ increasing from left to right. The curve for feed at stage one is different than the others because these results correspond to a sweep stream flow rate of zero. There is no potential benefit to a sweep stream entering at the same stage as the feed and so this was not simulated.
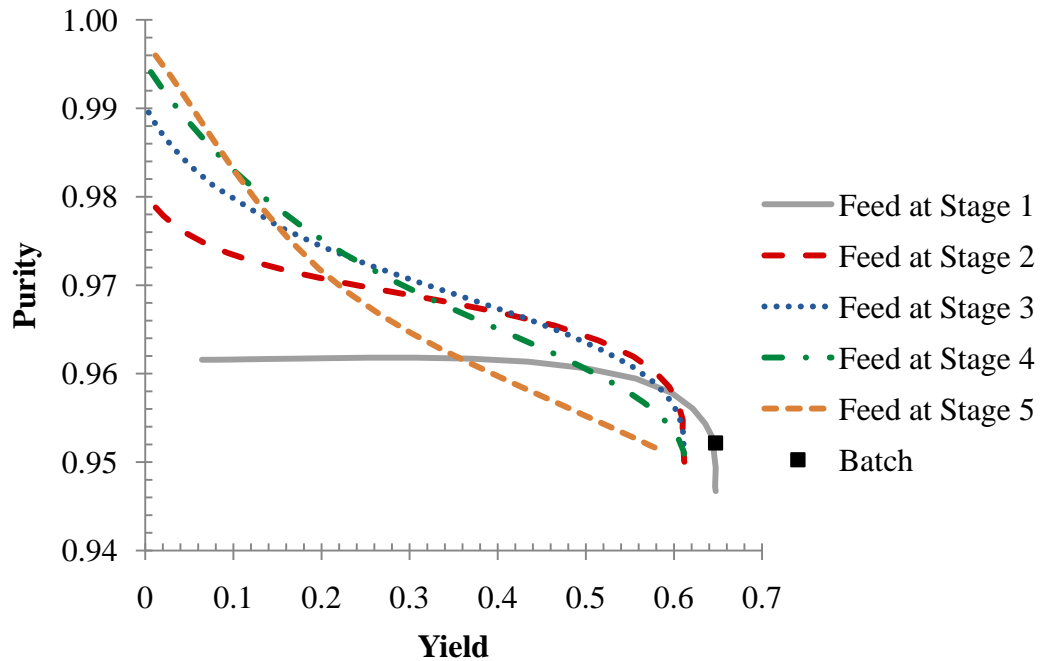
**Figure 29.** Plot of purity vs. yield when $\beta_A$ is varied at various feed stages. $\tau_f=3$, $\psi=0.1$, $\gamma=0.5$, $K=0.5$, 5 stages, and T=273.15 K. Purity of feed solution is 0.9259. $\beta_A$ varies from 0.1 to 100 moving left to right in each individual line. The curve for feed at stage one has a sweep stream flow rate of zero.

The behavior with changing incorporation rate constant is the same as before; as $\beta_A$ increases, the yield increases and the purity decreases. As the feed stage moves farther downstream in the cascade, the yield decreases and the purity increases. Introducing the feed at stage 2 and using a sweep stream gives lower yield but increased purity compared to feeding at stage 1 with no sweep stream. A lower sweep stream flow rate would decrease the gap between the cases for feed at stage 1 and stage 2 but would also diminish the increase in purity achieved by feeding at tank 2. Again any increase in purity due to the sweep stream is accompanied by a decrease in yield.

103
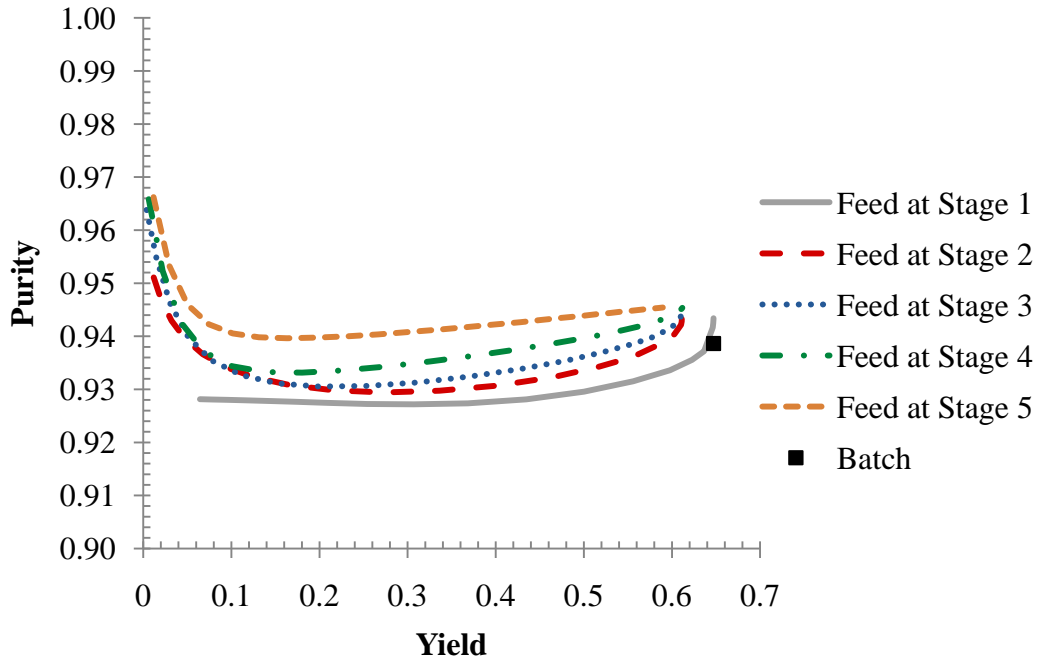
**Figure 30. Plot of purity vs. yield when** $\beta_A$ **is varied at various feed stages.** $\tau_f$=3, $\psi$ =0.1, $\gamma$=2, $K$=0.5, **5 stages, and T=273.15 K. Purity of feed solution is 0.9259.** $\beta_A$ **varies from 0.1 to 100 moving left to right in each individual line. The curve for feed at stage one has a sweep stream flow rate of zero.**

When the ratio of incorporation rate constants, $\gamma$, is 2, the manipulation of the feed stage has no significant effect on the product purity and yield. In this case as before, the sweep stream results in a decrease in the overall yield of the process but now the sweep stream does not provide any increase in purity. When is $\gamma$ greater than two the maximum purity from the counter-current crystallization process occurs at very high values of $\beta_A$ with yields approaching the batch yield. Similar to the behavior shown in section 2.4.1, it is seen that as $\beta_A$ becomes very large the variation of the feed stage has no effect on the yield and purity of the counter-current process. There is no sweep stream for 5 stage cascade with feed at stage 1 which explains why the yield for the case of feeding at stage 1 is higher than for feeding at any other stage.

The previously discussed results indicate that the sweep stream does not provide a positive benefit to the counter-current crystallization process. The sweep stream results in a decrease in yield while only providing an appreciable increase in purity when $\gamma$ is less than one. When $\gamma$ is large, the sweep stream does not provide an increase in purity of the counter-current

crystallization while it does result in a decrease in yield. Subsequent simulation results will not make use of a sweep stream because it does not provide an increase in performance.

Figure 31 and Figure 32 show the effects of varying the total number of stages and $\beta_A$ for $\gamma$ values of 0.5 and 2 respectively.

When $\gamma$=0.5, increasing the number of stages gives higher purity at higher yields. A larger number of stages results in a sharper corner between the high purity results and the highest yield results. This is exactly the desired result when this process was proposed; higher purity compared to batch crystallization at yields that are nearly the same. The semi-continuous process for systems with $\gamma$ >1 and a large number of stages will provide a distinct benefit over batch crystallization.

The exact number of stages used under these favorable conditions must consider that adding stages has decreasing returns on improvements in yield and purity. The maximum performance will be achieved at the maximum purity but using a much smaller number of stages can result in only a small decrease in performance. Simulations can be used to judge the benefits of different total numbers of stages for specific separations. The added costs for equipment, liquid handling and control should also be considered when designing the process and choosing the length of the cascade for a specific separation.

The value of $\beta_A$ necessary to achieve the optimal results is not the largest value used in the simulation. The optimal value of $\beta_A$ in the 9 stage cascade is found to be approximately 1.5-2. The optimal point will occur somewhere near the corner shown in Figure 31. The optimal point must still be determined by some value judgment that specifies a minimum deviation from the batch yield. The best operating point will occur at the value of $\beta_A$ giving the minimum yield and the purity corresponding to those operating conditions.
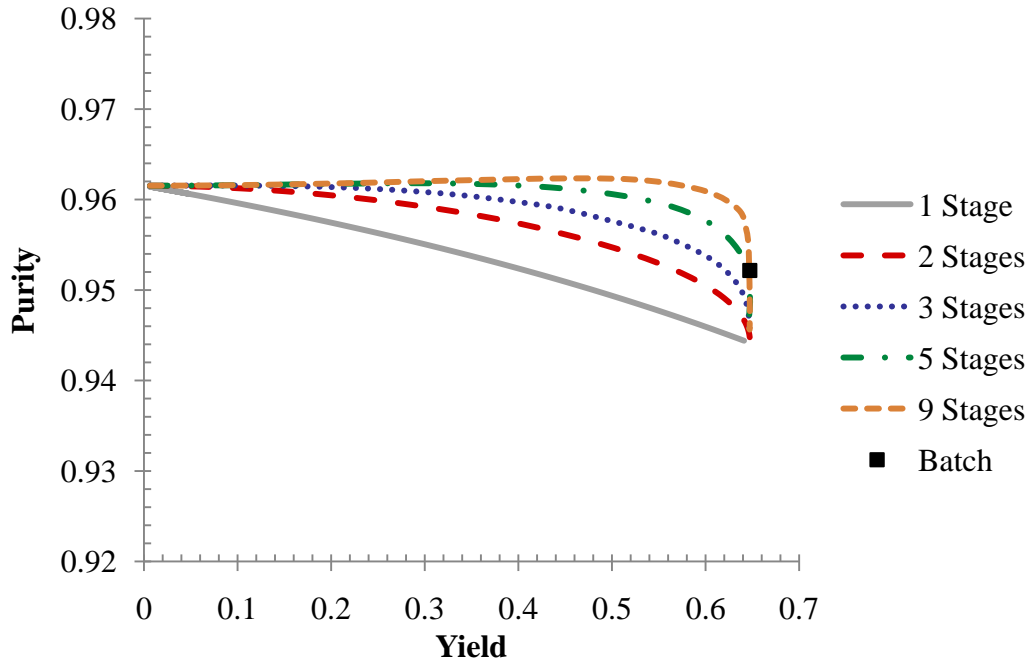
**Figure 31.** Plot of purity vs. yield when $\beta_A$ is varied for different cascade lengths. $\tau_f$=3, $\psi$ =0, $\gamma$=0.5, $K$=0.5, feed at stage 1 and T=273.15 K. Feed solution purity is 0.9259. $\beta_A$ varies from 0.1 to 30 from left to right in each line.
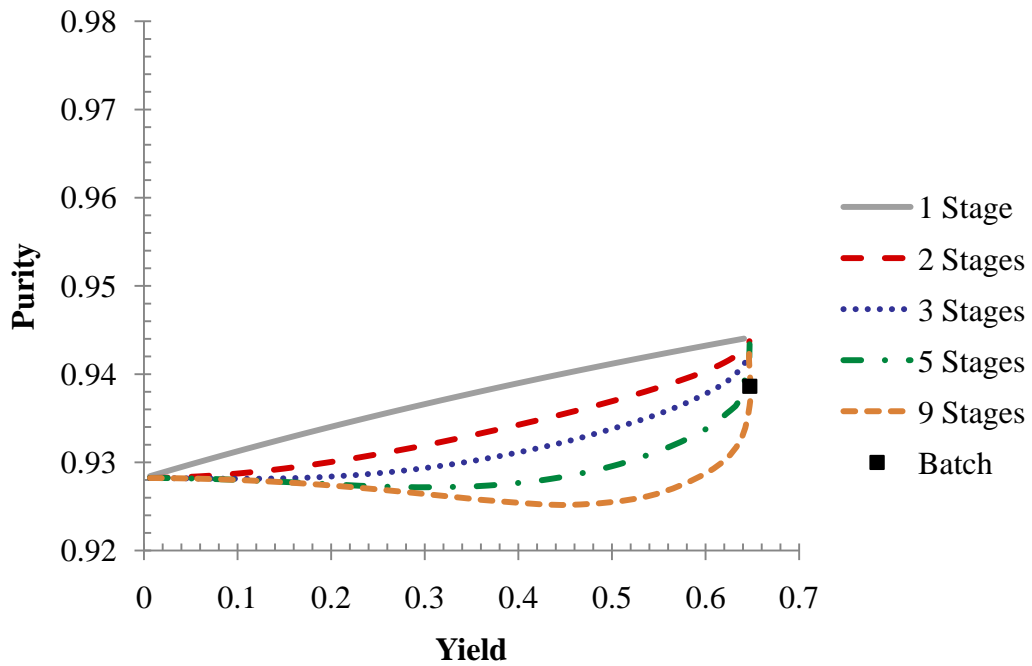


**Figure 32.** Plot of purity vs. yield when $\beta_A$ is varied for different cascade lengths. $\tau_f$=3, $\psi$ =0, $\gamma$=2, $K$=0.5, feed at stage 1 and T=273.15 K. Feed solution purity is 0.9259. $\beta_A$ varies from 0.1 to 30 from left to right in each line.

For $\gamma=2$, the behavior is roughly a mirror image with lower purity being maintained at higher yields. Figure 32 shows that the proposed crystallization process with the solid output taken as the product should not be used for systems with $\gamma>1$. In this situation the results are worse than batch crystallization until very high $\beta_A$ at which point the results are the same no matter the number of stages. A single stage gives the same results as multiple stages and the extra costs of using multiple stages makes use of a large cascade impractical and unnecessary when $\gamma>1$.

These simulation results indicate that in order to maximize yield the incorporation rate constant of A must be as large as possible. This can be accomplished by decreasing the flow rate through the process which results in higher residence times in each tank. The incorporation could also be increased by increasing the available surface area for crystallization. It will always be better to have larger surface area for crystallization so systems should be designed with as much surface area for growth as possible. If this is the case then the flow rate through the process will be the only method of manipulating the dimensionless incorporation rate constant for an existing set of equipment. While the yield always increases with increasing $\beta_A$, the best value of $\beta_A$ must also be chosen with the purity in mind and this will occur at a smaller value of $\beta_A$.

Variation of the total number of stages has shown that the counter-current simulation process can produce better purity than a batch crystallization at comparable when the ratio of incorporation rate constants is less than one, the surface equilibrium constant is order one or less and $\beta_A$ is chosen carefully. This is the stated goal of the proposed process and the conditions under which it is attainable have been made clearer. For systems with $\gamma>1$ the variation of the cascade length shows that a multi-stage process has no benefit over a single stage. It was seen in section 2.4.1 that higher values of $\gamma$ result in lower purities except at very high values of $\beta_A$ but in this section it was seen that this is the case at any number of stages and the proposed process has no benefit when $\gamma>1$. The semi-continuous process will be advantageous for systems with $\gamma<1$ and $K<O(1)$ in cascades with the largest possible number of stages and no sweep stream.

### 2.4.4    *Variation of $\gamma$ necessary for purity to depend on $\beta_A$*

It was shown in sections 2.4.1.2 and 2.4.3 that the staged process offers no benefit when $\gamma \geq 1$.  The amount by which $\gamma$ must be less than one in order for the semi-continuous process to provide a benefit is studied in Figure 33 with a plot of purity vs. yield for different values of $\gamma$ while $\beta_A$ is varied for a 9 stage cascade with feed at stage 1, $\tau_f=3$, $\psi=0$, $y=2$, $K=0.5$ and $T=273.15$ K.  The purity of the feed solution is 0.9259.
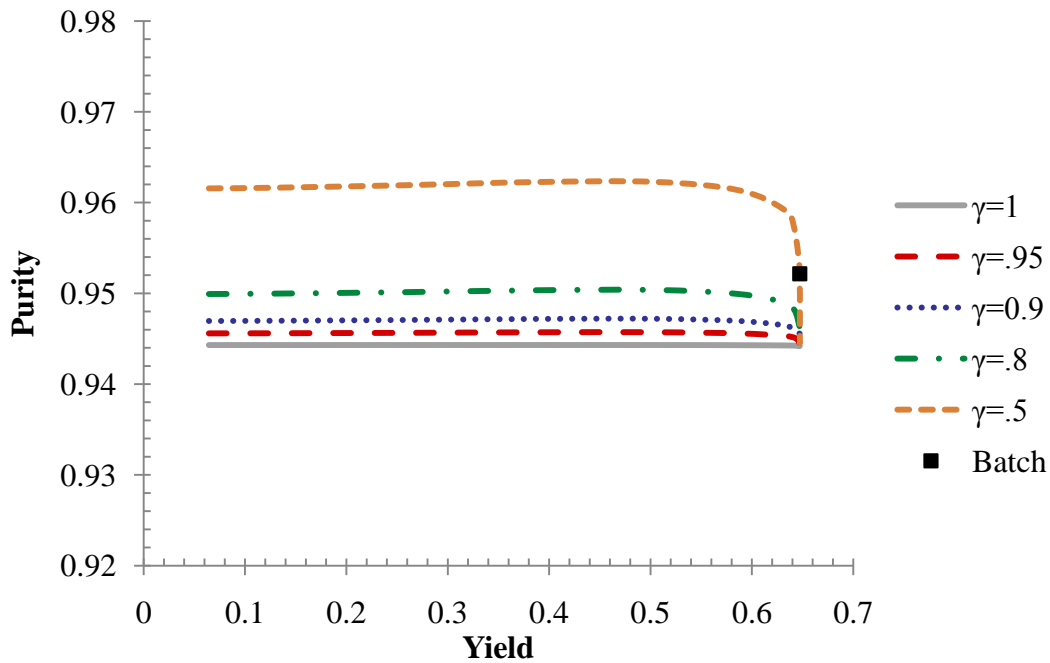


**Figure 33.  Plot of purity vs. yield when $\beta_A$ is varied for different values of $\gamma$ near 1.  $\tau_f=3$, $\psi =0$, $K=0.5$, 9 stages, feed at stage 1 and T=273.15 K. Feed purity is 0.9259. $\beta_A$ varies from 0.1 to 70 moving left to right in each individual line.**

Figure 33 shows that even when $\gamma$ is 0.95 there is a small but appreciable change in purity when $\beta_A$ is varied.  This indicates that the driving force ratio for crystallization is not uniform for values of $\gamma$ that are even a little less than one.  More importantly Figure 33 shows that In order to improve upon the batch performance the value of $\gamma$ must be significantly less than one.

This further limits the set of systems that will benefit from the counter-current crystallization process to those with incorporation rate constant ratios that are significantly less than one.  The value of $\gamma$ at which the semi-continuous process becomes useful will depend on the other system parameters, the available equipment and the value of an increment of purity for a

specific chemical system. Numerical simulations can be used to determine the necessary value if the other chemical parameters are known. In general, the lowest possible value of $\gamma$ will result in the best performance in comparison to batch crystallization as long as that value is below a threshold value determined by all of the chemical system parameters

### 2.4.5 Consideration of possible combinations of K and γ

The previous figures have shown that the crystallization process as described in section 2.1 is useful only when $K$ is less than order one and $\gamma$ is less than one. But it is useful to consider alternative methods of employing the proposed process in order to achieve productive results from a wider array of chemical systems. The possible combinations of $K$ and $\gamma$ can be broken down as $K$ and $\gamma$ greater than 1; $K$ and $\gamma$ less than one; $K$ greater than one and $\gamma$ less than one; and $K$ less than one and $\gamma$ greater than one. The previous results have shown that when $K$ and $\gamma$ are both less than one the crystallization process as described above produces the desired outcome as long as $\gamma$ is a system specific amount less than unity.

The process proposed in section 2.1 has two outputs; the crystal that is taken as the product and the liquid effluent from the growth operation. For systems where $K$ and $\gamma$ are not both less than one, analysis of the effluent stream concentration is informative. The following plots will show the purity vs. yield for both the crystal product and the liquid effluent stream for different values of the chemical system specific parameters

The reported values of yield and purity of the effluent stream are an average over the entire growth cycle. The yield of the effluent stream ($y_L$) is determined by integrating the product of the flow rate out of the final tank and the concentration of component A in the final tank and then dividing this integral by the total amount of component A put into the system.

$$y_L = \frac{\int_0^{\tau_f} \phi_N \theta_{AN} d\tau}{\tau_f} \tag{2.96}$$

where the subscript N denotes a property of the last tank in the cascade.

The purity ($p_L$) is found by integrating the product of the outlet flow rate and the concentration of component A in the final tank and dividing by the integral of the product of the outlet flow rate and the concentration of A plus the concentration of B in the final tank.

$$p_L = \frac{\int_0^{\tau_f} \phi_N \theta_{AN} d\tau}{\int_0^{\tau_f} \phi_N \left( \theta_{AN} + \theta_{BN} \right) d\tau} \tag{2.97}$$

The first situation to be considered is the case when $K$ is less than one and $\gamma$ is greater than one. This is shown in Figure 36 for $K$=0.5 and $\gamma$=2 and in Figure 35 for $K$=0.8 and $\gamma$=2. Each curve is composed of points at different values of $\beta_A$, with $\beta_A$ increasing in the direction of the arrow. Individual points on the curves represent specific values of $\beta_A$. The case where $K$ is greater than one and $\gamma$ is less than one as demonstrated with $K$=2 and $\gamma$=0.5 is shown in Figure 36 and the last case with both parameters greater than one is shown in Figure 37 with $K$=2 and $\gamma$=2.

For all of these figures, the sum of the yield of the crystal product and the effluent stream is one at a fixed value of $\beta_A$. This indicates that all of the material being put into the system is being removed from the system as expected. Figure 34 and Figure 35 show that for $\gamma$>1 and $K$<1 the effluent stream can be a viable product but only if $K$ is close to one. As $K$ approaches one the effluent stream purity becomes increasingly larger than the batch product purity and the purity of the feed stream. The value of $K$ at which the effluent stream becomes a viable product must be determined by simulation with the chemical and operational parameter values for a specific system.

Figure 36 shows that the effluent stream again is not a viable product for $\gamma$<1 and $K$>1. As studied before the batch crystallization gives a product that is less pure than the feed stream but there is the potential for the continuous process with no sweep stream to give higher purity than the batch crystallization and the feed purity while approaching the batch yield. Systems with parameter values in this range will then show benefits when used with the proposed continuous process some of the time. The amount of purity increase over the feed stage may be small and will decrease as $K$ increases.
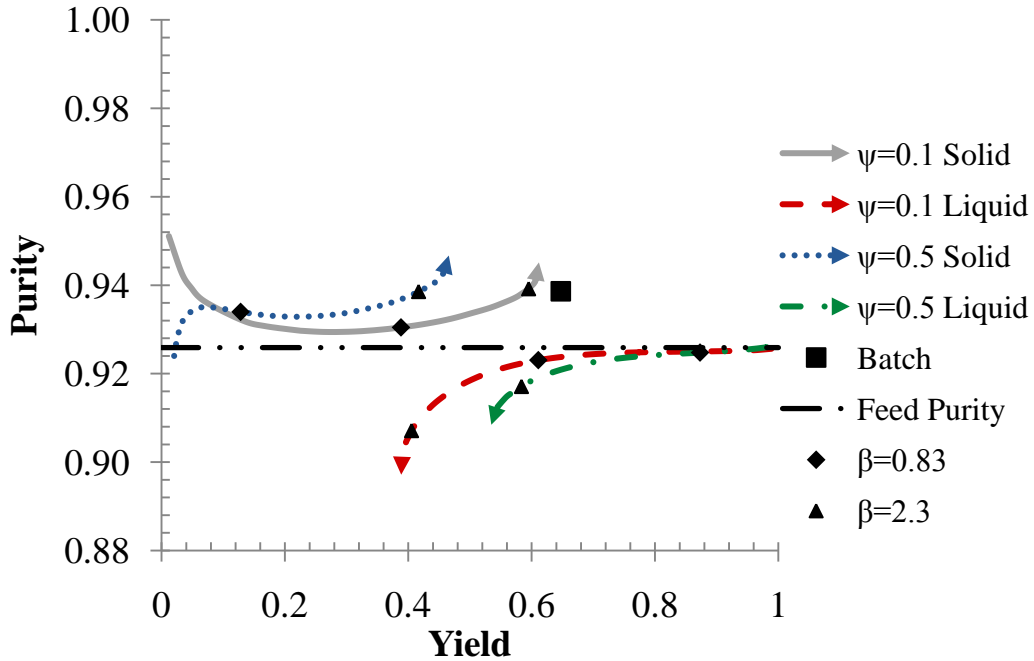
**Figure 34.** Plot of purity vs. yield for the solid product and the liquid effluent when $\beta_A$ is varied at two different sweep stream flow rates. $\tau_f$=3, $\gamma$=2, $K$=0.5, feed at stage 2, 5 total stages and T=273.15 K. Feed solution purity is 0.9259. $\beta_A$ increases in the direction indicated by the arrow on each curve. Points of the same shape correspond to the same value of $\beta_A$.
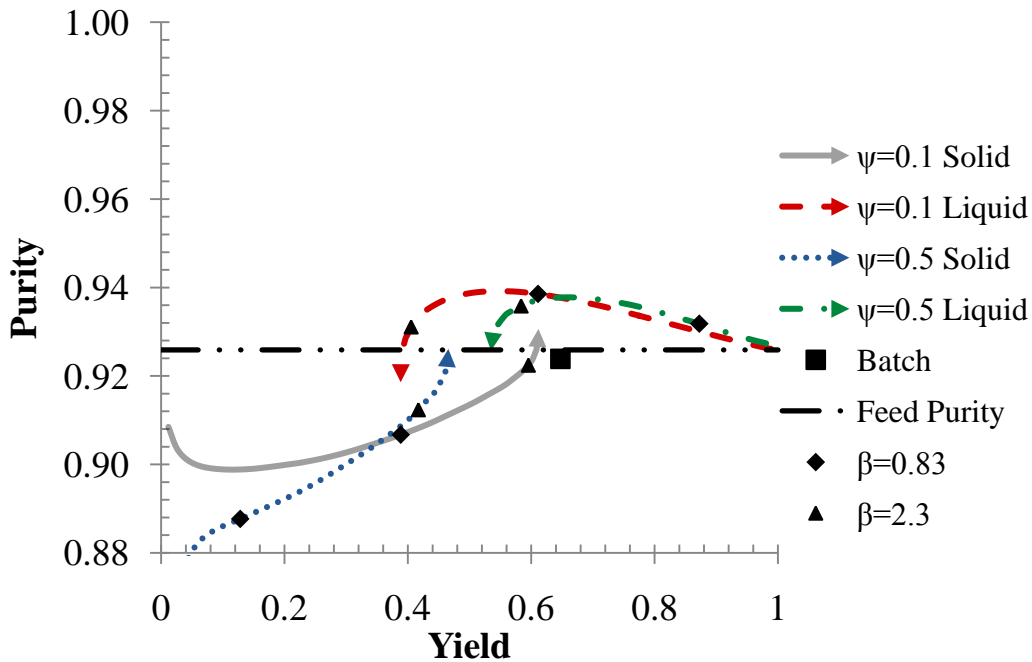


**Figure 35.** Plot of purity vs. yield for the solid product and the liquid effluent when $\beta_A$ is varied at two different sweep stream flow rates. $\tau_f$=3, $\gamma$=2, $K$=0.8, feed at stage 2, 5 total stages and T=273.15 K. Feed solution purity is 0.9259. $\beta_A$ increases in the direction indicated by the arrow on each curve. Points of the same shape correspond to the same value of $\beta_A$.
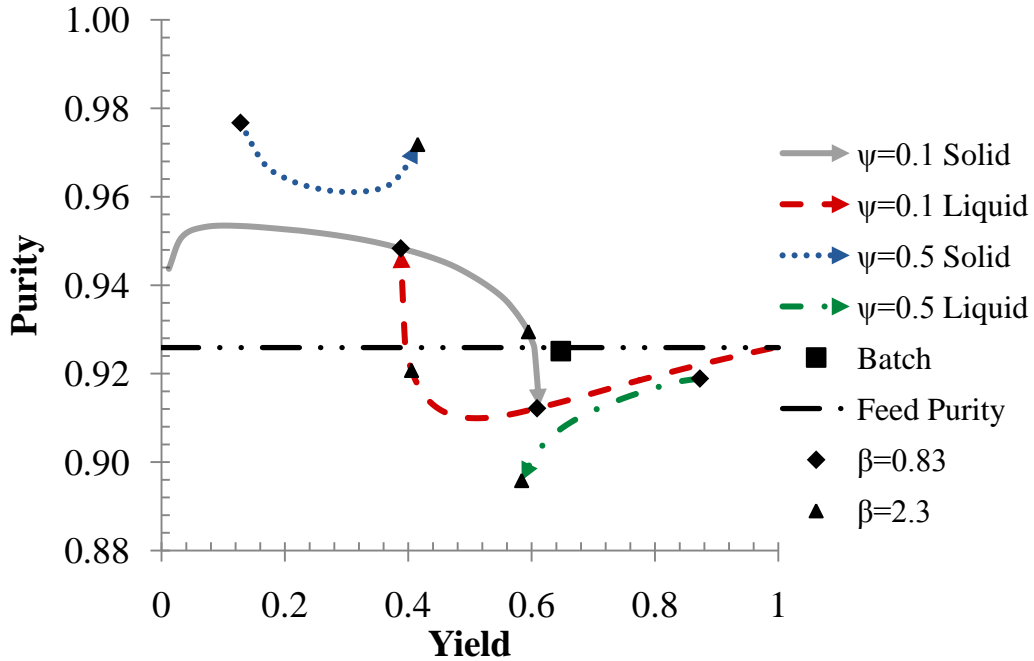
**Figure 36.** Plot of purity vs. yield for the solid product and the liquid effluent when $\beta_A$ is varied at two different sweep stream flow rates. $\tau_f$=3, $\gamma$=0.5, $K$=2, feed at stage 2, 5 total stages and T=273.15 K. Feed solution purity is 0.9259. $\beta_A$ increases in the direction indicated by the arrow on each curve. Points of the same shape correspond to the same value of $\beta_A$.
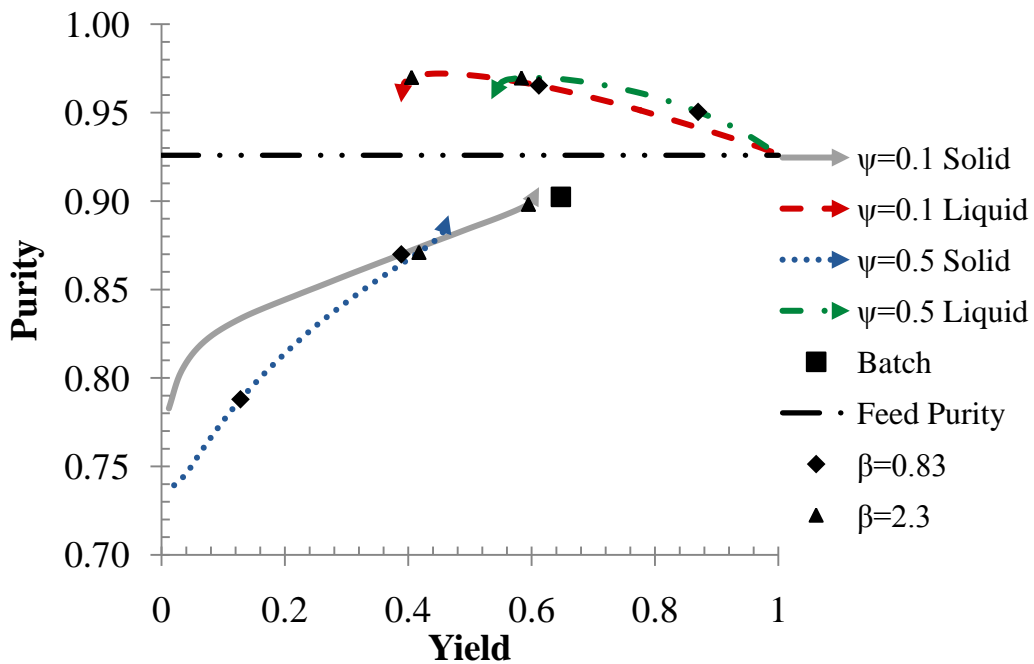


**Figure 37.** Plot of purity vs. yield for the solid product and the liquid effluent when $\beta_A$ is varied at two different sweep stream flow rates. $\tau_f$=3, $\gamma$=2, $K$=2, feed at stage 2, 5 total stages and T=273.15 K. Feed solution purity is 0.9259. $\beta_A$ increases in the direction indicated by the arrow on each curve. Points of the same shape correspond to the same value of $\beta_A$.

When both $\gamma$ and $K$ are greater than one, as in Figure 37, the effluent stream has higher purity and higher yield than the batch result. This is an ideal result as the yield is seen to be significantly greater than the batch yield while still allowing increased purity. The proposed crystallization process is beneficial for systems with $\gamma$ and $K$ greater than one except that the stream previously called the "waste" stream should now be taken as the product. The crystal product is now waste and can be discarded.

This situation is ideal because the product is a liquid with high yield and purity in comparison to batch crystallization but is not expected to be common. $K$ greater than one indicates that the impurity has a higher concentration in the crystal than the component of interest and $\gamma > 1$ indicates that the impurity is incorporated into the crystal faster than the component of interest. These two properties may tend to happen together but it is expected that in general the component of interest will favor incorporation of itself in both rate and amount. Systems with $\gamma > 1$ and $K > 1$ are expected to be very rare but will provide excellent results with the proposed process if the liquid effluent is taken as the product.

A summary of the benefits of the proposed process for different combinations of the chemical system specific parameters is given in Figure 38. The actual parameter values for real systems are expected to most often fall in the lower-left quadrant but these parameters must be determined experimentally.

| | $K < 1$ | $K > 1$ |
|---|---|---|
| $\gamma > 1$ | SOMETIMES use with counter-current process with liquid effluent taken as product. | DO use with counter-current process with liquid effluent taken as product. |
| $\gamma < 1$ | DO use with counter-current process with solid taken as product. | SOMETIMES use with counter-current process with solid taken as product. |

**Figure 38. Diagram of different combinations of the chemical system specific parameter and their utility with the proposed counter-current crystallization process.**

### 2.4.6  Comparison of Operation with and without a Liquid Handling Tank

To this point the simulation has been used to study the system when the liquid contents of the final tank are retained between growth cycles. The results from a process where this liquid is discarded will now be compared to the previous results.

First the purity vs. yield of the solid product will be shown for a range of $\beta_A$ values at different values of $\gamma$ for the process with and without the liquid handling tank. These results are for a system with the same number of active tanks such that the overall process when a liquid handling tank is used has one additional tank. These results are shown in Figure 39.
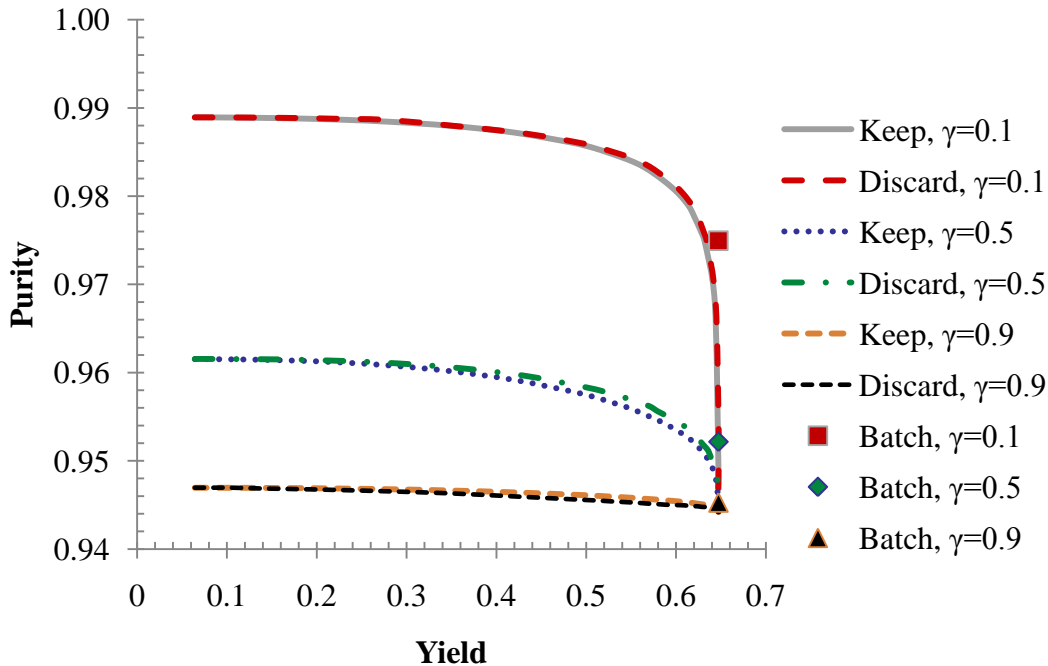
**Figure 39.  Plot of purity vs. yield comparing process with retention of liquid from final stage with removal of liquid from final stage when $\beta_A$ is varied at various values of the constant ratio $\gamma$. $\tau_f$=2, $\psi$=0, 3 stages, feed at stage 1, $K$=0.5, and T=273.15 K.  $\beta_A$ varies from 0.1 to 30 moving left to right in each individual line. Individual points correspond to the batch comparison points for different values of $\gamma$.  The purity of the feed solution is 0.9259.**

Figure 39 indicates that there is a very small difference in the performance of the process with and without the liquid handling tank.  These results indicate that the decision to keep or discard the liquid contents of the last tank depend on the value of $\gamma$.  At $\gamma$=0.9 better results are achieved when keeping the liquid while at $\gamma$=0.5 discarding the liquid gives better results.  The difference though in all cases is slight and a different comparison is necessary to decide which approach is better in general.

The comparison so far has been between systems with the same number of active tanks but a more appropriate comparison could be processes with the same number of total tanks. So that a cascade with three active tanks and a liquid handling tank where the liquid from the last tank is retained should be compared to a process with four active tanks where the liquid from the last tank is discarded.  The results for this comparison are given in Figure 40 as a plot of yield vs. purity at different values of $\beta_A$.
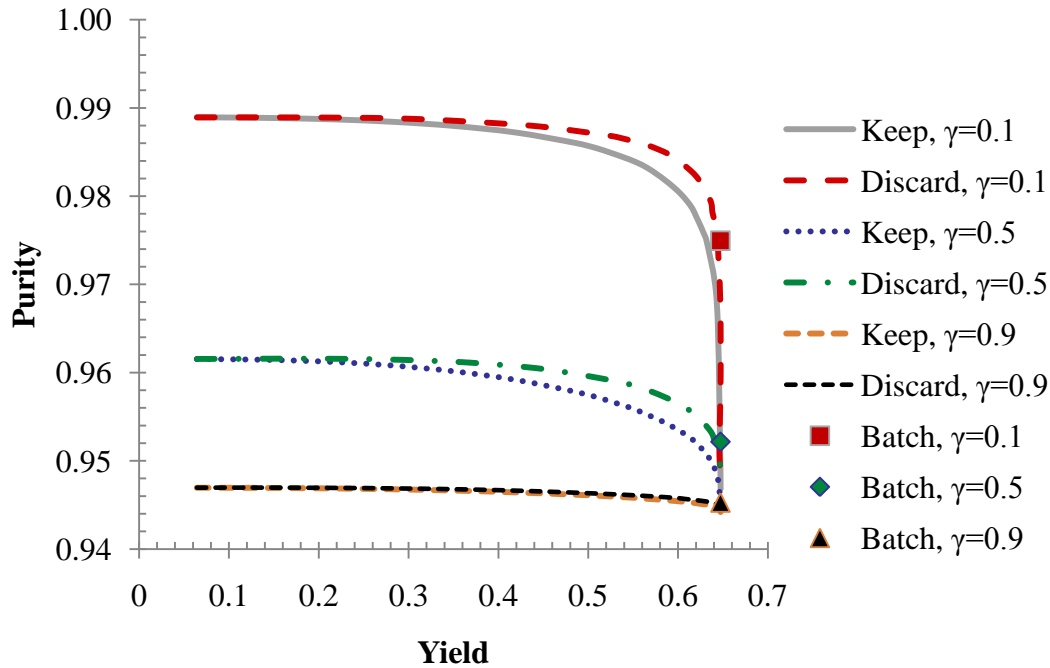
**Figure 40. Plot of purity vs. yield comparing a 3 stage process with retention of liquid from final stage to a 4 stage process with removal of liquid from final stage when $\beta_A$ is varied at different values of $\gamma$. $\tau_f$=2, $\psi$=0, feed at stage 1, $K$=0.5, and T=273.15 K. $\beta_A$ varies from 0.1 to 30 moving left to right in each individual line. Individual points correspond to the batch comparison points for different values of $\gamma$. The purity of the feed solution is 0.9259.**

Use of a liquid handling tank is now seen to be unfavorable because the liquid handling tank will provide a much larger benefit if used as an active tank while discarding the liquid from the last tank in each growth stage. This result might have been expected given the previous results indicating that additional tanks provide improved performance and that there was only a slight difference between operation when the liquid in the final tank is retained and when it is discarded.

This discussion indicates that retaining the liquid from the last tank is not beneficial. The empty tank will provide more utility if used as an active tank during the growth process when the liquid from the last tank is discarded. It is also apparent that the results for these two processing options are almost identical when the same number of active tanks is employed. This means that the conclusions drawn in the previous sections still apply to the process when the liquid from the effluent tank is discarded.

## 2.5     Summary of Process Description and Simulation

A counter-current crystallization process has been proposed that operates in a semi-continuous manner and seeks to eliminate multi-phase flows.  This is done by confining crystal growth to fixed growth surfaces and performing a liquid transfer operation along with systematic shifting of the feed and outlet points along a cascade of tanks.  The two outputs from this process are a solid crystalline product and a liquid effluent stream.  This process is complicated but has operational similarities to simulated moving bed chromatography.  The benefits of the proposed process are multiple recrystallizations to allow for improved purity and the elimination of multi-phase flow handling.

The yield of a crystallization process is determined by the concentration and flow rate of the effluent stream.  The concentration of the effluent is constrained by the solubility of species A in the solvent of interest.  A batch crystallization run until completion will provide the maximum possible yield and any continuous crystallization process will at best be able to match this batch yield unless the effluent stream is altered.

A model has been developed for batch crystallization and the proposed semi-continuous, counter-current crystallization operation.  The system specific parameters $C_A^*(T)$, $K$, $\gamma$ and $n$ must be measured experimentally before using this simulation to predict the separation performance in the proposed counter-current crystallization operation.  This simulation indicates that this process can give superior purity and comparable yield to batch crystallization run until completion from both the crystalline product and the liquid effluent for different values of the parameters $K$ and $\gamma$.

The solid crystalline output is the appropriate product to use when the ratio of the incorporation rate constants of the impurity to the incorporation rate constant of the product ($\gamma$) is less than one and $K$ is order one or less.  The liquid effluent should be taken as the product when $\gamma>1$ and $K$ is very close to or greater than one.  This liquid effluent is the waste stream as described in the original description of the process but for certain parameter values the simulation results indicate that it will provide a liquid product with higher purity and yield than batch crystallization.  In this scenario the crystallized solid should be discarded as waste.

Simulation results also indicate that the use of a sweep stream and tanks upstream of the feed point should not be employed when the solid is taken as the product because of the negative effect on yield. The sweep stream was seen to give increased purity but only at a significant cost in product yield. A large number of stages was found to provide higher purity at yields approaching the batch yield when $\gamma < 1$. The benefit of increasing the number of stages decreases as more stages are added so this must be weighed against capital and operational costs of larger cascades.

Use of the process with the liquid contents from the effluent tank discarded after each growth cycle was found to be better than operation with retention of the liquid in the effluent tank by use of an extra liquid handling tank. The difference in performance for these two operating principles was found to be very small when an equal number of active tanks were compared but use of the liquid handling tank as an active tank for crystallization provides superior results. This is in agreement with the conclusion that more tanks provide better performance. Results generated from simulations making use of the liquid handling tank are also appropriate for the system without a liquid handling tank if the number of active stages is held constant..

Key assumptions involved in developing this model are the equilibrium expression at the liquid-solid interface and the expressions for crystal growth. The equilibrium constant $K$ is assumed to be only a function of temperature. Experimental work must be done to validate the assumptions in this model and provide input to help refine this model to better predict real behavior. Batch experiments used to test the validity of this model are discussed in Chapters 3 and 4.

# 3.    Preliminary Batch Experiments

Initial investigations of the impurity distribution between the liquid and solid phases during batch crystallization were performed before development of the model described in Chapter 2.  This work was done at the St. Johann campus of Novartis International AG in Basel, Switzerland, to take advantage of existing experimental setups for performing traditional seeded, batch crystallizations.

The goal of these experiments was to measure how different parameters affect the distribution of impurity between solid and liquid phases.  The effect of the final temperature, initial concentration of the component of interest and the initial purity of the solution were studied.  The chemical compounds used in these experiments will be described first followed by an outline of the experimental method and finally the results from the batch experiments.


## 3.1    Chemical System for Experimentation

Cyclosporine A is a member of a family of similar structures that was used as the chemical system for these batch experiments.  Cyclosporine A is a large ring shaped compound composed of 11 amino acids.  The structure of cyclosporine is shown in Figure 41.  The cyclosporines are a good choice for batch experimentation because they have a strongly temperature dependent solubility and consequently readily crystallize from solution.

Cyclosporine A is the desired compound but the raw material contains at least 11 discernible impurities which are relatives of cyclosporine A.  These impurities have a range of very small structural differences including the presence of an extra double bond, an ethyl instead of a methyl group or a single chemical bond connecting two adjacent amino acids in a slightly different way.  These very slight structural differences make it likely that cyclosporine A forms solid solutions with at least some of the other cyclosporines.  It is very difficult to obtain extremely pure samples of different cyclosporines due to their similar structures and so phase behavior for pairs of cyclosporines has not been measured and solid solution behavior has not been proven in the literature.

119
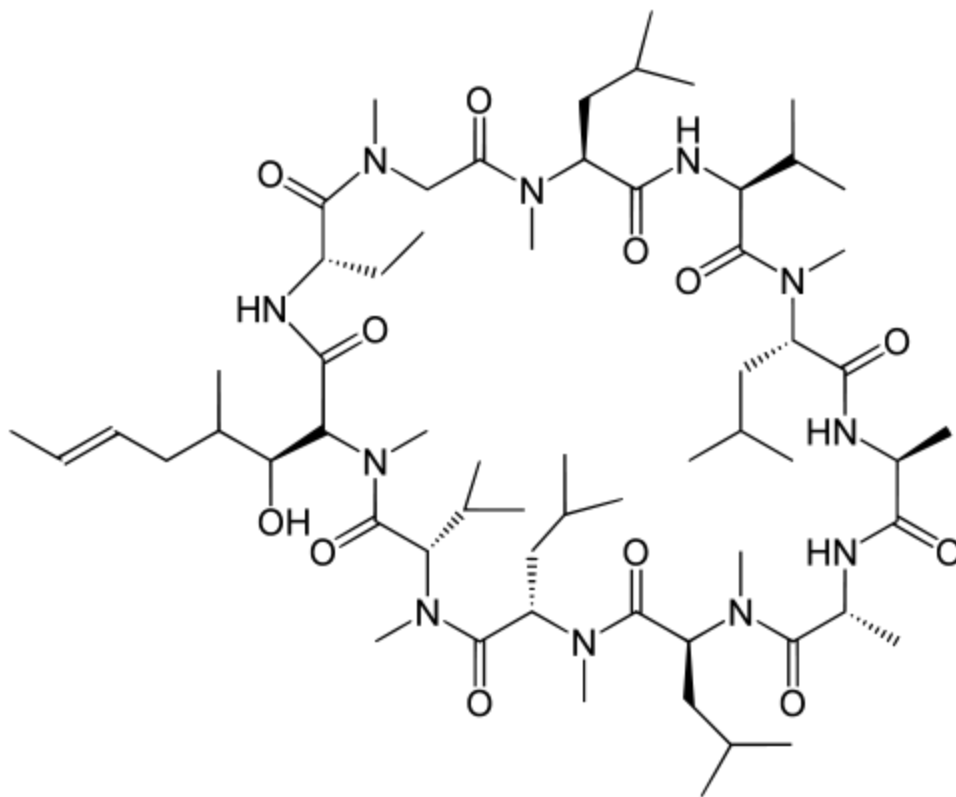
**Figure 41.  Chemical Structure of Cyclosporine A.**

The raw material for these experiments as supplied by Novartis consisted of 89% by mass cyclosporine A and 11% total impurities.  Of those 11% impurities, 9-10% are other cyclosporine molecules and the remaining 1-2% are solvents or other trace materials.

## 3.2    Experimental Method

The experiments were conducted in a stirred batch vessel under temperature control. Experimental data consisted of the temperature profile and HPLC analysis of the starting material, product, mother liquor and wash liquor.  Additionally, UV-Vis measurements were collected for some experiments.  The UV-Vis measurements were obtained from a probe placed in the reaction vessel which provided real-time absorption information.

All experiments were carried out using the following approach.  The starting solution was heated to $50^0$ C in order to dissolve all of the solids.  The solution was then cooled at a rate of 0.5 K/min to the temperature at which the solution was 2.5 times supersaturated as deter-

mined from the solubility curve for cyclosporine A. The solution was then seeded and the temperature was held constant for 1 hour. The solution was then cooled or heated to the final temperature at a rate of 0.3-0.5 K/min after which it was held at this temperature for 0-15 hours.

Experiments were conducted in a FlexyLab controlled lab reactor. A 100 mL reactor vessel equipped with mechanical stirrer and temperature probe were used. Temperature control was achieved through cooling or heating of the external wall of the reactor. The crystals grown during an experiment were vacuum filtered and washed with a small amount of acetone before being dried in an oven overnight.

The mother liquor and wash liquid were collected separately in order to determine if the wash liquid was resulting in significant dissolution of the crystals. If the wash liquid concentration is very similar to the mother liquor concentration then the wash is likely succeeding in removing some of the mother liquor stuck to crystals as opposed to dissolving some of the crystalline product.

The concentrations from the starting material, crystalline product, mother liquor and wash liquid were calculated from HPLC data in the following manner. The liquid phases were used directly while a little of the solid product was dissolved in acetone for HPLC analysis. A calibration chart for cyclosporine A was provided by Novartis and it was used to calculate the concentration of all the cyclosporines in a HPLC sample. The use of the cyclosporine A calibration chart for all cyclosporines assumes that absorbtivity for all cyclosporines is the same. Given the large size and similar structure of the molecules, this was deemed a good assumption.

The amounts for each species in the feed, product, mother liquor and wash liquor were entered into a mass balance. Good results were achieved in general with the overall mass balances closing to within 10% in most cases, and often closer to 5%. Individual data points for different impurities were neglected in separation analysis if the mass balance was off by more than 15%.

The variables of interest in this study were the final temperature, the initial concentration and the initial purity. The final temperatures used were 2.5, 20, 30 and 35$^0$C. The initial concentrations were 0.18, 0.264 and 0.131 mass of cyclosporine A per unit mass total solution.

The initial purities used were 0.79, 0.89 and 0.94 mass of cyclosporine A per unit mass solids. Other possible variables include the cooling rate and the holding time. In order to minimize experiments and to focus on the most important factors, the cooling rate and the holding time were chosen so that they had as little effect as possible on the result. Experiments were done to show that holding times greater than or equal to 4 hours have no effect on the product composition and that cooling rates less than 0.7 K/min after seeding also did not affect the results.

## 3.3    Experimental Results

The representation of the depletion behavior that was determined to be most useful is the separation factor. It is defined by the following equation.

$$\alpha_{Aj} = \frac{C_{j,S}/C_{j,L}}{C_{A,S}/C_{A,L}} \qquad (3.1)$$

where $C$ is a concentration, subscript A refers to cyclosporine A (or more generally the component of interest), subscript $j$ refers to a specific impurity, $L$ refers to the liquid phase and $S$ refers to the crystal phase. This quantity represents the ratio of the distributions of an impurity and the component of interest between the crystal and the liquid phases. A separation factor of 1 indicates that no purification has taken place; the crystal product has the same purity as the initial solution. A separation factor of 0 indicates that there is none of that impurity in the crystal which means that a perfect separation has occurred. A separation factor that is greater than one indicates that the impurity has been concentrated in the crystal compared to the target component.

The separation factor measured in these experiments is not an equilibrium property. The time dependent concentration profiles of the solid and liquid phases during crystallization affect the measured value. If the crystallization were to be operated at a constant temperature with very small crystal particles until equilibrium is reached in both the solid and liquid phases,

then the measured separation factor will be equal to the surface equilibrium constant at the temperature of the crystallization as defined in the model presented in Chapter 2.  This would be a difficult condition to approach experimentally because enough time must be allowed for diffusion to occur in the solid phase so that any concentration profiles are smoothed out.

### 3.3.1   Cyclosporine C, U and V

The measured separation factors and yield as functions of final temperature, initial concentration and initial purity for three cyclosporine impurities are shown in Figure 42 through Figure 48.  The points in each graph correspond to the situation where all parameters are held constant except for the one varied along the x-axis.  For example, in a plot where temperature is varied the initial concentration and purity are held constant for each experiment.
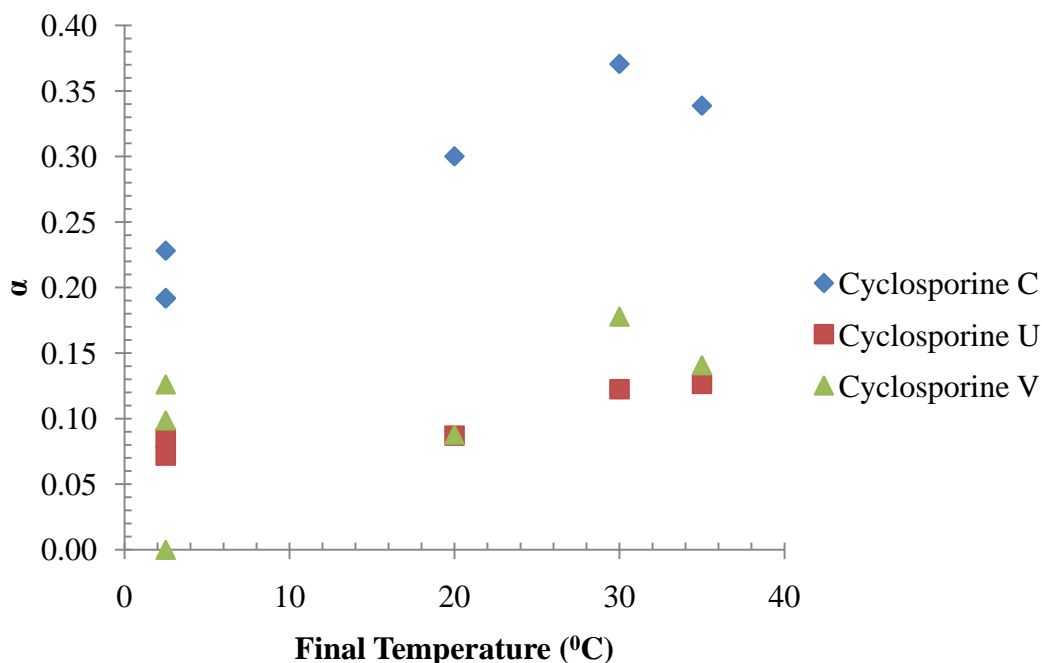


**Figure 42.  Experimental separation factors as a function of final temperature from batch experiments for three cyclosporine impurities.**
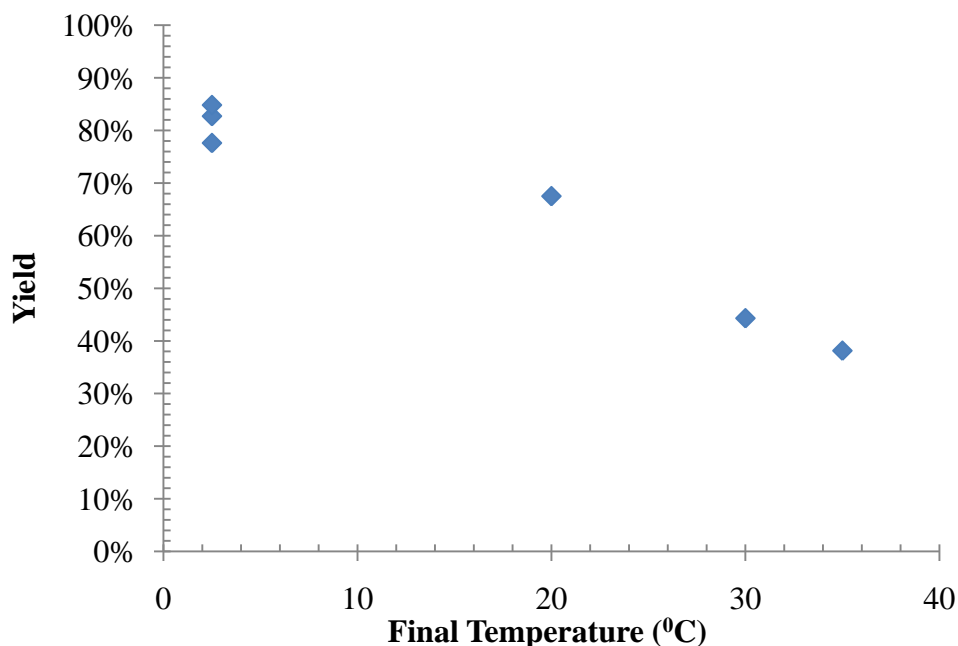
**Figure 43.  Yield as a function of final temperature from batch experiments.**

Figure 42 shows that there is generally a clear trend with the final temperature showing that the separation factor increases with increasing temperature.  Increasing values of the separation factor indicate worse separations so increasing temperature results in less separation of the impurity from cyclosporine A.

It is also seen in Figure 43 that yield decreases with increasing final temperature.  As temperature increases the solubility of cyclosporine A in the solvent increases and so yield must decrease while at higher temperatures it is more likely for the impurity molecules to be included in the crystal and so it is expected that the separation will be worse. This is the behavior shown in these plots.  The relationship between the separation factor and temperature is seen to be generally linear.
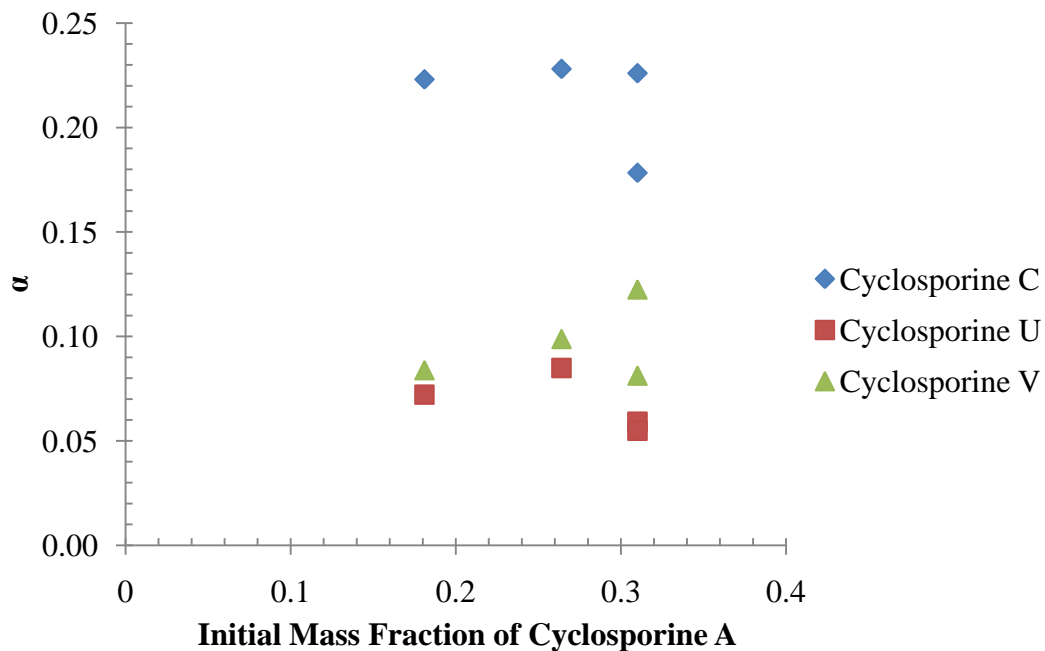
**Figure 44.** Separation factor as a function of initial concentration for three cyclosporine impurities from batch experiments.
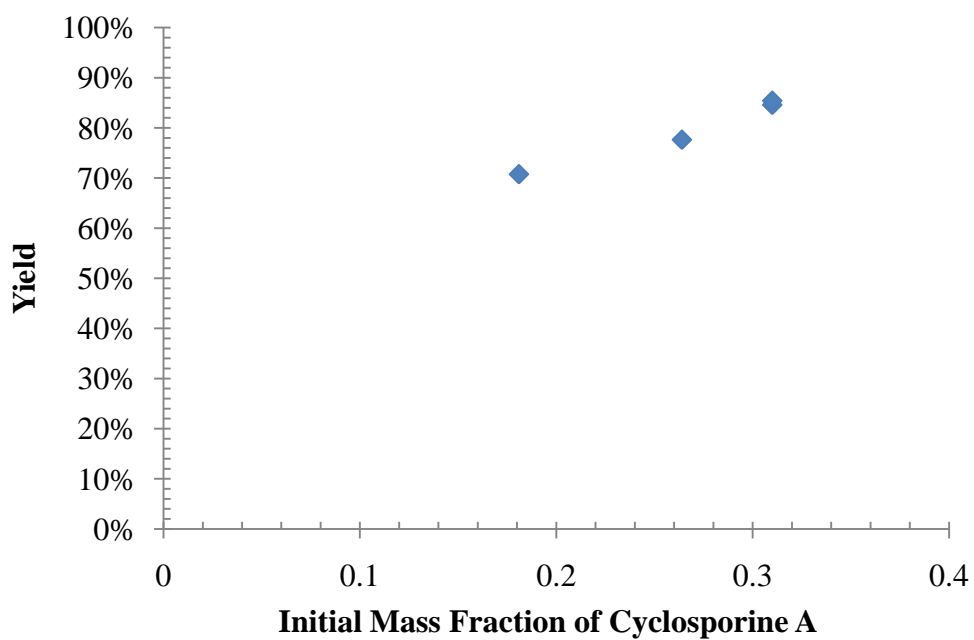


**Figure 45.** Yield as a function of initial cyclosporine A concentration from batch experiments.

Figure 44 shows that there is no apparent trend of the separation factor with the initial concentration. The yield is seen in Figure 45 to increase as the initial concentration increases. At a given temperature, increasing the starting concentration means the initial supersaturation is increased while the saturation concentration is unchanged. A larger driving force allows more crystal to be generated under experimental conditions where steady state is approached. Steady state is approached under the conditions of these experiments.

Figure 46 shows that the separation factor decreases slightly with increasing initial purity. This indicates that purer starting materials lead to purer products. This result indicates that multiple recrystallizations would result in better purity when separating cyclosporine A from its impurities. The yield is seen in Figure 47 to not depend on the initial purity. The fact that the yield does not change is good because it supports the assumption that the solubility behavior can be determined by ignoring all of the impurities in solution. When approaching equilibrium, the yield is determined by the initial supersaturation. If the initial concentration of cyclosporine A is unchanged then the supersaturation is unchanged and the same yield will be achieved if the amount of impurities does not affect the solubility of cyclosporine A in the solvent.

### 3.3.2 Cyclosporine D

Cyclosporine D gave very different results than any of the other cyclosporine impurities. The structural difference between cyclosporine D and A is that cyclosporine D has one less methyl group on the side chain of one amino acid residue. Plots of the separation factor vs. final temperature and initial concentration are shown in Figure 48 and Figure 49. No plot is included for initial purity due to lack of data. The mass balance on cyclosporine D was only within the stated tolerance (15%) for one of the experiments where initial purity was varied. Note that the plots for yield as a function of final temperature and initial concentration from above (Figure 43, Figure 45 and Figure 47 ) are the appropriate plots here as well.

Although the data does not indicate clear trends with the variables studied, the key difference in this case is that the separation factors are greater than one. This means that cyclosporine D is added to the crystal preferentially to cyclosporine A. Because cyclosporine D is more concentratd in the solid versus the liquid than cyclosporine A, it is more difficult to separate A from D using crystallization. Multiple crystallizations would be necessary with higher purities of cyclosporine A in each stage in order to decrease the concentration of cyclosporine D in the crystal. More recrysatllization steps would be required than for an impurity with separation factor less than one. This situation is expected to be relatively rare and will not be the focus of subsequent work.
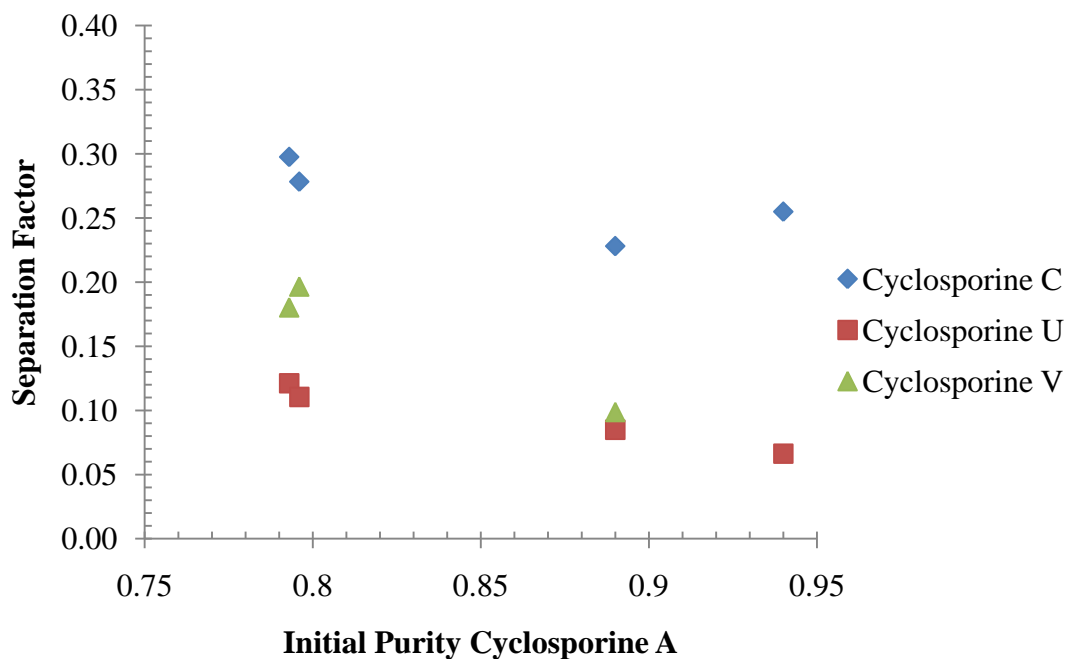
**Figure 46.** Separation factor as a function of initial purity of cyclosporine A for three cyclosporine impurities from batch experiments. Purity is defined as mass fraction of cyclosporine A on a solvent free basis.
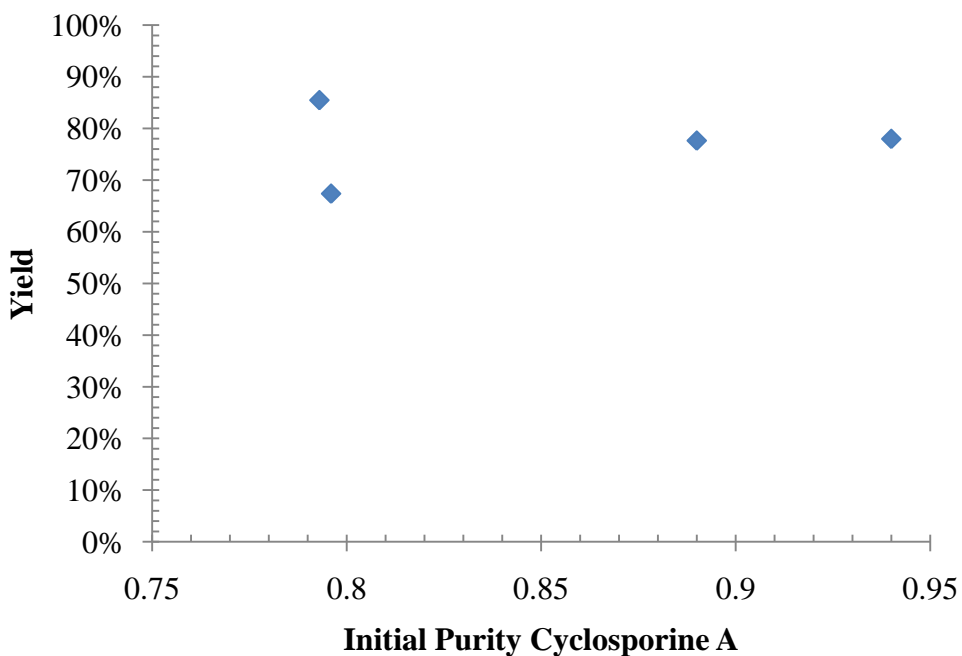


**Figure 47.** Yield as a function of initial purity from batch experiments. Purity is defined as mass fraction of cyclosporine A on a solvent free basis.
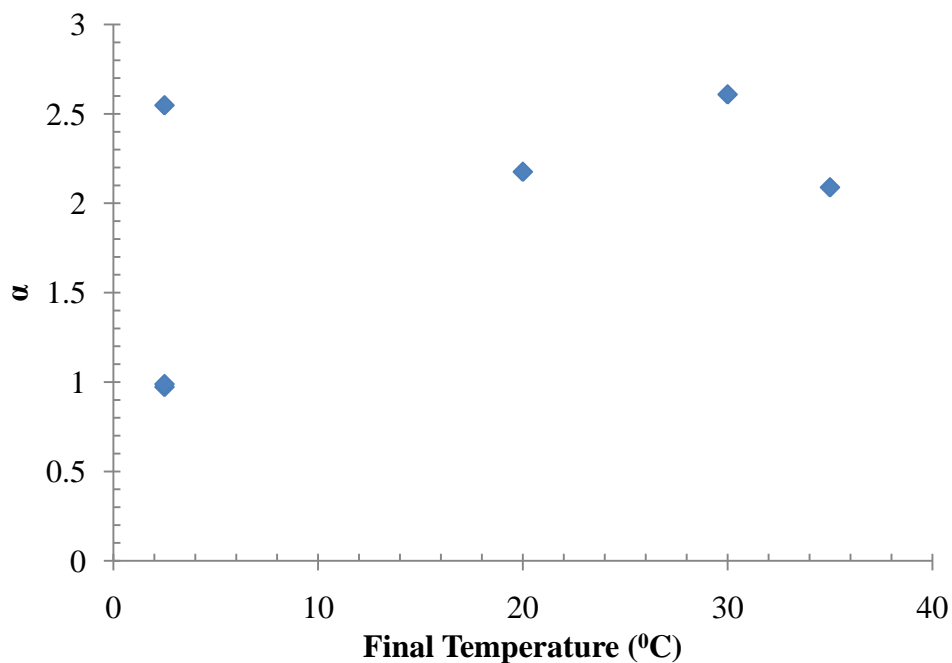
**Figure 48. Separation factor as function of final temperature for cyclosporine D from batch experiments.**
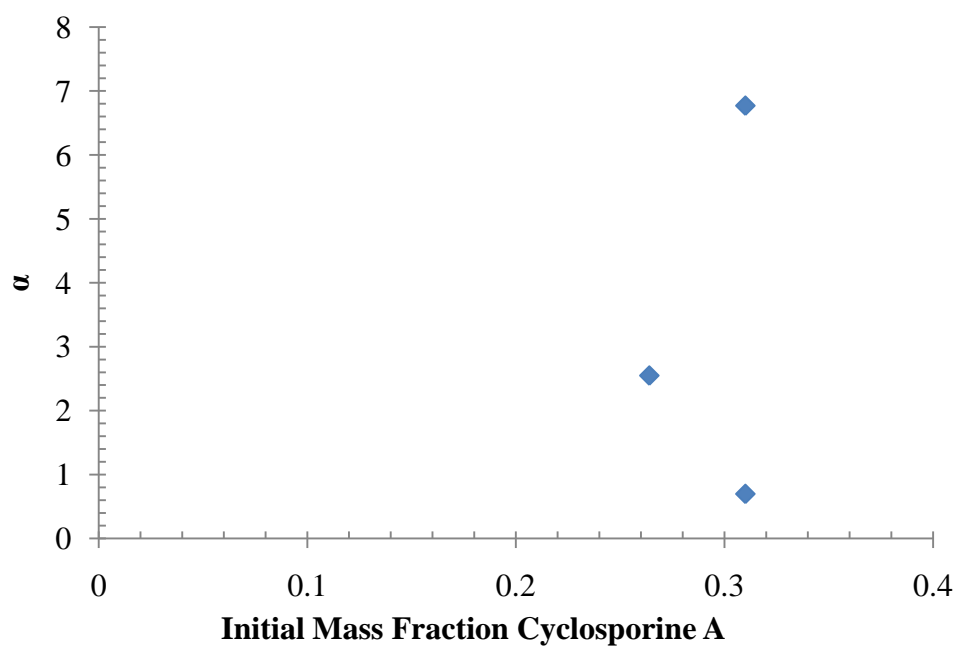


**Figure 49. Separation Factor of cyclosporine D as a function of initial concentration of cyclosporine A from batch experiments.**

## 3.4    Summary and Conclusions

Experimental studies of seeded batch crystallization operations have been performed in order to gain understanding of the impurity distribution in the crystal product. The separation factor given by the ratio of impurity and component of interest partitioning between the crystal and liquid phase was used to quantify this impurity distribution. Separation factors were calculated from experimental measurements where the final temperature, initial concentration of cyclosporine A and initial purity of cyclosporine A were varied.

Most of the separation factors were found to be less than one indicating the crystal is more pure than the starting material in terms of that impurity. Cyclosporine D was conversely found to have a separation factor greater than one indicating that the crystal is less pure with respect to D than the starting material. Impurities with separation factors greater than one will require more re-crystallizations to achieve high purity.

The majority of impurities had separation factors that were found to be linearly dependence on final temperature, independent of initial concentration and slightly dependent on initial purity. These results suggest that for modeling purposes the separation factor should be treated solely as a function of temperature.

The yield was unaffected by the purity of the starting material which means the saturation data as a function of temperature for the component of interest can be used in the presence of impurities when the impurities are similar and they are present in small quantity. This is an assumption used in the model development in Chapter 2 and is found to be valid here for cyclosporine A and its impurities.

The conclusions drawn from these experiments must be treated carefully when applied to the process described and modeled in Chapter 2. These experiments were performed on batch systems with a large distribution of crystal particle sizes. For processes where crystallization is confined to a surface there could be significantly different behavior.

The batch experiments in this chapter also used a series of temperature gradients that will affect the generated crystals. Chapter 4 will discuss experiments performed that are more directly applicable to the semi-continuous counter-current crystallization operation proposed in Chapter 2.

# 4.    Model Validation by Batch Crystallization

The process defined in the chapter 2 required a number of assumptions and those assumptions must be tested against experimental data.  Experimental data are also required to determine the necessary model parameters for a particular chemical system.  Setting up the full semi-continuous process would require a large amount of equipment and time so batch experiments are used instead because they are simpler to setup and perform and can provide the necessary information for model validation and parameter estimation.

The model developed for batch crystallization in Chapter 2 can be used for experimental model validation.  This chapter will detail further analysis of the batch model to gain insight into the expected behavior during experimentation and discuss the experimental setup and results.

## 4.1    Further Analysis of Batch Model

The liquid phase concentration expressions developed in section 2.2.2 can be extended further to give information about the overall distribution of impurity between liquid and solid phases and the concentration profile in the solid phase.  The dimensionless concentration profiles for A and B during batch crystallization are given again in equations (4.1) and (4.2).  Recall that these expressions were derived assuming the liquid volume is constant (dilute system), the temperature is constant and the parameter $n$ is equal to one.

$$\theta_A\left(\tau_2\right) = \theta_A^* + \left(1 - \theta_A^*\right)e^{-\tau_2}$$

(4.1)

$$\theta_B = \left(\frac{1 + e^{-\tau_2}\dfrac{K}{\gamma}\left(\dfrac{1}{\theta_A^*} - 1\right)}{1 + \dfrac{K}{\gamma}\left(\dfrac{1}{\theta_A^*} - 1\right)}\right)^{\gamma}$$

(4.2)

An overall separation factor and the mole fraction of impurity in the solid were derived.  The overall separation factor is defined in equation (4.3).  This factor is also discussed in section 1.2.2.

$$\alpha = \frac{\theta_A}{\theta_B}\frac{\theta_{Bc}}{\theta_{Ac}} \tag{4.3}$$

The difference between the separation factor and the surface equilibrium expression used in the model is that the separation factor is defined with the average concentration of the phases instead of surface solid and equilibrium liquid concentrations. Also, the separation factor is not an equilibrium quantity because its value depends on the history of the solution which defines the growth of crystal and incorporation of impurity. The surface equilibrium expression establishes a temperature dependent relationship between the equilibrium liquid phase concentrations and the surface solid phase concentrations no matter what the concentration profiles of the two phases have looked like up to that point.

The separation factor can be expressed as follows by recalling that the total mass of each component is constant and that the liquid volume is assumed constant.

$$\alpha = \frac{\theta_A}{\theta_B}\frac{\theta_{Bc}}{\theta_{Ac}} = \frac{\theta_A}{\theta_b}\left(\frac{1-\theta_B}{1-\theta_A}\right) = \frac{\frac{1}{\theta_B}-1}{\frac{1}{\theta_A}-1} = \frac{e^{\gamma\tau}\left(\dfrac{e^{\tau}+\dfrac{K}{\gamma}\left(\dfrac{1}{\theta_A^*}-1\right)}{1+\dfrac{K}{\gamma}\left(\dfrac{1}{\theta_A^*}-1\right)}\right)^{-\gamma}-1}{\dfrac{1}{\theta_A^*+\left(1-\theta_A^*\right)e^{-\tau}}-1} \tag{4.4}$$

The other quantity derived from this model is the surface mole fraction of impurity in the crystal ($x_{Bc}{}^S$). This variable as a function of time or total crystal mass gives the concentration gradient in the crystal. First combine equations (2.32), (2.33), (2.34) and (2.36) to give equation (4.5).

$$\frac{\theta_{Ac}^s}{\theta_{bc}^s} = \frac{\left(\theta_A-\theta_A^*\right)}{\gamma\left(\theta_B-\dfrac{\gamma\theta_A^*\theta_B}{K\left(\theta_A-\theta_A^*\right)+\gamma\theta_A^*}\right)} = \frac{\theta_A-\theta_A^*+\dfrac{\gamma}{K}\theta_A^*}{\gamma\theta_B} \tag{4.5}$$

The mole fraction of the impurity in the solid at the surface is then given by equation (4.6).

$$x_{Bc}^s = \frac{C_{Bc}^s}{C_{Bc}^s + C_{Ac}^s} = \frac{1}{1 + \dfrac{C_{Ac}^s}{C_A^0}\dfrac{C_A^0}{C_B^0}\dfrac{C_B^0}{C_{Bc}^s}} = \frac{1}{1 + \dfrac{\theta_{Ac}^s}{\eta\theta_{Bc}^s}} \tag{4.6}$$

where $\eta$ is the ratio of the initial concentrations of species B to species A as defined in equation (2.19).

Substituting (2.32), (2.36) and (4.5) into (4.6) gives the desired result which is presented in equation (4.7).

$$x_{bc}^s = \frac{1}{1 + \dfrac{\theta_{Ac}^s}{\eta\theta_{Bc}^s}} = \frac{1}{1 + \left(\dfrac{1}{\eta}\right)\left(\dfrac{\left(1-\theta_A^*\right)e^{-\tau_2} + \dfrac{\gamma}{K}\theta_A^*}{\gamma}\right)\left(\dfrac{1 + e^{-\tau_2}\dfrac{K}{\gamma}\left(\dfrac{1}{\theta_A^*}-1\right)}{1 + \dfrac{K}{\gamma}\left(\dfrac{1}{\theta_A^*}-1\right)}\right)^{-\gamma}} \tag{4.7}$$

The variables that remain in this expression are: $\eta$, the ratio of initial concentration of B to the initial concentration of A; $\gamma$, the ratio of incorporation rate constants B to A; $K$, the equilibrium constant at the surface; $\tau_2$, the time of the experiment; and $\theta_A^*$, the saturation concentration of A.

The change in mole fraction from the initial value is given by equation (4.8).

$$\Delta x_{bc}^s = x_{bc}^s\left(\tau\right) - x_{bc}^s\left(\tau = 0\right)$$

$$= \frac{1}{1 + \left(\dfrac{\left(1-\theta_A^*\right)e^{-\tau} + \dfrac{\gamma}{K}\theta_A^*}{\eta\gamma}\right)\left(\dfrac{1 + e^{-\tau}\dfrac{K}{\gamma}\left(\dfrac{1}{\theta_A^*}-1\right)}{1 + \dfrac{K}{\gamma}\left(\dfrac{1}{\theta_A^*}-1\right)}\right)^{-\gamma}} - \frac{1}{1 + \left(\dfrac{\left(1-\theta_A^*\right) + \dfrac{\gamma}{K}\theta_A^*}{\eta\gamma}\right)} \tag{4.8}$$

### 4.1.1 Analysis of the Liquid Phase Concentration of Impurity

Values for $\gamma$ and $K$ can be determined experimentally by fitting data to equation (2.36). This equation requires further examination because $K$ occurs only as its ratio to $\gamma$. Letting the ratio of $K$ to $\gamma$ be represented as $R$ allows equation (2.36) to be rewritten in the following form.

$$\theta_B = \left( \frac{1 + e^{-\tau_2} R\left(\frac{1}{\theta_A^*} - 1\right)}{1 + R\left(\frac{1}{\theta_A^*} - 1\right)} \right)^{\gamma} \tag{4.9}$$

First, the behavior when $R$ is small is analyzed by taking a Taylor expansion around $R=0$ and keeping the first non-constant term.

$$\theta_B = 1 - K\left(\frac{1}{\theta_A^*} - 1\right)\left(1 - e^{-\tau_2}\right)\left(1 - O\left(\frac{K}{\gamma}\left(2 + \left(1 - e^{-\tau_2}\right)(\gamma - 1)\right)\right)\right) \tag{4.10}$$

In order for this approximation to hold the error term must be much smaller than the other terms. At short times the relative error will be of order $K/\gamma$, or $R$. $R<<1$ was the condition for generating this expansion so no new information is obtained. When tau is large the relative error is of order $K(\gamma + 1)/\gamma$. This quantity must also be much less than one for equation (4.10) to be valid. For $\gamma$ greater than one the second constraint will require that $K$ be much less than one and if $\gamma$ is less than one then $K$ must also be much less than one since $R<<1$. The conditions under which this expansion are valid then can be simplified to $R<<1$ and $K<<1$ with no restriction on the time.

The situation with $R$ very large is given by the following equation.

$$\theta_B = e^{-\gamma\tau_2}\left(1 + O\left(\frac{\gamma^2}{K}\left(e^{\tau_2} - 1\right)\right)\right) \tag{4.11}$$

The error in the above approximation includes the parameters $\gamma$ and $K$ in addition to the operating time $\tau_2$. The ratio of the error to the term that has been retained is $\gamma^2/K(e^{\tau_2}-1)$ which must be much less than one for this expansion to apply. The leading term in this expansion, $e^{-\gamma\tau_2}$, will be of most interest when $\gamma\tau_2$ is approximately one so the relative error constraint can be written as $\gamma^2/K(e^{1/\gamma}-1)<<1$. Since an exponential function is much stronger than an algebraic one, it follows that the expansion fails for very small values of gamma. For values of gamma that are not very small, this simply represents an additional constraint that must be satisfied.

The approximations given in (4.10) and (4.11) indicate that data fitting to the analytical expression for the liquid phase impurity concentration can be complicated. Both of the two approximations have the same functional form, decreasing exponential, but each only depends on one of the two parameters. Multiple minima may be possible for different relative values of $\gamma$ and $K$. Further information about the correct relation of $\gamma$ to $K$ would be useful and will be provided by analysis of the mole fraction of impurity in the solid phase.

### 4.1.2   Analysis of the concentration gradient of impurity in the solid

The expression for $\Delta x_{Bc}{}^s$ can provide information about the direction of the concentration gradient in the solid depending on the relative values of the parameters $K$ and $\gamma$. Analysis of the final crystal deposition (growth at long times) can provide this information. First find the limit as $\tau$ approaches infinity in equation (4.8).

$$\lim_{\tau\to\infty}\Delta x_{Bc}^s = \frac{1}{1+\left(\dfrac{1}{\eta}\right)\left(\dfrac{\theta_A^*}{K}\right)\left(1+\dfrac{K}{\gamma}\left(\dfrac{1}{\theta_A^*}-1\right)\right)^\gamma} - \frac{1}{1+\left(\dfrac{\left(1-\theta_A^*\right)+\dfrac{\gamma}{K}\theta_A^*}{\eta\gamma}\right)} \tag{4.12}$$

When $\gamma=1$ in equation (4.12) the mole fraction difference is always zero.

$$\lim_{\tau \to \infty} \Delta x_{bc}^{s} \left( \gamma = 1 \right) = \cfrac{1}{1 + \left( \cfrac{1}{\eta} \right) \left( \cfrac{\theta_A^*}{K} \right) \left( 1 + \cfrac{K}{1} \left( \cfrac{1}{\theta_A^*} - 1 \right) \right)} - \cfrac{1}{1 + \left( \cfrac{1}{\eta} \right) \left( \cfrac{\left( 1 - \theta_A^* \right) + \cfrac{1}{K} \theta_A^*}{1} \right)}$$

$$= \cfrac{1}{1 + \left( \cfrac{1}{\eta} \right) \left( \cfrac{\theta_A^*}{K} + \left( 1 - \theta_A^* \right) \right)} - \cfrac{1}{1 + \left( \cfrac{1}{\eta} \right) \left( \left( 1 - \theta_A^* \right) + \cfrac{1}{K} \theta_A^* \right)} = 0$$

(4.13)

This indicates that, if the incorporation rate constants of A and B are the same, then there is no concentration gradient in the crystal. A flat concentration profile in the crystal can only occur when the ratio of A to B being added to the crystal remains constant at all times. This is true if the total incorporation rate is constant. Therefore the driving force ratio of A to B must also be constant for this result to be true and this was shown to be the case when $\gamma = 1$ in section 2.4.1.2.

If $K$ is equal to one, the following result is obtained.

$$\lim_{\tau \to \infty} \Delta x_{bc}^{s} \left( K = 1 \right) = \cfrac{1}{1 + \left( \cfrac{1}{\eta} \right) \left( \theta_A^* \right) \left( 1 + \cfrac{1}{\gamma} \left( \cfrac{1}{\theta_A^*} - 1 \right) \right)^{\gamma}} - \cfrac{1}{1 + \left( \cfrac{1}{\eta} \right) \left( \cfrac{\left( 1 - \theta_A^* \right) + \gamma \theta_A^*}{\gamma} \right)}$$

$$= \cfrac{1}{1 + \left( \cfrac{1}{\eta} \right) \left( \theta_A^* \right) \left( 1 + \cfrac{1}{\gamma} \left( \cfrac{1}{\theta_A^*} - 1 \right) \right)^{\gamma}} - \cfrac{1}{1 + \left( \cfrac{1}{\eta} \right) \left( \theta_A^* \right) \left( 1 + \cfrac{1}{\gamma} \left( \cfrac{1}{\theta_A^*} - 1 \right) \right)}$$

(4.14)

This indicates that even if the equilibrium behavior gives no separation in the solid phase, there will be a concentration gradient in the crystal if the incorporation rate constants of A and B are different. If $\gamma$ is greater than one, then the final layer of crystal grown will have a smaller impurity concentration than the initial layer. If $\gamma$ is less than one, the final crystal layer will have more impurity than the initial impurity layer.

It is also interesting to look at the cases where $K$ and $\gamma$ approach zero. The limit in the case that either $K$ or $\gamma$ approaches zero of equation (4.8) is zero.

$$\lim_{K \to 0} \Delta x_{bc}^s = 0 \tag{4.15}$$

$$\lim_{\gamma \to 0} \Delta x_{bc}^s = 0 \tag{4.16}$$

In both of these cases the gradient is zero but the total amount of impurity present in the crystal is also zero. This can be verified by noting that the limits of equation (4.7) as $K$ and $\gamma$ approach zero are zero. If $K$ is equal to zero then no impurity is present in the crystal and no concentration gradient is present. Kinetic factors do not matter when the equilibrium at the surface of the crystal does not include some impurity in the crystal. No impurity will be present in the crystal as well if there is no transfer from the liquid to the solid phase.

It is important to consider the case of low $\gamma$ and very long times. The limit in this case is given in equation (4.17).

$$\lim_{\gamma \to 0} \left( \lim_{\tau \to \infty} \Delta x_{bc}^s \right) = \frac{1}{1 + \left( \dfrac{1}{\eta} \right) \left( \dfrac{\theta_A^*}{K} \right)} = \frac{\eta K}{\eta K + \theta_A^*} \tag{4.17}$$

Even for very low incorporation rate constants there can be an appreciable impurity gradient at steady state. The equilibrium behavior of the system will dominate if enough time is given for equilibrium to be achieved. This is true unless K is equal to zero in which case the equilibrium scenario has no impurity in the crystal and therefore no gradient will exist in the crystal.

### 4.1.3   Analysis of the separation factor

Analyzing the expression for $\alpha$ (equation (4.4)), it can be seen that the limit of $\alpha$ as $K$ or $\gamma$ approaches zero is zero.  A value of zero for the separation factor indicates that no impurity is present in the crystal and a perfect separation has occurred.

For long times the liquid concentrations will approach their steady state values. The expression for $\alpha$ can be simplified at long times as follows.

$$\lim_{\tau \to \infty} \alpha = \frac{\left(1 + \frac{K}{\gamma}\left(\frac{1}{\theta_A^*} - 1\right)\right)^\gamma - 1}{\frac{1}{\theta_A^*} - 1} = \frac{1}{\frac{1}{\theta_A^*} - 1}\left(\left(\gamma + K\left(\frac{1}{\theta_A^*} - 1\right)\right)^\gamma \gamma^{-\gamma} - 1\right)$$ (4.18)

The best separations will occur for values of $K$ and $\gamma$ approaching zero. The behavior at these limits can be approximated by taking a Taylor expansion of equation (4.18) about $K=0$ and $\gamma=0$. The derivation of the limit about $\gamma=0$ is described in section 6.1 . Keeping only first order terms gives the following results.

$$\alpha(K) = K + O(K^2)$$ (4.19)

$$\alpha(\gamma) = \frac{\ln\left(\frac{K}{\gamma}\left(\frac{1}{\theta_A^*} - 1\right)\right)}{\frac{1}{\theta_A^*} - 1}\gamma + O(\gamma^2)$$ (4.20)

These limiting expressions indicate that the average concentration of the crystal phase at long times are functions of the physical properties of the system; $K$, $\gamma$ and $\theta_A^*$. In the case of $K$ approaching zero, the value of $\alpha$ becomes equal to $K$ indicating that the separation factor is determined by the equilibrium relationship between the solid and liquid phases. For $\gamma$ approaching zero, the expression for $\alpha$ is more complicated and depends on all three physical parameters.

## 4.2    Batch Crystallization Experiments

Batch experiments were performed in order to provide data to validate and to fit parameter values to the previously defined model. The model has been developed for crystallization occurring on fixed surfaces and so a method for doing this experimentally has been determined. The description of the experimental apparatus will be followed by discussion of the chemical system used during experimentation and then the experimental results.

### 4.2.1 Experimental Apparatus

The necessary components of the experimental apparatus are a temperature controlled solution of known initial composition and a fixed, temperature controlled surface upon which crystal growth occurs. A means of taking samples from the liquid over the course of time and a method for analyzing those samples are also required.

Experiments were conducted in a single-necked 100 mL round bottom flask submerged in a constant temperature water bath. The constant temperature bath was maintained by circulation from a Neslab RTE-1100 water circulator. The mixture was stirred with a magnetic stir bar using a stir plate that allowed digital control of the rotation speed.

The crystallization solutions were made as follows. A measured amount of the component of interest (A) and the impurity (B) were added to the round bottom flask along with 100 g of water. This mixture was heated until the solids were dissolved. The temperature was then cooled to the desired working temperature via the external water bath. During this heating and cooling process, the growth surface was not present in the solution. The experiments were designed such that the solution was not supersaturated at the bulk temperature. No nucleation or growth would be expected until the seed plate is added to the solution.

The seeding device is a pre-coated length of metal tubing. The tube is bent into a U-shape and pushed through a rubber septum that serves to seal the flask from the outside environment. Both stainless steel and aluminum tubing was used with similar results. Aluminum was chosen as a better material because it can be bent more smoothly to give a more uniform seed surface.

The metal tube is made into a seed by evaporative coating from a saturated solution of the component of interest. The tube is first lightly sanded using a rotary hand tool in order to roughen the surface. The surface is then wiped with phosphoric acid in order to remove the surface oxide layer and enhance wetting of the surface. The surface is then washed with water to remove the acid and immediately is dipped into a saturated solution of the component of interest. The tube is dipped three times in succession and then is allowed to dry in an $80^0$C oven. This coating process is then repeated 10-12 times or until a visible coating of solid is present on the tube surface. The amount of solid deposited by this coating process is deter-

mined by weighing.  The coating of seed that is developed is stable to mechanical agitation.  A picture of a coated seed tube is shown in Figure 50.
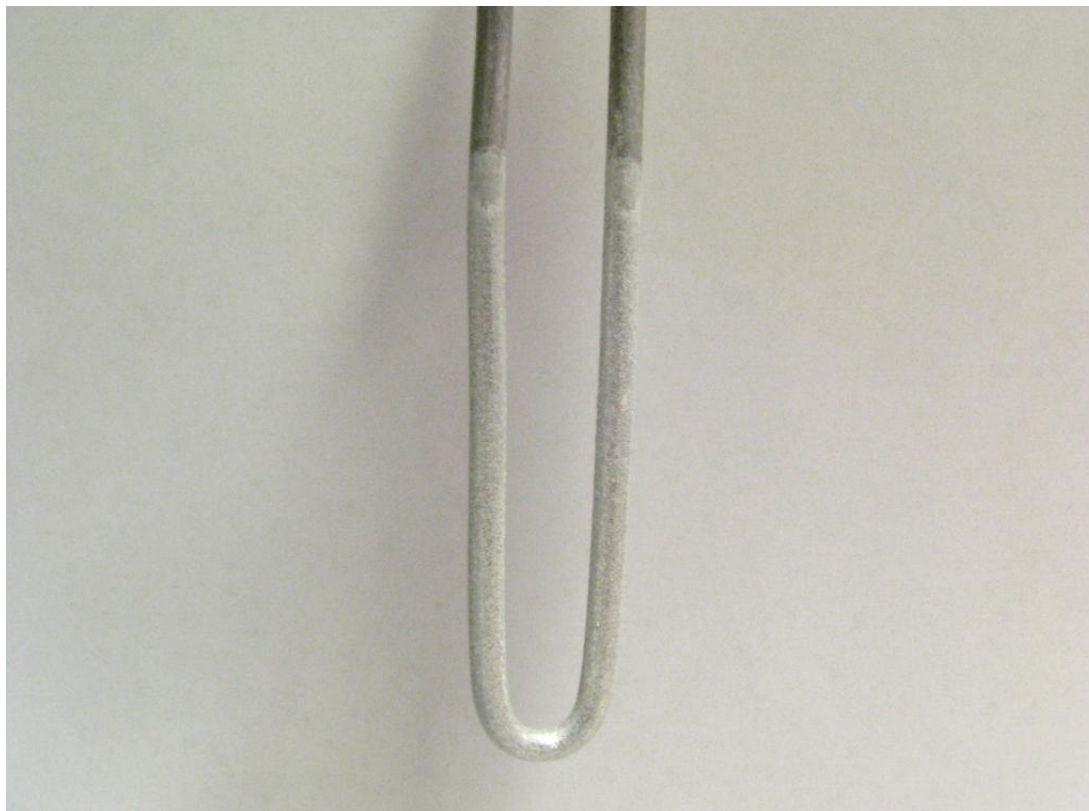


**Figure 50.  Picture of aluminum seed tube coated with asparagine.**

The purpose of using metal tubing instead of a metal rod is temperature control of the crystallization surface.  Controlled temperature water is passed through the metal tube in order to maintain the surface at a constant temperature.  Initial experiments were done with no cooling of the seed surface and a supersaturated initial solution.  Although this approach did result in preferential growth on the seed surface, most experiments also had a visible, significant amount of bulk crystallization, due to secondary or homogeneous nucleation.  Because the purpose of the experiment is to study the impurity incorporation into crystal grown on a solid surface bulk crystallization should be minimized.  By cooling the seed surface, the bulk solution can be kept at very small supersaturations or even slight undersaturation.  This will eliminate the possibility of homogeneous nucleation and will diminish the effects of secondary nucleation because crystals that are dislodged from the growth surface can dissolve in the bulk solution.

The cooling of the seed surface is accomplished using a Netzsch NM011SY mini-metering progressive cavity pump and a controlled temperature water bath. This pump was connected to a DC motor and delivered a flow rate of 1.4 liters per minute at 500 RPM. The controlled temperature water bath was capable of temperature control to within less than $0.1^0$C. Fluid connections in the flow path from the pump through the seed loop are made using double sleeved compression tube fittings.

A progressing cavity pump is a positive displacement pump that operates by moving fluid with a helical rotor turning inside of an elastomeric rubber stator. This rotation creates discrete pockets of fluid that are moved through the pump. The stator is designed so that the pockets start to overlap towards the discharge end of the pump in order to minimize pulsing fluid flow.

The progressive cavity pump cavity pump is the best choice for this application because it provides very smooth flow with a minimum of vibration. Vibrations are undesirable because they propagate through the tubing and can result in oscillations of the seed tube. Oscillations of the seed tube are expected to affect the amount of secondary nucleation arising from crystals breaking away from the seed tube. Minimizing these oscillations is desired in order to simplify experimental analysis.
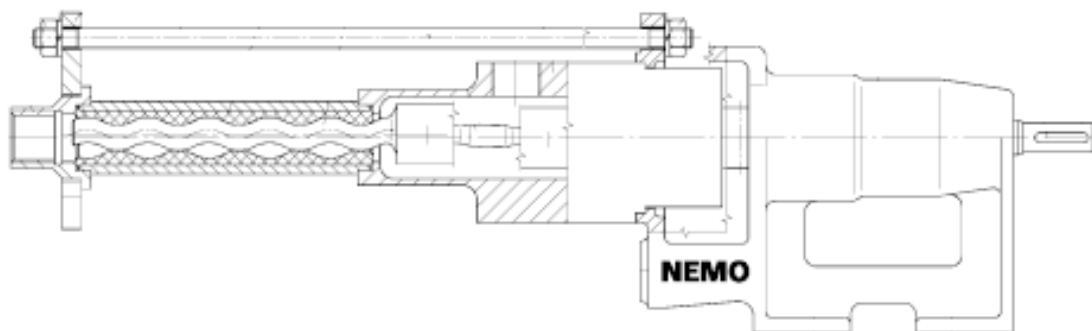


**Figure 51. Schematic of Nemo progressive cavity pump used during experimentation.**[151]

The overall system is composed of the crystallization vessel, the seed tube with flow loop and the temperature control system for the external bath. The inflow and outflow from the Neslab chiller was not balanced and so an extra pump was necessary in order to deal with overflow. A Cole-Parmer peristaltic pump was used for this purpose. A picture of the overall experimental setup is given in Figure 52.
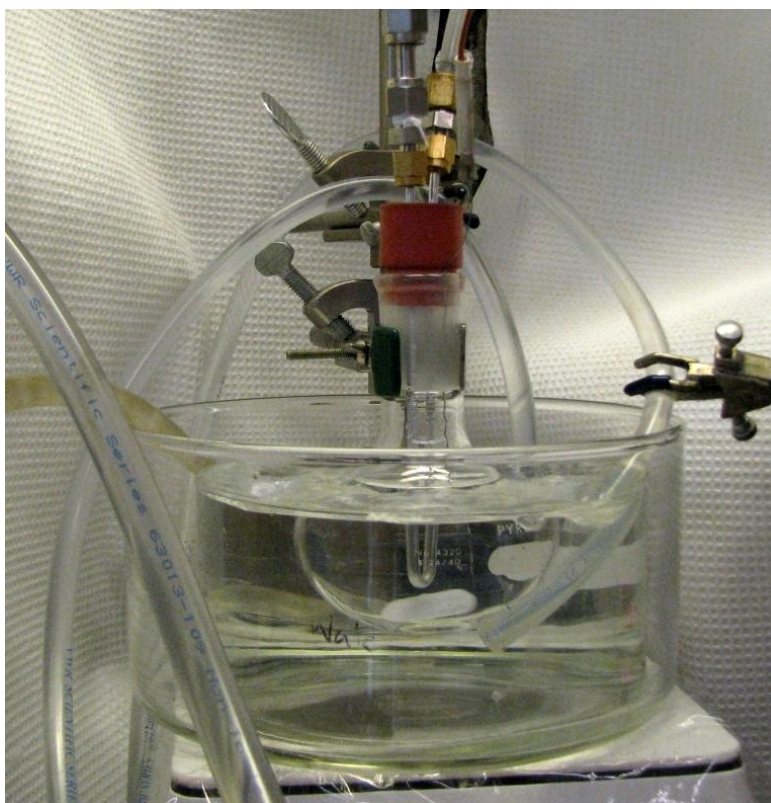


**Figure 52. Experimental setup showing external temperature bath, crystallization flask and seed tube with attached tubing for surface temperature control.**

Sampling of the liquid phase is accomplished by a needle inserted through the rubber septum into the crystallization flask. The needle is left in the solution at all times and the end is covered when liquid is not being extracted in order to limit solvent evaporation. To prepare each sample, a volume of between 0.1 and 0.2 mL is taken from the solution. No more than 20 total samples were taken during a single experiment so that the total volume lost is less than 3

mL, or approximately 3 % of the total volume. Multiple samples were taken at some time points in order to test the homogeneity of the solution.

From the liquid removed from the vessel, 0.1 mL is diluted with 4.9 g of water to give the final sample to be analyzed for that time point. This level of dilution is used in order to operate in an absorption regime far removed from the saturation limit of the UV-Vis detector. The sample is taken via a calibrated pipette but the actual sample amount is also determined by weighing in order to get more accurate data.

Accurate sample preparation is important because the concentrations involved are relatively small and sampling errors can result in large uncertainties in the measured concentrations. A 10% variance in sample volume leads to a roughly 10% change in the absorbance during HPLC analysis via UV-Vis detection. But the overall change in absorbance from the feed to the final solution for a typical experiment is often on the order to 10%. Careful sampling then is very important.

Sampling of the solid phase was done by sequential dissolution. Once an experiment is finished, the wet weight of the resulting crystal is recorded. The crystal was then air dried and reweighed to give the dry product weight. Subsequent samples of the solid are collected by placing the crystal in an unstirred vial of water for a specified period of time. The crystal was then allowed to air dry before the weight was recorded. This process was repeated until the entire crystal was dissolved. Air drying was used because oven drying was found to make the crystal more brittle and prone to uneven dissolution.

This sampling method will be most appropriate when the crystal grown on the seed plate is very uniform. The seed method used here does result in very uniform crystal growth over the entire submerged surface of the seed tube. The product on the seed tube is not a single crystal but a uniform, polycrystalline coating. A picture of the final crystal grown from one experiment is shown in Figure 53.

**Figure 53. Crystalline product grown on a seed tube during a batch experiment.**

The first sample from the solid crystal was only placed in water for a very short period of time. This was done in order to remove any material deposited on the surface by evaporation of the solution after removal of the seed tube from the experimental vessel. The solid deposited from evaporation of the mother liquor is less likely to be incorporated into the crystal lattice because it is deposited in a shorter time scale due to evaporation and so it can be removed with the first dissolution operation. The first solid sample was generally only placed in water for 15 s and the data from this sample was not included in analysis of the concentration profile in the solid.

### 4.2.2 Modification to Model Due to Experimental Setup

The experimental setup that was used provides a constant temperature at the surface of the seed tube but the growth of crystal will result in a changing temperature at the solid-liquid interface. The growing crystal will provide a significant resistance to heat transfer that will eventually limit the growth of crystal. Growth will stop when the saturation concentration given by the temperature at the surface of the crystal is equal to the bulk concentration. At this point the driving force for crystallization becomes zero.

144

This changing surface temperature requires removal of one of the key assumptions made when deriving the analytical solution above. Because the surface temperature is not constant, the saturation concentration at that surface ($C_A^*$) is also not constant. It is not required that $C_A^*$ be constant to use the model defined earlier but it is necessary that its value be known as a function of time. This can be accomplished by relating the temperature at the liquid-crystal interface to the total mass of crystal present through an energy balance. This energy balance will require estimation of heat transfer coefficients inside the seed tube and from the bulk fluid to the surface of the seed tube in addition to a thermal conductivity for the crystal layer. The shape of the growing crystal layer is also necessary and in this system will be cylindrical due to the use of tubing as the seed surface.

The varying temperature at the liquid-crystal surface is also expected to affect the values of the incorporation rate constant $k_A$, the equilibrium constant $K$ and the ratio of incorporation rate constants $\gamma$. Fitting of the model to experimental data will result in average values of these parameters over the temperature range experienced at the growth surface. The value determined from fitting the model to the experimental data will give an order of magnitude understanding of these parameters but cannot give parameter values at specific temperatures due to the experimental setup.

An energy balance over the system can be used to find the temperature at the surface of the crystal as a function of time. The energy balance is done at quasi-steady state because the growth rate of crystal is expected to be much slower than the time necessary to establish thermal equilibrium. The total amount of energy transferred between the liquid inside the seed tube and the bulk liquid will be constant because the water in the tube is at constant flow rate and inlet temperature while the bulk temperature is also constant. The unknown variables then are the total heat added to the seed tube and the temperatures at the interior surface of the seed tube, the exterior surface of the seed tube and at the crystal surface.

For purposes of this energy balance, the system will be assumed to have the form shown in Figure 54. In this figure the growth surface is a straight tube in the bulk solution. This assumption eliminates consideration of the bends in the tube for interior heat transfer and as-

sumes the bulk solution is mixed well enough that the region between the U-shaped seed tube legs has the same temperature as the bulk solution.
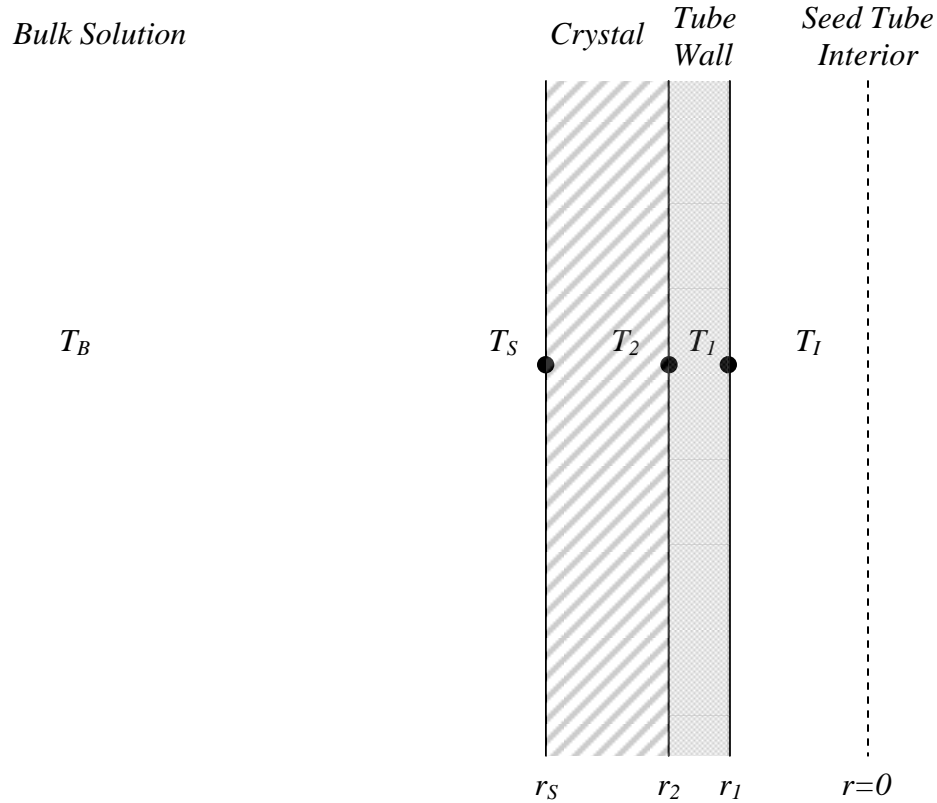


**Figure 54. Diagram of heterogeneous batch crystallization system for energy balance purposes. Half of system is shown with mirror plane of symmetry at $r=0$. $T_j$ and $r_j$ represent the temperature and radial distance at location $j$.**

A heat transfer equation can be written for each of the four regions in Figure 54 (seed tube interior, tube wall, crystal and bulk solution). These equations are presented in equations (4.21) to (4.24).

$$q_I = h_I a_1 (T_I - T_1) \tag{4.21}$$

$$q_1 = \frac{2\pi L k_{tw}}{\ln \frac{r_2}{r_1}} (T_1 - T_2) \tag{4.22}$$

$$q_2 = \frac{2\pi L k_c}{\ln \left. r_S \middle/ r_2 \right.} (T_2 - T_S)$$ (4.23)

$$q_B = h_B a_c (T_S - T_B)$$ (4.24)

where $q_j$ is the heat transfer in watts of region $j$, $h_I$ is the heat transfer coefficient for the fluid inside the seed tube to the tube wall, $h_B$ is the heat transfer coefficient from the bulk to the crystal surface, $k_{tw}$ is the thermal conductivity of the tube wall, $k_c$ is the thermal conductivity of the crystal, $a_I$ is the interior surface area of the seed tube, $a_c$ is the surface area of the crystal and $L$ is the length of the seed tube submerged in the solution.

The thermal conductivity of the crystal layer is assumed to be equal to the thermal conductivity of the component of interest. This is a good assumption because the impurity will only be present in a small quantity and in a solid solution the impurity will have a very similar structure to the component of interest and cause only slight disturbance of the crystalline lattice. The heat of crystallization released by growth of the crystal will be assumed small compared to the heat transferred from the bulk liquid to the interior of the seed tube. This will be demonstrated for the model system that will be described in the next section.

For a system at quasi steady state the heat transferred between two adjacent regions will be equal. For the system outlined in Figure 54 and equations (4.21)-(4.24) all values of $q$ will be equal at steady state. The five unknown quantities then are $q$, $T_1$, $T_2$, $T_S$ and $r_S$ and the four equations can be solved for the desired quantity $T_S$ as a function of the crystal thickness $r_S$. The expression for $T_S$ is presented in equation (4.25).

$$T_S = \frac{\dfrac{2\pi L k_{tw}}{\ln(r_2/r_1)} \left( T_I + T_B h_B a_c \left( \dfrac{1}{h_I a_1} + \dfrac{\ln(r_s/r_2)}{2\pi L k_c} \right) \right) + T_B h_B a_c}{h_B a_c \left( 1 + \dfrac{2\pi L k_{tw}}{h_I a_1 \ln(r_2/r_1)} + \dfrac{k_{tw}}{k_c} \dfrac{\ln(r_s/r_2)}{\ln(r_2/r_1)} \right) + \dfrac{2\pi L k_{tw}}{\ln(r_2/r_1)}}$$ (4.25)

The crystal thickness $r_S$ must be related to the solution phase concentrations in order for equation (4.25) to be used in the proposed model for batch crystallization. This is done by finding the total mass of the crystal and using the conservation of mass in a batch system. The shape of the crystal will be a cylindrical shell for the cylindrical seed tube used in these experiments.

$$m_C = m_{AC} + m_{BC} = m_A^0 - m_A + m_B^0 - m_B = V\left(C_A^0 - C_A + C_B^0 - C_B\right) = \rho_C L\pi\left(r_S^2 - r_2^2\right) \text{(4.26)}$$

Equation (4.26) can then be solved for $r_S$ which is given in equation (4.27).

$$r_S = \sqrt{\frac{V}{\rho_C L\pi}\left(C_A^0 - C_A + C_B^0 - C_B\right) + r_2^2} \tag{4.27}$$

The remaining information needed to solve equation (4.25) is physical parameters of the experimental setup and the chemical system in use. The thermal conductivities of the tube wall and the crystal can be looked up while the values of $r_1$, $r_2$, $L$, $T_B$, $T_I$ and $a_1$ are known from the established system materials and parameters and the surface area of the crystal, $a_C$, can be related to $r_S$ ($a_c = 2\pi r_s L$). The last two values that are required to solve for the temperature at the crystal surface are the heat transfer coefficients from the bulk to the crystal surface and from the interior to the wall of the seed tube.

The heat transfer coefficient inside the seed tube can be found from a correlation for heat transfer inside a pipe. The submerged portion of the seed tube was in all cases at least 10 cm from the beginning of the seed tube. The inner diameter of the seed tube ($D_I$) is 0.2 cm so the ratio of length before the growth area to tube diameter is 50 and entrance effects can be neglected. In order to choose the appropriate heat transfer correlation the Reynolds number of the water flowing through the seed tube must be known. The volumetric flow rate in the pipe ($Q$) is 1.4 liters per minute or $2.3 * 10^{-5}$ m$^3$/s. The calculation of the Reynolds number is shown in equation (4.28).

$$\mathrm{Re} = \frac{QD_1}{\pi r_1^2 \upsilon} = \frac{\left(2.3*10^{-5}\right)\left(0.002\right)}{\pi\left(0.001^2\right)\left(10^{-6}\right)} = 15000 \tag{4.28}$$

Where the kinematic viscosity of water ($\upsilon$) at room temperature is $10^{-6}$ m$^2$/s. This Reynolds number is in the turbulent flow regime and the Dittus-Boelter correlation[152] is appropriate.

$$Nu = \frac{h_I D_1}{k_w} = 0.023\,\mathrm{Re}^{0.8}\,\mathrm{Pr}^{0.4} \tag{4.29}$$

Pr is the Prandtl number of the fluid as defined in equation (4.30) and $k_w$ is the thermal conductivity of water which is equal to 0.58 W/mK. For the Prandtl number, the heat capacity at constant pressure ($c_P$), the viscosity ($\mu$) and the thermal conductivity are all properties of the fluid.

$$\mathrm{Pr} = \frac{c_P \mu}{k} \tag{4.30}$$

The Prandtl number for water at room temperature is approximately 7. The Nusselt number for this situation is then equal to 110 which gives a heat transfer coefficient of 33,000 W/m$^2$K for transfer from the liquid flowing inside the seed tube to the surface of the seed tube. This coefficient can only be considered constant throughout the entire seed tube if the flow rate through the seed tube is high enough that the temperature change of the water from entrance to exit of the seed tube is small. This temperature difference from inlet to outlet was measured to be $0.25^0$C so the assumption of constant internal heat transfer coefficient is reasonable.

The heat transfer coefficient from the bulk to the crystal surface was measured. Appropriate heat transfer correlations for stirred tank systems are difficult to find so a simple experiment was done in order to measure this value for the conditions used during the batch crystallization experiments. A piece of aluminum tubing, the same as used for seed tubing but without any surface treatment, was inserted into a 100 mL solution of water held at $25^0$C. Water was passed through the tube from a controlled temperature water source and the inlet and

outlet temperatures from the aluminum tube were recorded. The same flow rate through the seed tube used during crystallization experiments was used in order to find the most appropriate heat transfer coefficient.

The measured inlet and outlet temperature along with the internal heat transfer coefficient from a correlation and the thermal conductivity of the aluminum tube allow for the bulk heat transfer coefficient to be calculated. The total energy transfer is first found from the change in temperature of the water during flow through the seed tube. This amount of heat transfer is then used to find an overall heat transfer coefficient. The overall heat transfer coefficient can then be used to find the bulk heat transfer coefficient. The equations for these three steps are given in equation (4.31) to (4.33) where $\dot{m}$ is the mass flow rate of water in the seed tube, $c_p$ is the heat capacity at constant pressure of water, $T_{out}$ and $T_{in}$ are the outlet and inlet temperatures respectively of the water in the feed tube, $q$ is the heat transfer in watts, $\Delta T_{lm}$ is the log mean temperature difference between the water in the seed tube and the bulk, and $a_2$ is the outside surface area of the seed tube.

$$q = \dot{m}c_p\left(T_{out} - T_{in}\right) \tag{4.31}$$

$$q = U_O a_2 \Delta T_{lm} \tag{4.32}$$

$$U_O = \cfrac{1}{\cfrac{1}{h_B} + \cfrac{D_2}{k_{tw}}\cfrac{\ln\left(D_2/D_1\right)}{2} + \cfrac{D_2}{D_1}\cfrac{1}{h_I}} \tag{4.33}$$

For the previously discussed flow rate of 1.4 liters per minute and a bath temperature of $10^0$C the temperatures of water entering and exiting the seed tube are 11.38 and 11.62$^0$C respectively. This corresponds to heat transfer ($q$) of 31 W and a bulk heat transfer coefficient equal to 3,100 W/m$^2$K.

The values of the heat transfer coefficients and equation (4.25) can be added to the batch model outlined in section 2.2 in order to allow numeric simulation of the proposed batch experiments. The collected experimental data can then be fit to this model using a least squares approach in order to give values for the model parameters $k_A$, $\gamma$ and $K$.

150

### 4.2.3 Model Chemical System

The chemical system chosen for experimentation was the amino acids asparagine and aspartic acid in water. The structures of asparagine (asn) and aspartic acid (asp) are shown in Figure 55.
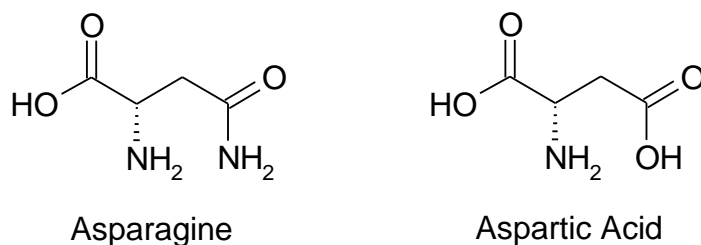


**Figure 55. Structure of the amino acids asparagine and aspartic acid.**

It has been previously found[153, 154] that asparagine and aspartic acid form a solid solution with up to 20% by weight of aspartic acid in the asparagine crystalline lattice. The formation of a solid solution was also verified experimentally for the range of concentrations of interest in this study. The details of this are given in section 6.5. The similar shape of these two molecules also supports the formation of a solid solution.

Another benefit of asparagine as the component of interest is that it exhibits a strongly temperature dependent solubility in water[149]. The strong dependence on temperature allows for larger amounts of crystal to be grown with smaller temperature differences. This is important because in this system only a small amount of impurity is present in the crystal and larger total amounts of crystal facilitate concentration measurement.

Both asparagine and aspartic acid crystallize as a mono-hydrate. This means that the crystal structure of pure asparagine or aspartic acid will contain one water molecule for every molecule of asparagine or aspartic acid. The solid solution formed between asparagine and aspartic acid will also be a mono-hydrate.

Because the solubility of these amino acids in water is small the amount of water in the crystal is also small and will not affect the concentration of the liquid phase. Every gram of asparagine crystal will contain 0.14 g of water. The saturation of asparagine at $20^0$C is roughly 2 g asparagine per 100 g water. If the initial solution has a supersaturation ratio of 1.5 and the crystallization proceeds to equilibrium then 1 gram of crystal will form containing 0.14 g water.

151

The change in the amount of water present will be 0.1%. The assumption in the batch model development that the amount of solvent in the liquid phase was constant will still be appropriate.

The presence of a mono-hydrate can explain why oven drying is not a good strategy when analyzing the solid crystals of asparagine and aspartic acid. High temperatures allow the bound water in the crystal matrix to evaporate which results in a significant change in the stability of the crystal. The crystal becomes very brittle and prone to breaking off in large pieces which makes uniform sampling of the crystal very difficult. Air drying allows surface moisture to evaporate without removing water from the crystalline lattice so that the crystal does not become brittle.

The heat of crystallization for asparagine monohydrate is 33 kJ/mol[155]. For the same conditions discussed previously, 1 g of asparagine crystal will require 250 J of energy for crystallization. If this growth is spread out over the course of one hour a power input of 0.07 W will be required. This growth will in fact generally be spread over multiple hours decreasing the necessary power even further. This heat input is much less than the heat transfer from the cooling loop to the bulk solution in the batch experimental setup and so the assumption that the heat of crystallization can be ignored is justified.

Asparagine and aspartic acid were purchased from Sigma-Aldrich at 99.5% purity and used without further purification.

### 4.2.4   Estimation of Maximum Mass Transfer Rate

The estimated outside heat transfer coefficient allows estimation of a mass transfer coefficient for asparagine and aspartic acid in water by use of the Chilton-Colburn analogy.[156, 157] This relationship is given by

$$\mathrm{St}\,\mathrm{Pr}^{2/3} = \mathrm{St}_m \mathrm{Sc}^{2/3} \tag{4.34}$$

where St is the Stanton number, Pr is the Prandtl number, $\mathrm{St}_m$ is the mass transfer Stanton number and Sc is the Schmidt number. These dimensionless variables are defined as follows.

$$St = \frac{h}{\rho V c_p} \tag{4.35}$$

$$St_m = \frac{h_m}{V} \tag{4.36}$$

$$Pr = \frac{c_p \mu}{k} \tag{4.37}$$

$$Sc = \frac{v}{D_{ij}} \tag{4.38}$$

where $h$ is the heat transfer coefficient (W/m² K), $\rho$ is the density of the fluid (kg/m³), $V$ is the fluid velocity (m/s), $c_p$ is the heat capacity at constant pressure (J/kg K), $h_m$ is the mass transfer coefficient (m/s), $\mu$ is the viscosity (kg/m s), $k$ is the thermal conductivity (W/m K), $v$ is the kinematic viscosity (m²/s) and $D_{ij}$ is the diffusivity of $j$ in $i$ (m²/s).

Equation (4.34) can be rearranged to give the following expression for the mass transfer coefficient.

$$h_m = \frac{h}{\rho c_p} \left( \frac{Pr}{Sc} \right)^{2/3} \tag{4.39}$$

The only unknown parameter in equation is the Schmidt number. The heat transfer coefficient was found in the last section to be 3,100 W/m²K and the density of water is approximately 1,000 kg/m³, the heat capacity at constant pressure of water is 4,183 J/kg K, and the Prandtl number of water is 7 at room temperature. Also, the kinematic viscosity of water is $10^{-6}$ m²/s so the only unknown quantity is the diffusivity of asparagine or aspartic acid in water. The diffusivity can be estimated using the Hayduk-Laudie correlation[158] which is given in the following equation.

$$D_{wA} = \frac{13.16 * 10^{-5}}{\mu_w^{1.14} V_A^{0.589}} \tag{4.40}$$

where $\mu_w$ is the viscosity of water (cP) which is 1 at room temperature and $V_A$ is the molar volume of the solute at its normal boiling point (cm$^3$/mol) and $D_{wA}$ is the diffusivity of asparagine in water with units of cm$^2$/s.

The value of the molar volume of asparagine at its normal boiling point was not found and instead was estimated using the simple additive method developed by Schroeder.[159] This gives the molar volume in cm$^3$/mole by taking the sum of the number of carbon, hydrogen, nitrogen and oxygen atoms, adding the number of double bonds and multiplying the resulting number by seven. For asparagine this gives an estimate of 126 cm$^3$/mole. Using equation (4.40) with this molar volume results in a diffusivity of 8*10$^{-6}$ cm$^2$/s. This value compares very favorably with measured values of the diffusivity of other amino acids in water as reported by Ma et al.[160]

The Schmidt number for this system is then 1250 and the mass transfer coefficient can be calculated as

$$h_m = \frac{h}{\rho c_p}\left(\frac{\text{Pr}}{\text{Sc}}\right)^{\!2/3} = \frac{3100}{(1000)(4183)}\left(\frac{7}{1250}\right)^{\!2/3} = 2.3*10^{-5}\,m/s \qquad (4.41)$$

This estimated value of the mass transfer coefficient will be the maximum possible value for the crystallization incorporation rate constants $k_A$ and $k_B$. This will give an upper limit when fitting the model to experimental data. The values of $k_A$ and $k_B$ are expected to be smaller than this mass transfer limit because the crystallization process consists of diffusion to the surface and addition to the growing crystal.

The value of the mass transfer coefficient can be tested by performing dissolution experiments on a pure species. The dissolution process is expected to occur entirely due to mass transfer and so measurement of the rate constant for this process should provide support for the estimate in this section. This experiment will be discussed with the experimental results.

### 4.2.5   Concentration Measurements

All concentration measurements were done using high pressure liquid chromatography (HPLC).  The instrument used was an Agilent 1200 series HPLC with a diode array detector. Amino acids are not directly detectible by UV/Vis spectroscopy so a pre-column derivatization reaction is necessary before analysis.  The amino acids are reacted with ortho-phthalaldehyde (OPA) in the presence of 3-mercaptopropionic acid.  This reaction is shown in Figure 56.  The functionalized amino acids produced in this reaction are unstable and reproducibility of the de-rivatization method is very important in order to compare data between samples.[161]  This deri-vatization reaction can be carried out automatically by the Agilent 1200 series auto-sampler in a reproducible manner.
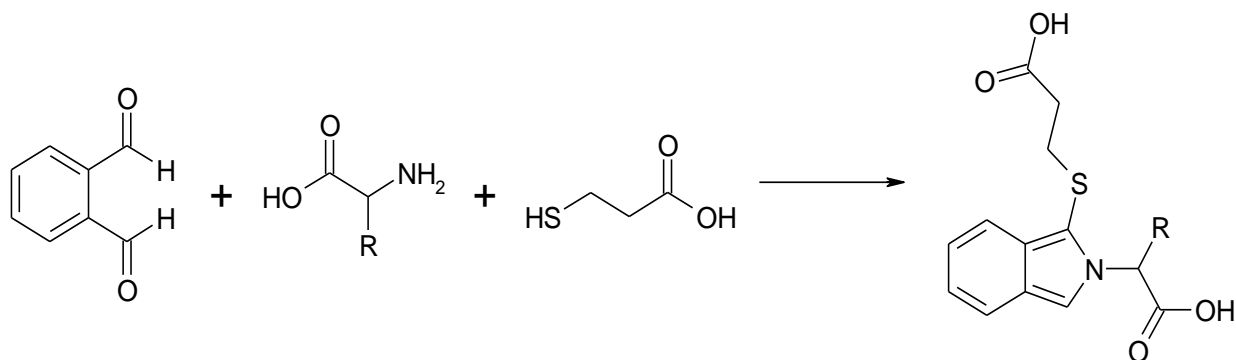


**Figure 56.   Schematic of reaction of primary amino acid with o-phthalaldehyde in the presence of 3-mercaptopropionic acid to give a derivative detectable with absorbance spectroscopy.**

A HPLC method for separating amino acids published by the Agilent Corporation was used as the basis for the experimental method in this investigation[162].  The separation is done using a gradient elution profile with two solvents.   Solvent A is 5 mM sodium phosphate and 5 mM sodium borate in water with the pH adjusted to 8.2.  Solvent B is a 45:45:10 mixture of ace-tonitrile, methanol and water.  The gradient conditions are shown in Figure 57 as the percen-tage of solvent B as a function of time for a total flow rate of 1 mL/min.  Each HPLC measure-ment takes a total of 14.5 minutes.  Data are collected during the first 8.4 minutes while the last 6.1 minutes are used for re-equilibration of the column and for preparation of the next sample in the autosampler.  The program used by the autosampler is detailed in Table 2.
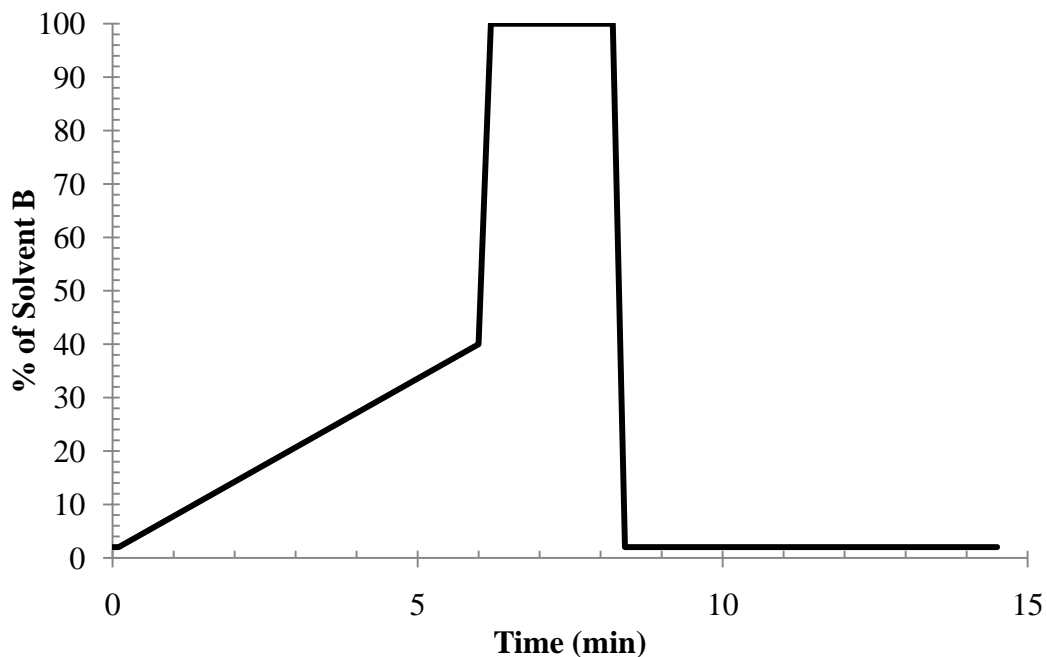
**Figure 57.** Percentage of solvent B in HPLC effluent vs. time for separation of amino acids asparagine and aspartic acid.

| |
|---|
| 1. Draw 2.5 µL borate buffer into syringe. |
| 2. Draw 0.5 µL 1 mM valine solution into syringe. |
| 3. Draw 0.5 µL sample into syringe. |
| 4. Mix syringe contents 5 times. |
| 5. Wait 0.2 minutes. |
| 6. Draw 0.5 µL OPA solution into syringe. |
| 7. Mix syringe contents 6 times. |
| 8. Draw 32 µL water into syringe. |
| 9. Mix syringe contents 8 times. |
| 10. Inject syringe contents onto column. |

**Table 2.** Autosampler program used with the Agilent 1200 autosampler in order to perform pre-column derivatization reaction of amino acids with o-phthalaldehyde. Mixing of syringe contents is done by moving the injector piston back and forth in air.

In order to account for variabilities in individual HPLC measurements, quantification was done using an internal standard and a calibration curve prepared from samples of known concentration. The internal standard was added automatically to each sample using the auto-sampler. The chosen internal standard was the amino acid valine. This amino acid appears in the chromatogram at an appreciable distance from the peaks for asparagine and aspartic acid allowing for easy resolution. A sample chromatogram is given in Figure 58. Calibration curves were made by plotting the ratio of the measured area of the peak of interest (asparagine or aspartic acid) and the measured area of the valine internal standard versus the known concentration of the standard solution. This provides a calibration constant for the ratio of the area of the peak of interest to the area of the internal standard.
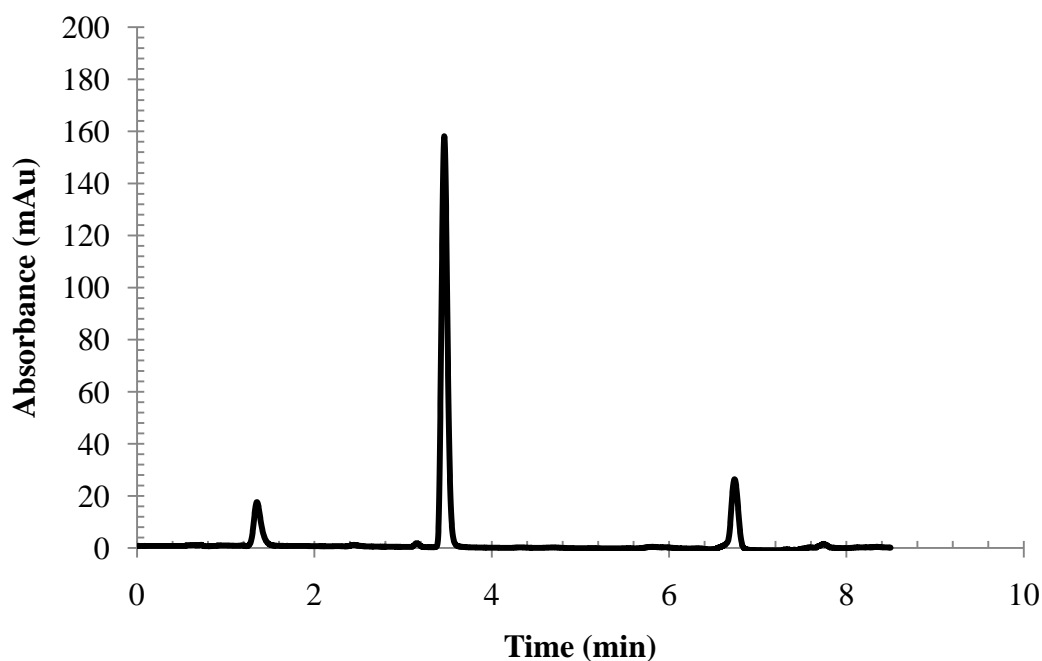


**Figure 58. Typical chromatogram from HPLC separation of aspartic acid, asparagine and valine.**

The liquid samples described in section 4.2.1 can be used directly for HPLC analysis. Solid samples from dissolution of the product crystal as described above can also be used directly when the amount of solid dissolved is roughly 0.02 g or less in 20 mL of water.

Variability in concentration determination via HPLC was tested in terms of sampling variability and instrument variability. Experimental variability results from incomplete mixing of

the liquid phase and from small crystals present in solution that dissolve upon dilution of the liquid sample while instrument variability can arise from the uncertainty for volume measurement in the syringe.

The variability due to the Agilent instrument was tested by performing multiple injections of the same sample. The injection-to-injection variability in peak area ratio of asparagine to valine was found to be 1.7 $\pm$ 1.3 % for asparagine and 1.4 $\pm$ 1.3 % for the aspartic acid to valine area ratio. Variability due to sampling was tested by taking two samples at one time point and comparing the resulting HPLC areas. The variability due to sampling was found to be 1.7 $\pm$ 1.7% for the asparagine to valine and 2.8 $\pm$ 2.8% for aspartic acid to valine area ratio. The sampling variability is then indistinguishable from the instrument variability and in both cases the amount of variability is small.

## 4.3    Experimental Results and Discussion

### 4.3.1    Experimental Results

Experiments were performed at three different temperatures of the controlled temperature water bath used for cooling of the seed tube in order to explore the effect of temperature on the impurity incorporation during batch growth. Three experiments were performed at each of these temperatures in order to test the reproducibility of the proposed experimental method.

The initial concentrations of asparagine and aspartic acid were held constant in these experiments at 2.6 g of asparagine and 0.4 g of aspartic acid in 100.0 g of water. The concentration of asparagine was chosen so that the asparagine super-saturation at the bulk temperature of $25^0$C is roughly zero. Industrial crystallizations can have a wide range of impurity concentrations. The mass ratio of aspartic acid to asparagine in these experiments is 8 % which is a reasonable value for the impurity concentrations in industrial crystallization.

All experiments were conducted with a stirring rate of 200 rpm using a magnetic stir bar with a length of 1 inch. The pump was operated at 500 rpm for all experiments resulting in a flow rate of water through the seed tube of 1.4 liters per minute. The duration of each experiment was between 8 and 10 hours.

The overall mass balance for each experiment was checked by taking the known initial amounts of asparagine and aspartic acid and subtracting the weighed amount of crystal product and the final amounts in the liquid phase as determined by HPLC. Mass balances on asparagine and aspartic acid were performed as well by using HPLC analysis of the solid phase to determine the amount of each species that was deposited.

The discrepancy between mass in and the measured mass out is the accumulation. This can also be measured directly with the following procedure. After the seed tube with product is removed from the crystallization vessel, the vessel is sealed and heated before additional samples are taken for HPLC analysis. The purpose of this operation is to measure the amount of solid material present on surfaces other than the seed tube; such as the stir bar or the vessel walls. A large amount of solid being deposited on surfaces other than the seed tube could invalidate model fitting to the liquid phase concentration data.

The error in the mass balance will be compared to the initial amount of material used and also to the amount of crystal grown. The amount of crystal grown will be small in relation to the initial amount of material so a small percentage error in relation to the initial amount of material will be a much larger error in relation to the amount of product.

The liquid phase concentration and the solid phase impurity mole fraction data are fitted to the model using least squares regression. The batch model developed in section 2.2 along with the modification for non-constant surface temperature from section 4.2.2 were used with MATLAB to find the parameter values that provide the best fit of the measured data. The liquid phase concentration data are fit first to give a value for $k_A$, $\gamma$ and $K$. The asparagine concentration data are used to fit $k_A$ and the aspartic acid concentration data are then used with the value of $k_A$ to fit $\gamma$ and $K$. The values of $k_A$ fitted to the asparagine liquid phase data are then used with the solid phase data to find values of $\gamma$ and $K$ from the solid phase dissolution measurements.

Because the model has been modified to account for a variable temperature at the crystal-liquid interface the concentration of asparagine does depend slightly on the parameters $\gamma$ and $K$. The total amount of crystal depends on the parameters $\gamma$ and $K$ and the surface temperature depends on the total amount of crystal. In order to account for this the parameter

fitting is iterated until the difference in parameter values between sequential fittings is less than 0.1% of the value from the newest fit. Fitting of the solid phase data are done after this iterative fitting so that the final value of $k_A$ is used when fitting the solid phase data.

A plot representing one experiment is presented for each of the three temperatures of the seed tube water source. Each plot will show the measured concentration data as a function of time along with the best fit curve generated from model fitting to the data for that individual experiment. Reported values of the fitted parameters for each seed tube water source temperature represent averages over multiple experiments.

### 4.3.1.1 Experiments with a seed tube water source temperature of $5^0C$

The first set of experiments was conducted with the seed tube water source temperature at $5^0$C. The temperature at the inlet to the seed tube under these conditions was $7.0^0$C and the temperature at the outlet of the feed tube was $7.3^0$C. The concentration vs. time data along with best fit curves are shown in Figure 59 and Figure 60 for asparagine and aspartic acid respectively. The solid phase data collected by sequential dissolution of the crystal grown on the seed tube is presented in plots of mole fraction of aspartic acid versus relative mass of crystal. The relative mass of crystal is the mass of crystal from the seed tube wall to the point of measurement normalized by the total mass of crystal grown. A value of zero corresponds to the beginning of crystallization at the seed tube surface and a value of one is the exposed surface of the grown crystal. Samples are collected starting from a relative mass of one and proceeding towards zero. The solid phase data and best fit curve for the same experiment shown in Figure 59 and Figure 60 are shown in Figure 61.
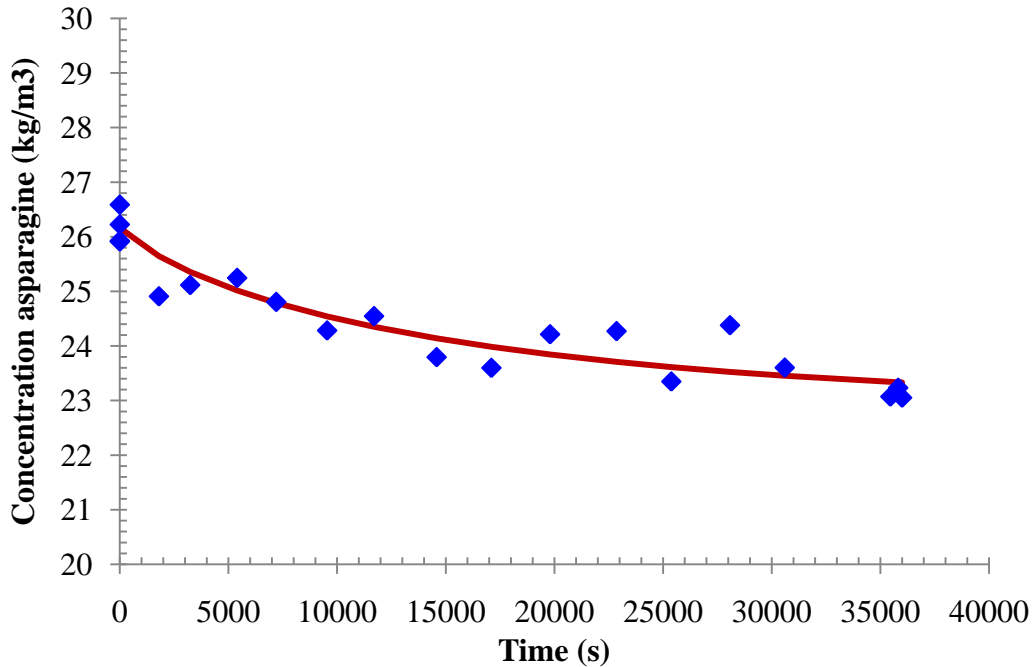
**Figure 59. Concentration of asparagine versus time as determined by HPLC for a batch experiment with the seed tube water source at 5$^0$C and 2.6 g of asparagine and 0.4 g of aspartic acid in 100 g of water. The solid line is the curve representing the best fit of the model for this crystallization process to the data. The solution is stirred at 200 rpm and the water is passed through the seed tube at 1.4 LPM.**
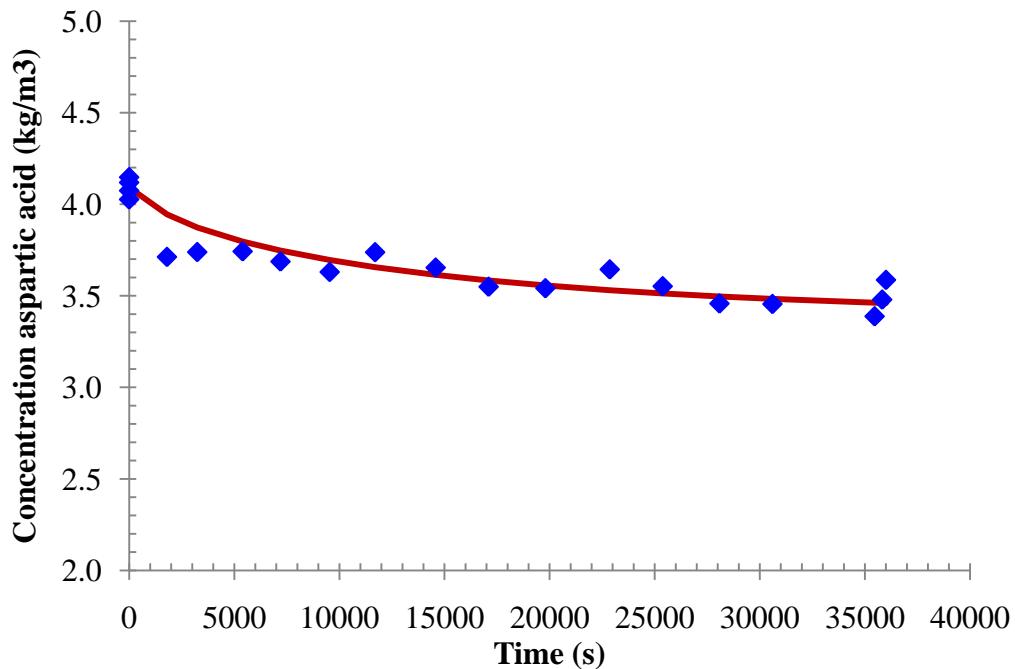


**Figure 60. Concentration of asparagine versus time as determined by HPLC for a batch experiment with the seed tube water source at 5$^0$C and 2.6 g of asparagine and 0.4 g of aspartic acid in 100 g of water. The solid line is the curve representing the best fit of the model for this crystallization process to the data. The solution is stirred at 200 rpm and the water is passed through the seed tube at 1.4 LPM.**
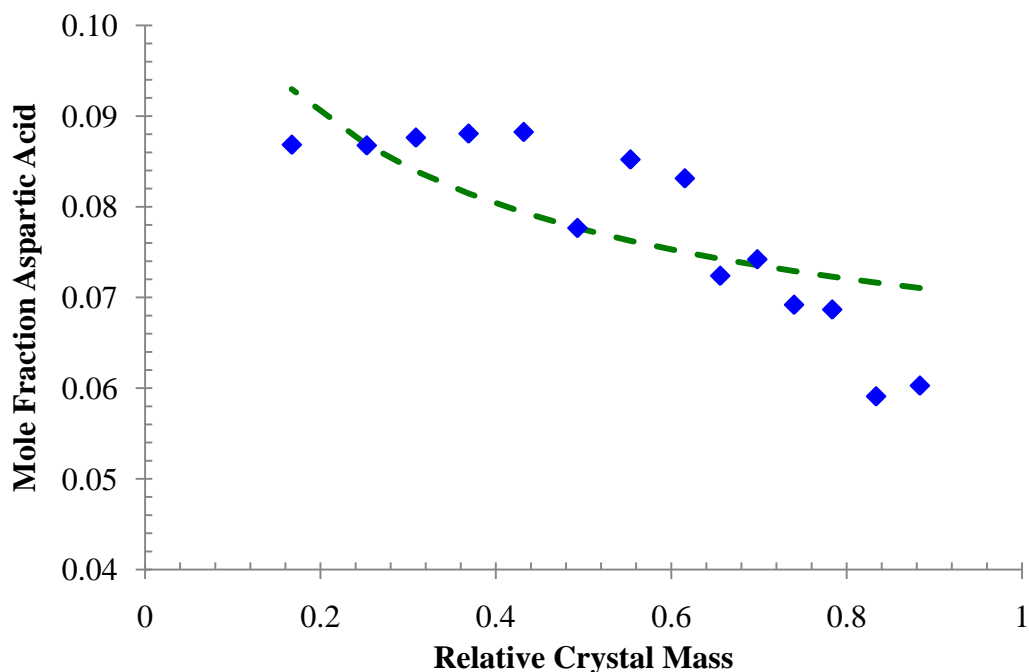
**Figure 61. Mole fraction of aspartic acid versus relative crystal mass as determined by HPLC for a batch experiment with the seed tube water source at 5$^0$C and 2.6 g of asparagine and 0.4 g of aspartic acid in 100 g of water. The dashed line is the curve representing the best fit of the model for this crystallization process to the data. The solution is stirred at 200 rpm and the water is passed through the seed tube at 1.4 LPM.**

The average values of the parameters $k_A$, $\gamma$ and $K$ for experiments with the cold water source at 5$^0$C are listed in Table 3 along with the average yield of asparagine, the average amount of crystal grown and the average accumulation in the liquid phase for these experiments. The yield is the weighed amount of product on the seed tube divided by the initial amount of asparagine and the accumulation is determined by the difference between the concentration of the heated solution remaining after the seed tube is removed and the final concentration of the liquid phase as determined by HPLC.

| Phase | $k_A$ (m/s) | $\gamma$ | $K$ | Yield (%) | Product (g) | Accumulation (g) |
|-------|-------------|----------|-----|-----------|-------------|------------------|
|  | $2.9 \pm 1.2*10^{-6}$ |  |  | $9.7 \pm 0.3$ | $0.252 \pm 0.008$ | $0.10 \pm 0.04$ |
| Liquid |  | $11 \pm 4$ | $1.2 \pm 0.1$ |  |  |  |
| Solid |  | $3.3 \pm 3.2$ | $0.49 \pm 0.04$ |  |  |  |

**Table 3. Average experimentally determined values for parameters $k_A$, $\gamma$ and $K$ along with the yield of asparagine, the mass of product and the mass of accumulation in the system for experiments with starting amounts of 2.6 g of asparagine, 0.4 g aspartic acid in 100 g water, stirred at 200 rpm with water flowing through the seed tube at 1.4 LPM with a seed tube water source temperature of $5^0$C. Parameters $\gamma$ and $K$ were determined from both liquid and solid phase data.**

### 4.3.1.2   Experiments with a seed tube water source temperature of $10^0C$

The next set of experiments used a cold source temperature of $10^0$C. The temperature at the inlet and outlet of the seed tube was $11.4^0$C and $11.6^0$C respectively. The concentration vs. time data for asparagine and aspartic acid are shown in Figure 62 and Figure 63 while the mole fraction aspartic acid in the crystal as a function of relative mass is given in Figure 64.
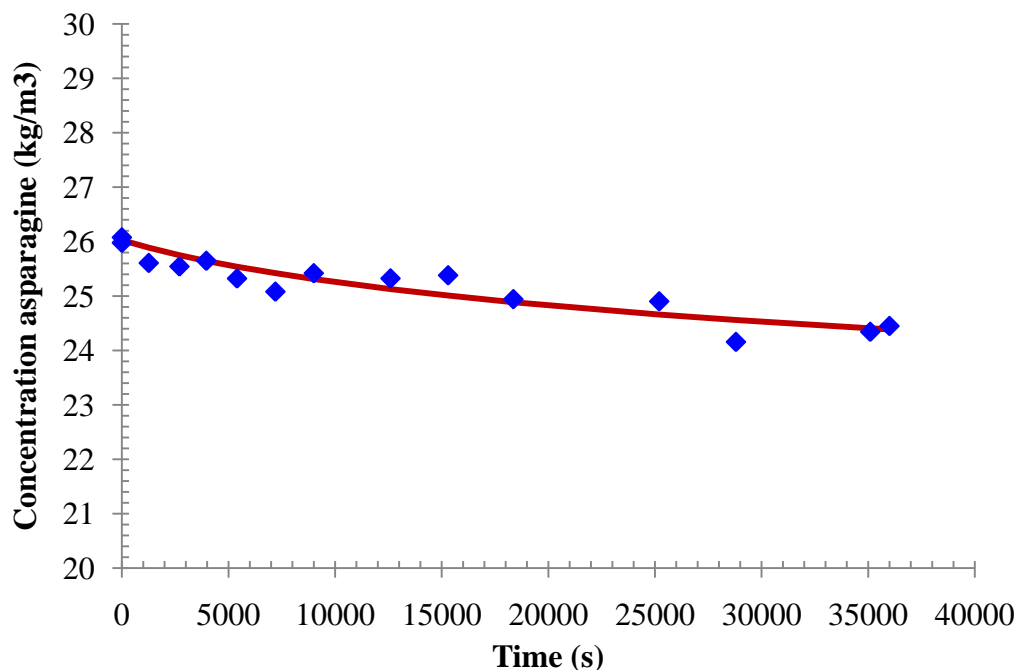


**Figure 62. Concentration of asparagine versus time as determined by HPLC for a batch experiment with the seed tube water source at $10^0$C and 2.6 g of asparagine and 0.4 g of aspartic acid in 100 g of water. The solid line is the curve representing the best fit of the model for this crystallization process to the data. The solution is stirred at 200 rpm and the water is passed through the seed tube at 1.4 LPM.**
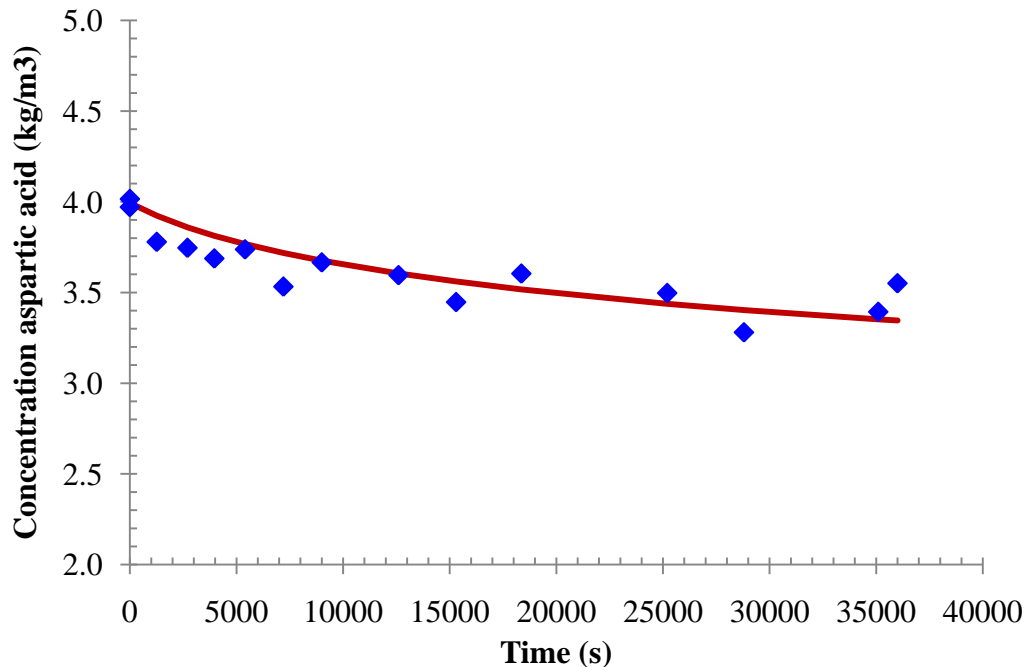
**Figure 63. Concentration of aspartic acid versus time as determined by HPLC for a batch experiment with the seed tube water source at 10⁰C and 2.6 g of asparagine and 0.4 g of aspartic acid in 100 g of water. The solid line is the curve representing the best fit of the model for this crystallization process to the data. The solution is stirred at 200 rpm and the water is passed through the seed tube at 1.4 LPM.**
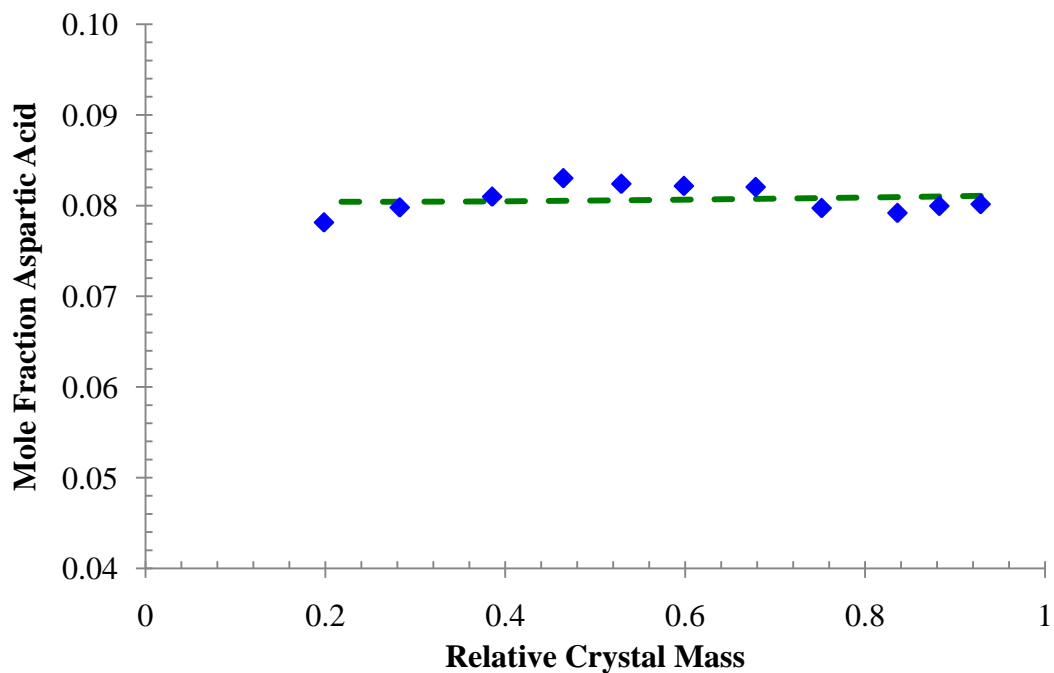


**Figure 64. Mole fraction of aspartic acid versus relative crystal mass as determined by HPLC for a batch experiment with the seed tube water source at 10⁰C and 2.6 g of asparagine and 0.4 g of aspartic acid in 100 g of water. The dashed line is the curve representing the best fit of the model for this crystallization process to the data. The solution is stirred at 200 rpm and the water is passed through the seed tube at 1.4 LPM.**

The average values of the parameters $k_A$, $\gamma$ and $K$ for experiments with the cold water source at 10$^0$C are listed in Table 4 along with the average yield of asparagine, amount of product and amount of accumulation for these experiments.

| Phase | $k_A$ (m/s) | $\gamma$ | $K$ | Yield (%) | Product (g) | Accumulation (g) |
|---|---|---|---|---|---|---|
| | $1.4 \pm 0.4 * 10^{-6}$ | | | $5.6 \pm 0.8$ | $0.15 \pm 0.02$ | $0.14 \pm 0.05$ |
| Liquid | | $13 \pm 10$ | $3.3 \pm 2.4$ | | | |
| Solid | | $0.63 \pm 0.22$ | $0.53 \pm 0.04$ | | | |

**Table 4.  Average experimentally determined values for parameters $k_A$, $\gamma$ and $K$ along with the yield of asparagine, the mass of product and the mass of accumulation in the system for experiments with starting amounts of 2.6 g of asparagine, 0.4 g aspartic acid in 100 g water, stirred at 200 rpm with water flowing through the seed tube at 1.4 LPM with a seed tube water source temperature of 10$^0$C.  Parameters $\gamma$ and $K$ were determined from both liquid and solid phase data.**

### 4.3.1.3        Experiments with a seed tube water source temperature of 15$^0$C

Experiments were also conducted using a cold source temperature of 15$^0$C.  The temperature at the inlet and outlet of the seed tube was 16.4$^0$C and 16.6$^0$C respectively.  The concentration vs. time data for asparagine and aspartic acid are shown in Figure 65 and Figure 66 while the mole fraction aspartic acid in the crystal as a function of relative mass is given in Figure 67.  The average values of the parameters $k_A$, $\gamma$ and $K$ for experiments with the cold water source at 15$^0$C are listed in Table 4 along with the average yield of asparagine, amount of product and amount of accumulation for these experiments.
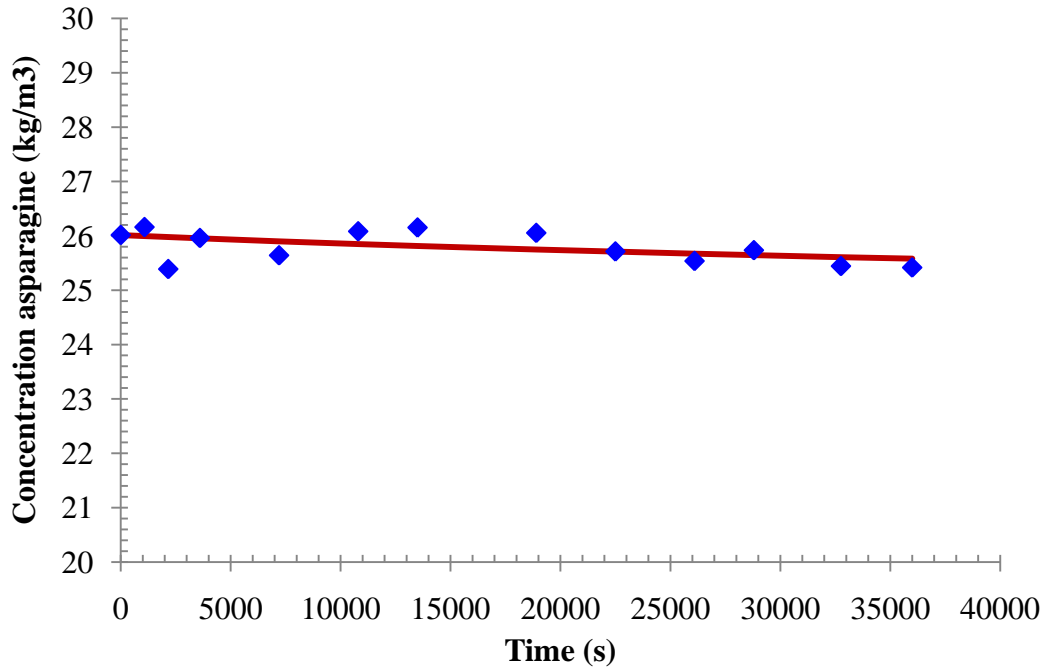
**Figure 65. Concentration of asparagine versus time as determined by HPLC for a batch experiment with the seed tube water source at 15$^0$C and 2.6 g of asparagine and 0.4 g of aspartic acid in 100 g of water. The solid line is the curve representing the best fit of the model for this crystallization process to the data. The solution is stirred at 200 rpm and the water is passed through the seed tube at 1.4 LPM.**
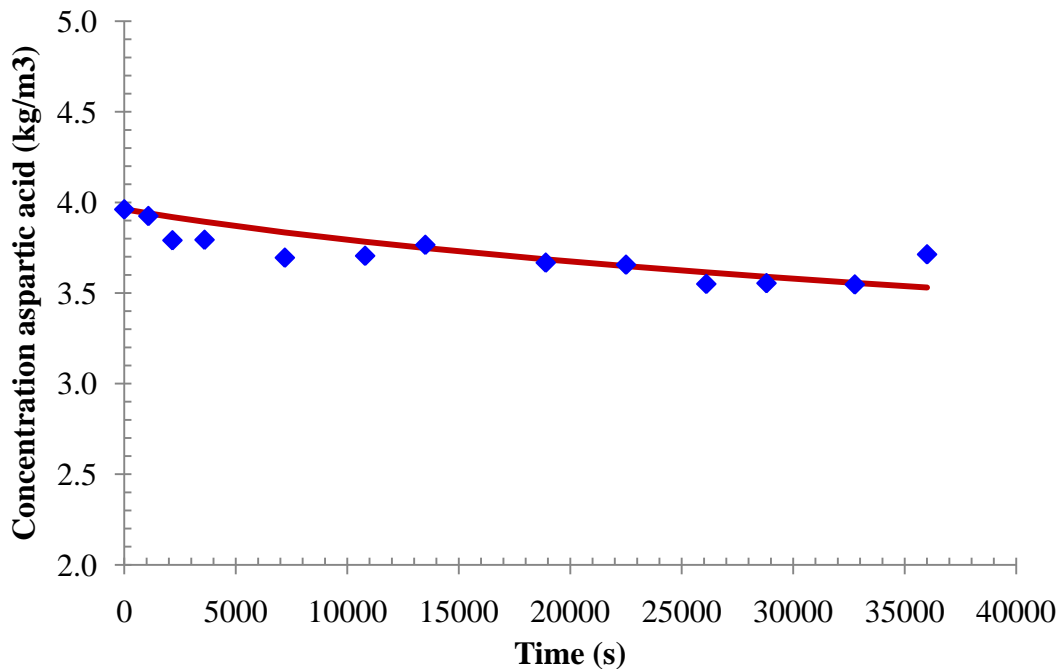


**Figure 66. Concentration of aspartic acid versus time as determined by HPLC for a batch experiment with the seed tube water source at 15$^0$C and 2.6 g of asparagine and 0.4 g of aspartic acid in 100 g of water. The solid line is the curve representing the best fit of the model for this crystallization process to the data. The solution is stirred at 200 rpm and the water is passed through the seed tube at 1.4 LPM.**

166
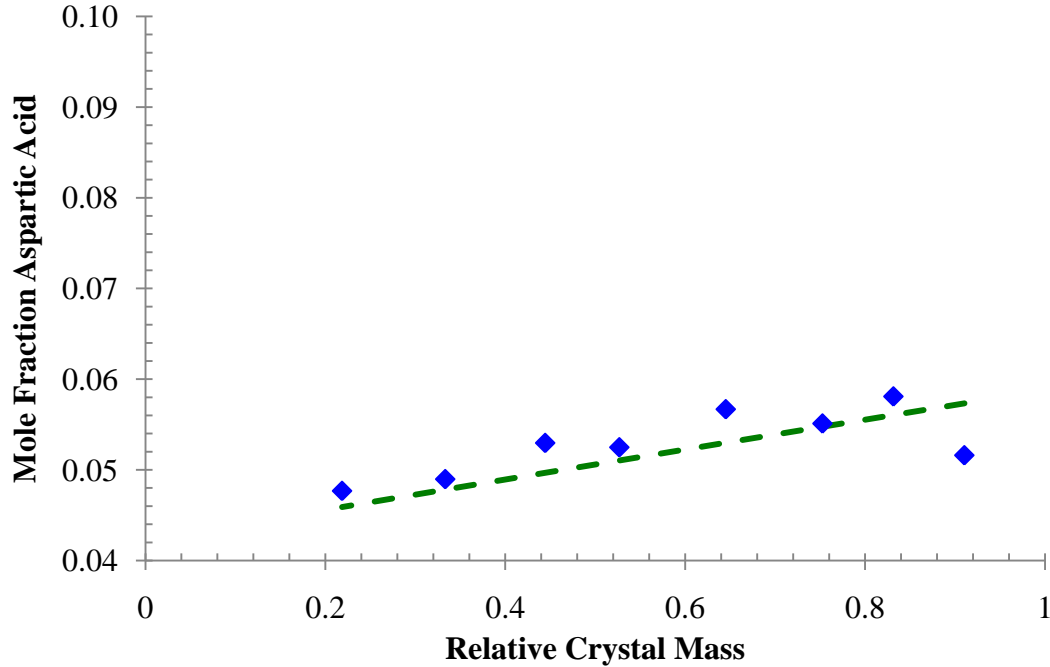
**Figure 67. Mole fraction of aspartic acid versus relative crystal mass as determined by HPLC for a batch experiment with the seed tube water source at 15⁰C and 2.6 g of asparagine and 0.4 g of aspartic acid in 100 g of water. The dashed line is the curve representing the best fit of the model for this crystallization process to the data. The solution is stirred at 200 rpm and the water is passed through the seed tube at 1.4 LPM.**

| Phase | $k_A$ (m/s) | $\gamma$ | $K$ | Yield (%) | Product (g) | Accumulation (g) |
|-------|------------|----------|-----|-----------|-------------|------------------|
|       | $5.3 \pm 4.6 \times 10^{-6}$ |  |  | $0.9 \pm 0.2$ | $0.024 \pm 0.004$ | $0.10 \pm 0.06$ |
| Liquid |  | $30 \pm 50$ | $8.8 \pm 5.0$ |  |  |  |
| Solid |  | $0.12 \pm 0.02$ | $0.60 \pm 0.38$ |  |  |  |

**Table 5. Average experimentally determined values for parameters $k_A$, $\gamma$ and $K$ along with the yield of asparagine, the mass of product and the mass of accumulation in the system for experiments with starting amounts of 2.6 g of asparagine, 0.4 g aspartic acid in 100 g water, stirred at 200 rpm with water flowing through the seed tube at 1.4 LPM with a seed tube water source temperature of 15⁰C. Parameters $\gamma$ and $K$ were determined from both liquid and solid phase data.**

### 4.3.1.4  Experimental separation factors

The separation factor as defined in section 1.2.2 was calculated for each experiment. The value was determined using the final concentration ratio of A to B in the liquid phase as given by the HPLC results and the total amount of asparagine and aspartic acid in the solid phase by summing the HPLC results from product dissolution. The separation factor was also determined from the model (equation (4.4)) using the best fit parameters for the liquid and sol-

id phase data.  The average calculated values of the separation factor are shown in Table 6 for the three seed tube water source temperatures used.

| Seed Tube Water Source Temperature ($^0$C) | $\alpha_{exp}$ | $\alpha_{L,fit}$ | $\alpha_{S,fit}$ |
|:---:|:---:|:---:|:---:|
| 5 | $0.60 \pm 0.04$ | $1.6 \pm 0.2$ | $0.55 \pm 0.03$ |
| 10 | $0.57 \pm 0.05$ | $2.7 \pm 0.6$ | $0.54 \pm 0.03$ |
| 15 | $0.6 \pm 0.2$ | $10 \pm 7$ | $0.32 \pm 0.09$ |

**Table 6.  Separation factors as a function of seed tube water source temperature from experimental data ($\alpha_{exp}$) and from the batch model using the best fit parameters for both the liquid ($\alpha_{L,fit}$) and solid ($\alpha_{S,fit}$) phase experimental data.  Data was collected for experiments with 2.6 g of asparagine, 0.4 g aspartic acid in 100 g water, stirred at 200 rpm with water flowing through the seed tube at 1.4 LPM with a seed tube water source temperature of 5, 10 or 15$^0$C.**

### 4.3.1.5   Experiments with pure asparagine

Experiments were performed with pure asparagine in order to determine the dissolution rate for asparagine.  These experiments were performed by taking a seed tube with pure asparagine crystal and submerging it in a stirred solution of water at 25$^0$C.  The pure asparagine coated seed tube was obtained by performing an experiment similar to the ones described above with no aspartic acid.  No water is passed through the seed tube during this operation.  Samples are then taken with time and the concentration is determined by HPLC analysis.

The dissolution is limited by the amount of crystal on the seed tube which rapidly approaches zero for the large driving forces used in these experiments.  The dissolution rate is estimated using only the first few data points to approximate the tangent to the dissolution profile.  The temperature during this dissolution experiment is constant and so data fitting is done to the simple equation given in equation (2.32).  A graph of one experiment along with the fitted tangent line is given in Figure 68.
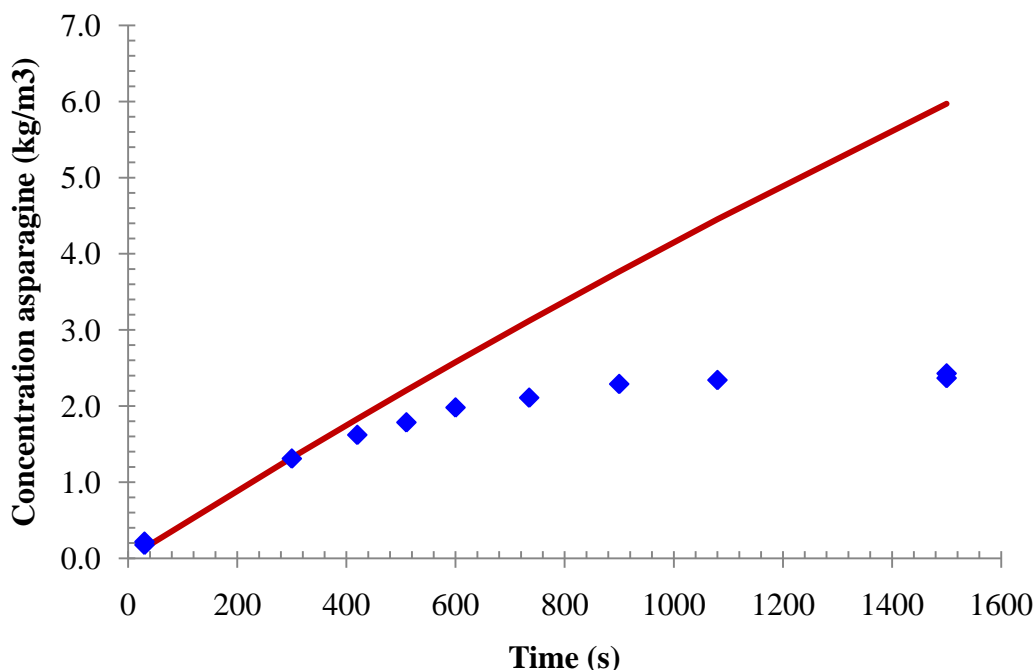
**Figure 68. Concentration of asparagine versus time as determined by HPLC for a batch dissolution experiment of 0.25 g of asparagine on a seed tube placed in 100 g of water. The solid line is the curve representing the best fit of the model to the initial data points. The solution is stirred at 200 rpm and the bulk temperature is maintained at 25⁰C.**

The average value of the dissolution rate constant calculated in this manner from two experiments was $(2.4 \pm 0.4)*10^{-5}$ m/s.

### 4.3.2 Discussion of Experimental Results

#### 4.3.2.1 Discussion of mass balance

The average yield, amount of product and the amount of accumulation are collected in Table 7. The product is the weighed amount of material deposited on the seed tube, the yield is the product divided by the initial amount of asparagine and the accumulation is the difference in concentration between the heated solution after the seed tube is removed and the final concentration of the liquid phase during the experiment as determined by HPLC.

| Seed Tube Water Source Temperature ($^0$C) | Yield (%) | Product (g) | Accumulation (g) |
|---|---|---|---|
| 5 | 9.7 $\pm$ 0.3 | 0.252 $\pm$ 0.008 | 0.10 $\pm$ 0.04 |
| 10 | 5.6 $\pm$ 0.8 | 0.15 $\pm$ 0.02 | 0.14 $\pm$ 0.05 |
| 15 | 0.9 $\pm$ 0.2 | 0.024 $\pm$ 0.004 | 0.10 $\pm$ 0.06 |

**Table 7.  Average experimentally determined values for yield (in relation to initial amount of asparagine), product and accumulation for experiments with 2.6 g of asparagine, 0.4 g aspartic acid in 100 g water, stirred at 200 rpm with water flowing through the seed tube at 1.4**

It is apparent from Table 7 that the amount of accumulation in the liquid phase during these experiments is of the same order of magnitude as the total amount of product generated in these experiments.  This means that the concentration depletion in the liquid phase is caused by a significant amount of crystallization on surfaces other than the seed tube. Fitting of the model parameters to the liquid phase concentration profiles will result in significant overestimation because of this extra crystallization occurring in the liquid phase.

Even though the amount of accumulation is comparable to the amount of crystal grown on the seed tube the overall mass balance with respect to the initial amounts of material in all cases has less than 10% error.  This is possible because the overall change in concentration of the liquid phase is small compared to the initial concentrations.  The amount of material (asparagine and aspartic acid) at the beginning of every experiment is 3 g.  For one experiment performed with the seed tube water source temperate at 5$^0$C the total amount of material in the liquid phase and on the seed tube at the end of the experiment as determined by HPLC and weighing was 2.9 g.  The 0.1 g difference corresponds to a 3% error in relation to the total initial mass but in relation to the 0.25 g of product grown on the seed tube this is a 40 % error.  The concentration profile in the liquid then represents 40% more depletion of material than is accounted for on the seed tube surface and so a large error in the parameters fitted to the liquid phase data is expected.

A larger ratio of crystal grown to accumulation in the liquid phase is necessary to obtain reasonable parameters from liquid phase concentration data.  This could be done by increasing the amount of crystal growth if the accumulation stays constant or by decreasing the amount of

accumulation. More growth could be obtained by increasing the surface area for growth or increasing the supersaturation. The supersaturation can be increased by lowering the temperature of the water flowing through the seed tube or by increasing the initial concentration. Increasing the initial concentration though is not expected to be a good approach to this problem because higher concentrations of the bulk liquid will increase the possibility of nucleation in the bulk and it will likely not address the issue of the total growth being small compared to the initial amount of material.

Lowering the temperature in the seed tube is a good option because the bulk temperature and concentration remain the same but more growth will occur on the seed tube. This is seen for the experiments conducted here with the lowest temperature of water flowing through the seed tube loop. These experiments correspond to the largest amount of product and the smallest ratio of accumulation to product. In fact the accumulation is roughly constant for the experiments at the three different seed tube water source temperatures which if true for even lower temperatures of the seed tube water source would support this strategy.

The accumulation may depend on the stirring speed or the bulk temperature. Raising the temperature of the bulk liquid may help to reduce accumulation in the liquid phase but this would also likely result in smaller amounts of crystal growth for a fixed temperature in the seed tube so this strategy should be pursued in conjunction with a lower seed tube water temperature. Experiments varying the bulk temperature and the stirring speed may provide insight that would allow accumulation to be minimized by appropriate choices of the operating parameters. Both of these parameters also are expected to have an impact on the kinetic parameters of the crystallization and this must be accounted for as well when attempting to minimize accumulation.

### 4.3.2.2 Discussion of fitted parameters

The fitted parameters for the three different seed tube water source temperatures are listed again in Table 8.

| Seed Tube Water Source Temperature ($^0$C) | $k_A*10^6$ (m/s) | Liquid Phase | | Solid Phase | |
|---|---|---|---|---|---|
| | | $\gamma$ | $K$ | $\gamma$ | $K$ |
| 5 | 2.9 ± 1.2 | 11 ± 4 | 1.2 ± 0.1 | 3.3 ± 3.2 | 0.49 ± 0.04 |
| 10 | 1.4 ± 0.4 | 13 ± 10 | 3.3 ± 2.4 | 0.63 ± 0.22 | 0.53 ± 0.04 |
| 15 | 5.3 ± 4.6 | 30 ± 50 | 8.8 ± 5.0 | 0.12 ± 0.02 | 0.60 ± 0.38 |

**Table 8. Average experimentally determined values for the parameters $k_A$, $\gamma$ and $K$ for experiments with 2.6 g of asparagine, 0.4 g aspartic acid in 100 g water, stirred at 200 rpm with water flowing through the seed tube at 1.4 LPM with a seed tube water source temperature of 5, 10 or 15$^0$C. Parameters $\gamma$ and $K$ were determined from both liquid and solid phase data.**

The experimental method used complicates the interpretation of these average parameter values. The model parameters are expected to depend on temperature so the fitted values from these experiments are an average over the temperature range experienced at the liquid-solid interface. The fitted parameters from these experiments then do not represent the parameter values at a specific temperature which would be the most useful information for modeling purposes. The fitted values can be used to understand the magnitude of the constants which is very important because the value of $\gamma$ in relation to one has a significant impact on the utility of the proposed counter-current process as seen in section 2.4.

The bulk temperature in all experiments was held at the same value so that there is overlap in the temperature range experienced at the solid-liquid interface for all three temperatures of the seed tube water source. This means that the average parameters from different sets of experiments will overlap. Variation of the fitted parameters with temperature will be somewhat underrepresented due to the overlap of solid-liquid temperature profiles. A large variation in the fitted parameters at different temperatures will indicate a strong dependence of that parameter on temperature. The fitted parameters in Table 8 do not indicate strong temperature dependence except possibly in the case of $\gamma$ from the solid phase data.

The experiments performed with the seed tube water source temperature at 15$^0$C were not as reliable as other experiments. The uncertainty in the fitted parameters for these experiments is large and the parameter values are in some cases very different from the fitted parameters at the other two temperatures. The total amount of crystal grown at this tempera-

ture was small, 0.02 g on average, which is 5 times less than the average amount of accumulation and therefore the parameter values fitted to the liquid concentration data will be almost entirely due to crystallization on surfaces other than the seed tube. Only a very thin layer of crystal is grown on the seed tube with a small impurity concentration gradient which makes the sampling method difficult to employ reliably and may lead to unrealistic values for the fitted parameters. This point will be explored further after discussion of general issues with the solid phase analysis is presented.

The fitted values of $\gamma$ are much greater than one for the liquid phase data but order one or less from the solid phase data. The values of $K$ from both the liquid and solid phase data are roughly order one in all cases. Because the liquid phase data represents crystallization on surfaces other than the seed tube these values are not considered to be reliable and the solid phase values are more applicable to this system.

For the solid phase data the fitted value of $\gamma$ is greater than one for the experiments at $5^{0}$C and less than one for experiments at 10 or $15^{0}$C. The simplified analysis of the batch model from section 4.1.2 predicts that the concentration of impurity in the solid will increase with growth when $\gamma<1$ and decrease with growth when $\gamma>1$. Both of these statements can be considered true when analyzing the measured solid phase data which illustrates a major issue with the solid phase data which will be discussed in section 4.3.2.6. The values of $K$ from the solid phase data are all less than one which indicates that the component of interest is preferentially incorporated into the crystal lattice.

The separation factors ($\alpha$) calculated from the batch model using the fitted parameters from the liquid phase data are greater than one while $\alpha$ from the solid phase fitted parameters are less than one. The values of $\alpha$ calculated directly from the experimental data are in good agreement with the values predicted by the solid phase data fitted parameters. This again indicates that the parameters fitted to the liquid phase data are not an accurate representation of the system behavior. Comparison of the predicted liquid phase concentration profile using solid phase fitted parameters and vice versa will further demonstrate this observation.

### 4.3.2.3 Discussion of Sum of Squared Residuals for Liquid and Solid Phase Data

In order to better understand the parameters fit to the liquid and solid phase data, the sum of squared residuals (SSR) for a wide range of values for $\gamma$ and $K$ were calculated and plotted. The range of values for $\gamma$ in these plots is larger than the possible range of values for data fitting when the value of $k_B$ is constrained by the mass transfer rate calculated in section 4.2.4. This was done to show that the behavior is consistent in the limits of high $\gamma$ and high $K$ even though these values are physically unattainable. The maximum value of $\gamma$ found from data fitting with the mass transfer constraint was order 10.

A contour plot of the sum of squared residuals vs. $\gamma$ and $K$ from fitting to the liquid phase data for an experiment with a seed tube water source temperature of $10^0$C is shown in Figure 69.
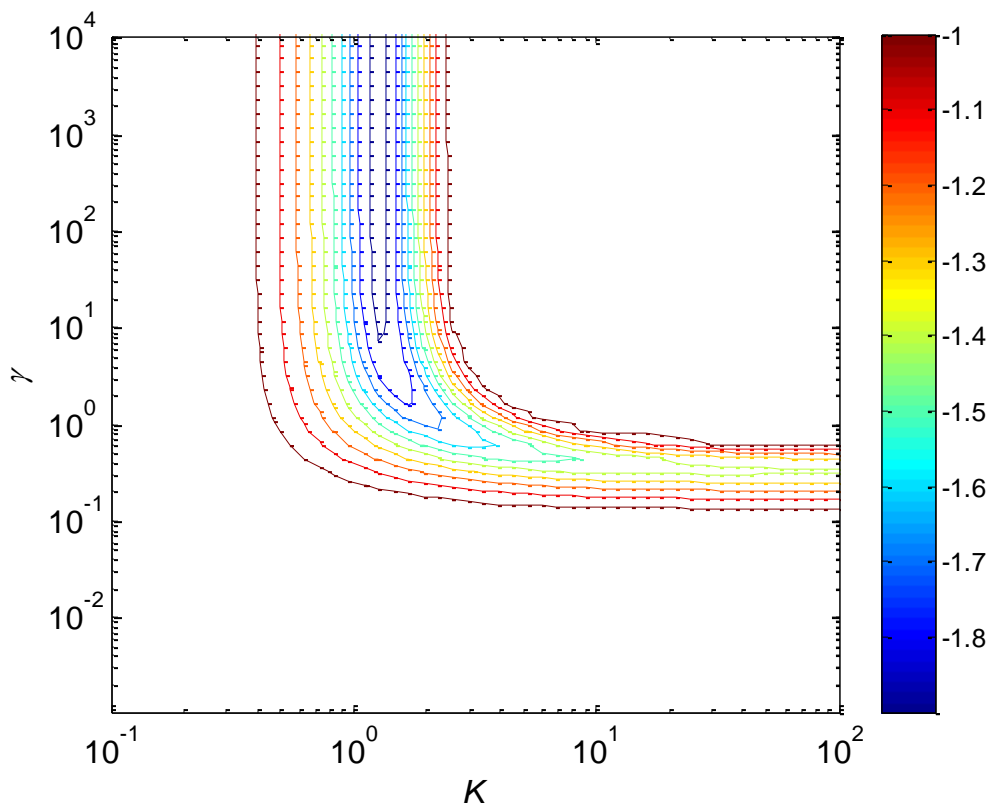


**Figure 69. Log of the sum of squared residuals for fitting of liquid phase data for an experiment with seed tube water source temperature of $10^0$C at various $\gamma$ and $K$ values. SSR values that are more than 100 times greater than the minimum value have been set equal to 100 times the minimum value so that the minimum values are easier to see.**

The corresponding plot for fits to the solid phase data from the same experiment is shown in Figure 70.
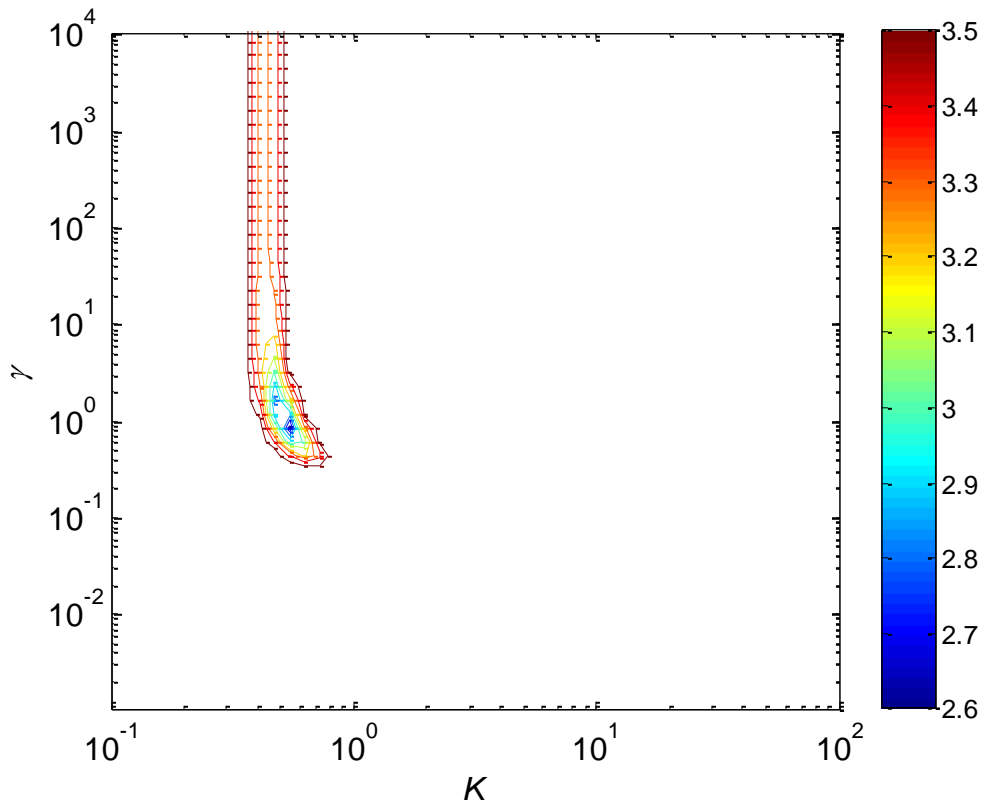


**Figure 70. Log of the sum of squared residuals for fitting of solid phase data for an experiment with seed tube water source temperature of 10⁰C at various $\gamma$ and $K$ values.  SSR values that are more than 100 times greater than the minimum value have been set equal to 100 times the minimum value so that the minimum values are easier to see.**

It is seen in Figure 69 that there is no distinct minima when fitting the liquid phase data. The best fit corresponds to a large value of $\gamma$ but many specific values of $\gamma$ will give essentially the same fit.  As discussed in section 2.2.3 a very large value of $\gamma$ corresponds to the case where there is no resistance to impurity incorporation in the crystal.  This will be equally true for any value of $\gamma$ that is sufficiently large.

The maximum value of $\gamma$ that is allowed by the constraint on $k_B$ for the above experiment is approximately 13.  Looking at Figure 69 this value of $\gamma$ corresponds to a value of $K$ equal to 1.3.  Using these parameter values along with the value of $k_A$ determined for this experiment

a plot showing the concentration profile of the impurity in the liquid phase and the concentration driving force for the impurity was prepared.  This is shown in Figure 71.
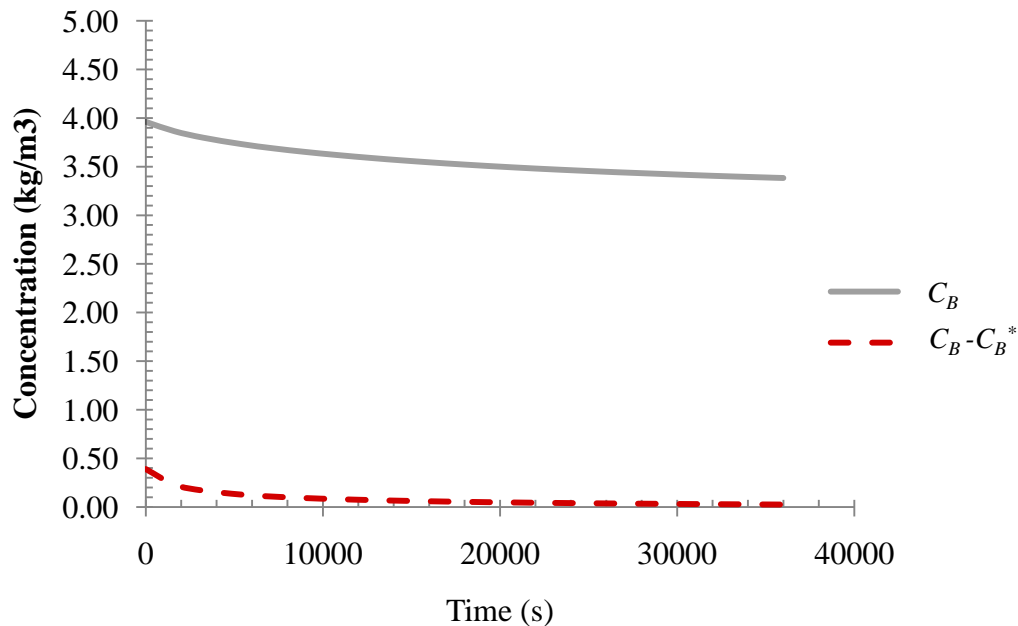


**Figure 71.  Concentration profile of aspartic acid and aspartic acid concentration driving force from model using best fit parameters for experiment performed with seed tube water source temperature of 10$^0$C.**

Figure 71 indicates that the concentration driving force of the impurity does very rapidly approach zero.  The time constant for the change in the concentration driving force is approximately 4,000 s while the time constant for change of the concentration of the impurity much larger.  The value of the time constant for the concentration of the impurity is hard to estimate from these plots because not enough of the profile was measured experimentally.  These time constants indicate that the change in concentration of the impurity is not controlled by the concentration driving force for impurity incorporation.  Larger values of $\gamma$ result in concentration driving force values that start closer to zero and decay even faster.  As $\gamma$ becomes even larger, the concentration driving force will eventually become uniformly zero.

When $\gamma$ is large it is also expected that the change in concentration of the impurity will closely follow the change of the component of interest because the limiting factor for impurity incorporation is the amount of crystal available for incorporation.  This can be studied by comparing the concentration profiles for species A and B.  If they have the same time constant then

the change in the concentration of the impurity will be seen to be driven by the change in concentration of the component of interest. A plot of the concentration of the component of interest using the model and the fitted parameters for the same experiment as shown in Figure 71 is shown in Figure 72. The concentration change of species A is seen to very closely resemble the concentration change for species B and the change of species B is controlled by the change in species A as expected.
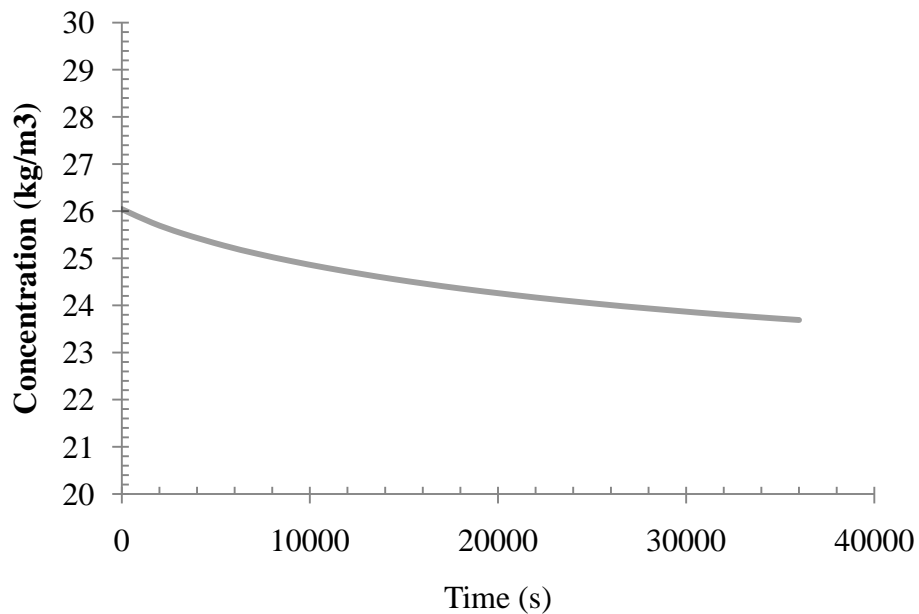


**Figure 72. Concentration profile of asparagine from model using best fit parameters for experiment performed with seed tube water source temperature of 10⁰C.**

Although the previous analysis has explained the behavior given by the parameters fitted to the liquid phase data, the parameter values fitted to the liquid phase data should not be considered accurate values for the desired behavior because the change in the liquid phase concentration corresponds to crystallization on multiple surfaces. The incorporation rate constant for species B is equal to the rate constant $k_B$ times the area for growth $a$. This area is represented in the model by the surface area of the seed tube and if crystallization occurs on other surfaces the model will overestimate the value of $k_B$ in order to compensate for the small value of $a$.

The plot of the SSR for the solid phase data shown in Figure 70 also has a valley at large $\gamma$ but there is now a distinct minimum point indicating a best fit set of parameter values. The parameter values at this minimum are expected to provide a better representation of the system and are considered the most representative values for describing asparagine and aspartic acid in water.

### 4.3.2.4 Comparison of model predictions to the data using the fitted parameters

Predicted liquid phase concentration profiles for asparagine and aspartic acid using the parameters fitted to the liquid and solid phase experimental data are shown in Figure 73 and Figure 74 along with experimental data for an experiment performed with a seed tube water source temperature of $5^0$C. The solid phase data with predicted concentration profiles using the best fit parameters from the liquid and solid phase data for the same experiment are presented in Figure 75. A plot of the solid phase data along with fitted curves using parameters fitted to both liquid and solid phase data for an experiment performed with the seed tube water source temperature at $15^0$C is given in Figure 76.

The slight difference in the fit to the asparagine concentration in the liquid phase for the two sets of parameters shown in Figure 73 occurs because the value of $k_A$ was the same for liquid and solid phase fitting. Different values for $\gamma$ and $K$ affect the total amount of crystal grown which affects the asparagine concentration in the batch model because the liquid-crystal interface temperature depends on the total amount of crystal grown. The value of $k_A$ from the liquid phase fit was used for solid phase analysis because the mole fraction of impurity (equation (4.7)) has only a weak dependence on $k_A$ but a strong dependence on $\gamma$ so that if $k_A$ is not fixed a wide range of $k_A$ values can give the same fit.

These plots further indicate that the parameters fitted to the liquid phase concentration profile are not representative of the modeled behavior. The presence of crystals on surfaces other than the seed tube results in parameters fitted to the liquid phase data that are too large. When these parameters are used to predict the impurity concentration profile in the solid phase the predicted values are 2-10 times larger than the measured values as can be seen in Figure 75 and Figure 76.
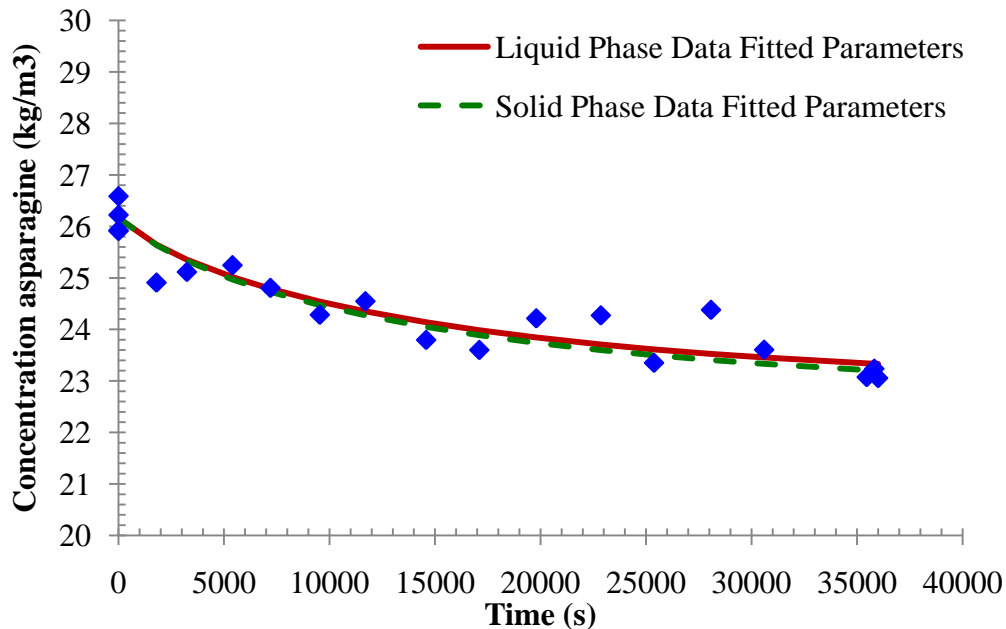
**Figure 73.** Concentration of asparagine versus time as determined by HPLC for a batch experiment with the seed tube water source at 5⁰C and 2.6 g of asparagine and 0.4 g of aspartic acid in 100 g of water. The solid line is the curve representing the best fit of the batch crystallization model to the liquid phase data and the dashed line is the concentration profile predicted using the best fit parameters from the solid phase data for this experiment. The solution is stirred at 200 rpm and the water is passed through the seed tube at 1.4 LPM.
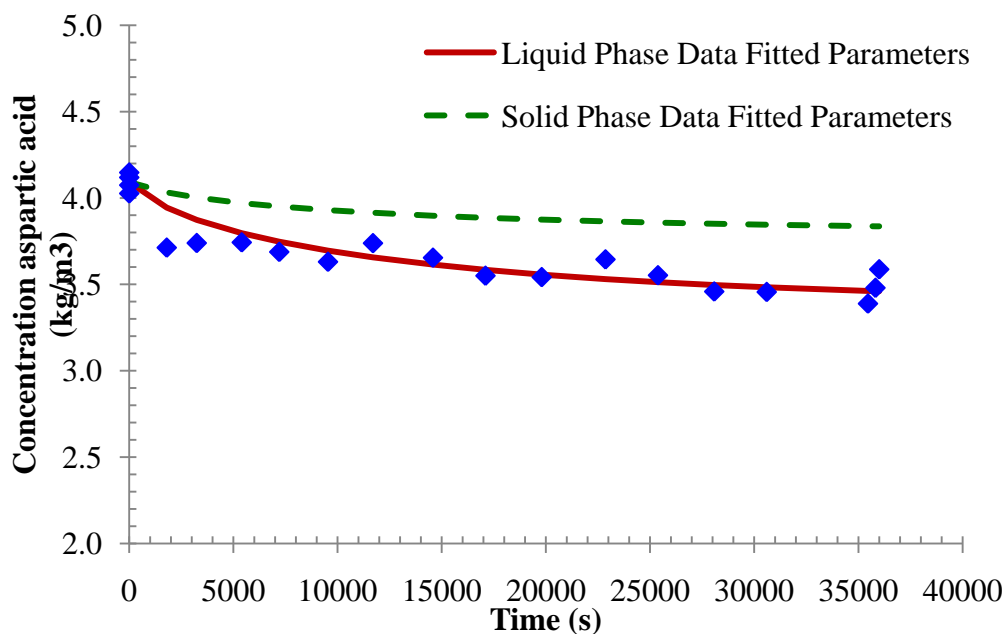


**Figure 74.** Concentration of aspartic acid versus time as determined by HPLC for a batch experiment with the seed tube water source at 5⁰C and 2.6 g of asparagine and 0.4 g of aspartic acid in 100 g of water. The solid line is the curve representing the best fit of the batch crystallization model to the liquid phase data and the dashed line is the concentration profile predicted using the best fit parameters from the solid phase data for this experiment. The solution is stirred at 200 rpm and the water is passed through the seed tube at 1.4 LPM.

179
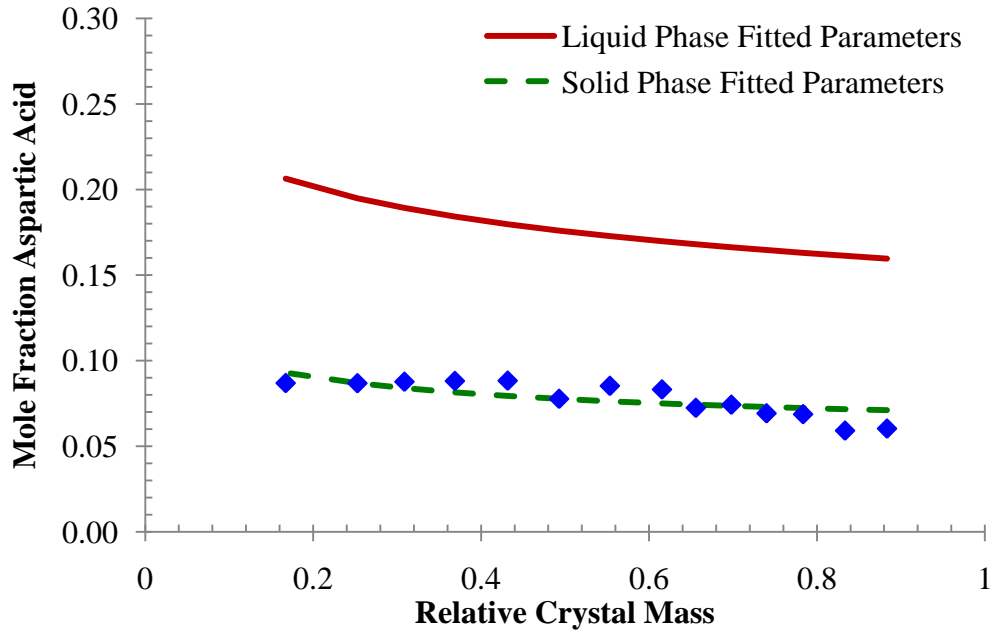
**Figure 75. Mole fraction of aspartic acid versus relative crystal mass as determined by HPLC for a batch experiment with the seed tube water source at 5$^0$C and 2.6 g of asparagine and 0.4 g of aspartic acid in 100 g of water. The dashed line is the curve representing the best fit of surface mole fraction of impurity equation derived from the batch crystallization model to the data and the solid line is the prediction for the impurity mole fraction using the parameters fitted to the liquid phase data. The solution is stirred at 200 rpm and the water is passed through the seed tube at 1.4 LPM.**
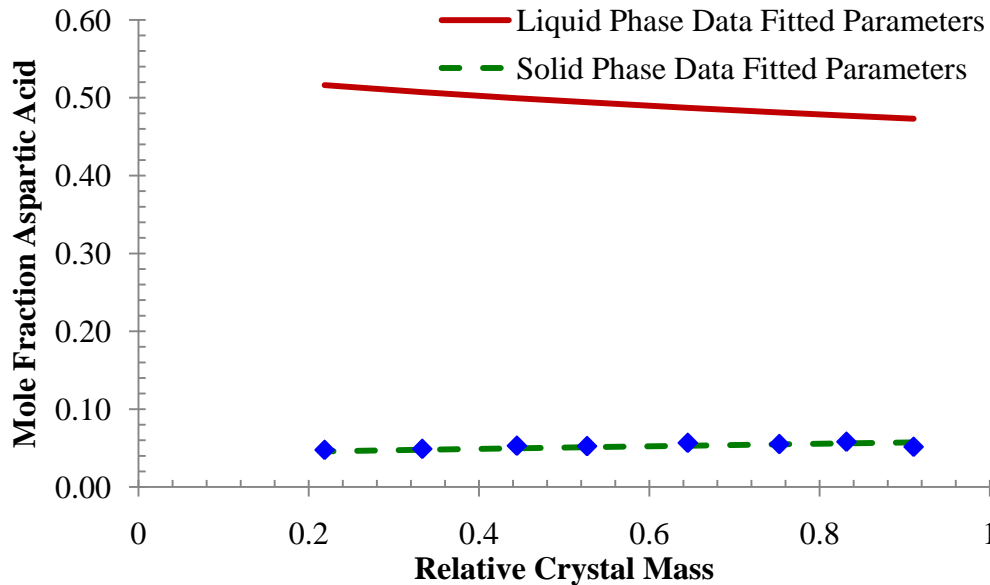


**Figure 76. Mole fraction of aspartic acid versus relative crystal mass as determined by HPLC for a batch experiment with the seed tube water source at 15$^0$C and 2.6 g of asparagine and 0.4 g of aspartic acid in 100 g of water. The dashed line is the curve representing the best fit of surface mole fraction of impurity equation derived from the batch crystallization model to the data and the solid line is the prediction for the impurity mole fraction using the parameters fitted to the liquid phase data. The solution is stirred at 200 rpm and the water is passed through the seed tube at 1.4 LPM.**

The liquid phase concentration profile of aspartic acid predicted by the parameters fitted to the solid phase data predict a smaller change in concentration than observed experimentally. This is seen in Figure 74. The difference between these two curves is a measure of how much asparagine is deposited in the liquid phase on surfaces other than the seed tube. For the current experiments, the parameters fitted to the solid phase data are a more appropriate representation of the asparagine and aspartic acid system in water.

Although the parameters fitted to the solid phase are likely more representative of the modeled behavior there are issues with the solid phase data. The measured solid phase data shown in Figure 75 show a concave trend while the best fit curve is convex. Possible explanations for this discrepancy will be discussed in section 4.3.2.6.

### 4.3.2.5   Adjustment of $k_A$ to account for accumulation in the liquid phase

The large amount of accumulation with respect to the amount of crystal grown will also affect the value of $k_A$ fitted to the liquid phase concentration data. This is especially important because this value of $k_A$ is used when fitting the solid phase data. To determine the possible impact of this overestimation, the solid phase data were re-fitted using a value of $k_A$ scaled by the ratio of product to accumulation plus product. The average results are listed in Table 9.

| Seed Tube Water Source Temperature ($^0$C) | Solid Phase | | | |
| --- | --- | --- | --- | --- |
| | $k_A*10^6$ (m/s) | $\gamma$ | $K$ | $\alpha_{S,fit}$ |
| 5 | $2.0 \pm 0.6$ | $4.7 \pm 5.5$ | $0.48 \pm 0.05$ | $0.57 \pm 0.04$ |
| 10 | $0.7 \pm 0.2$ | $0.58 \pm 0.33$ | $0.57 \pm 0.09$ | $0.53 \pm 0.02$ |
| 15 | $0.8 \pm 0.6$ | $0.09 \pm 0.03$ | $0.93 \pm 0.11$ | $0.33 \pm 0.06$ |

Table 9.  Average values for the parameters $\gamma$ and $K$ fitted to experiments with 2.6 g of asparagine, 0.4 g aspartic acid in 100 g water, stirred at 200 rpm with water flowing through the seed tube at 1.4 LPM with a seed tube water source temperature of 5, 10 or 15$^0$C.  The value of $k_A$ is the value of $k_A$ fitted to the liquid phase data and multiplied by the amount of crystal product divided by the amount of crystal product plus the amount of accumulation in the liquid phase.  The separation factor, $\alpha_{S,fit}$, is the value calculated from the model using the parameter values in this table.

The change in the parameters $\gamma$ and $K$ from Table 8 to Table 9 is small. The equivalent parameter values show significant overlap between the two tables when considering the uncertainties. This indicates that changing the value of $k_A$ has essentially no effect on the parameters controlling impurity incorporation into the crystal. This is consistent with the expected behavior based on analysis of the expression for the mole fraction of impurity in the crystal (equation (4.7)) and justifies use of the value of $k_A$ from liquid phase data fitting for solid phase data fitting.

### 4.3.2.6   Discussion of surface impurity mole fraction trends from solid phase data

Although the parameters fitted to the solid phase data are more consistent with the experimental results, the fits to the solid phase data are qualitatively worse than the fits to the liquid phase data. This occurs because of inconsistencies in the collected solid phase data. The impurity concentration increases or stays constant as the total amount of crystal increases at the beginning of the experiment but for experiments with cold water source at 5 and $10^0$C the aspartic acid concentration starts to decrease at some point during the experiment. The impurity concentration in the solid for the experiments performed with a cold water source of $15^0$C continually increased during the entire growth process.

This two regime behavior is not expected to result from the fundamental growth process because the concentrations of both species in the liquid phase decrease monotonically. Additionally, the ratio of aspartic acid to asparagine in the liquid phase as characterized by the solvent free mole fraction also decreases monotonically. With no inflection point in the liquid phase data it is difficult to envision a mechanism by which the incorporation of impurity into the solid phase undergoes the transition observed in the experimental data. It is possible that the presence of crystallization on surfaces other than the seed tube is hiding any change in the relative depletion of asparagine to aspartic acid caused by crystallization on the seed tube but this cannot be determined from these experiments. Other factors involved with the experimental setup or sampling procedure also must be explored as the cause of the observed behavior.

The behavior of the solid data could be explained by errors in the solid phase analysis or by a more complicated growth mechanism on the seed tube for the initial layers of crystal. During the sequential dissolution of the solid phase uniform dissolution was not observed for the entire crystal mass. The initial dissolution operations maintained a qualitatively uniform crystal layer on the seed tube but eventually some areas of the seed tube were dissolved more rapidly than others leading to bare seed tube being exposed in some places. This often happened near the top of the crystal. At this point, water is able to interact with the side of the crystal instead of just the surface and dissolution can occur in two dimensions. This results in dissolution near the top of the seed tube at a faster rate than over the total crystal mass. At this point subsequent dissolutions will contain material from different layers of the grown crystal and so the impurity concentration measured will not correspond to the impurity concentration at the surface.

If the total crystal had the same trend in impurity concentrations as the last few layers of crystal grown, then the solid near the seed tube surface would have a higher impurity concentration and so would raise measured impurity concentration. Early dissolution of the higher impurity concentration layers would serve to flatten the observed increase in impurity concentration. This is consistent with some of the collected data where the measured impurity concentration is flat over the first portion of crystal growth before decreasing. This cannot explain the data showing an initial increase in impurity concentration followed by a decrease in impurity concentration so dissolution from the top of the seed tube alone cannot account for all of the trends observed in the solid impurity concentration results.

Variation in the growth of the first few layers of crystal could lead to the observed impurity concentration behavior. The seed tube is initially coated with polycrystalline pure asparagine. A pure asparagine seed may alter the crystallization behavior by favoring the incorporation of asparagine. The aspartic acid would be incorporated into the crystal gradually over the first few layers before the full asparagine-aspartic acid solid solution is established. This is consistent with an initial increase in impurity concentration that is observed in some experiments.

The initial variation in growth could also occur spatially. If different regions of the seed tube grow at faster rates initially then the concentration in the initial layers of crystal would

represent an average from crystals grown at different time points. This disparity in initial growth could result by inconsistent seeding on the surface of the seed tube but the crystal would grow into a uniform surface over a period of time after which the impurity concentration profile would be determined by the modeled behavior.

In the experiments conducted with the cold water source at $15^0$C the monotonically increasing impurity concentration could result from the initial growth behavior instead of fundamentally different parameter values. The amount of crystal growth in these experiments is very small and there may not be enough crystal grown to overcome the initial growth process and to establish a uniform surface for further growth.

It is also possible that there is a transition between high and low $\gamma$ behavior between a source water temperature of 5 and $15^0$C. The predicted behavior with $\gamma>1$ is decreasing impurity concentration with growth and with $\gamma<1$ is increasing impurity concentration. A change in the value of $\gamma$ with respect to one seems unlikely because the temperature at the surface varies with crystal growth and there is a large amount of overlap in the range of temperature experienced at the crystal surface. Any issues leading to the non-monotonic nature of the collected solid phase data must also be addressed before addressing this possibility.

The discussion in this section has given possible explanations for the observed behavior in the solid phase data but the major finding is that further experimental work is necessary. Experiments that generate larger amounts of crystal and experimental techniques that give more consistent sampling of the grown crystal are needed for comparison to model predictions. The parameter values fitted to the collected solid phase data in these experiments were found to give reasonable average results through comparison of the separation factor but further work is necessary for comparing model predictions to the impurity concentration profile in the crystal.

### 4.3.2.7  Discussion of dissolution rate

The dissolution experiments performed on pure asparagine indicate that mass transfer to the surface is not the rate limiting step in the crystal growth process. This conclusion assumes that the dissolution rate is a reasonable approximation to the mass transfer rate. This is

184

supported by the estimation of the mass transfer coefficient using the Chilton-Colburn analogy in section 4.2.4. The estimated value of the mass transfer coefficient in that section was $2.3*10^{-5}$ m/s which compares favorably to the value of $(2.4\pm0.4)*10^{-5}$ m/s determined by parameter fitting to data obtained from dissolution experiments at $25^{0}$C

The dissolution rate determined from experiment is 10-50 times larger than any of the fitted values for the incorporation rate constant of asparagine. The most appropriate values of $k_A$ to use for comparison are those for experiments with seed tube water source temperature at $15^{0}$C because this temperature range is the closest to the conditions at which the dissolution rate was measured.

The estimated values of $k_A$ for those experiments were $0.3*10^{-5}$ m/s directly from fitting of the liquid phase concentration and $0.04*10^{-5}$ m/s if the fitted parameter is scaled by the ratio of product to product plus accumulation. The most appropriate comparison point is the smaller value because of the previously discussed overestimation of parameters from the liquid phase concentration data. This smaller value is nearly two orders of magnitude less than the measured dissolution rate and would be expected to be even smaller if the temperature of the seed tube water source was moved closer to $25^{0}$C. This indicates that the growth of crystal on the seed tube is not diffusion limited. Surface incorporation kinetics are the rate determining step.

### 4.3.2.8 Summary of Experimental Discussion

Due to the presence of solid in the bulk liquid the parameters fitted to the solid phase data are the most appropriate for describing the crystallization behavior of asparagine and aspartic acid in water. The parameters fitted to the solid phase data do a better job of explaining the overall impurity distribution in the solid and separation factor between the solid and liquid phases when an appreciable amount of solid is grown but the solid phase data does not allow clear interpretation.

Larger amounts of crystal growth and improved solid sampling methods are important in order to generate clearer data from the solid phase analysis to determine the value of $\gamma$ in relation to one and determine the appropriate trend in the surface mole fraction of impurity. Further experiments that severely limit the amount of crystallization on surfaces other than the

seed tube or at least give much larger ratios of growth on the seed tube to growth on other surfaces in the liquid phase are needed so that the accurate parameters can be found from liquid phase concentration data.

## 4.4    <u>Summary of Experimental Work</u>

Batch experiments with asparagine as the component of interest and aspartic acid as the impurity have been conducted in order to provide data to validate the model proposed in Chapter 2.  The model system for experimentation was asparagine and aspartic acid in water which forms a solid solution with up to 15% aspartic acid in the asparagine crystal lattice.  The crystal growth surface is a piece of aluminum tubing coated with asparagine and with water flowing through the interior to provide temperature control.  The growth of crystal in this system provides a significant thermal resistance which results in a changing temperature at the solid-liquid interface.  The model for the batch experiment was modified to account for the changing temperature at the solid-liquid interface.

The parameters fitted to the solid phase data were found to be more representative of the experimental results than the parameters fitted to the liquid phase data.  This is due to the presence of crystals in the liquid phase on surfaces other than the seed tube which affect the parameter values fitted to liquid phase concentration measurements.  The presence of crystals in the bulk also results in overprediction of $k_A$ but this was not found to have an effect on the parameters fitted to the solid phase data.  This indicates that the value of $k_A$ does not have a strong effect on the fitting of the solid phase data collected in these experiments.

The measurement of the solid phase concentration profile by sequential dissolution was not perfect.  The concentration profile showed non-monotonic behavior which may result from uneven dissolution of the sample or from a different mechanism for the initial crystal growth on the seed tube.  Uneven dissolution was observed but cannot entirely account for the observed behavior so a combination of these two mechanisms or other factors seems likely.

The parameters fitted to the solid phase were able to more closely match the measured concentration profiles and separation factor than the liquid phase fitted parameters even with this uncertainty.  Due to the experimental method, these parameters represent an average val-

ue over the range of temperature experienced at the solid-liquid interface. The magnitude of these values is instructive but the absolute values as a function of temperature cannot be determined.

The experimental method described here provides evidence that the proposed model can reasonably describe crystallization of a solid solution but it is far from conclusive. Avoiding crystals in the bulk solution was not possible in these experiments but should be improved upon for future experimentation. Additionally, the solid phase analysis was not as reliable as the liquid phase analysis and further adaptation of the analysis method should be explored in order to get more reliable data.

The experiments have been shown to be very reproducible in terms of crystal yield. One possibility for improved solid phase analysis is to perform a series of experiments with the same initial conditions but different end times. The total solid could then be dissolved and a differential analysis of the solid behavior could be performed with the results from multiple experiments. This would eliminate issues related to product sampling.

# 5.    Conclusions

## 5.1    <u>Summary of Findings</u>

A staged, semi-continuous, counter current crystallization process has been proposed that seeks to constrain crystal growth to solid surfaces in order to avoid multi-phase fluid handling while allowing for multiple recrystallizations to provide improved purity but comparable yield to batch crystallization. Processes that avoid multi-phase flow handling problems and that can be run in a continuous manner would be beneficial for integration into new continuous processing schemes.

A model for crystallization of solid solutions was proposed and applied to batch crystallization and the new process. The proposed model was tested against batch crystallization experiments. The new process was proposed with the goal of providing increased purity compared to batch crystallization with yield approaching that of batch crystallization run until completion. The yield is constrained by the solubility of the component of interest in the system solvent and therefore batch crystallization run until completion will give the maximum yield at a specified temperature.

Analysis shows that the proposed crystallization model is capable of predicting concentration gradients in the solid phase. This is an important characteristic of a model seeking to describe crystallization of solid solutions on surfaces because the amount of impurity incorporated into the crystal will vary with concentration for a solid solution. This has been demonstrated for crystallization of solid solutions in melt crystallization.[113]

The impurity incorporation behavior is controlled by two model parameters, $\gamma$ and $K$. These parameters are characteristic of the particular chemical system in use and must be measured experimentally. The ratio of the incorporation rate constants of the impurity to the component of interest is $\gamma$ and $K$ is an equilibrium constant describing the relationship between the concentrations at the solid surface and the equilibrium concentrations in the bulk. These parameters are expected to depend on temperature but not concentration.

Variation of these model specific parameters resulted in determination of parameter regimes in which the proposed crystallization process can provide better performance than

batch crystallization. The proposed process with the solid removed as the product was found to be advantageous when $\gamma<1$ and $K$ less than order 1 with smaller values of $K$ providing better results.

When $\gamma>1$ and $K$ is close to or greater than one the process can also deliver a favorable result if the liquid effluent is taken as the product and the solid output is discarded as waste. This situation results in a high yield, high purity liquid product ready for the next processing operation but these parameter values are not expected to happen for a large number of systems.

Additional operating variables such as the sweep stream flow rate and the number of stages were also explored. It was found that a sweep stream offers an increase in purity at the cost of a significant decrease in yield indicating that the use of a sweep stream is not desirable. Increasing the number of stages was shown to be favorable and resulted in higher purities at yields close to the maximum yield. The benefit of increasing the number of stages diminishes as more and more stages are added and the cost of construction and operation of a large cascade should also be considered when designing the process.

The proposed process provides the best results when the liquid from the last tank is discarded at the end of every growth stage. Any tank used during the process will provide a larger benefit as an active tank for crystal growth than as a vessel to facilitate liquid transfer which means that the use of a liquid handling tank is not favorable and the process should be operated with removal of the liquid from the last tank at the end of each growth stage.

Experiments conducted with asparagine as the component of interest and aspartic acid as the impurity in water in order to test the validity of the model encountered some difficulties. The seed tube used as the designated growth surface does not present a constant temperature at the crystallization surface because the growing crystal layer will resist heat transfer and the temperature at the liquid-solid interface will increase with time. The fitted parameters represent an average over the temperature profile observed at the liquid-solid interface. An experimental design that allows for constant temperature at the solid-liquid interface would simplify data analysis and provide more valuable information. This could potentially be achieved by varying the flow rate or temperature of the coolant in the seed tube flow loop.

Constraint of crystal growth is an important principle of the new process but is difficult to achieve in practice. The batch experiments that were performed were unable to eliminate crystallization on surfaces other than the seed tube and this resulted in significant depletion from the liquid phase due to undesired crystallization. The model fitted to the liquid phase concentration data did not generate reasonable values for the model parameters because of this undesired crystallization.

The amount of crystallization occurring on undesired surfaces could be limited by decreasing the overall supersaturation or increasing the bulk temperature. Decreasing the supersaturation would also result in smaller amount of product on the desired surface but this option could be pursued by using a large number of tanks with a small amount of supersaturation in each tank. This could be accomplished by implementing a decreasing temperature profile along the length of the cascade.

If the bulk temperature is raised in relation to the temperature at the surface for crystallization the amount of undesired crystallization should decrease. Raising the bulk temperature will raise the solubility in the bulk so that crystal will be less likely to be present on a non-cooled surface.

Fitting the model to the experimental solid phase data indicate that the value of $K$ was roughly 0.5-1 for experiments with a temperature range of 5-25$^0$C. The value of $\gamma$ was found to be less than one for experiments conducted with seed tube water source temperatures 10 and 15$^0$C but greater than one with a large standard deviation for a seed tube water source temperature of 5$^0$C. The fitted parameter values for experiments performed with a seed tube water source temperature of 10 and 15$^0$C are in the range where the proposed process is predicted to give favorable results with the crystal being removed as the product.

The point of these experiments was not to determine if asparagine and aspartic acid could be separated by the proposed process but instead to determine if the proposed model was able to describe a real system. Batch experiments indicate that the proposed model is reasonably consistent with the collected data but inconsistencies in the experimental data make this conclusion uncertain.

The collected solid phase data were somewhat ambiguous resulting in uncertainty as to the fitted parameter values. For most of the experiments an initial increase was followed by a decrease in the mole fraction of impurity across the growing crystal. This change in behavior is unexpected because the liquid phase data indicates a monotonic change in concentration and liquid phase mole fraction. Model fitting resulted in best fit curves that were in some cases convex while the data itself was concave. The presence of undesired crystallization in the liquid phase may be masking a change in the liquid phase concentrations capable of explaining the observed solid phase behavior but this cannot be learned from the current experiments and issues with the solid phase growth process and data collection seem more likely culprits.

The observed behavior for the solid phase concentration profile could be explained by any uneven growth during the initial crystallization and/or complications with the solid phase analysis procedure. The initial growth may not be uniform over the entire surface. If islands of material grow at different rates initially before eventually joining together the sampling method would then remove samples from different time points which would change the measured concentrations. After an initial period the islands join together and then are constrained to grow in one direction which gives the final macroscopically uniform product. The initial seed layer was pure asparagine and this may impact the initial growth of crystal. The incorporation of aspartic acid into the crystal may change as the crystal changes from pure asparagine into a solid solution of asparagine and aspartic acid.

Growing thicker layers of crystal would help to address both of these issues by minimizing the uncertain layers of growth with respect to the total amount of growth. Thicker layers of crystal could be grown by decreasing the initial temperature at the seed tube surface or by decreasing the diameter of the seed tube. Other experimental designs with different seed surfaces may also be useful in circumventing this problem.

The solid phase analysis also resulted in uneven dissolution of crystal after a certain amount of crystal was dissolved. The initial dissolutions give qualitatively even dissolution but eventually the crystal at the top of the seed tube is totally removed and the bare seed tube is exposed. At this point dissolution continues from exterior face of the crystal but also from the edge exposed by total dissolution at the top of the seed tube. This impact of this problem could

be minimized by increasing the thickness of the collected crystal so that the effect dissolutions represent only a small fraction of the total crystal grown.

As an alternative analysis method to the sequential dissolution of the solid phase, multiple experiments could be performed with identical conditions but different end times. The total concentration of the crystals grown in these experiments could then be measured and a differential analysis could be used to find the concentration profile in the crystal. The amount of crystal growth was found to be reproducible in these experiments indicating that a differential analysis may be possible.

Further experiments are necessary to determine if the proposed model is capable of describing crystallization on solid surfaces for a solid solution forming system. These experiments need to further minimize crystallization on surfaces other than the seed tube to make fitting of parameters to the liquid phase concentrations useful and increase the total amount and thickness of product so that more consistent solid data can be collected.

## 5.2    **Future Work**

Validation of the proposed model by experiment should be the focus of any future work. In order to do this, experiments must be designed that provide even growth on a defined surface while minimizing any other growth in the system. Minimizing growth in undesired locations could possibly be done by increasing the bulk temperature of the liquid so that particles are less likely to exist on non-cooled surfaces or by changing the stirring rate or stir bar type to minimize contact nucleation and particle attrition from the seed tube.

Finding a new way to promote growth on a specific surface may also be advantageous. Designed surfaces for nucleation of a specific chemical would simplify processing and might promote growth on the desired surface in relation to growth on other surfaces in the vessel.

Alternative shapes for the seed tube could also be studied. A flat plate would be more appropriate for use with the model as implemented in this work and this becomes more important as the thickness of the crystal layer increases. The challenge of using a flat plate is to design the heat transfer such that the temperature across the plate could be held at a constant value.

If the proposed model is found to be appropriate then the effect of varying the temperature profile along the cascade should be explored. A temperature profile will allow control over the degree of supersaturation in each tank which will be important for minimizing homogeneous nucleation and may also provide some benefit to the product purity. A temperature profile will result in a larger number of stages being needed to achieve high yields but the magnitude of this difference can be estimated by simulation.

If the proposed model is found to not be appropriate then a new model for crystallization should be proposed and used to study the semi-continuous process. The same procedure outlined in this document can be followed with a different model to determine whether the proposed process has benefits compared to batch crystallization.

# 6.    Appendices

## 6.1    Batch separation factor limit derivation

The separation factor at steady state as given originally in equation (4.18) is presented again in equation (6.1).

$$\lim_{\tau \to \infty} \alpha = \frac{\left(1 + \frac{K}{\gamma}\left(\frac{1}{\theta_A^*} - 1\right)\right)^{\gamma} - 1}{\frac{1}{\theta_A^*} - 1} = \frac{1}{\frac{1}{\theta_A^*} - 1}\left(\left(\gamma + K\left(\frac{1}{\theta_A^*} - 1\right)\right)^{\gamma} \gamma^{-\gamma} - 1\right) \tag{6.1}$$

The series expansion for equation (6.1) as $\gamma$ approaches zero can be found by finding the individual series expansions for $\left(\gamma + K\left(\frac{1}{\theta_A^*} - 1\right)\right)^{\gamma}$ and $\gamma^{-\gamma}$ and then substituting them into equation (6.1). This is done for both expressions using the following approach. Rewrite the two expressions as follows.

$$\left(\gamma + K\left(\frac{1}{\theta_A^*} - 1\right)\right)^{\gamma} = e^{\ln\left(\gamma + K\left(\frac{1}{\theta_A^*} - 1\right)\right)^{\gamma}} = e^{\gamma \ln\left(\gamma + K\left(\frac{1}{\theta_A^*} - 1\right)\right)} \tag{6.2}$$

$$\gamma^{-\gamma} = e^{\ln \gamma^{-\gamma}} = e^{-\gamma \ln \gamma} \tag{6.3}$$

Next note that a substitution can be made in both cases ($u_1 = \gamma \ln\left(\gamma + K\left(\frac{1}{\theta_A^*} - 1\right)\right)$ in (6.2) and $u_2 = -\gamma \ln \gamma$ in (6.3)) to simplify both expressions to the functional form $e^u$. Take the Taylor expansion around zero for $e^u$ to give the following.

$$e^u = 1 + u + O\left(u^2\right) \tag{6.4}$$

To finish, insert the appropriate u for each of the two expressions into equation (6.4).

$$\left(\gamma + K\left(\frac{1}{\theta_A^*} - 1\right)\right)^{\gamma} = 1 + \gamma \ln\left(K\left(\frac{1}{\theta_A^*} - 1\right)\right) + O(\gamma^2)$$

(6.5)

$$\gamma^{-\gamma} = 1 - \gamma \ln \gamma + O\left((\gamma \ln \gamma)^2\right)$$

(6.6)

## 6.2    Analytical Yield for Counter-Current Crystallization Process

The following derivation is for a three stage cascade with the feed entering at stage two and sweep stream entering at stage one. The volume of liquid in each tank is assumed to be constant (dilute solution), the temperature is the same and constant in every tank, the order of the supersaturation dependence is one and the surface area of crystal growth is constant (1-dimensional plane growth). The dimensionless variables are defined as in section 2.3.1. This analysis will only deal with species A so all $\theta$ values will omit the subscript A. $\theta_i$ will indicate the concentration of species A in tank $i$. Because the temperature is assumed constant the saturation concentration and incorporation rate constants in all tanks are equal and will be represented by $\theta^*$ and $\beta$. Additionally the liquid transfer considerations dealing with over and under filled tanks will not be taken into account during this derivation.

The differential equation describing tank one is presented in equation (6.7).

$$\frac{d\theta_1}{d\tau} = \psi\theta_0 - \psi\theta_1 - \beta\left(\theta_1 - \theta^*\right) \tag{6.7}$$

The Laplace transform of equation (6.7) is taken and this equation can be solved and inverted to give the concentration profile as a function of time for tank one. This is shown in equations through (6.8)-(6.10).

$$s\Theta_1 - \theta_1^0 = -\left(\psi + \beta\right)\Theta_1 + \frac{\psi\theta_0 + \beta\theta^*}{\psi + \beta} \tag{6.8}$$

$$\Theta_1 = \frac{\theta_1^0}{s + \psi + \beta} + \frac{\psi\theta_0 + \beta\theta^*}{s\left(s + \psi + \beta\right)} \tag{6.9}$$

$$\theta_1\left(\tau_f\right) = \theta_1^0 e^{-(\psi+\beta)\tau} + \frac{\psi\theta_0 + \beta\theta^*}{\psi + \beta}\left(1 - e^{-(\psi+\beta)\tau}\right) \tag{6.10}$$

The following substitutions will be used to simplify notation during this derivation.

$$\lambda_1 = -(\psi + \beta) \tag{6.11}$$

$$\lambda_2 = -(1 + \psi + \beta) \tag{6.12}$$

$$b_1 = \frac{\psi \theta_0 + \beta \theta^*}{\psi + \beta} \tag{6.13}$$

$$b_2 = \frac{1 + \psi b_1 + \beta \theta^*}{1 + \psi + \beta} \tag{6.14}$$

$$b_3 = \frac{(1 + \psi) b_2 + \beta \theta^*}{1 + \psi + \beta} \tag{6.15}$$

If the total time of the growth operation is $\tau_f$ then the total amount of crystal grown in tank 1 is give in equation (6.16).

$$\tilde{m}_{c1}(\tau_f) = \int_0^{\tau_f} \beta(\theta_1 - \theta^*) d\tau = \int_0^{\tau_f} \beta(\theta_1^0 e^{\lambda_1 \tau} + b_1(1 - e^{\lambda_1 \tau}) - \theta^*) d\tau$$
$$= \frac{\beta}{\lambda_1}(\theta_1^0 - b_1)(e^{\lambda_1 \tau_f} - 1) + \beta(b_1 - \theta^*)\tau_f \tag{6.16}$$

This procedure is then repeated for tank 2 making use of the concentration in tank 1.

$$\frac{d\theta_2}{d\tau} = 1 + \psi \theta_1 - (1 + \psi)\theta_2 - \beta(\theta_2 - \theta^*) = -(1 + \psi + \beta)\theta_2 + \psi(\theta_1^0 - b_1)e^{\lambda_1 \tau} + \psi b_1 + \beta \theta^* \tag{6.17}$$

$$s\Theta_2 - \theta_2^0 = \lambda_2 \Theta_2 + \frac{\psi(\theta_1^0 - b_1)}{s - \lambda_1} + \frac{1 + \psi b_1 + \beta \theta^*}{s} \tag{6.18}$$

$$\Theta_2 = \frac{\theta_2^0}{s - \lambda_2} + \psi(\theta_1^0 - b_1)\left(\frac{1}{s - \lambda_1} - \frac{1}{s - \lambda_2}\right) + \frac{1 + \psi b_1 + \beta \theta^*}{\lambda_2}\left(\frac{1}{s - \lambda_2} - \frac{1}{s}\right) \tag{6.19}$$

$$\theta_2(\tau_f) = (\theta_2^0 - \psi(\theta_1^0 - b_1) - b_2)e^{\lambda_2 \tau} + \psi(\theta_1^0 - b_1)e^{\lambda_1 \tau} + b_2 \tag{6.20}$$

$$\tilde{m}_{c2}(\tau_f) = \int_0^{\tau_f} \beta(\theta_2 - \theta^*) d\tau =$$

$$= \frac{\beta}{\lambda_2}\left(\theta_2^0 - \psi(\theta_1^0 - b_1) - b_2\right)\left(e^{\lambda_2 \tau_f} - 1\right) + \frac{\beta\psi}{\lambda_1}\left(\theta_1^0 - b_1\right)\left(e^{\lambda_1 \tau_f} - 1\right) + \beta(b_2 - \theta^*)\tau_f \qquad (6.21)$$

The concentration in tank 3 can then be found making use of the concentrations in tanks 1 and 2.

$$\frac{d\theta_3}{d\tau} = (1+\psi)\theta_2 - (1+\psi)\theta_3 - \beta(\theta_3 - \theta^*)$$

$$= -(1+\psi+\beta)\theta_3 + (1+\psi)\left(\left(\theta_2^0 - \psi(\theta_1^0 - b_1) - b_2\right)e^{\lambda_2 \tau} + \psi(\theta_1^0 - b_1)e^{\lambda_1 \tau} + b_2\right) + \beta\theta^* \qquad (6.22)$$

$$s\Theta_3 - \theta_3^0 = \lambda_2\Theta_3 + \frac{(1+\psi)\left(\theta_2^0 - \psi(\theta_1^0 - b_1) - b_2\right)}{s - \lambda_2} + \frac{\psi(1+\psi)\left(\theta_1^0 - b_1\right)}{s - \lambda_1}$$

$$+ \frac{(1+\psi)b_2 + \beta\theta^*}{s} \qquad (6.23)$$

$$\Theta_3 = \frac{\theta_3^0}{s - \lambda_2} + \frac{(1+\psi)\left(\theta_2^0 - \psi(\theta_1^0 - b_1) - b_2\right)}{(s - \lambda_2)^2} + \frac{\psi(1+\psi)\left(\theta_1^0 - b_1\right)}{(s - \lambda_1)(s - \lambda_2)}$$

$$+ \frac{(1+\psi)b_2 + \beta\theta^*}{s(s - \lambda_2)} \qquad (6.24)$$

$$\theta_3(\tau_f) = \left(\theta_3^0 - \psi(1+\psi)(\theta_1^0 - b_1) - b_3\right)e^{\lambda_2 \tau} + (1+\psi)\left(\theta_2^0 - \psi(\theta_1^0 - b_1) - b_2\right)\tau e^{\lambda_2 \tau}$$

$$+ \psi(1+\psi)\left(\theta_1^0 - b_1\right)e^{\lambda_1 \tau} + b_3 \qquad (6.25)$$

$$\tilde{m}_{c3}\left(\tau_f\right) = \int_0^{\tau_f} \beta\left(\theta_3 - \theta^*\right) d\tau =$$

$$= \frac{\beta}{\lambda_2}\left(\theta_3^0 - \psi\left(1+\psi\right)\left(\theta_1^0 - b_1\right) - b_3\right)\left(e^{\lambda_2\tau_f} - 1\right)$$

$$+ \frac{\beta}{\lambda_2}\left(1+\psi\right)\left(\theta_2^0 - \psi\left(\theta_1^0 - b_1\right) - b_2\right)\left(\tau_f e^{\lambda_2\tau_f} - \frac{e^{\lambda_2\tau_f} - 1}{\lambda_2}\right) \qquad (6.26)$$

$$+ \frac{\beta}{\lambda_1}\psi\left(\theta_1^0 - b_1\right)\left(e^{\lambda_1\tau_f} - 1\right) + \beta\left(b_3 - \theta^*\right)\tau_f$$

The initial conditions for the next growth cycle are determined by the final concentrations during the previous growth cycle. This relationship for each of the three tanks is detailed below where the subscript $j$ will indicate a particular growth cycle.

$$\theta_{1,j}^0 = \theta_{1,j-1}\left(\tau_f\right) + \tilde{m}_{c2,j-1}\left(\tau_f\right) \qquad (6.27)$$

$$\theta_{2,j}^0 = \theta_{2,j-1}\left(\tau_f\right) + \tilde{m}_{c3,j-1}\left(\tau_f\right) \qquad (6.28)$$

$$\theta_{3,j}^0 = \theta_{3,j-1}\left(\tau_f\right) \qquad (6.29)$$

The condition of cyclic steady state occurs when $\theta_{i,j}^0 = \theta_{i,j-1}^0$. When this is the case, equations (6.27)-(6.29) can be solved to give explicit expressions for $\theta_i^0$. This is done starting with tank 3 and working backwards. The algebra involved in generating the expressions for $\theta_i^0$ is substantial and will be omitted in this derivation.

$$\theta_3^0 = \left(\theta_3^0 - \psi\left(1+\psi\right)\left(\theta_1^0 - b_1\right) - b_3\right)e^{\lambda_2\tau} + \left(1+\psi\right)\left(\theta_2^0 - \psi\left(\theta_1^0 - b_1\right) - b_2\right)\tau e^{\lambda_2\tau}$$

$$+ \psi\left(1+\psi\right)\left(\theta_1^0 - b_1\right)e^{\lambda_1\tau} + b_3 \qquad (6.30)$$

$$\theta_3^0 = \frac{1}{1-e^{\lambda_2\tau_f}}\begin{bmatrix} \left(-\psi\left(1+\psi\right)\left(\theta_1^0 - b_1\right)-b_3\right)e^{\lambda_2\tau_f} \\ +\left(1+\psi\right)\left(\theta_2^0 - \psi\left(\theta_1^0 - b_1\right)-b_2\right)\tau_f e^{\lambda_2\tau_f} \\ +\psi\left(1+\psi\right)\left(\theta_1^0 - b_1\right)e^{\lambda_1\tau_f} + b_3 \end{bmatrix} \tag{6.31}$$

$$\begin{aligned} \theta_2^0 &= \left(\theta_2^0 - \psi\left(\theta_1^0 - b_1\right)-b_2\right)e^{\lambda_2\tau} + \psi\left(\theta_1^0 - b_1\right)e^{\lambda_1\tau} + b_2 \\ &+ \frac{\beta}{\lambda_2}\left(\theta_3^0 - \psi\left(1+\psi\right)\left(\theta_1^0 - b_1\right)-b_3\right)\left(e^{\lambda_2\tau_f}-1\right) \\ &+ \frac{\beta}{\lambda_2}\left(1+\psi\right)\left(\theta_2^0 - \psi\left(\theta_1^0 - b_1\right)-b_2\right)\left(\tau_f e^{\lambda_2\tau_f} - \frac{e^{\lambda_2\tau_f}-1}{\lambda_2}\right) \\ &+ \frac{\beta}{\lambda_1}\psi\left(\theta_1^0 - b_1\right)\left(e^{\lambda_1\tau_f}-1\right) + \beta\left(b_3 - \theta^*\right)\tau_f \end{aligned} \tag{6.32}$$

$$\theta_2^0 = \frac{1}{\left(1-e^{\lambda_2\tau_f}\right)\left(1-\frac{\beta}{\lambda_2^2}\left(1+\psi\right)\right)}\begin{bmatrix} \left(-\psi\left(\theta_1^0 - b_1\right)-b_2\right)\left(e^{\lambda_2\tau_f} - \frac{\beta}{\lambda_2^2}\left(1+\psi\right)\left(e^{\lambda_2\tau_f}-1\right)\right) \\ +\psi\left(\theta_1^0 - b_1\right)e^{\lambda_1\tau_f} + b_2 \\ -\frac{\beta}{\lambda_1\lambda_2}\psi\left(1+\psi\right)\left(\theta_1^0 - b_1\right)\left(e^{\lambda_1\tau_f}-1\right) \\ +\beta\left(b_3 - \theta^*\right)\tau_f \end{bmatrix} \tag{6.33}$$

$$\begin{aligned} \theta_1^0 &= \left(\theta_1^0 - b_1\right)e^{-(\psi+\beta)\tau_f} + b_1 \\ &+ \frac{\beta}{\lambda_2}\left(\theta_2^0 - \psi\left(\theta_1^0 - b_1\right)-b_2\right)\left(e^{\lambda_2\tau_f}-1\right) \\ &+ \frac{\beta}{\lambda_1}\psi\left(\theta_1^0 - b_1\right)\left(e^{\lambda_1\tau_f}-1\right) + \beta\left(b_2 - \theta^*\right)\tau_f \end{aligned} \tag{6.34}$$

$$\theta_1^0 = \frac{\left[\begin{array}{l}b_1\left(1-e^{\lambda_1\tau_f}\right)\left(1-\dfrac{\beta\psi\lambda_2}{\lambda_1\left(\lambda_2^2-\beta(1+\psi)\right)}\right)\\[2mm] +\beta\left(b_2-\theta^*\right)\tau_f-\beta^2\lambda_2\dfrac{\left(b_3-\theta^*\right)\tau_f}{\lambda_2^2-\beta(1+\psi)}\end{array}\right]}{\left(1-e^{\lambda_1\tau_f}\right)\left(1-\dfrac{\beta\psi\lambda_2}{\lambda_1\left(\lambda_2^2-\beta(1+\psi)\right)}\right)} \tag{6.35}$$

The yield from this process at cyclic steady state is given by the expression in equation (6.36).

$$y = \frac{\tilde{m}_{c1}}{\tau_f} \tag{6.36}$$

The expressions for $\theta_i^0$ can be used to find the final expression for $\tilde{m}_{c1}$.

$$\tilde{m}_{c1}\left(\tau_f\right) = \frac{\beta}{\lambda_1}\left(\frac{\left[\begin{array}{l}b_1\left(1-e^{\lambda_1\tau_f}\right)\left(1-\dfrac{\beta\psi\lambda_2}{\lambda_1\left(\lambda_2^2-\beta(1+\psi)\right)}\right)\\[2mm] +\beta\left(b_2-\theta^*\right)\tau_f-\beta^2\lambda_2\dfrac{\left(b_3-\theta^*\right)\tau_f}{\lambda_2^2-\beta(1+\psi)}\end{array}\right]}{\left(1-e^{\lambda_1\tau_f}\right)\left(1-\dfrac{\beta\psi\lambda_2}{\lambda_1\left(\lambda_2^2-\beta(1+\psi)\right)}\right)}-b_1\right)\left(e^{\lambda_1\tau_f}-1\right)+\beta\left(b_1-\theta^*\right)\tau_f$$

$$= \beta\left(b_1-\theta^*\right)\tau_f - \frac{\beta}{\lambda_1}\left(\frac{\beta\left(b_2-\theta^*\right)\tau_f-\beta^2\lambda_2\dfrac{\left(b_3-\theta^*\right)\tau_f}{\lambda_2^2-\beta(1+\psi)}}{1-\dfrac{\beta\psi\lambda_2}{\lambda_1\left(\lambda_2^2-\beta(1+\psi)\right)}}\right)$$

$$= \beta\left(b_1-\theta^*\right)\tau_f$$

$$+ \frac{\beta\left(b_2-\theta^*\right)\tau_f}{-\dfrac{\lambda_1}{\beta}+\dfrac{\psi\lambda_2}{\left(\lambda_2^2-\beta(1+\psi)\right)}}$$

$$+ \frac{\beta\left(b_3-\theta^*\right)\tau_f}{\left(-\dfrac{\lambda_2}{\beta}+\dfrac{1+\psi}{\lambda_2}\right)\left(-\dfrac{\lambda_1}{\beta}+\dfrac{\psi\lambda_2}{\left(\lambda_2^2-\beta(1+\psi)\right)}\right)} \tag{6.37}$$

$$y = \beta\left(b_1 - \theta^*\right)$$

$$+ \frac{\beta\left(b_2 - \theta^*\right)}{-\dfrac{\lambda_1}{\beta} + \dfrac{\psi\lambda_2}{\left(\lambda_2^2 - \beta(1+\psi)\right)}} \tag{6.38}$$

$$+ \frac{\beta\left(b_3 - \theta^*\right)}{\left(-\dfrac{\lambda_2}{\beta} + \dfrac{1+\psi}{\lambda_2}\right)\left(-\dfrac{\lambda_1}{\beta} + \dfrac{\psi\lambda_2}{\left(\lambda_2^2 - \beta(1+\psi)\right)}\right)}$$

Replacing all of the substituting variables with their definitions gives equation (6.39) which is the result presented in section 2.3.2.

$$y = \beta\left(\frac{\psi\theta_0 + \beta\theta^*}{\psi + \beta} - \theta^*\right)$$

$$+ \frac{\beta\left(\dfrac{1+\psi\left(\dfrac{\psi\theta_0 + \beta\theta^*}{\psi + \beta}\right) + \beta\theta^*}{1+\psi+\beta} - \theta^*\right)}{\dfrac{\psi + \beta}{\beta} - \dfrac{\psi(1+\psi+\beta)}{(1+\psi+\beta)^2 - \beta(1+\psi)}}$$

$$+ \frac{\beta\left(\dfrac{(1+\psi)\left(\dfrac{1+\psi\left(\dfrac{\psi\theta_0 + \beta\theta^*}{\psi + \beta}\right) + \beta\theta^*}{1+\psi+\beta}\right) + \beta\theta^*}{1+\psi+\beta} - \theta^*\right)}{\left(\dfrac{1+\psi+\beta}{\beta} - \dfrac{1+\psi}{1+\psi+\beta}\right)\left(\dfrac{\psi + \beta}{\beta} - \dfrac{\psi(1+\psi+\beta)}{(1+\psi+\beta)^2 - \beta(1+\psi)}\right)} \tag{6.39}$$

If the sweep stream flow rate is set equal to zero in equation (6.39) the result is equal to the yield from a two stream cascade with feed at stage 1 and no sweep stream. This result is shown in equation (6.40).

$$y = \beta\left(\frac{1+\beta\theta^*}{1+\beta} - \theta^*\right) + \frac{\beta\left(\dfrac{\left(\dfrac{1+\beta\theta^*}{1+\beta}\right)+\beta\theta^*}{1+\beta} - \theta^*\right)}{\left(\dfrac{1+\beta}{\beta} - \dfrac{1}{1+\beta}\right)}$$

$$= \frac{\beta}{1+\beta}\left(1-\theta^*\right) + \frac{\beta}{(1+\beta)^2\left(\dfrac{1+\beta}{\beta} - \dfrac{1}{1+\beta}\right)}\left(1-\theta^*\right) \qquad (6.40)$$

$$= \frac{\beta + \beta^2}{1+\beta+\beta^2}\left(1-\theta^*\right)$$

The maximum possible yield at steady state from a single tank would be $\dfrac{\beta}{1+\beta}\left(1-\theta^*\right)$.

Because $\beta$ is strictly greater than one it is evident that multiple tanks employing this cyclical process result in a higher maximum attainable yield.

## 6.3 Analytical Concentration Profile for Species B When $\gamma<<1$ or $\gamma>>1$ and $K<<1$

The following derivations are for a one stage cascade with the feed entering and sweep stream entering at stage one. Solutions to equations can be done using the same methods as outlined in appendix 6.2. A one stage system is not expected to employ a sweep stream in practice but it is used for this derivation in order to provide a simpler final expression for the purity. The expression giving the product purity is

$$p = \frac{\tilde{m}_{Ac}}{\tilde{m}_{Ac} + \eta_B \tilde{m}_{Bc}} = \frac{1}{1 + \eta_B \dfrac{\tilde{m}_{Bc}}{\tilde{m}_{Ac}}} \tag{6.41}$$

where all values are at cyclical steady state. The volume of liquid in each tank is assumed to be constant (dilute solution), the temperature is the same and constant in every tank, the order of the supersaturation dependence is one and the surface area of crystal growth is constant (1-dimensional plane growth). The dimensionless variables are defined as in section 2.3.1. The liquid transfer considerations dealing with over and under filled tanks are not needed for a one stage system.

The general solution to the impurity concentration profile cannot be determined analytically. The model defined in section 2.3 defines the equilibrium concentration of the impurity species in terms of the time dependent concentrations of species A and B. This leads to a differential equation that cannot be solved. In order to generate analytical solutions, two special cases were considered.

The first case is $\gamma<<1$. In this situation the incorporation rate constant of the impurity into the crystal is much smaller than the incorporation of the component of interest so only a small amount of B will be included in the crystal. In this case the equilibrium concentration of species B in the liquid phase will be nearly constant at the initial value. Assuming that the equilibrium concentration of B in the liquid phase is constant allows for the model to be solved analytically.

The second special case is $\gamma \gg 1$ and $K \ll 1$. When $\gamma \gg 1$ the concentration of species B in the liquid will at all times be equal to $\theta_B^*$.

$$K = \frac{\theta_A^*}{\theta_B^*} \frac{\theta_{Bc}^s}{\theta_{Ac}^s} = \frac{\theta_A^*}{\theta_B} \frac{\theta_{Bc}^s}{\theta_{Ac}^s} = \frac{\theta_A^*}{\theta_B} \frac{d\tilde{m}_{Bc}}{d\tilde{m}_{Ac}} \tag{6.42}$$

where the last equality follows from equation (2.69). This allows the differential equation for impurity in the crystal phase to be rewritten as follows.

$$\frac{d\tilde{m}_{Bc}}{dt} = K \frac{\theta_B}{\theta_A^*} \frac{d\tilde{m}_{Ac}}{dt} = K \frac{\theta_B}{\theta_A^*} \beta_A \left( \theta_A - \theta_A^* \right) \tag{6.43}$$

The differential equation for the liquid phase concentration of species B can then be written as

$$\frac{d\theta_B}{dt} = 1 - \theta_B - K \frac{\theta_B}{\theta_A^*} \beta_A \left( \theta_A - \theta_A^* \right) \tag{6.44}$$

This equation can still not be solved explicitly for the purity. The second assumption that $K \ll 1$ is now employed so that again only a small amount of impurity will be included in the crystal and therefore not only will $\theta_B^*$ be equal to $\theta_B$ but it will also be equal to $\theta_B^0$ since there is very little impurity incorporated into the crystal. These assumptions allow an analytical concentration profile for the impurity to be determined.

For both special cases the concentration profile of species A is required. This profile is independent of the assumptions made about the impurity behavior and so the same profile will apply to both cases for species B. The differential equation describing species A is presented in equation (6.45).

$$\frac{d\theta_A}{d\tau} = 1 - (1 + \psi) \theta_A - \beta_A \left( \theta_A - \theta_A^* \right) \tag{6.45}$$

The solution to this equation with the concentration of species A at time zero equal to $\theta_A{}^0$ is

$$\theta_A = \theta_A^0 e^{-(1+\psi)\tau} + \frac{1+\beta_A\theta_A^*}{1+\psi+\beta_A}\left(1-e^{-(1+\psi)\tau}\right)$$

(6.46)

At cyclical steady state the following relation will be true.

$$\theta_A^0 = \theta_A\left(\tau_f\right)$$

(6.47)

This expression is very simple because in the one stage system the solid contents are removed after every growth stage as the product. This derivation can be extended to multiple tank systems but the resulting profiles are complicated and difficult to analyze.

Equation (6.47) can then be solved to give the concentration profile of species A during a growth stage when cyclic steady state has been achieved.

$$\theta_A = \frac{1+\beta_A\theta_A^*}{1+\psi+\beta_A}e^{-(1+\psi)\tau} + \frac{1+\beta_A\theta_A^*}{1+\psi+\beta_A}\left(1-e^{-(1+\psi)\tau}\right) = \frac{1+\beta_A\theta_A^*}{1+\psi+\beta_A}$$

(6.48)

The concentration of species A in the liquid phase is seen to be constant at all times when cyclical steady state is achieved in a one stage system. This answer makes sense because the liquid is not changed between successive growth stages so that the conditions at the end of one growth stage are identical to those at the beginning of the next.

The amount of species A in the solid phase is also necessary and is given by the following equation.

$$\frac{d\tilde{m}_{Ac}}{dt} = \beta_A\left(\theta_A - \theta_A^*\right) = \beta_A\left(\frac{1-(1+\psi)\theta_A^*}{1+\psi+\beta_A}\right)$$

(6.49)

$$\tilde{m}_{Ac} = \beta_A \left( \theta_A^0 - \theta_A^* \right) \tau = \beta_A \left( \frac{1 - (1+\psi)\theta_A^*}{1+\psi+\beta_A} \right) \tau \tag{6.50}$$

### 6.3.1 *Impurity concentration profile when γ<<1*

The differential equation for the impurity in this case is given by

$$\frac{d\theta_B}{d\tau} = 1 - (1+\psi)\theta_B - \beta_B \left( \theta_B - \theta_B^* \right) \tag{6.51}$$

When $\theta_B^*$ is constant as it is in this case that this is the exact same functional form as for species A. The solutions for species A can then be used directly when the subscript A is replaced with a subscript B.

$$\theta_B = \theta_B^0 e^{-(1+\psi)\tau} + \frac{1 + \beta_B \theta_B^*}{1+\psi+\beta_B} \left( 1 - e^{-(1+\psi)\tau} \right) \tag{6.52}$$

Determination of the initial concentration at cyclical steady state is slightly complicated because $\theta_B^*$ depends on the value of $\theta_B^0$. This dependence is given by

$$\theta_B^* = \frac{\theta_B^0}{1 + \dfrac{K}{\gamma \theta_A^*} \left( \theta_A^0 - \theta_A^* \right)} \tag{6.53}$$

The value of $\theta_B^0$ is then found to be

$$\theta_B^0 = \frac{1}{1+\psi+\beta_B \left( \dfrac{1}{1 + \dfrac{\gamma \theta_A^*}{K \left( \theta_A^0 - \theta_A^* \right)}} \right)} \tag{6.54}$$

Substituting this expression into equation (6.52) gives the impurity profile at cyclical steady state.

$$\theta_B = \frac{1}{1 + \psi + \beta_B \left( \dfrac{1}{1 + \dfrac{\gamma \theta_A^*}{K\left(\theta_A^0 - \theta_A^*\right)}} \right)} \tag{6.55}$$

As in the case of species A, the concentration of species B at cyclical steady state is constant.

The amount of species B in the crystal phase is then found as

$$\frac{d\tilde{m}_{Bc}}{dt} = \beta_B \left( \theta_B - \theta_B^* \right) = \beta_B \theta_B^0 \left( 1 - \frac{1}{1 + \dfrac{K}{\gamma \theta_A^*}\left(\theta_A^0 - \theta_A^*\right)} \right)$$

$$= \beta_B \theta_B^0 \left( \frac{1}{1 + \dfrac{\gamma \theta_A^*}{K\left(\theta_A^0 - \theta_A^*\right)}} \right) = \beta_B \left( \frac{1}{1 + \psi + \beta_B \left( \dfrac{1}{1 + \dfrac{\gamma \theta_A^*}{K\left(\theta_A^0 - \theta_A^*\right)}} \right)} \right) \left( \frac{1}{1 + \dfrac{\gamma \theta_A^*}{K\left(\theta_A^0 - \theta_A^*\right)}} \right) \tag{6.56}$$

$$= \beta_B \left( \frac{1}{(1 + \psi)\left(1 + \dfrac{\gamma \theta_A^*}{K\left(\theta_A^0 - \theta_A^*\right)}\right) + \beta_B} \right)$$

$$\tilde{m}_{Bc} = \beta_B \tau \left( \frac{1}{(1 + \psi)\left(1 + \dfrac{\gamma \theta_A^*}{K\left(\theta_A^0 - \theta_A^*\right)}\right) + \beta_B} \right) \tag{6.57}$$

The purity is given by

$$p = \cfrac{1}{1 + \eta_B \dfrac{\beta_B}{\beta_A} \cfrac{\left( (1+\psi)\left( 1 + \dfrac{\gamma\theta_A^*}{K\left(\theta_A^0 - \theta_A^*\right)} \right) + \beta_B \right)}{\left(\theta_A^0 - \theta_A^*\right)}}$$

$$= \cfrac{1}{1 + \eta_B \gamma \left( \cfrac{1}{(1+\psi)\left( \left(\theta_A^0 - \theta_A^*\right) + \dfrac{\gamma\theta_A^*}{K} \right) + \beta_B \left(\theta_A^0 - \theta_A^*\right)} \right)}$$

$$= \cfrac{1}{1 + \eta_B \gamma \left( \cfrac{1}{(1+\psi)\left( \dfrac{1-(1+\psi)\theta_A^*}{1+\psi+\beta_A} + \dfrac{\gamma\theta_A^*}{K} \right) + \beta_B \left( \dfrac{1-(1+\psi)\theta_A^*}{1+\psi+\beta_A} \right)} \right)}$$

$$= \cfrac{1}{1 + \eta_B \gamma \left( \cfrac{1}{(1+\psi+\beta_B)\left( \dfrac{1-(1+\psi)\theta_A^*}{1+\psi+\beta_A} \right) + \dfrac{\gamma\theta_A^*}{K}(1+\psi)} \right)} \tag{6.58}$$

### 6.3.2  *Impurity concentration profile when γ>>1 and K<<1*

The differential equation for the impurity in this case is given by

$$\frac{d\theta_B}{d\tau} = 1 - (1+\psi)\theta_B - K\frac{\theta_B^0}{\theta_A^*}\beta_A\left(\theta_A - \theta_A^*\right) \tag{6.59}$$

This equation can be solved for $\theta_B$ after substituting in the expression for $\theta_A$ to give the following.

$$\theta_B = \theta_B^0 e^{-(1+\psi)\tau} + \left( 1 - K\frac{\theta_B^0}{\theta_A^*}\beta_A\left( \frac{1-(1+\psi)\theta_A^*}{1+\psi+\beta_A} \right) \right)\left( \frac{1-e^{-(1+\psi)\tau}}{1+\psi} \right) \tag{6.60}$$

Applying the cyclic steady state condition allows for determination of $\theta_B{}^0$.

$$\theta_B^0 = \cfrac{1}{1+\psi+\cfrac{K\beta_A}{\theta_A^*}\left(\cfrac{1-(1+\psi)\theta_A^*}{1+\psi+\beta_A}\right)} \tag{6.61}$$

When this is substituted into equation (6.60) the concentration profile for the impurity at cyclical steady can be determined and it is found again to be constant at the initial value.

$$\theta_B = \theta_B^0 \tag{6.62}$$

The determination of the purity in this case is slightly simpler than in the previous case because the explicit expression for the amount of impurity in the solid phase does not need to be calculated. Equation (6.43) allows this quantity to be determined in relation to the amount of species A in the solid phase with the initial condition that there is no solid present.

$$\tilde{m}_{Bc} = K\frac{\theta_B^0}{\theta_A^*}\tilde{m}_{Ac} \tag{6.63}$$

The purity can then be written as follows.

$$
\begin{aligned}
p &= \frac{\tilde{m}_{Ac}}{\tilde{m}_{Ac}+\eta_B\tilde{m}_{Bc}} = \frac{1}{1+\eta_B\dfrac{\tilde{m}_{Bc}}{\tilde{m}_{Ac}}} \\[2em]
&= \frac{1}{1+\eta_B\dfrac{K\theta_B^0}{\theta_A^*}} = \cfrac{1}{1+\eta_B\cfrac{K}{\theta_A^*}\left(\cfrac{1}{1+\psi+\cfrac{K\beta_A}{\theta_A^*}\left(\cfrac{1-(1+\psi)\theta_A^*}{1+\psi+\beta_A}\right)}\right)}
\end{aligned} \tag{6.64}
$$

## 6.4    Analytical Concentration Profile for Species B in Tank 1 When $\gamma=1$

For a system with N stages, feed at stage 1, no sweep stream, dilute concentrations, and short times an analytical expression for the concentration of the impurity in tank 1 can be determined for an arbitrary growth cycle.  The value at cyclic steady state cannot be determined though so the solution will contain the initial concentrations at the beginning of the growth cycle, $\theta_A{}^0$ and $\theta_B{}^0$.  The differential equations governing the concentration profile of species A and B in tank 1 are given in equations (6.65) and (6.66).

$$\frac{d\theta_{A1}}{d\tau} = -\beta_A\left(\theta_{A1} - \theta_A^*\right) + 1 - \theta_{A1} \tag{6.65}$$

$$\frac{d\theta_{B1}}{d\tau} = -\beta_B\left(\theta_{B1} - \theta_B^*\right) + 1 - \theta_{B1} \tag{6.66}$$

Equation (6.65) can be solved readily to give the concentration profile of species A in tank 1.

$$\theta_{A1} = \left(\theta_{A1}^0 - \frac{1 + \beta_A\theta_A^*}{1 + \beta_A}\right)e^{-(1+\beta_A)\tau} + \frac{1 + \beta_A\theta_A^*}{1 + \beta_A} \tag{6.67}$$

The critical concentration of the impurity, $\theta_B^*$, is given by the following expression as shown in section 2.2.2.

$$\theta_B^* = \frac{\theta_B}{\dfrac{K}{\gamma\theta_A^*}\left(\theta_A - \theta_A^*\right) + 1} = \frac{\theta_B}{\dfrac{K}{\gamma\theta_A^*}\left(\left(\theta_{A1}^0 - \dfrac{1 + \beta_A\theta_A^*}{1 + \beta_A}\right)e^{-(1+\beta_A)\tau} + \dfrac{1 - \theta_A^*}{1 + \beta_A}\right) + 1} \tag{6.68}$$

Substituting equation (6.68) into equation (6.66) and rearranging gives

$$\frac{d\theta_{B1}}{d\tau} = 1 - \left(1 + \beta_B - \frac{\beta_B}{\frac{K}{\gamma\theta_A^*}\left(\left(\theta_{A1}^0 - \frac{1+\beta_A\theta_A^*}{1+\beta_A}\right)e^{-(1+\beta_A)\tau} + \frac{1-\theta_A^*}{1+\beta_A}\right) + 1}\right)\theta_{B1}$$

(6.69)

This equation is a first order differential equation and can be solved using an integrating factor. To find the integrating factor the following integral must be evaluated

$$\int\left(1 + \beta_B - \frac{\beta_B}{\frac{K}{\gamma\theta_A^*}\left(\left(\theta_{A1}^0 - \frac{1+\beta_A\theta_A^*}{1+\beta_A}\right)e^{-(1+\beta_A)\tau} + \frac{1-\theta_A^*}{1+\beta_A}\right) + 1}\right)d\tau$$

$$= (1+\beta_B)\tau - \int\left(\frac{\beta_B}{\frac{K}{\gamma\theta_A^*}\left(\left(\theta_{A1}^0 - \frac{1+\beta_A\theta_A^*}{1+\beta_A}\right)e^{-(1+\beta_A)\tau} + \frac{1-\theta_A^*}{1+\beta_A}\right) + 1}\right)d\tau$$

$$= (1+\beta_B)\tau - \beta_B\int\left(\frac{1}{\frac{K}{\gamma\theta_A^*}\left(\theta_{A1}^0 - \frac{1+\beta_A\theta_A^*}{1+\beta_A}\right)e^{-(1+\beta_A)\tau} + \frac{K}{\gamma\theta_A^*}\left(\frac{1-\theta_A^*}{1+\beta_A}\right) + 1}\right)d\tau$$

$$= (1+\beta_B)\tau - \beta_B\int\left(\frac{e^{(1+\beta_A)\tau}}{\frac{K}{\gamma\theta_A^*}\left(\theta_{A1}^0 - \frac{1+\beta_A\theta_A^*}{1+\beta_A}\right) + \left(\frac{K}{\gamma\theta_A^*}\left(\frac{1-\theta_A^*}{1+\beta_A}\right) + 1\right)e^{(1+\beta_A)\tau}}\right)d\tau$$

$$= (1+\beta_B)\tau - \frac{\beta_B\Big/(1+\beta_A)}{\left(\frac{K}{\gamma\theta_A^*}\left(\frac{1-\theta_A^*}{1+\beta_A}\right) + 1\right)}\ln\left(\frac{K}{\gamma\theta_A^*}\left(\theta_{A1}^0 - \frac{1+\beta_A\theta_A^*}{1+\beta_A}\right) + \left(\frac{K}{\gamma\theta_A^*}\left(\frac{1-\theta_A^*}{1+\beta_A}\right) + 1\right)e^{(1+\beta_A)\tau}\right)$$

(6.70)

The integrating factor is then given by

$$\mu = \exp\left[(1+\beta_B)\tau - \frac{\beta_B\Big/(1+\beta_A)}{\left(\frac{K}{\gamma\theta_A^*}\left(\frac{1-\theta_A^*}{1+\beta_A}\right) + 1\right)}\ln\left(\frac{K}{\gamma\theta_A^*}\left(\theta_{A1}^0 - \frac{1+\beta_A\theta_A^*}{1+\beta_A}\right) + \left(\frac{K}{\gamma\theta_A^*}\left(\frac{1-\theta_A^*}{1+\beta_A}\right) + 1\right)e^{(1+\beta_A)\tau}\right)\right]$$

$$= e^{(1+\beta_B)\tau}\left[\frac{K}{\gamma\theta_A^*}\left(\theta_{A1}^0 - \frac{1+\beta_A\theta_A^*}{1+\beta_A}\right) + \left(\frac{K}{\gamma\theta_A^*}\left(\frac{1-\theta_A^*}{1+\beta_A}\right)+1\right)e^{(1+\beta_A)\tau}\right]^{\frac{-\beta_B}{(1+\beta_A)\left(\frac{K}{\gamma\theta_A^*}\left(\frac{1-\theta_A^*}{1+\beta_A}\right)+1\right)}} \qquad (6.71)$$

The concentration profile for species B in tank 1 is given by

$$\theta_{B1} = \frac{\int \mu d\tau + C}{\mu} \qquad (6.72)$$

where $C$ is the constant of integration. Evaluating the integral of $\mu$ will be simpler to follow with use of the following constants.

$$B = \frac{K}{\theta_A^*}\left(\theta_{A1}^0 - \frac{1+\beta_A\theta_A^*}{1+\beta_A}\right) \qquad (6.73)$$

$$D = \frac{K}{\gamma\theta_A^*}\left(\frac{1-\theta_A^*}{1+\beta_A}\right) + 1 \qquad (6.74)$$

The integral to be evaluated is

$$\int e^{(1+\beta_B)\tau}\left(B + De^{(1+\beta_A)\tau}\right)^{\frac{-\beta_B}{(1+\beta_A)D}}d\tau \qquad (6.75)$$

This equation cannot be evaluated analytically unless $\beta_B$ is equal to $\beta_A$, or $\gamma=1$. If all values of $\beta_B$ are set equal to $\beta_A$, equation (6.75) can be evaluated to give

$$\int e^{(1+\beta_A)\tau}\left(B + De^{(1+\beta_A)\tau}\right)^{\frac{-\beta_A}{(1+\beta_A)D}}d\tau = \frac{\left(B + De^{(1+\beta_A)\tau}\right)^{1-\frac{\beta_A}{(1+\beta_A)C}}}{D(1+\beta_A)\left(1 - \frac{\beta_A}{(1+\beta_A)D}\right)} \qquad (6.76)$$

Substituting into equation (6.72) gives the concentration profile for B in terms of the integration constant.

$$\theta_{B1} = \frac{\dfrac{\left(B+De^{(1+\beta_A)\tau}\right)^{1-\frac{\beta_A}{(1+\beta_A)C}}}{D\left(1+\beta_A\right)\left(1-\dfrac{\beta_A}{\left(1+\beta_A\right)D}\right)} + C}{e^{(1+\beta_A)\tau}\left(B+De^{(1+\beta_A)\tau}\right)^{\frac{-\beta_A}{(1+\beta_A)C}}}$$

(6.77)

The concentration at $\tau=0$ is $\theta_{B1}{}^0$.  Using this to evaluate the integration constant $C$ gives the final result.

$$\theta_{B1} = \frac{\dfrac{\left(B+De^{(1+\beta_A)\tau}\right)^{1-\frac{\beta_A}{(1+\beta_A)C}}}{D\left(1+\beta_A\right)\left(1-\dfrac{\beta_A}{\left(1+\beta_A\right)D}\right)} + \dfrac{\theta_{B1}^0}{(B+C)^{\frac{-\beta_A}{(1+\beta_A)C}}} - \dfrac{(B+D)^{1-\frac{\beta_A}{(1+\beta_A)C}}}{D\left(1+\beta_A\right)\left(1-\dfrac{\beta_A}{\left(1+\beta_A\right)D}\right)}}{e^{(1+\beta_A)\tau}\left(B+De^{(1+\beta_A)\tau}\right)^{\frac{-\beta_A}{(1+\beta_A)C}}}$$

(6.78)

$$= \frac{\dfrac{\left(B+De^{(1+\beta_A)\tau}\right)^{1-\frac{\beta_A}{(1+\beta_A)C}} - (B+D)^{1-\frac{\beta_A}{(1+\beta_A)C}}}{D\left(1+\beta_A\right)\left(1-\dfrac{\beta_A}{\left(1+\beta_A\right)D}\right)} + \dfrac{\theta_{B1}^0}{(B+C)^{\frac{-\beta_A}{(1+\beta_A)C}}}}{e^{(1+\beta_A)\tau}\left(B+De^{(1+\beta_A)\tau}\right)^{\frac{-\beta_A}{(1+\beta_A)C}}}$$

Now rewrite equation (6.68) as

$$\theta_{B1}^* = \frac{\theta_{B1}}{\frac{K}{\gamma\theta_A^*}\left(\left(\theta_{A1}^0 - \frac{1+\beta_A\theta_A^*}{1+\beta_A}\right)e^{-(1+\beta_A)\tau} + \frac{1-\theta_A^*}{1+\beta_A}\right)+1} = \frac{\theta_{B1}e^{(1+\beta_A)\tau}}{B+De^{(1+\beta_A)\tau}}$$

$$= \frac{\dfrac{\left(B+De^{(1+\beta_A)\tau}\right)^{1-\frac{\beta_A}{(1+\beta_A)D}} - (B+D)^{1-\frac{\beta_A}{(1+\beta_A)D}}}{D(1+\beta_A)\left(1-\dfrac{\beta_A}{(1+\beta_A)D}\right)} + \dfrac{\theta_{B1}^0}{(B+D)^{\frac{-\beta_A}{(1+\beta_A)D}}}}{\left(B+De^{(1+\beta_A)\tau}\right)^{1-\frac{\beta_A}{(1+\beta_A)D}}}$$

$$= \frac{1-\left(\dfrac{(B+D)}{\left(B+De^{(1+\beta_A)\tau}\right)^{1-\frac{\beta_A}{(1+\beta_A)D}}}\right)^{1-\frac{\beta_A}{(1+\beta_A)D}}}{D(1+\beta_A)-\beta_A} + \dfrac{\theta_{B1}^0\left(B+De^{(1+\beta_A)\tau}\right)^{-1+\frac{\beta_A}{(1+\beta_A)D}}}{(B+D)^{\frac{-\beta_A}{(1+\beta_A)D}}}$$

$$= \frac{1-\left(\dfrac{(B+D)}{\left(B+De^{(1+\beta_A)\tau}\right)^{1-\frac{\beta_A}{(1+\beta_A)D}}}\right)^{1-\frac{\beta_A}{(1+\beta_A)D}}}{D(1+\beta_A)-\beta_A} + \dfrac{\theta_{B1}^0}{(B+D)}\left(\dfrac{(B+D)}{\left(B+De^{(1+\beta_A)\tau}\right)^{1-\frac{\beta_A}{(1+\beta_A)D}}}\right)^{1-\frac{\beta_A}{(1+\beta_A)D}}$$

$$= \frac{1}{D(1+\beta_A)-\beta_A} + \left(\dfrac{\theta_{B1}^0}{(B+D)} - \dfrac{1}{D(1+\beta_A)-\beta_A}\right)\left(\dfrac{(B+D)}{\left(B+De^{(1+\beta_A)\tau}\right)^{1-\frac{\beta_A}{(1+\beta_A)D}}}\right)^{1-\frac{\beta_A}{(1+\beta_A)D}} \tag{6.79}$$

The following equations will simplify the final result

$$D(1+\beta_A)-\beta_A = \left(\frac{K}{\theta_A^*}\left(\frac{1-\theta_A^*}{1+\beta_A}\right)+1\right)(1+\beta_A)-\beta_A = \frac{K}{\theta_A^*}(1-\theta_A^*)+1 \tag{6.80}$$

$$B+D = \frac{K}{\theta_A^*}\left(\theta_{A1}^0 - \frac{1+\beta_A\theta_A^*}{1+\beta_A}\right) + \frac{K}{\theta_A^*}\left(\frac{1-\theta_A^*}{1+\beta_A}\right)+1 = 1 + \frac{K}{\theta_A^*}\left(\theta_{A1}^0 - \theta_A^*\right) \tag{6.81}$$

$$1-\frac{\beta_A}{(1+\beta_A)D} = 1 - \frac{\beta_A}{(1+\beta_A)\frac{K}{\theta_A^*}\left(\frac{1-\theta_A^*}{1+\beta_A}\right)+1} = 1 - \frac{\beta_A}{(1+\beta_A)+\frac{K}{\theta_A^*}(1-\theta_A^*)}$$

$$= \frac{1+\frac{K}{\theta_A^*}(1-\theta_A^*)}{(1+\beta_A)+\frac{K}{\theta_A^*}(1-\theta_A^*)} \tag{6.82}$$

The expression for $\theta_{B1}{}^*$ can now be written as

$$\theta_{B1}^* = \cfrac{1}{1+\dfrac{K}{\theta_A^*}\left(1-\theta_A^*\right)} + \left(\cfrac{\theta_{B1}^0}{1+\dfrac{K}{\theta_A^*}\left(\theta_{A1}^0-\theta_A^*\right)} - \cfrac{1}{1+\dfrac{K}{\theta_A^*}\left(1-\theta_A^*\right)}\right)*$$

$$\left(\cfrac{1+\dfrac{K}{\theta_A^*}\left(\theta_{A1}^0-\theta_A^*\right)}{\dfrac{K}{\theta_A^*}\left(\theta_{A1}^0-\dfrac{1+\beta_A\theta_A^*}{1+\beta_A}\right)+\left(\dfrac{K}{\gamma\theta_A^*}\left(\dfrac{1-\theta_A^*}{1+\beta_A}\right)+1\right)e^{(1+\beta_A)\tau}}\right)^{\frac{1+\frac{K}{\theta_A^*}\left(1-\theta_A^*\right)}{(1+\beta_A)+\frac{K}{\theta_A^*}\left(1-\theta_A^*\right)}}$$

(6.83)

This is the result presented in equation (2.93).

## 6.5    Solid Solution Verification

Asparagine and aspartic acid have been found in the literature to form a solid solution containing up to 20% aspartic acid in asparagine.[148, 149] In order to validate this, supersaturated solutions at five different concentrations were prepared. The compositions of these solutions are listed in Table 10.

| Asparagine (g) | Aspartic Acid (g) | Water (g) | $x_{ASN}*10^3$ | $x_{ASP}*10^3$ |
|:---:|:---:|:---:|:---:|:---:|
| 3 | 0.5 | 100 | 4.07 | 0.68 |
| 3.1 | 0.4 | 100 | 4.20 | 0.54 |
| 3.2 | 0.3 | 100 | 4.34 | 0.41 |
| 3.3 | 0.2 | 100 | 4.48 | 0.27 |
| 3.4 | 0.1 | 100 | 4.61 | 0.14 |

**Table 10. Composition of solutions prepared in order to check for solid solution formation by asparagine and aspartic acid in water. $x_i$ is the mole fraction of species $i$.**

The asparagine, aspartic acid and water were heated to $80^0$C until the solids had completely dissolved. The mixtures were then allowed to cool to room temperature at which point a liquid sample was taken for HPLC analysis. The solutions were then stirred for 5 days at room temperature. Crystals were observed in the first four solutions after 24 hrs and the fifth solution contained crystals after 48 hrs. Stirring is continued for 5 days to allow equilibrium to be approached in both the liquid and solid phase.

Once the 5 days had elapsed, each solution was filtered and the solid and liquid phases were collected. A sample was prepared from the liquid and solid phases for HPLC analysis. The liquid phase samples were prepared in the same manner as samples from batch crystallization experiments (section 4.2.1). The solid phase was prepared for HPLC analysis by dissolving approximately 70 mg of solid in 100 ml of water. The concentrations of asparagine and aspartic acid in the prepared samples were then measured with HPLC.

The phase behavior will be shown using a standard 2-dimensional plot with the mole fraction of asparagine on the x-axis and the mole fraction of aspartic acid on the y-axis. The

mole fraction of water can be found by subtracting the sum of these two mole fractions from one. The crystal grown is a mono-hydrate so the highest possible mole fraction of asparagine in the solid phase is 0.5 corresponding to a pure asparagine crystal. A plot of the phase behavior showing primarily the solid phase compositions is given in Figure 77. The liquid phase concentrations are too small to be seen on the same plot as the solid phase concentrations so they will be addressed in a different figure.
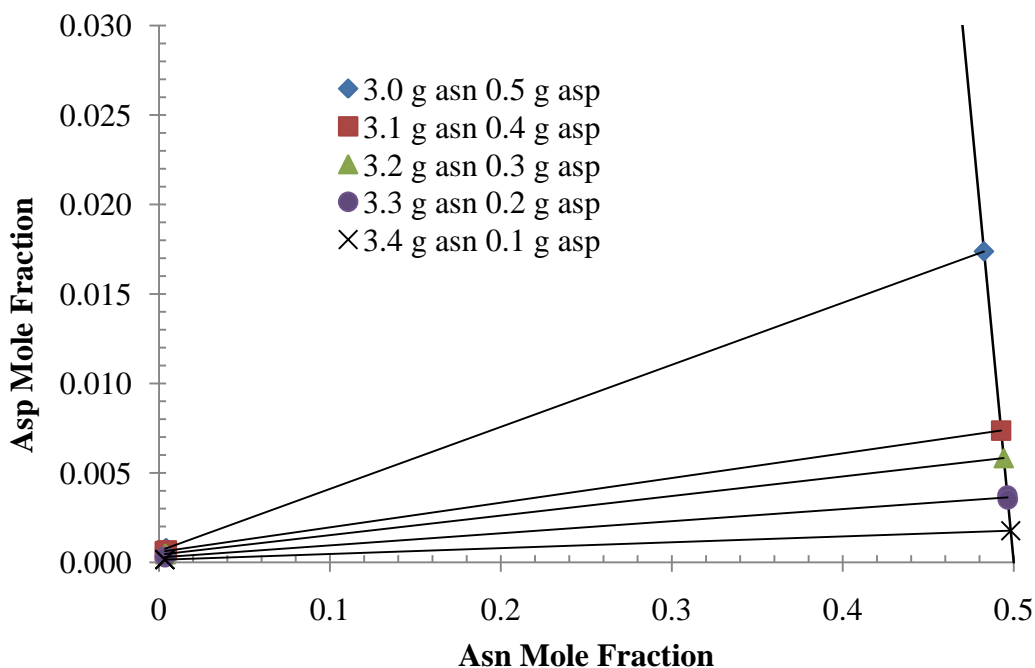


**Figure 77. Partial phase diagram for asparagine and aspartic acid in water.**

It is clear in Figure 77 that the solid phase compositions for the five test solutions are all different. This is the expected result as a eutectic or compound forming system would a constant solid composition.

Figure 78 shows the initial and liquid phase concentrations.
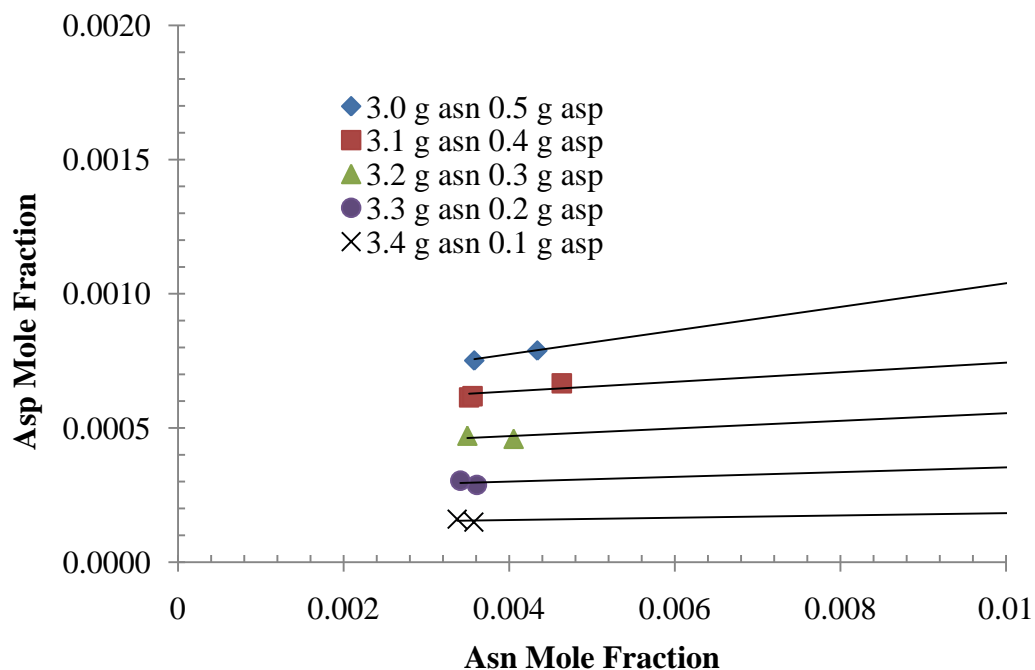
**Figure 78.** Partial phase diagram for asparagine and aspartic acid in water showing primarily the initial and liquid phase concentrations. Liquid phase concentrations are the left most point in each set.

All solutions have unique liquid phase concentrations and the initial concentration of the supersaturated liquid phase lies on the line between the liquid and solid phase concentrations which indicates that the mass balance is satisfied.

The measured phase behavior is consistent with the formation of a solid solution. The expected behavior published in the literature has been verified.

# 7.    References

1.    W. H. Power, B. M. Fabuss and C. N. Satterfield, Journal of Chemical & Engineering Data **9** (3), 437-442 (1964).

2.    V. Costodes and A. Lewis, Chem. Eng. Sci. **61** (5), 1377-1385 (2006).

3.    I. D. G. A. Putrawan and T. H. Soerawidjaja, Separation and Purification Technology **39**, 79-88 (2004).

4.    L. F. Filobelo, O. Galkin and P. G. Vekilov, The Journal of Chemical Physics **123** (1), 014904-014901 - 014904-014907 (2005).

5.    A. Che and C. Rey, Journal of Materials Science: Materials in Medicine **10**, 231-237 (1999).

6.    D. G. Georgieva, M. E. Kuil, T. H. Oosterkamp, H. W. Zandbergen and J. P. Abrahams, Acta Crystallographica Section D Biological Crystallography **63** (5), 564-570 (2007).

7.    M. Järn, S. Areva, V. Pore, J. Peltonen and M. Lindén, Langmuir **22**, 8209-8213 (2006).

8.    X. Y. Liu, Langmuir **16**, 7337-7345 (2000).

9.    X. Y. Liu, Journal of Physical Chemistry B **105**, 11550-11558 (2001).

10.    T. E. Paxton, A. Sambanis and R. W. Rousseau, Langmuir **17**, 3076-3079 (2001).

11.    R. P. Sear, Physical Review E **67** (6) (2003).

12.    N. E. Chayen, E. Saridakis and R. P. Sear, Proceedings of the National Academy of Sciences **103** (3), 597-601 (2005).

13.    V. F. Komarov, J. Garside and J. W. Mullin, Chem. Ind. (3), 119-120 (1976).

14.    M. L. White and A. A. Frost, Journal of Colloid Science **14** (3), 247-251 (1959).

15.    J. L. Kenty and J. P. Hirth, Surface Science **15** (3), 403-& (1969).

16.    J. Aizenberg, Nature **1720** (1971), 1997-2000 (1999).

17.    K. Fujiwara, S. Nagahisa, J. Yano, S. Ueno and K. Sato, Journal of Physical Chemistry B, 8116-8123 (2000).

18.    T. Kubo, Journal of Crystal Growth **269** (2-4), 535-541 (2004).

19.    E. M. Landau, S., M. Levanon, L. Leiserowitz, M. Lahav and J. Sagiv, Journal of the American Chemical Society **111**, 1436-1445 (1989).

20.    D. Palms, C. Priest, R. Sedev, J. Ralston and G. Wegner, Journal of Colloid and Interface Science **303** (2), 333-336 (2006).

21.    H. Takiguchi, K. Iida, S. Ueno, J. Yano and K. Sato, Journal of Crystal Growth **193**, 641-647 (1998).

22.    A. M. Travaille, E. G. A. Steijven, H. Meekes and H. Kempen, Journal of Physical Chemistry B **109**, 5618-5626 (2005).

23.    P. W. Carter and M. D. Ward, Journal of the American Chemical Society **115**, 11521-11535 (1993).

24.    P. W. Carter and M. D. Ward, Journal of the American Chemical Society (116), 769-770 (1994).

25.    N. B. J. Hetherington, A. N. Kulak, K. Sheard and F. C. Meldrum, Langmuir **22** (5), 1955-1958 (2006).

26.    A. McPherson and P. Shlichta, Science **239** (4838), 385-387 (1988).

27.    N. A. Clontz and W. L. McCabe, Chemical Engineering Progress Symposium Series, No. 110 **67**, 6-17 (1971).

28.    R. T. Johnson, R. W. Rousseau and W. L. McCabe, AICHE Symposium Series No. 121 **68**, 31-41 (1972).

29.    J. W. Mullin and S. J. Jancic, Transactions of the Institution of Chemical Engineers **57** (3), 188-193 (1979).

30.    A. H. Janse and E. J. Dejong, Transactions of the Institution of Chemical Engineers **56** (3), 187-193 (1978).

31.    M. Volmer, *Kinetik der phasenbildung*. (T. Steinkopff, Dresden und Leipzig, 1939).

32.    D. Kashchiev and G. M. van Rosmalen, Crystal Research and Technology **38** (78), 555-574 (2003).

33.    D. Knezic, J. Zaccaro and A. S. Myerson, Journal of Physical Chemistry B **108** (30), 10672-10677 (2004).

34.    O. Sohnel and J. W. Mullin, Journal of Colloid and Interface Science **123** (1), 43-50 (1988).

35.    J. W. Gibbs, *The collected works of J. Willard Gibbs*. (Yale Univ. Press, New Haven, 1948).

36.    R. Becker and W. Döring, Annalen der Physik **416** (8), 719-752 (1935).

37.    M. Avrami, Journal of Chemical Physics **7**, 1103-1112 (1939).

38.    W. A. Johnson and R. F. Mehl, TRANSACTIONS OF THE AMERICAN INSTITUTE OF MINING AND METALLURGICAL ENGINEERS **135**, 416-442 (1939).

39.    A. N. Kolmogorov, IZV AKAD NAUK SSSR Ser Math **1**, 355-359 (1937).

40.    M. Castro, Physical Review B **67** (3), 1-8 (2003).

41. P. Chaing, M. D. Donohue and J. L. Katz, Journal of Colloid and Interface Science **122** (1), 251-265 (1988).

42. M. Iwamatsu, The Journal of Chemical Physics **126** (13), 134703-134703 (2007).

43. X. Y. Liu, Journal of Chemical Physics **111** (4), 1628-1635 (1999).

44. R. Mohanty, S. Bhandarkar and J. Estrin, AIChE Journal **36** (10), 1536-1544 (1990).

45. P. C. Rieke, **182**, 472-484 (1997).

46. J. W. P. Schmelzer, Materials Physics and Mechanics **6**, 21-33 (2003).

47. R. M. Tromp and J. B. Hannon, Surface Review and Letters **9** (3 & 4), 1565-1593 (2002).

48. W. Wu and G. H. Nancollas, Journal of Colloid and Interface Science **182**, 365-373 (1996).

49. Y. Kousaka, T. Nomura and M. Alonso, Advanced Powder Technology **12** (3), 291-309 (2001).

50. A. D. J. Haymet and D. W. Oxtoby, The Journal of Chemical Physics **74** (4), 2559-2565 (1981).

51. T. V. Ramakrishnan and M. Yussouff, Physical Review B **19** (5), 2775 (1979).

52. S. M. Kathmann, Theoretical Chemistry Accounts **116** (1-3), 169-182 (2006).

53. L. A. Baez and P. Clancy, The Journal of Chemical Physics **102** (20), 8138-8148 (1995).

54. Y. G. Chushak and L. S. Bartell, The Journal of Physical Chemistry B **103** (50), 11196-11204 (1999).

55. Y. Chushak and L. S. Bartell, The Journal of Physical Chemistry A **104** (41), 9328-9336 (2000).

56. J. Anwar and P. K. Boateng, Journal of the American Chemical Society **104** (15), 9600-9604 (1998).

57. D. Frenkel and J. P. McTague, Annual Review of Physical Chemistry **31** (1), 491-521 (1980).

58. E. S. Boek, W. J. Briels and D. Feil, The Journal of Physical Chemistry **98** (6), 1674-1681 (1994).

59. P. Chiang and M. D. Donohue, Journal of Colloid and Interface Science **122** (1), 230-250 (1988).

60. A. A. Chernov, (1989), pp. 391-417.

61. W. K. Burton, N. Cabrera and F. C. Frank, Philosophical Transactions of the Royal Society A: Mathematical, Physical and Engineering Sciences **243** (866), 299-358 (1951).

62. A. A. Chernov, Soviet Physics Uspekhi **4** (1), 116-148 (1961).

63. G. H. Gilmer, R. Ghez and N. Cabrera, Journal of Crystal Growth **8** (1), 79-93 (1971).

64. A. Berthoud, Journal de Chimique Physique **10**, 624-635 (1912).

65. J. J. P. Valeton, Zeitschrift fur Kristallographie **59**, 483 (1924).

66. J. W. Mullin, *Crystallization*. (Elsevier Butterworth-Heinemann, Boston, 2001).

67. J. Garside, Chem. Eng. Sci. **40** (1), 3-26 (1985).

68. K. A. Jackson, in *Liquid metals and solidification; a seminar on liquid metals and solidification held during the thirty-ninth National Metal Congress and Exposition, Chicago, November 2 to 8, 1957*, edited by M. American Society for (Cleveland, 1958), pp. 174-186.

69. P. Bennema and J. P. van der Eerden, Journal of Crystal Growth **42**, 201-213 (1977).

70. J. R. Bourne and R. J. Davey, Journal of Crystal Growth **36** (2), 278-286 (1976).

71. S. Briarqon, D. Colson and J. P. Klein, Chemical Engineering Journal **70**, 55-64 (1998).

72. T. R. Bott, Experimental Thermal and Fluid Science **14**, 356-360 (1997).

73. P. Martins and F. Rocha, Chem. Eng. Sci. **61** (17), 5686-5695 (2006).

74. G. H. Montillon and W. L. Badger, Industrial & Engineering Chemistry **19** (7), 809-816 (1927).

75. W. L. McCabe, Industrial & Engineering Chemistry **21** (1), 30-33 (1929).

76. W. L. McCabe, Industrial & Engineering Chemistry **21** (2), 112-119 (1929).

77. A. D. Randolph and M. A. Larson, AIChE Journal **8** (5), 639-645 (1962).

78. J. Garside and R. J. Davey, Chem. Eng. Commun. **4** (4-5), 393-424 (1980).

79. M. Bavin, Chem. Ind. (16), 527-529 (1989).

80. A. Asmadi, M. A. Neumann, J. Kendrick, P. Girard, M.-A. Perrin and F. J. J. Leusen, The Journal of Physical Chemistry B **113** (51), 16303-16313 (2009).

81. B. B. Averkiev, M. Y. Antipin, A. B. Sheremetev and T. V. Timofeeva, Crystal Growth & Design **5** (2), 631-641 (2004).

82. A. R. Browning, M. F. Doherty and G. H. Fredrickson, Physical Review E **77** (4), 041604 (2008).

83. R. J. Davey and J. W. Mullin, Kristall und Technik **11** (3), 229-233 (1976).

84. R. J. Davey, Journal of Crystal Growth **34**, 109-119 (1976).

85. A. S. Michaels and A. R. Colville, The Journal of Physical Chemistry **64** (1), 13-19 (1960).

86. J. W. Mullin and Amataviv.A, Journal of Applied Chemistry of the Ussr **17** (5), 151-& (1967).

87.    N. Kubota and J. W. Mullin, Journal of Crystal Growth **152** (3), 203-208 (1995).

88.    R. J. Davey and J. W. Mullin, Journal of Crystal Growth **26** (1), 45-51 (1974).

89.    S. Al-Jibbouri and J. Ulrich, Crystal Research and Technology **39** (6), 540-547 (2004).

90.    K. G. Denbigh and E. T. White, Chem. Eng. Sci. **21** (9), 739-& (1966).

91.    A. S. Myerson and M. Saska, Aiche Journal **30** (5), 865-867 (1984).

92.    K. Sato, Japanese Journal of Applied Physics **19** (7), 1257-1266 (1980).

93.    K. Sato, Japanese Journal of Applied Physics **19** (10), 1829-1836 (1980).

94.    A. S. Dzyuba, Soviet Physics Crystallography **28** (1), 111-112 (1983).

95.    A. S. Myerson and D. J. Kirwan, Industrial & Engineering Chemistry Fundamentals **16** (4), 414-420 (1977).

96.    N. Clavaguera, V. Palumbo-Romand, M. Ferriol and M. T. Cohen-Adad, Growth (Lakeland) **180**, 248-254 (1997).

97.    Q. Nie, J. Wang and Q. Yin, Chem. Eng. Sci. **61** (18), 5962-5968 (2006).

98.    G. G. Z. Zhang and D. J. W. Grant, International Journal of Pharmaceutics **181**, 61-70 (1999).

99.    L. Bonpunt, R. Courchinoux, Y. Haget, E. Estop, T. Calvet, M. a. Cuevas-Diarte and M. Labrador, Journal of Applied Crystallography **24** (2), 164-170 (1991).

100.   A.-L. Chow, P. K. K. Chow, W. Zhongshan and D. J. W. Grant, International Journal of Pharmaceutics **24**, 239-258 (1985).

101.   A. S. Teja, J. C. Givand and R. W. Rousseau, AIChE Journal **48** (11), 2629-2634 (2002).

102.   R. M. Myasnikova, Molecular Crystals and Liquid Crystals **90** (1), 195-204 (1983).

103.   G. T. Didrikhsons and H. Pfeiffer, PHYSICA STATUS SOLIDI A-APPLIED RESEARCH **169**, 169-178 (1982).

104.   A. G. Shtukenberg, Y. O. Punin and P. Azimov, American Journal of Science **306**, 553-574 (2006).

105.   H. A. Doerner and W. H. Hoskins, Journal of the American Chemical Society **47** (3), 662-675 (1925).

106.   R. Meadhra and R. Lin, Chemical Engineering Research and Design **84** (8), 711-720 (2006).

107.   J. C. Givand, A. S. Teja and R. W. Rousseau, AIChE Journal **47** (12), 2705-2712 (2001).

108.   J. Givand, B.-K. Chang, A. S. Teja and R. W. Rousseau, Industrial & Engineering Chemistry Research **41** (7), 1873-1876 (2002).

109.    F. Rosenberger and H. G. Riveros, The Journal of Chemical Physics **60** (2), 668-673 (1974).

110.    J. A. Burton, R. C. Prim and W. P. Slichter, The Journal of Chemical Physics **21** (11), 1987-1991 (1953).

111.    P. A. Meenan, S. R. Anderson and D. L. Klug, in *Handbook of industrial crystallization*, edited by A. S. Myerson (Butterworth-Heinemann, Boston, 1993).

112.    B. R. Thomas, A. A. Chernov, P. G. Vekilov and D. C. Carter, Journal of Crystal Growth **211** (1-4), 149-156 (2000).

113.    G. J. Sloan and A. R. McGhie, *Techniques of Melt Crystallization*. (Wiley-Interscience, New York, 1988).

114.    M. Oullion, F. Puel, G. Fevotte, S. Righini and P. Carvin, Chem. Eng. Sci. **62** (3), 820-832 (2007).

115.    F. Ricard, C. Brechtelsbauer, X. Y. Xu and C. J. Lawrence, Chemical Engineering Research and Design **83** (7), 794-805 (2005).

116.    A. G. Jones and J. W. Mullin, Chem. Eng. Sci. **29** (1), 105-118 (1974).

117.    J. W. Mullin and J. Nyvlt, Chem. Eng. Sci. **26** (3), 369-& (1971).

118.    K. Hanaki, N. Nonoyama, Y. Yabuki, Y. Kato and I. Hirasawa, Journal of Chemical Engineering of Japan **40** (1), 63-71 (2007).

119.    M. A. Novomeysky, Transactions of the Institution of Chemical Engineers **14**, 60-84 (1936).

120.    J. L. Manganaro and J. C. Schwartz, Industrial & Engineering Chemistry Process Design and Development **24** (4), 1245-1251 (1985).

121.    F. Jeremiassen and H. Svanoe, Chemical and Metallurgical Engineering **39**, 594-596 (1932).

122.    I. GEA Process Engineering, in *http://www.niroinc.com/evaporators_crystallizers/Oslo_type_crystallizer.asp*, edited by Oslo_type_crystallizer_fg4.jpg (2010).

123.    H. H. Newman and R. C. Bennett, Chemical Engineering Progress **55** (3), 65-70 (1959).

124.    R. Castelnuovo, in *http://en.wikipedia.org/wiki/File:DTB_2.PNG* (2006).

125.    J. N. Robinson and J. E. Roberts, Canadian Journal of Chemical Engineering **35**, 105-112 (1957).

126.    J. S. Wey and J. P. Terwilliger, Industrial & Engineering Chemistry Process Design and Development **15** (3), 467-469 (1976).

127.    H. S. Weng, Journal of Chemical Engineering of Japan **13** (5), 407-409 (1980).

128.    A. E. Bailey, *Melting and solidification of fats*. (Interscience Publishers, New York, 1950).

129.    A. E. Bailey, D. Swern, M. W. Formo and T. H. Applewhite, *Bailey's Industrial oil and fat products*. (Wiley, New York, 1979).

130.    W. KLOEK, T. VAN VLIET and P. WALSTRA, Journal of Texture Studies **36** (5-6), 544-568 (2005).

131.    L. Chen, J. Li and M. Matsuoka, Industrial and Engineering Chemistry Research **45**, 2818-2823 (2006).

132.    M. A. van der Gun, O. S. L. Bruinsma and G. M. van Rosmalen, Chem. Eng. Sci. **56** (7), 2381-2388 (2001).

133.    G. G. Devyatykh, Y. E. Elliev, Y. P. Kirillov and A. Y. Malyshev, Inorg. Mater. **36** (10), 1050-1055 (2000).

134.    H. Schildknecht, *Zone melting*. (Verlag Chemie;Academic Press, Weinheim/Bergstr.,New York, 1966).

135.    J. A. Brodie, Mechanical and Chemical Engineering Transactions **7** (1), 37-44 (1971).

136.    O. Fischer, S. J. Jancic and K. Saxer, in *Industrial Crystallization 84 (9th Symposium, The Hague)*, edited by S. J. Jancic and E. J. de Jong (Elsevier, Amsterdam, 1984), pp. 153-157.

137.    K.-J. Kim and A. Mersmann, Chemical Engineering Research and Design **75** (2), 176-182 (1997).

138.    J. Sobesto and J. Mydlarz, Chemische Technik **43** (6), 227-230 (1991).

139.    J. W. Mullin and J. R. Williams, Chemical Engineering Research & Design **62** (5), 296-302 (1984).

140.    K. Bartosch and A. Mersmann, Chem. Eng. Sci. **56** (7), 2347-2356 (2001).

141.    E. W. Merrow, Chemical Engineering Progress **81** (5), 14-22 (1985).

142.    E. W. Merrow, Chemical Engineering **95** (15), 89-92 (1988).

143.    D. Schulze, *Powders and bulk solids : behavior, characterization, storage and flow*. (Springer, Berlin; New York, 2007).

144.    W. L. Godfrey and R. D. Benham, Simulation **4** (1), 27-33 (1965).

145.    W. L. Godfrey,  (1969).

146.    J. P. Roodenrijs and W. H. J. M.,  (1988).

147.    A. Poulos, J. W. Greiner and G. A. Fevig, Industrial and Engineering Chemistry **53** (12), 949-962 (1961).

148.    D. M. Ruthven and C. B. Ching, Chem. Eng. Sci. **44** (5), 1011-1038 (1989).

149.    J. B. Dalton and C. L. A. Schmidt, Journal of Biological Chemistry **109**, 241-248 (1935).

150. CRC handbook of chemistry and physics. (1978).

151. Netzsch, *Operating and Maintenance Instructions for Mini-Metering Pumps*. (1999).

152. F. W. Dittus and L. M. K. Boelter, International Communications in Heat and Mass Transfer **12** (1), 3-22.

153. L. Addadi, Z. Berkovitch-Yellin, N. Domb, E. Gati, M. Lahave and L. Leiserowitz, Nature **296** (4), 21-26 (1982).

154. J. L. Wang, Z. Berkovitch-Yellin and L. Leiserowitz, Acta Crystallographica Section B Structural Science **41** (5), 341-348 (1985).

155. C. A. Zittle and C. L. A. Schmidt, Journal of Chemical Biology **108**, 161-185 (1934).

156. T. H. Chilton and A. P. Colburn, Industrial and Engineering Chemistry **26**, 1183-1187 (1934).

157. A. P. Colburn, Transactions of the American Institute of Chemical Engineers **29**, 174-210 (1933).

158. W. Hayduk and H. Laudie, AIChE Journal **20** (3), 611-615 (1974).

159. J. R. Partington, *An advanced treatise on physical chemistry, Vol. 1 Fundamental Principles: the Properties of Gases*. (Longmans, Green, London; New York, 1949).

160. Y. Ma, C. Zhu, P. Ma and K. T. Yu, Journal of Chemical & Engineering Data **50** (4), 1192-1196 (2005).

161. R. C. Dorresteijn, L. G. Berwald, G. Zomer, C. D. de Gooijer, G. Wieten and E. C. Beuvery, Journal of Chromatography A **724** (1-2), 159-167 (1996).

162. J. W. J. Henderson and A. Brooks, (Agilent Technologies 5990-4547EN, 2010).